**August 29, 2016 (Monday)**

# Superconducting qubit systems: recent experimental progress towards fault-tolerant quantum computing at IBM

Antonio D. Córcoles

*IBM*

**Abstract.** Quantum information processing has experienced dramatic experimental breakthroughs over the last couple of years in many physical platforms. With current attained metrics, the horizon appears promising for building increasingly powerful quantum processors. In this talk I will review recent progress on quantum error detection and correction on superconducting qubit systems at IBM. Our experiments, which are implemented within the stabilizer formalism present in the surface code architecture, aim at demonstrating quantum error correcting protocols for fault-tolerant quantum computing. As a conclusion, I will describe and reflect on the main experimental hurdles our field will have to tackle in the incoming years.

# Observation of frequency-domain Hong-Ou-Mandel interference

Toshiki Kobayashi[1] * Rikizo Ikuta[1] Shuto Yasui[1] Shigehito Miki[2]
Taro Yamashita[2] Hirotaka Terai[2] Takashi Yamamoto[1] Masato Koashi[3]
Nobuyuki Imoto[1]

[1] *Graduate School of Engineering Science, Osaka University, Toyonaka, Osaka 560-8531, Japan*
[2] *Advanced ICT Research Institute, National Institute of Information and Communications Technology (NICT), Kobe 651-2492, Japan*
[3] *Photon Science Center, Graduate School of Engineering, The University of Tokyo, Bunkyo-ku, Tokyo 113-8656, Japan*

**Abstract.** Hong-Ou-Mandel (HOM) interference plays a key role in quantum optics and quantum information processing. Although many types of HOM interference have been demonstrated by using photons, plasmons, atoms and phonons, all of them essentially used the spatial or polarization degree of freedom. In this work, we report the first observation of the HOM interference between two photons with different frequencies. The frequency-domain HOM interferometer is implemented by a partial frequency conversion in a nonlinear optical medium with a strong pump light. Our results have important consequences for manipulating the photonic quantum states encoded in the frequency domain.

**Keywords:** Quantum interference, Nonlinear optics

## 1 Introduction

In the past three decades since the HOM interference has been proposed and demonstrated with two photons from spontaneous parametric down-conversion (SPDC) process [1], huge varieties of experiments based on the HOM interference revealed fundamental properties in quantum physics, especially in quantum optics, and its applications are widely spreading over quantum information processing. The HOM interference has been observed with not only photons but also other bosonic particles, e.g., surface plasmons[2], Helium 4 atoms[3] and phonons[4]. In spite of such demonstrations using various kinds of physical systems, to the best of our knowledge, all of them essentially used the spatial degree of freedom for the HOM interference, including the use of polarization modes of photons that are easily converted to and from spatial modes. The demonstrations use a beamsplitter (BS) which mixes the two particles in different spatial/polarization modes.

In this work[5], we report the first observation of the HOM interference between two photons with different frequencies in optical region. In contrast to the spatial interferometer, the frequency-domain HOM interferometer is implemented in a single spatial mode with a nonlinear optical frequency conversion[6, 7, 8]. In the experiment, we input a 780 nm photon and a 1522 nm photon to the frequency converter that partially converts the wavelengths of the photons between 780 nm and 1522 nm[8]. We measured coincidence counts between the output photons at 780 nm and those at 1522 nm from the frequency converter. The observed visibility of the HOM interference was $0.71 \pm 0.04$, which clearly exceeds the maximum value of 0.5 in the classical wave theory.

## 2 Experimental setup

The experimental setup for the frequency-domain HOM interference by using the partial frequency converter[8] is shown in Fig. 1(a). We prepare a heralded single photon at 780 nm in mode A and a weak coherent light at 1522 nm in mode B with an average photon number of $\sim 0.1$. The two light pulses are combined by a dichroic mirror ($\mathrm{DM}_2$) and then focused on a type-0 quasi-phase-matched periodically-poled $\mathrm{LiNbO}_3$ (PPLN) waveguide for the frequency conversion.

The time difference between the two light pulses is adjusted by mirrors (M) on a motorized stage. The vertically polarized cw pump laser at 1600 nm is combined with the two input light pulses by $\mathrm{DM}_3$ and focused on the PPLN waveguide. The effective pump power was set to 140 mW which corresponds to the conversion efficiency of $\sim 0.4$. After the frequency converter, the light pulses at 780 nm and 1522 nm are separated by $\mathrm{DM}_4$ and Bragg gratings ($\mathrm{BG}_{\mathrm{U2}}$ and $\mathrm{BG}_{\mathrm{L2}}$). They are then measured by an avalanche photodiode with the quantum efficiency of about 60% for 780-nm photons ($\mathrm{D}_{\mathrm{U2}}$) and by a superconducting single-photon detector (SSPD)[9] with the quantum efficiency of about 60% for the 1522-nm photons ($\mathrm{D}_{\mathrm{L}}$). In order to observe the HOM interference, we collect the threefold coincidence events among the three detectors $\mathrm{D}_{\mathrm{U1}}, \mathrm{D}_{\mathrm{U2}}$ and $\mathrm{D}_{\mathrm{L}}$.

## 3 Experimental result

The experimental result of the dependency of the threefold coincidence counts on the optical delay is shown in Fig. 1(b). The observed visibility of $0.71 \pm 0.04$ at the zero delay point was obtained by the best fit to the experimental data with a Gaussian. The high visibility clearly shows the nonclassical HOM interference between the two light pulses in a single spatial mode with different frequencies. We also measured the visibilities at the

*kobayashi-t@qi.mp.es.osaka-u.ac.jp

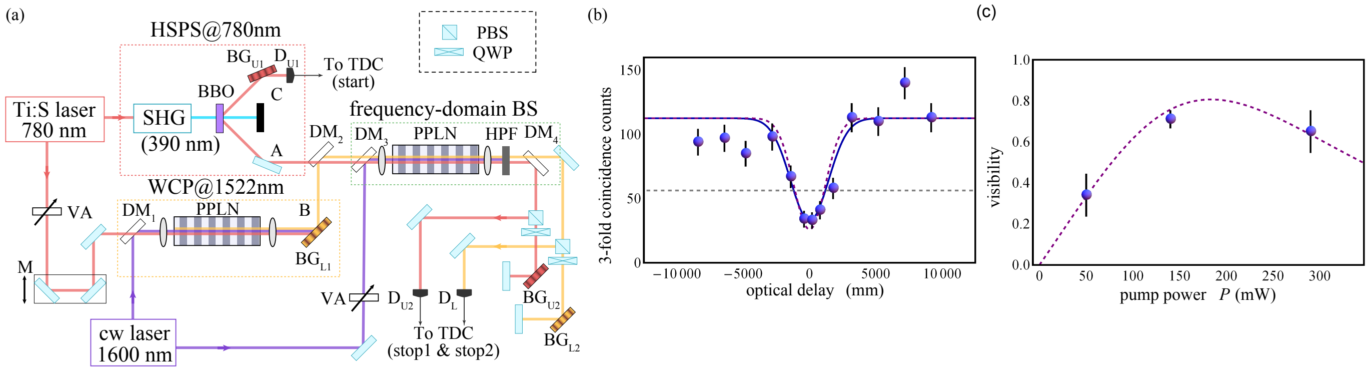

Figure 1: (a) The experimental setup of the frequency-domain HOM interference. In the experiment, the heralded single photon source (HSPS) at 780 nm and the weak coherent pulse (WCP) at 1522 nm are prepared to serve as two input photons to the frequency-domain BS. (b) The observed HOM dip at 140-mW pump power. The circles represent the experimental threefold coincidence counts. The solid curve is the Gaussian fit to the experimental counts. The dashed curve is obtained from our theoretical model with the experimental parameters. The dashed horizontal line describes the half values of the maximum of the fitting result. (c) The pump power dependence of the visibility. The circles are obtained from the experimental result. The dashed curve is obtained from our theoretical model with the experimental parameters.

pump power 50 mW and 290 mW, which corresponds to the conversion efficiencies ∼ 0.2 and ∼ 0.7, respectively. The experimental result is shown in Fig. 1(c). The observed visibilities are 0.34±0.10 at 50 mW and 0.65±0.10 at 290 mW. From our theoretical model, main reasons for the degradation of the visibility comes from the input light pulses; the effect of the multiphoton components in the coherent light pulse at 1522 nm and the broad bandwidth of the heralded single photon at 780 nm. If we use two single photons with the same bandwidth as that of the coherent light pulse, the visibility will be 0.98 at 190-mW pump power.

## 4 Conclusion

In conclusion, we have demonstrated the frequency-domain HOM interference between a heralded single photon at 780 nm and a weak laser light at 1522 nm in a single spatial mode by using the partial frequency converter based on the nonlinear optical effect. We observed the visibility of 0.71±0.04, which clearly shows the nonclassical interference. We believe that our results give a novel tool for exploiting frequency-domain quantum phenomena and a way of scaling up the quantum information processing.

## Acknowledgements

This work was supported by the JSPS Grant-in-Aid for JSPS Fellows Grant No. JP14J04677 and MEXT/JSPS KAKENHI Grant Nos JP25247068, JP15H03704, JP15KK0164 and JP25286077.

## References

[1] C. K. Hong, Z. Y. Ou, & L. Mandel, Measurement of subpicosecond time intervals between two photons by interference. *Phys. Rev. Lett.* 59, 2044-2046 (1987).

[2] G. Di Martino *et al.* Observation of Quantum Interference in the Plasmonic Hong-Ou-Mandel Effect. *Phys. Rev. Applied* 1, 034004 (2014); J. S. Fakonas *et al.* Two-plasmon quantum interference. *Nat. Photon.* 8, 317 (2014).

[3] R. Lopes *et al.* Atomic Hong-Ou-Mandel experiment. *Nature* 520, 66 (2015).

[4] K. Toyoda, R. Hiji, A. Noguchi & S. Urabe, Hong-Ou-Mandel interference of two phonons in trapped ions. *Nature* 527, 74 (2015).

[5] T. Kobayashi *et al.* Frequency-domain Hong-Ou-Mandel interference *Nat. Photon.* 10, 441 (2016).

[6] S. Tanzilli *et al.* A photonic quantum information interface. *Nature* 437, 116 (2005).

[7] R. Ikuta, *et al.* Wide-band quantum interface for visible-to-telecommunication wavelength conversion. *Nat. Commun.* 2, 537 (2011).

[8] R. Ikuta *et al.* Observation of two output light pulses from a partial wavelength converter preserving phase of an input light at a single-photon level. *Opt. Express* 21, 27865 (2013).

[9] S. Miki, T. Yamashita, H. Terai & Z. Wang, High performance fiber-coupled NbTiN superconducting nanowire single photon detectors with Gifford-McMahon cryocooler. *Opt. Express* 21, 10208 (2013).

# Realization of the contextuality-nonlocality tradeoff with a qubit-qutrit photon pair

Peng Xue[1] * Xiang Zhan[1] Xin Zhang[1] Jian Li[1] Yongsheng Zhang[2]
Barry C. Sanders[3]

[1] *Department of Physics, Southeast University, Nanjing 211189, China*
[2] *Key Laboratory of Quantum Information, University of Science and Technology of China, CAS, Hefei 230026, China*
[3] *Institute for Quantum Science and Technology, University of Calgary, Alberta T2N 1N4, Canada*

**Abstract.** We report our experimental results on the no-disturbance principle, which imposes a fundamental monogamy relation on contextuality vs non-locality. We employ a photonic qutrit-qubit hybrid to explore no-disturbance monogamy at the quantum boundary spanned by non-contextuality and locality inequalities. In particular we realize the single point where the quantum boundary meets the no-disturbance boundary. Our results agree with quantum theory and satisfy the stringent monogamy relation thereby providing direct experimental evidence of a tradeoff between locally contextual correlations and spatially separated correlations. Thus, our experiment provides evidence that entanglement is a particular manifestation of a more fundamental quantum resource.

**Keywords:** nonlocality, contextuality, monogamy relation, entanglement

Quantum systems exhibit a wide range of non-classical and counter-intuitive phenomena. Corresponding experimental tests have been performed and support the necessity of quantum mechanics. The relation between contextual correlations and non-local correlations has been studied recently. It has been proven that the no-disturbance (ND) principle imposes monogamy relation between contextuality and non-locality and the quantum version of this monogamy relation is even more stringent.

We demonstrate no-disturbance monogamy spanned by non-contextuality and locality inequalities [1], which was theoretically proposed by Kurzyński et al. in [2]. Consider a scenario with two spatial separated observers Alice and Bob. Alice randomly chooses two compatible measurements from five measurements $\{A_i\}$ $(i = 1, ..., 5)$ and performs them on her system. Each two of $A_i$ and $A_{(i+1) \bmod 5}$ are compatible. Whereas Bob chooses one of two incompatible measurements $B_1$, $B_2$ and performs them on his system. Each measurement has two outcomes ±1.

One can test contextuality on Alice's system via KCBS inequality

$$\kappa_A = \langle A_1A_2\rangle + \langle A_2A_3\rangle + \langle A_3A_4\rangle + \langle A_4A_5\rangle + \langle A_5A_1\rangle \overset{\text{NCHV}}{\geqslant} -3. \quad (1)$$

Whereas CHSH locality inequality

$$\beta_{AB} = \langle A_1B_1\rangle + \langle A_1B_2\rangle + \langle A_4B_1\rangle - \langle A_4B_2\rangle \overset{\text{LHV}}{\geqslant} -2 \quad (2)$$

can be tested on the systems of Alice and Bob.

The ND principle imposes a nontrivial tradeoff between the violations of CHSH and KCBS inequalities, i.e.,

$$\beta_{AB} + \kappa_A \overset{\text{ND}}{\geqslant} -5. \quad (3)$$

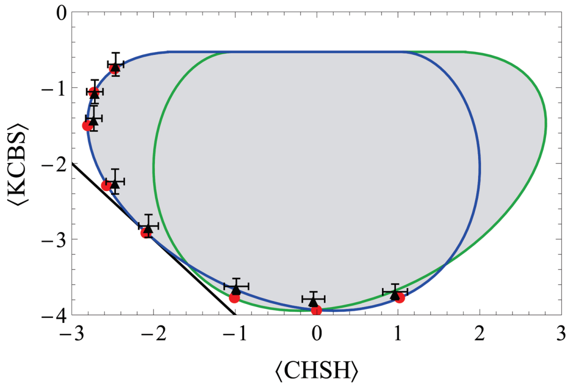

Figure 1: The region spanned by the allowed average values of CHSH and KCBS operators $\langle CHSH\rangle$ and $\langle KCBS\rangle$ can be divided into two overlapping parts and bounded by the solid curves. Every quantum state produces a point inside the region. However only the specific states can produce the points on the boundaries. The solid black straight line denotes the ND boundary. Experimental results of $\langle CHSH\rangle$ and $\langle KCBS\rangle$ are represented by the black triangles and compared to their theoretical predictions (red dots), producing the points on the boundary of the quantum region.

According to the ND principle, only one of these inequalities can be violated at a time. Quantum theory shows an additional monogamy relation between NCHV and LHV by restricting the possible values of $(\beta_{AB}, \kappa_A)$ within a region in the parametric space spanned by the value of these two inequalities. The more stringent monogamy relation makes the quantum region to be smaller than that imposed by the ND principle. Therefore the boundary of the quantum region is more interesting. The quantum boundary touches the ND boundary in a single point.

To experimentally investigate quantum monogamy re-

*gnep.eux@gmail.com

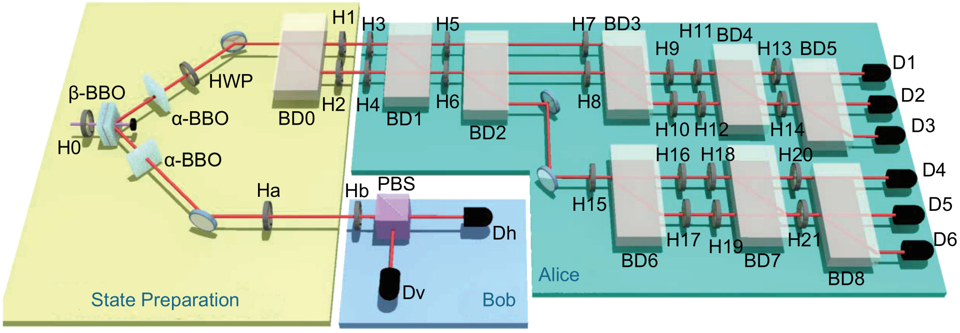

Figure 2: Experimental setup. Alice and Bob share entangled photon pairs which are generated via type-I SPDC. For Alice, cascade setup for sequentially measuring $A_i$ and $A_{i+1}$ is used to test KCBS inequality. Whereas, to test CHSH inequality $B_j$ is measured via standard polarization measurements using HWP (Hb) and PBS.

lation between KCBS and CHSH inequalities, we produce the boundary of the quantum region in the parametric space spanned by the value of the two inequalities and especially the single point where the quantum boundary touches the ND boundary.

As illustrated in Fig. 2, our experimental setup consists of three modules: state preparation, Alice's measurement, and Bob's measurement. In the state preparation module, entangled photons of 801.6nm wavelength are generated in a type-I spontaneous parametric down-conversion (SPDC) process where two joint 0.5mm-thick $\beta$-barium-borate ($\beta$-BBO) crystals are pumped by a CW diode laser with 90mW of power. The visibility of entangled photonic state is larger than 95%. One of the photons as a qubit system is sent to Bob for his measurement. The other is then split by a birefringent calcite beam displacer (BD) into two parallel spatial modes. By employing the polarizations and spatial modes of a single photon, we can prepare arbitrary state of a qutrit.

To measure Alice's observables $A_i$ and their correlations, we use cascaded Mach-Zehnder interferometers in three steps. The first step is to realize the measurement of $A_i$. Measuring $A_iA_{i+1}$ requires two sequential measurements on the same photon. Since the single-observable measuring devices map its eigenstates to a fixed spatial path and polarization, with HWPs and BDs we can re-create the corresponding eigenstates of $A_i$ for further measurement $A_{i+1}$ in the second step. Two outcomes of $A_i$ are each directed into identical but separated devices. In the third step we use the same interferometers in the first step to measurement $A_{i+1}$. Two identical $A_{i+1}$ measuring devices are built, each of which is connected to the corresponding output port of the measuring device of $A_i$. The outcomes of the measurement $A_iA_{i+1}$ are given by the responses of the detectors.

For Bob, the measurement of observable $B_j$ is standard polarization measurement using HWP (Hb) and PBS. The photons are detected by Dh and Dv right after the PBS. For the photon detection, we only register the coincidence rates between the detectors of Alice and Bob.

We produce eight points on the quantum boundary corresponding to eight different input states. The experimental results on the average values of CHSH and KCBS operators are shown in Fig. 1. It is clear that the inequality (3) is always satisfied in experiment, and the violation of either KCBS or CHSH inequality forbids the violation of the other, in agreement with the quantum theory predictions. Especially, our results show the inequality (3) is tight, i.e., there is a state for which the inequality becomes an equality. We present the measured values $\langle CHSH\rangle_{\text{ex}} = -2.061 \pm 0.120$, $\langle KCBS\rangle_{\text{ex}} = -2.826 \pm 0.151$ in the single point where the quantum boundary touches the ND boundary and the inequality becomes an equality, i.e., $\beta_{AB} + \kappa_A = -5$ is satisfied within error bars.

The fact that the origin of Bell inequalities and contextual inequalities is the existence of joint probability distributions naturally raises the question as to whether similar monogamy relations exist between contextual correlations and nonlocal correlations. Our experiment provides an answer to this question. We observe the fundamental monogamy relation between contextuality and non-locality in a photonic qutrit-qubit system and show the first experimental evidence of a tradeoff between locally contextual correlations and spatially separated correlations imposed by quantum theory. The existence of the monogamy relation suggests the existence of a quantum resource of which entanglement is a particular form. The resource required to violate KCBS inequality can be transformed into entanglement which consumes to violate CHSH inequality. Our experiment sheds new light for further explorations of this quantum resource. Furthermore our results suggest monogamy relations between different types of correlations might be ubiquitous in nature and pave the way for further research on these monogamy relations.

## References

[1] X. Zhan, X. Zhang, J. Li, Y. S. Zhang, B. C. Sanders, and P. Xue, Phys. Rev. Lett. 116, 090401 (2016).

[2] P. Kurzyński, A. Cabello and D. Kaszlikowski, Phys. Rev. Lett. **112**, 100401 (2014).

# One-way and reference-frame independent EPR-steering

Sabine Wollmann,[1] * Raj B. Patel,[1] Nathan Walk,[1 2] Michael J. W. Hall,[1]
Howard M. Wiseman,[1] Geoff J. Pryde[1 †]

[1] *Centre for Quantum Computation and Communication Technology (Australian Research Council), Centre for Quantum Dynamics, Griffith University, Brisbane, Queensland 4111, Australia*
[2] *Department of Computer Science, University of Oxford, Oxford OX1 3QD, United Kingdom*

**Abstract.** Einstein-Podolsky-Rosen steering is a type of quantum correlation intermediate to entanglement and Bell nonlocality. It is widely investigated for its foundational aspects and applications in quantum information and communication tasks. Here, we prove and experimentally observe that steering can be *one-way*, i.e. the ability to complete the protocol is asymmetric under change of the parties. We also prove and experimentally observe that steering can be demonstrated with 100% probability that this is invariant to rotations of the measurement settings.

**Keywords:** Quantum optics, Quantum information, EPR, nonlocality, steering, reference frame

Quantum entanglement is a key resource for quantum information and communication tasks, such as teleportation, entanglement swapping and quantum key distribution. Einstein-Podolsky-Rosen (EPR) steering is a quantum correlation that is distinct from other nonclassical correlations such as Bell nonlocality (1) and quantum nonseparability. Because of the nonlocal correlations, measuring one system affects the measurement results on the other system, hence the name 'steering'.

## 1 Asymmetric steering

Moving through the classes of quantum nonlocality, from Bell nonlocality towards nonseparability gives access to protocols which are more robust to noise (2) for projective measurements at the expense of increasing the number of parties and apparatus that need to be trusted. For entanglement witness tests and Bell inequality violations, both observers are untrusted or trusted respectively. However, EPR-steering, which was only recently formalized by Wiseman et al. (3), features a fundamental asymmetry in the sense that in a steering test the observers play different roles: one party is trusted while the other is untrusted. While the previous classes are symmetric —the effects persist under exchange of the parties - this does not necessarily hold for EPR-steering. The question which arises is whether sharing an asymmetric state can result in one-way EPR steering, where e.g. Alice can steer Bob's measurement outcomes, but not the other way around.

This question was first experimentally addressed by Händchen et al., who demonstrated Gaussian one-way EPR steering (4). However their investigation was restricted to Gaussian measurements on Gaussian states. However, there exists explicit examples of supposedly one-way steerable Gaussian states actually being two-way steerable using a broader class of measurements (5). Do states exist which are one-way steerable for arbitrary measurements? The answer is yes. Two independent groups, Nicolas Brunner's in Geneva and Howard Wiseman's in Brisbane, theoretically proved the existence of such states. Brunner's approach holds for arbitrary measurements with infinite settings, the so-called infinite-setting positive-operator-valued measures (POVMs), with the cost of using an exotic family of states to demonstrate the effect over an extremely small parameter range, which is unsuitable for experimental observation (6). Independently, Evans et al. showed one-way steerability exists for projective measurements of Werner states and loss (7), which are easier to realise experimentally.

In our work (5) we ask if we can extend the result in Ref. (6) to find a simple state which is steerable in one direction but cannot be steered in the other direction, even for the case of arbitrary measurements and infinite settings. We consider a shared Werner state for optical polarisation qubits, $\rho_W(\mu) = \mu\,|\psi_s\rangle\,\langle\psi_s| + (1-\mu)/4\,\mathbf{I}_x$, where $\mu \in [0,1]$, $\mathbf{I}_x$ is the identity and $|\psi_s\rangle = (|01\rangle - |10\rangle)/\sqrt{2}$ (7). Using a theorem of Ref.(6) allowed us to construct a state $\rho_{AB} = \frac{1-p}{3}\rho_W + \frac{p+2}{3}\frac{\mathbf{I}_A}{2} \otimes |v\rangle\,\langle v|$, where $|v\rangle$ is the vacuum state of Bob's mode and the probability p represents adding asymmetric loss in his arm. This state is one-way steerable for POVMs, if we can fulfil the condition $p > \frac{2\mu+1}{3}$.

In our experiment we investigated three different regimes: two-way steering, one-way steering for projective measurements and one-way steering for POVMs. The state for each steering regime was reconstructed via quantum state tomography and its fidelity with the closest Werner state, and its parameter $\mu$, was determined (5). To demonstrate two-way steering, we measured Alice's steering parameter to be 8.4 standard deviations (SDs) above the classical bound and Bob's steering parameter violating the steering inequality by 5.1 SDs. Next we realized a one-way steerable state for projective measurements by inserting a loss in Bob's line (Fig.1). Alice remained able to steer Bob's state, violating the inequality by 7.3 SDs. The loss of information in Bob's arm made him unable to steer the other party. Finally, we investigated the regime where only one-way steering

[*] sabine.wollmann@griffithuni.edu.au

[†] g.pryde@griffith.edu.au

is possible, even for arbitrary POVMs. We were able to violate the inequality by 6.6 SDs in one direction. In the other direction, tomographic reconstruction verified the creation of a state that was provably unsteerable for POVMs. Thus, we observe genuine one-way EPR steering for the first time. We note that an independent demonstration was realised in Ref.(8). While their result is restricted to two measurement settings, our result holds for POVMs.

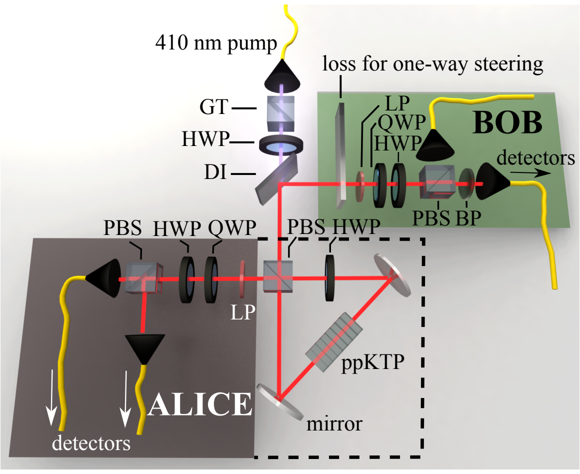

Figure 1: Experimental scheme. Both, Alice and Bob, are in control of their line and their detectors. The party which is steering is also in control of the source. Entangled photons at 820 nm were produced via SPDC (9). Different measurement settings are realized by rotating half- and quarter-wave plates relative to the polarizing beam splitters. The loss, inserted for one-way EPR-steering, was realized by a gradient neutral density filter mounted in front of Bob's line to control the fraction of photons received. Long pass (LP) filters remove pump photons co-propagating with the qubits before the latter are coupled into fibres and detected by photon counting modules and counting electronics.

## 2 Rotationally symmetric steering tests

In another experiment we also characterised the rotational invariance of EPR-steering. Establishing such a common reference frame —necessary for many quantum information tasks - is a nontrivial issue and can be highly resource intensive and technically demanding. The question is whether quantum nonlocality can be demonstrated without a shared reference frame. This question was experimentally (10; 11) answered for the CHSH inequality. Here, we formulate rotationally invariant steering inequalities for $m$ measurement directions for Alice and $n$ directions for Bob. In our experiment, they can estimate the average correlations $M_{jk} := \langle A_j B_k \rangle$ from their measurement outcomes. Alice has to violate the EPR-steering inequality $\|M\|_{tr} := tr\sqrt{M^T M} \leq \sqrt{m}$ for the trace-norm of the correlation matrix to demonstrate steering of Bob's state. For m=n=2, this trace-norm inequality is the best possible steering inequality that is invariant under local rotations that preserve the plane of Alice and Bob's measurement directions. If Alice's and Bob's measurement directions are sharing the same plane, EPR-steering is always possible, regardless of any rotations in the plane for a Werner state with $\mu > \frac{1}{\sqrt{2}}$. We compare our inequality with the CFFW inequality (12). In our experiment (Fig.1), we consider $m = n = 2$ orthogonal measurement directions for Alice and Bob in the $\sigma_x - \sigma_z$ plane (Fig.2). While Bob's measurement directions remained fixed along $\sigma_x$ and $\sigma_z$, Alice's were rotated by $w = 10°$steps. We compared our trace-norm inequality (blue squares) with the CFFW inequality (red circles) and observed for both a violation of the bound (Fig.2a). Rotating by angle $\Phi$ out of the shared plane demonstrated the dependency of both inequalities on a shared measurement plane. At our chosen angle, using the trace-norm inequality did not allow us to demonstrate steering, while we could still violate the CFFW inequality despite its dependence on the rotation $w$ along the plane (Fig.2b).

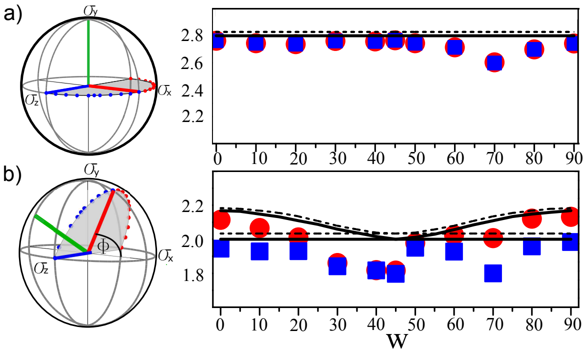

Figure 2: The Poincaré spheres show measurement directions (blue and red). Alice's measurement directions are rotated by 90° in 10° steps (dots) along the plane (grey) which was spanned by $a_1$(blue) and $a_2$ (red) forming an angle of $\Phi = 0°$ (a), and $\Phi = 64°$ (b) with the $\sigma_x$ axis. We compare experimental data for the trace-norm inequality (blue square) and CFFW inequality (red circles) with modeled curves using a maximally entangled state (dashed line) and a Werner state $\rho_W(\mu)$ (solid line).

## References

[1] J.S Bell, *Physics*, 1:195, 1964.
[2] A. J. Bennet et al., *Phys. Rev. X*, 2:031003, 2012.
[3] H. Wiseman et al., *Phys. Rev. Lett.*, 98:140402, 2007.
[4] V. Handchen et al., *Nat Photon*, 6:596, 2012.
[5] S. Wollmann et al., *Phys. Rev. Lett.*, 116:160403, 2016.
[6] M. T. Quintino et al., *Phys. Rev. A*, 92:032107, 2015.
[7] D.A. Evans et al., *Phys. Rev. A*, 90, 2014.
[8] K. Sun et al., *Phys. Rev. Lett.*, 116:160404, 2016.
[9] A. Fedrizzi et al., *Opt. Exp.*, 15:15377, 2007.
[10] P. Shadbolt et al., *Sci. Rep.*, 2:470, 2012.
[11] M. S. Palsson et al., *Phys. Rev. A*, 86:032322, 2012.
[12] E. G. Cavalcanti et al., *J. Opt. Soc. Am. B*, 32:A74, 2015.

# Are Incoherent Operations Physically Consistent? – A Physical Appraisal of Incoherent Operations and an Overview of Coherence Measures

Eric Chitambar[1] *  Gilad Gour[2] [3] †

[1] *Department of Physics and Astronomy, Southern Illinois University, Carbondale, Illinois 62901, USA*
[2] *Department of Mathematics and Statistics, University of Calgary, AB, Canada T2N 1N4*
[3] *Institute for Quantum Science and Technology, University of Calgary, AB, Canada T2N 1N4*

**Abstract.** In this paper we establish a criterion of physical consistency for any resource theory. We show that all currently proposed basis-dependent theories of coherence fail to satisfy this criterion. We further characterize the physically consistent resource theory of coherence and find its operational power to be quite limited. After relaxing the condition of physical consistency, a number of new coherence measures are introduced based on relative Rényi entropies, and we study incoherent state transformations under different operational classes, including the newly proposed dephasing-covariant operations. Necessary and sufficient conditions are derived for the convertibility of qubit states.

**Keywords:** Quantum coherence, Quantum resource theories

## 1 Introduction

In quantum systems, the notion of coherence is ubiquitous. For instance, the state $|+\rangle = \sqrt{1/2}(|0\rangle + |1\rangle)$ can be seen as a coherent superposition of the states $|0\rangle$ and $|1\rangle$, while the state $|0\rangle$ can itself be seen as a coherent superposition of $|+\rangle$ and $|-\rangle = \sqrt{1/2}(|0\rangle - |1\rangle)$. Thus, without further qualification, it is completely ambiguous to say that one state has coherence while another does not. One way to make such a statement meaningful involves first identifying a fixed reference basis, and then defining coherence with respect to this basis. More precisely, a basis for the system's state space is specified (called the incoherent basis), and then a given state is deemed incoherent if it is diagonal in this basis.

Recently, researchers have used this distinction between coherent and incoherent states to construct resource theories of quantum coherence [1, 2, 3, 4]. A general resource theory for a quantum system is characterized by a pair $(\mathcal{F}, \mathcal{O})$, where $\mathcal{F}$ is a set of "free" states and $\mathcal{O}$ is a set of "free" quantum operations. Any state that does not belong to $\mathcal{F}$ is then deemed a resource state. Entanglement theory provides a prototypical example of a resource theory in which the free states are the separable or unentangled states, and the free operations are local operations and classical communication (LOCC). For quantum coherence, the free states are the incoherent states $\mathcal{I}$. As for the free or "incoherent" operations, many different approaches have been proposed, and a primary objective of this paper is to consider the physical meaning behind these approaches.

Specifically, we propose one notion of what it means for a quantum resource theory to be "physical," and then we see what type of incoherent operations fits this prescription. In principle, any pair $(\mathcal{F}, \mathcal{O})$ defines a resource theory, provided the operations of $\mathcal{O}$ act invariantly on $\mathcal{F}$; i.e. $\mathcal{E}(\rho) \in \mathcal{F}$ for all $\rho \in \mathcal{F}$ and all $\mathcal{E} \in \mathcal{O}$. However, this is just a mathematical restriction placed on the maps belonging to $\mathcal{O}$. It does not imply that $\mathcal{E} \in \mathcal{O}$ can actually be physically implemented without generating or consuming additional resource. The issue is a bit subtle here since in quantum mechanics, physical operations on one system ultimately arise from unitary dynamics and projective measurements on a larger system, a process mathematically described by a Stinespring dilation. A resource theory $(\mathcal{F}, \mathcal{O})$ defined on system $A$ is said to be *physically consistent* if every free operation $\mathcal{E} \in \mathcal{O}$ can be obtained by an auxiliary state $\hat{\rho}_B$, a joint unitary $U_{AB}$, and a projective measurement $\{P_k\}_k$ that are all free in an extended resource theory $(\mathcal{F}', \mathcal{O}')$ defined a larger system $AB$, for which $\mathcal{F} = \text{Tr}_B\mathcal{F}' := \{\text{Tr}_B(\rho_{AB}) : \rho_{AB} \in \mathcal{F}'\}$. For example, LOCC renders a physically consistent resource theory of entanglement since any LOCC operation can be implemented using only local unitaries and projections.

The most well-known resources theories of quantum coherence are based on either Maximal Incoherent Operations (MIO) [1], Incoherent Operations (IO) [2], or Strictly Incoherent Operations (SIO) [3, 4]. We observe that none of these offer a physically consistent resource theory as just defined, and the true analog to LOCC in coherence theory has been lacking. We identify this hitherto missing piece as the class of *physically incoherent operations* (PIO). The previously studied operations MIO/IO/SIO are much closer akin to separable or non-entangling operations in entanglement theory, and we clarify what sort of physical interpretations can be given to these operations. The relationship between the different operational classes is depicted described by PIO ⊂ SIO ⊂ IO ⊂ MIO.

## 2 Results

The following summarizes our main results. First, we fully characterize the class of physically incoherent operations (PIO).

*echitamb@siu.edu
†gour@ucalgary.ca

**Proposition 1** *A CPTP map $\mathcal{E}$ is a physically incoherent operation if and only if it can be expressed as a convex combination of maps each having Kraus operators $\{K_j\}_{j=1}^r$ of the form*

$$K_j = U_j P_j = \sum_x e^{i\theta_x} |\pi_j(x)\rangle\langle x| P_j, \qquad (1)$$

*where the $P_j$ form an orthogonal and complete set of incoherent projectors on system $A$ and $\pi_j$ are permutations.*

Necessary and sufficient conditions for state transformations are derived.

**Proposition 2** *For any two state $|\psi\rangle$ and $|\phi\rangle$, the transformation $|\psi\rangle \to |\phi\rangle$ is possible by PIO if and only if*

$$|\psi\rangle = \sum_{i=1}^k \sqrt{p_i} U_i |\phi\rangle, \qquad (2)$$

*where the $U_i$ are incoherent isometries such that $P_i U_i |\phi\rangle = U_i |\phi\rangle$ for an orthogonal and complete set of incoherent projectors $\{P_i\}_i$.*

While we find that PIO allows for optimal distillation of maximal coherence from partially coherent pure states in the asymptotic limit of many copies, the process is strongly irreversible. That is, maximally coherent states cannot be diluted into weakly coherent states at a nonzero rate, and they are thus curiously found to be the *least* powerful among all coherent states in terms of asymptotic convertibility.

Given this limitation of PIO and its similar weakness on the finite-copy level, it is therefore desirable from a theoretical perspective to consider more general operations. Consequently, we shift our focus to the development of coherence resource theories under different relaxations of PIO. To this end, we introduce the class of dephasing-covariant incoherent operations (DIO), which to our knowledge has never discussed before in literature. We provide physical motivation for DIO and show that these operations are just as powerful as Maximal Incoherent Operations (MIO) when acting on qubits. It turns out that all classes of incoherent operations behave equivalently for this task, and in fact, state convertibability depends on just two incoherent monotones. The first is the *Robustness of Coherence*, and is defined as

$$C_R(\rho) = \min_{t \geq 0} \left\{ t \;\middle|\; \frac{\rho + t\sigma}{1+t} \in \mathcal{I},\ \sigma \geq 0 \right\}.$$

Here we introduce a new type of robustness measure that we call the $\Delta$-Robustness of Coherence:

$$C_{\Delta,R}(\rho) = \min_{t \geq 0} \left\{ t \;\middle|\; \frac{\rho + t\sigma}{1+t} \in \mathcal{I},\ \sigma \geq 0,\ \Delta(\sigma - \rho) = 0 \right\}.$$

While $C_R$ is a monotone under MIO in general, for qubits $C_{\Delta,R}$ is also a MIO monotone. These two measures completely characterize qubit state transformations, as we prove in this paper.

**Theorem 3** *For qubit state $\rho$ and $\sigma$, the transformation $\rho \to \sigma$ is possible by either SIO, DIO, IO, or MIO if and only if both $C_R(\rho) \geq C_R(\sigma)$ and $C_{\Delta,R}(\rho) \geq C_{\Delta,R}(\sigma)$.*

Additional results include:

- We show that the so-called majorization condition decides transformation feasibility for the classes SIO and a special subclass of IO that we denote by sIO. However, whether or not the majorization condition also holds for IO remains an open problem and we point out mistakes in recent proofs claiming it does. By constructing an explicit family of transformations, we show that the majorization condition can be violated by MIO - even stronger the Schmidt rank can be increased by MIO. In addition, we demonstrate an operational equivalence between incoherent pure state transformations using PIO/SIO/sIO and the transformation of bipartite maximally correlated states using zero-communication LOCC/one-way LOCC/ two-way LOCC, respectively.

- We introduce a number of new incoherent monotones/measures for the various operational classes based. All of these measures are unified within a very general framework for constructing incoherent measures. Two class of measures included in this framework are the relative Rényi $\alpha$-entropies of incoherence and the quantum relative Rényi $\alpha$-entropies of incoherence.

- We discuss in greater detail the relationship between coherence resource theories based on asymmetry and those using a basis-dependent definition of coherence. We develop the resource theories of $G$-asymmetry and $N$-asymmetry, where $G$ is the group of all incoherent unitaries and $N$ is the group of all diagonal incoherent unitaries.

## References

[1] J. Äberg. Quantifying Superposition. quant-ph/0612146, 2006.

[2] T. Baumgratz, M. Cramer, and M.B. Plenio. Quantifying Coherence. *Phys. Rev. Lett.*, 113(14):140401, 2014.

[3] A. Winter and D. Yang. Operational Resource Theory of Coherence. *Phys. Rev. Lett.*, 116(12):120404, 2015.

[4] B. Yadin, J. Ma, D. Girolami, M. Gu, V. Vedral. Quantum Processes which do not use Coherence. arXiv:1512.02085, 2015.

# Relating the Resource Theories of Entanglement and Quantum Coherence

Eric Chitambar[1] * Min-Hsiu Hsieh[2] †

[1] *Southern Illinois University*
[2] *University of Technology Sydney*

**Keywords:** Resource Theory; Coherence; Entanglement; LOCC

There has currently been much interest in constructing a resource theory of quantum coherence [1, 15, 2, 4, 13, 31, 29, 25, 20, 26, 30], in part because of recent experimental and numerical findings that suggest quantum coherence alone can enhance or impact physical dynamics in biology [17, 16, 12, 14], and thermodynamics [18, 21]. In a standard resource-theoretic treatment of quantum coherence, the free (or "incoherent") states are those that are diagonal in some fixed reference (or "incoherent") basis. Different classes of allowed (or "incoherent") operations have been proposed in the literature [1, 2, 20, 26, 30, 5, 19], however an essential requirement is that the incoherent operations act invariantly on the set of diagonal density matrices. Incoherent operations can then be seen as one of the most basic generalizations of classical operations since their action on diagonal states can always be simulated by classical processing.

In addition to coherence, entanglement is another precious resource in quantum information science. To properly unify coherence and entanglement under a common resource-theoretic framework, one must modify the scenario by adopting the "distant lab" perspective in which two or more parties share a quantum system but they are spatially separated from one another [24, 11]. In this setting, entanglement cannot be generated between the parties and it becomes another resource in play. When the constraint of locality is added to the incoherent framework, the allowable operations for Alice and Bob are then *local incoherent operations and classical communication* (LIOCC). The hybrid coherence-entanglement theory described here is similar in spirit to previous work on the locality-restricted resource theories of purity and asymmetry. The goal of this paper is to investigate the LIOCC convertibility between entanglement and coherence as resources in quantum information processing. For instance, how much local coherence and shared entanglement do Alice ($A$) and Bob ($B$) need to prepare a particular bipartite state $\rho^{AB}$ using LIOCC? Conversely, how much coherence and entanglement can be distilled from a given state $\rho^{AB}$ using LIOCC? We refer the detailed introduction of the bipartite coherence theory to the full paper [6]. The canonical resource states in the bipartite LIOCC framework are the maximally coherent bits (CoBits), $|\Phi_A\rangle := \sqrt{1/2}(|0\rangle^A + |1\rangle^A)$ and $|\Phi_B\rangle := \sqrt{1/2}(|0\rangle^B + |1\rangle^B)$ for Alice and Bob's systems respectively [2], as well as the entangled state $|\Phi_{AB}\rangle := \sqrt{1/2}(|00\rangle + |11\rangle)$, which we will call the maximally coherent entangled bit (eCoBit).

***Asymptotic Manipulations of Entanglement and Coherence:*** We now describe the primary tasks studied in this paper, which can be seen as the resource-theoretic tasks recently analyzed by Winter and Yang in Ref. [29] but now with additional locality constraints. All of the detailed proofs can be found in Ref. [6], and here we just present the results. Let us begin with the problem of asymptotic state formation. A triple $(R_A, R_B, E^{co})$ is an achievable *coherence-entanglement formation triple* for the state $\rho^{AB}$ if for every $\epsilon > 0$ there exists an LIOCC operation $\mathcal{L}$ and integer $n$ such that $\mathcal{L}\left(\Phi_A^{\otimes\lceil n(R_A+\epsilon)\rceil} \otimes \Phi_B^{\otimes\lceil n(R_B+\epsilon)\rceil} \otimes \Phi_{A'B'}^{\otimes\lceil n(E^{co}+\epsilon)\rceil}\right) \overset{\epsilon}{\approx} \rho^{\otimes n}$. Dual to the task of formation is resource distillation. A triple $(R_A, R_B, E^{co})$ is an achievable *coherence-entanglement distillation triple* for $\rho^{AB}$ if for every $\epsilon > 0$ there exists an LIOCC operation $\mathcal{L}$ and integer $n$ such that $\mathcal{L}(\rho^{\otimes n}) \overset{\epsilon}{\approx} \Phi_A^{\otimes\lfloor n(R_A-\epsilon)\rfloor} \otimes \Phi_B^{\otimes\lfloor n(R_B-\epsilon)\rfloor} \otimes \Phi_{AB}^{\otimes\lfloor n(E^{co}-\epsilon)\rfloor}$. As we are dealing with asymptotic transformations, we should expect the optimal rate triples to be given by entropic quantities. We will also be interested in these entropic quantities after sending our state $\omega^{AB}$ through the completely dephasing channel, $\Delta(\omega) := \sum_{xy} |xy\rangle\langle xy|\omega|xy\rangle\langle xy|$. It will be convenient to think of $\Delta(\omega)$ as encoding random variables $XY$ having joint distribution $p(x, y) = \langle xy|\Delta(\omega)|xy\rangle$. For this reason, we follow standard convention and replace the labels $(A, B) \to (X, Y)$ when discussing a dephased state. Our first main result completely characterizes the achievable rate region for the LIOCC formation of bipartite pure states.

**Theorem 1** *For a pure state $|\Psi\rangle^{AB}$ the following triples are achievable coherence-entanglement formation rates*

$$(R_A, R_B, E^{co}) = \big(\, 0,\ S(Y|X)_{\Delta(\Psi)}\ ,\ S(X)_{\Delta(\Psi)}\big) \tag{1}$$

$$(R_A, R_B, E^{co}) = \big(S(X)_{\Delta(\Psi)},\ S(Y|X)_{\Delta(\Psi)},\ \mathrm{E}(\Psi)\big) \tag{2}$$

$$(R_A, R_B, E^{co}) = \big(0,\ 0,\ S(XY)_{\Delta(\Psi)}\big) \tag{3}$$

*as well as the points obtained by interchanging $A \leftrightarrow B$ in Eqns. (1) – (3). Moreover, these points are optimal in the sense that any achievable rate triple must satisfy*

*echitamb@siu.edu

†Min-Hsiu.Hsieh@uts.edu.au

*(i) $E^{co} \geq \mathrm{E}(\Psi)$, (ii) $R_A + R_B \geq S(XY)_{\Delta(\Psi)}$, (iii) $R_B + E^{co} \geq S(XY)_{\Delta(\Psi)}$.*

For a mixed state $\rho^{AB}$, a formation protocol can be constructed that achieves the average rates for any ensemble $\{p_k, |\varphi_k\rangle^{AB}\}$ such that $\rho = \sum_k p_k|\varphi_k\rangle\langle\varphi_k|$ [3]. For instance, one can consider an ensemble whose average bipartite coherence attains the coherence of formation $C_F$ for $\rho$; i.e. it is an ensemble $\{p_k, |\varphi_k\rangle^{AB}\}$ for $\rho$ that minimizes $\sum_k p_k S(XY)_{\Delta(\varphi_k)}$ [31, 29]. Then for a mixed state $\rho$, the coherence rate sum $R_A + R_B$ of Eq. (2) can attain the coherence of formation $C_F(\rho)$. In the global setting where Alice and Bob are allowed to perform joint operations across system $AB$, it has been shown that $C_F(\rho)$ quantifies the optimal coherence consumption rate for generating $\rho$ using global incoherent operations [29]. Our result then intuitively says that in the restricted LIOCC setting, the same coherence rate is sufficient to generate $\rho$, however they now need additional entanglement at a rate $\sum_k p_k \mathrm{E}(\varphi_k)$, where the ensemble $\{p_k, |\varphi_k\rangle^{AB}\}$ minimizes the average coherence of $\rho$.

Next, we introduce a new LIOCC monotone and provide its operational interpretation. To do so, we recall the recently studied task of *assisted* coherence distillation, which involves one party helping another distill as much coherence as possible through general quantum operations performed on the helper side and incoherent operations performed on the distillation side [7]. For a given state $\rho^{AB}$, the optimal asymptotic rate of coherence distillation on Bob's side when Alice helps is denoted by $C_a^{A|B}(\rho^{AB})$. When the roles are switched, the optimal asymptotic rate is denoted by $C_a^{B|A}(\rho^{AB})$. It was shown in Ref. [7] that $C_a^{A|B}(\rho^{AB}) = S(Y)_{\Delta(\Psi)}$ and $C_a^{B|A}(\rho^{AB}) = S(X)_{\Delta(\Psi)}$. With these quantities in hand, we define for a bipartite pure state $|\Psi\rangle^{AB}$ the function

$$\begin{aligned} C_{\mathcal{L}}(\Psi) = & \quad C_a^{A|B}(\Psi) + C_a^{B|A}(\Psi) - \mathrm{E}(\Psi) \\ = & \quad S(X)_{\Delta(\Psi)} + S(Y)_{\Delta(\Psi)} - \mathrm{E}(\Psi). \end{aligned} \tag{4}$$

Its extension to mixed states can be defined by a convex roof optimization [27]: $C_{\mathcal{L}}(\rho^{AB}) = \inf_{\{p_k,|\varphi_k\rangle^{AB}\}} \sum_k p_k C_{\mathcal{L}}(\varphi_k^{AB})$ for which $\rho^{AB} = \sum_k p_k|\varphi_k\rangle\langle\varphi_k|$.

**Theorem 2** *The function $C_{\mathcal{L}}$ is an LIOCC monotone.*

We note that this is the first monotone of its kind since it behaves monotonically under LIOCC, but not general LOCC or even under LQICC, the latter being an operational class in which only one of the parties is required to perform incoherent operations (as opposed to LIOCC where *both* parties must perform incoherent operations) [7]. Using the monotonicity of $C_{\mathcal{L}}$, we are able to derive tight upper bounds on coherence distillation rates.

**Theorem 3** *For a pure state $|\Psi\rangle^{AB}$ the following triples are achievable coherence-entanglement distillation rates*

$$(R_A, R_B, E^{co}) = \big(S(X)_{\Delta(\Psi)} - \mathrm{E}(\Psi),\ S(Y)_{\Delta(\Psi)},\ 0\big) \tag{5}$$

$$(R_A, R_B, E^{co}) = \big(0,\ S(Y|X)_{\Delta(\Psi)},\ I(X:Y)_{\Delta(\Psi)}\big), \tag{6}$$

*as well as the points obtained by interchanging $A \leftrightarrow B$ in Eqn. (5) and (6). Moreover, these points are optimal in the sense that any achievable rate triple must satisfy (i) $R_A + R_B \leq C_{\mathcal{L}}(\Psi)$ and (ii) $R_B + E^{co} \leq S(Y)_{\Delta(\Psi)}$.*

This theorem endows $C_{\mathcal{L}}$ with the operational meaning of quantifying how much local coherence can be simultaneously distilled from a pure state. For a state $|\Psi\rangle$ the maximum that Alice can help Bob distill coherence is $C_a^{A|B}$ while the maximum that Bob can help Alice is $C_a^{B|A}$. Evidently, they cannot both simultaneously help each other at these optimal rates. Instead, they are bounded away from simultaneous optimality at a rate equaling their shared entanglement. It is still unknown the precise range of achievable distillation triples $(R_A, R_B, E_{max}^{co})$, where $E_{max}^{co}$ is the maximum eCoBit distillation rate. While we are able to prove that $E_{max}^{co}$ is the regularized version of $I(X:Y)_{\Delta(\Psi)}$ optimized over all LIOCC protocols, we have no single-letter expression for this rate nor do we know the achievable local coherence rates for optimal protocols.

A natural question is whether $E_{max}^{co}(\Psi) = \mathrm{E}(\Psi)$. While this question remains open, we can show that $\mathrm{E}(\Psi)$ is achievable if the Schmidt basis of the final state need not be incoherent. More precisely, we say a number $R$ is an achievable LIOCC entanglement distillation rate if for every $\epsilon > 0$, there exists an LIOCC protocol $\mathcal{L}$ acting on $n$ copies of $\Psi$ such that $\mathcal{L}(\Psi^{\otimes n}) \overset{\epsilon}{\approx} \Lambda_d$, where $\Lambda_d$ is a $d \otimes d$ maximally entangled pure state (i.e. $\Lambda^A = \Lambda^B = \mathbb{I}/d$) with $\frac{1}{n}\log d > R - \epsilon$. The largest achievable distillation rate will be denoted by $E_D^{LIOCC}(\Psi)$.

**Theorem 4** $E_D^{LIOCC}(\Psi) = \mathrm{E}(\Psi)$.

It is interesting to compare the coherence distillation rates using incoherent operations under different types of locality constraints. In Refs. [23, 8, 22, 10], similar comparisons were made in terms of purity (or work-information) extraction. Let $C_D^{Global}$, $C_D^{LIOCC}$, and $C_D^{LIO}$ denote the optimal rate sum $R_A + R_B$ of local coherence distillation using global incoherent operations, LIOCC, and local incoherent operations (with no classical communication), respectively. In complete analogy to [23, 8, 22, 10], we define the *nonlocal coherence deficit* of a bipartite state $\rho^{AB}$ as $\delta(\rho^{AB}) = C_D^{Global}(\rho^{AB}) - C_D^{LIOCC}(\rho^{AB})$ and the *LIOCC coherence deficit* as $\delta_c(\rho^{AB}) = C_D^{LIOCC}(\rho^{AB}) - C_D^{LIO}(\rho^{AB})$. Intuitively, the quantity $\delta(\rho^{AB})$ quantifies the coherence in a state that can only be accessed using nonlocal incoherent operations. Likewise, $\delta_c(\rho^{AB})$ gives the coherence in $\rho^{AB}$ that requires classical communication to be obtained. The results of Winter and Yang imply that $C_D^{Global}(\Psi) = S(XY)_{\Delta(\Psi)}$ and $C_D^{LIO}(\Psi) = S(X)_{\Delta(\Psi)} + S(Y)_{\Delta(\Psi)} - 2\mathrm{E}(\Psi)$ for a bipartite pure state $|\Psi\rangle^{AB}$ [28]. Combined with Theorem 3, we can compute the two coherence deficits for pure states:

$$\delta(\Psi) = \mathrm{E}(\Psi) - I(X:Y)_{\Delta(\Psi)} \tag{7}$$

$$\delta_c(\Psi) = \mathrm{E}(\Psi). \tag{8}$$

It is curious that the entanglement $\mathrm{E}(\Psi)$ quantifies the coherence gain unlocked by *classical* communication.

Note that a similar phenomenon exists in the resource theory of purity; namely, the quantum deficit $\overline{\Delta}(\Psi)$ and classical deficit $\overline{\Delta}_c(\Psi)$ measure the analogous differences in local purity distillation by so-called "closed operations" (CO), and they are given by $\overline{\Delta}(\Psi) = \overline{\Delta}_c(\Psi) = \mathrm{E}(\Psi)$ [23, 8]. For the task of distilling CoBits, every protocol using incoherent operations can be seen as one using closed operations by accounting for all ancilla systems at the start of protocol [5]. However, closed operations allow for arbitrary unitary rotations, which are forbidden in coherence theory. The term $I(X:Y)_{\Delta(\Psi)}$ in $\delta(\Psi)$ identifies precisely the basis dependence in coherence theory and shows how this decreases the deficit $\delta(\Psi)$ relative $\overline{\Delta}(\Psi)$. On the other hand, there is evidently no basis dependency in the classical deficit $\delta_c(\Psi)$ and it is equivalent to $\Delta_c(\Psi)$.

Although our distillation results so far have only applied to pure states, we can deduce a very general result concerning the distillability of mixed states.

**Theorem 5** *A mixed state $\rho^{AB}$ has (LOCC) distillable entanglement iff entanglement can be distilled using LIOCC.*

***Strengthening entanglement distillability criterion:*** As shown in Ref. [9], a state $\rho$ has distillable entanglement iff for some $k$ there exists rank two operators $A$ and $B$ such that the (unnormalized) state $A \otimes B\rho^{\otimes k} A \otimes B$ is entangled. By Theorem 3 and following the same argumentation of Ref. [9], we can further require that the $A$ and $B$ are incoherent operators; that is, they have the form $A = |0\rangle\langle\alpha_0| + |1\rangle\langle\alpha_1|$ and $B = |0\rangle\langle\beta_0| + |1\rangle\langle\beta_1|$ where $\Delta(\alpha_0) := \Delta(|\alpha_0\rangle\langle\alpha_0|)$ is orthogonal to $\Delta(\alpha_1) := \Delta(|\alpha_1\rangle\langle\alpha_1|)$, and likewise for $\Delta(\beta_0) := \Delta(|\beta_0\rangle\langle\beta_0|)$ for $\Delta(\beta_1) := \Delta(|\beta_1\rangle\langle\beta_1|)$. We are thus able to add an additional condition to the distillability criterion of Ref. [9]. We hope that the strengthened distillability criterion can be useful in the long-standing search for NPT bound entanglement.

***Discussion:*** We would like to comment on the particular type of incoherent operations studied in this letter. As noted in the introduction, there have been various proposals for the "free" class of operations in a resource theory of coherence. This letter has adopted the incoherent operations (IO) of Baumgratz *et al.* [2], where each Kraus operator in a measurement just needs to be incoherence-preserving. While the class IO has drawbacks in terms of formulating a full physically consistent resource theory of coherence [30, 5], it nevertheless seems unlikely that the results of this letter would remain true if other operational classes were considered. For example, the strictly incoherent operations (SIO) proposed by Yadin *et al.* are unable to convert one eCoBit into a CoBit [30]. Thus, we believe that the interesting connections between IO coherence theory and entanglement demonstrated in this letter make a positive case for why IO is important in quantum information theory, independent of any other motivation. In fact, one could even put coherence aside and view LIOCC as just being a simplified subset of LOCC. As we have shown here, nontrivial conclusions about entanglement can indeed be drawn by studying LOCC from "the inside." This approach is somewhat dual to the standard practice of studying LOCC using more general separable operations (SEP), the chain of inclusions being LIOCC $\subset$ LOCC $\subset$ SEP. Interesting future work would be to consider more general connections between coherence non-generating and entanglement non-generating operations.

## References

[1] J. Äberg, 2006. quant-ph/0612146.

[2] T. Baumgratz, M. Cramer, and M. B. Plenio. Quantifying coherence. *Phys. Rev. Lett.*, 113:140401, Sep 2014.

[3] C. H. Bennett, D. P. DiVincenzo, J. A. Smolin, and W. K. Wootters. Mixed-state entanglement and quantum error correction. *Phys. Rev. A*, 54(5):3824–3851, Nov 1996.

[4] T. R. Bromley, M. Cianciaruso, and G. Adesso. Frozen quantum coherence. *Phys. Rev. Lett.*, 114:210401, May 2015.

[5] E. Chitambar and G. Gour, 2016. arXiv:1602.06969.

[6] E. Chitambar and M.-H. Hsieh, 2016. arXiv:1509.07458.

[7] E. Chitambar, A. Streltsov, S. Rana, M. N. Bera, G. Adesso, and M. Lewenstein. Assisted distillation of quantum coherence. *Phys. Rev. Lett.*, 116:070402, Feb 2016.

[8] M. Horodecki, K. Horodecki, P. Horodecki, R. Horodecki, J. Oppenheim, A. Sen(De), and U. Sen. Local information as a resource in distributed quantum systems. *Phys. Rev. Lett.*, 90:100402, Mar 2003.

[9] M. Horodecki, P. Horodecki, and R. Horodecki. Mixed-state entanglement and distillation: is there a "bound" entanglement in nature? *Phys. Rev. Lett.*, 80(24):5239–5242, Jun 1998.

[10] M. Horodecki, P. Horodecki, R. Horodecki, J. Oppenheim, A. Sen(De), U. Sen, and B. Synak-Radtke. Local versus nonlocal information in quantum-information theory: Formalism and phenomena. *Phys. Rev. A*, 71(6):062307, 2005.

[11] R. Horodecki, P. Horodecki, M. Horodecki, and K. Horodecki. Quantum entanglement. *Rev. Mod. Phys.*, 81(2):865, 2009.

[12] S. F. Huelga and M. B. Plenio. Vibrations, quanta and biology. *Contemp. Phys.*, 54(4):181–207, 2013.

[13] K. Korzekwa, M. Lostaglio, J. Oppenheim, and D. Jennings. 2015.

[14] N. Lambert, Y.-N. Chen, Y.-C. Cheng, C.-M. Li, G.-Y. Chen, and F. Nori. Quantum biology. *Nature Physics*, 9:10, 2013.

[15] F. Levi and F. Mintert. A quantitative theory of coherent delocalization. *New J. Phys.*, 16(3):033007, 2014.

[16] C.-M. Li, N. Lambert, Y.-N. Chen, G.-Y. Chen, and F. Nori. Witnessing quantum coherence: from solid-state to biological systems. *Sci. Rep.*, 2(885), 2012.

[17] S. Lloyd. Quantum coherence in biological systems. *J. Phys.: Conf. Series*, 302(1):012037, 2011.

[18] M. Lostaglio, D. Jennings, and T. Rudolph. Description of quantum coherence in thermodynamic processes requires constraints beyond free energy. *Nature Communications*, 6:6383, 2015.

[19] I. Marvian and R. W. Spekkens, 2016. arXiv:1602.08049.

[20] I. Marvian, R. W. Spekkens, and P. Zanardil, 2015. arXiv:1510.06474.

[21] V. Narasimhachar and G. Gour. Low-temperature thermodynamics with quantum coherence. *Nature Communications*, 6:7689, 2015.

[22] J. Oppenheim, K. Horodecki, M. Horodecki, P. Horodecki, and R. Horodecki. Mutually exclusive aspects of information carried by physical systems: Complementarity between local and nonlocal information. *Phys. Rev. A*, 68:022307, Aug 2003.

[23] J. Oppenheim, M. Horodecki, P. Horodecki, and R. Horodecki. Thermodynamical Approach to Quantifying Quantum Correlations. *Phys. Rev. Lett.*, 89:180402, 2002.

[24] M. B. Plenio and S. Virmani. An introduction to entanglement measures. *Quant. Inf. Comput.*, 7(1&2):1–51, Jan 2007.

[25] U. Singh, M. N. Bera, A. Misra, and A. K. Pati. 2015.

[26] A. Streltsov, 2015. arXiv:1511.08346.

[27] G. Vidal. Entanglement monotones. *J. Mod. Opt.*, 47:355, 2000.

[28] A. Winter. Secret, public and quantum correlation cost of triples of random variables. In *Information Theory, 2005. ISIT 2005. Proceedings. International Symposium on*, pages 2270–2274, Sept 2005.

[29] A. Winter and D. Yang. Operational resource theory of coherence. *Phys. Rev. Lett.*, 116:120404, Mar 2016.

[30] B. Yadin, J. Ma, D. Girolami, M. Gu, and V. Vedral, 2015.

[31] X. Yuan, H. Zhou, Z. Cao, and X. Ma. Intrinsic randomness as a measure of quantum coherence. *Phys. Rev. A*, 92:022124, Aug 2015.

# An infinite dimensional Birkhoff's Theorem and LOCC-convertibility

Daiki Asakura[1] *

[1] *Graduate School of Information Systems, The University of Electro-Communications*

**Abstract.** Nielsen developed that the condition for the LOCC-convertibility of two pure states of a bipartite system in finite dimensional systems is given by a majorization relation of Schmidt cofficients of them. The key of the proof of this is Birkhoff's theorem in matrix theory. In this study, we establish an infinite dimensional version of Birkhoff's theorem and apply them to prove that the condition for LOCC convertibility holds in infinite dimensional systems as in the similar form in finite dimensional.

**Keywords:** LOCC-convertibility, Birkhoff's theorem, majorization

## 1 Introduction

Extensive efforts have been devoted to understand local operations and classical communications (LOCC), since LOCC protocols have many applications in quantum information theory. Among them, the convertibility under LOCC is one of the important topics in quantum information theory. Nielsen [1] developed the condition for the LOCC-convertibility of two pure states of a bipartite system in finite dimensional systems.

For pure states $|\psi\rangle\langle\psi|$ and $|\phi\rangle\langle\phi|$ of a bipartite system, we say that $|\psi\rangle\langle\psi|$ is majorized by $|\phi\rangle\langle\phi|$, if the Schmidt coefficients of $|\psi\rangle$ is majorized by those of $|\phi\rangle$. For state vectors $|\psi\rangle$ and $|\phi\rangle$, we say that $|\psi\rangle$ is majorized by $|\phi\rangle$, if the Schmidt coefficents of $|\psi\rangle$ is majorized by those of $|\phi\rangle$. Nielsen [1, 2] proved that

one can convert $|\psi\rangle$ to $|\phi\rangle$ by LOCC

$\iff$ $|\psi\rangle$ is majorized by $|\phi\rangle$.

Subsequently, Owari *et al.* [3] proved that the necessary condition for LOCC convertibility holds in infinite dimensional systems as in the same form in finite dimensional. Moreover, Owari *et al.* [3] introduced a notion of $\epsilon$-convertibility by LOCC in infinite dimensional systems and proved that $\epsilon$-convertibility for LOCC gives a characterization of the sufficient condition.

However, it has been open whether the sufficient condition also holds in infinite dimensional systems as in the same form.

In [2, Section12.5], the key tool and the essence of the Nielsen's proof of the sufficient condition for LOCC convertibility in finite dimensional systems is Birkhoff's theorem in matrix theory.

According to Birkhoff's theorem [4] [5, Section II.2],

(i) the extreme points of the convex set of doubly stochastic matrices are permutation matrices.

(ii) any doubly stochastic matrix can be represented as a convex combination of permutation matrices,

(iii) the set of doubly stochastic matrices coincides with the closed convex hull of the set of permutation matrices.

Moreover, (i), (ii), (iii) imply each other by Caratheodory Theorem.

Nielsen used Birkhoff's theorem (ii) in [2, Section12.5].

An infinite dimensional analogue of Birkhoff's theorem is known as Birkhoff's problem111, which was considered in [6, 7, 8, 9, 10, 11, 12] etc. Nevertheless, there is no study treated (ii). Unlike the finite dimensional case, (i), (ii) and (iii) are not always equivalent to each other in infinite dimensional case. Moreover in infinite dimensional cases (i) remained true, whereas the validity of (ii) and (iii) depend on the choice of topology. While in finite dimensional case (ii) is equivalent to (iii) by virtue of Caratheodory Theorem, in infinite dimensional case the assertion of (ii) can be stronger than the one of (iii).

In this study, we establish an infinite dimensional version of Birkhoff's theorem (i)(ii)(iii) with the weakly operator topology (WOT). In particular, we show that an infinite dimensional analogue of (ii) holds in WOT, and we apply this to prove a new characterization for LOCC-convertibility in infinite dimensional. Our characterization, of course, is a certain generalization of Nielsen's result. Moreover, our characterization implies the results of Owari *et al.* [3] as a corollary.

## 2 Main results

Let $\mathcal{H}$ be separable (at most countable infinite dimensional) Hilbert space. For a fixed CONS $(|i\rangle)_{i=1}^{\infty}$, let $\mathcal{P}(\mathcal{H})$, $\mathcal{D}(\mathcal{H})$ be the sets of bounded operators $\sum_{i,j=1}^{\infty} a_{ij}|i\rangle\langle j|$ satisfying the following $(P)$, $(D)$:

$$(P)\ a_{ij} = 0 \,\text{or}\, 1, \sum_{j=1}^{\infty} a_{ij} = 1, \sum_{i=1}^{\infty} a_{ij} = 1 \text{ (for any } i, j)$$

$$(D)\ a_{ij} \in [0,1], \sum_{j=1}^{\infty} a_{ij} = 1, \sum_{i=1}^{\infty} a_{ij} = 1 \text{ (for any } i, j).$$

Then, we can rewrite Birkhoff's theorem(ii) as following:

**Theorem1(Birkhoff [4])** When $\mathcal{H} = \mathbb{C}^d$ and $(|i\rangle)$ is the standard basis in $\mathbb{C}^d$, denoting $\mathcal{P}(\mathcal{H}) =: \{P_n\}_{n=1}^{d!}$, for any $D \in \mathcal{D}(\mathcal{H})$, there exists a probability mass $\{p_n\}_{n=1}^{d!}$ such that

$$D = \sum_{n=1}^{d!} p_n P_n.$$

In this study, we get the following result:

* asakura0d@gmail.com

**Theorem2(Asakura)** For any $D \in \mathcal{D}(\mathcal{H})$, there exists a probability measure $\mu_D$ on $\mathcal{P}(\mathcal{H})$ such that

$$D = \int_{\mathcal{P}(\mathcal{H})} X d\mu_D(X),$$

where the integral converges in WOT.

## 3 Main result(2) : LOCC-convertibility

Nielsen's theorem [1] [2, Section12.5] can be written mathematically as following:

**Theorem3(Nielsen[1, 2])** Let $\mathcal{H}$ and $\mathcal{K}$ be finite dimensional Hilbert spaces, and let $\psi$, $\phi \in \mathcal{H} \otimes \mathcal{K}$ be unit vectors. Then, the followings are equivalent.

- There exist a POVM $\{M_i\}_i$ on $\mathcal{H}$ and a set of unitary operators $\{U_i\}_i$ $\mathcal{K}$ such that
$$|\phi\rangle\langle\phi| = \sum_i (M_i \otimes U_i)|\psi\rangle\langle\psi|(M_i^* \otimes U_i^*), \quad (1)$$
where the sum is finite sum.
- $\mathrm{Tr}_\mathcal{K} |\psi\rangle\langle\psi| \prec \mathrm{Tr}_\mathcal{K} |\phi\rangle\langle\phi|$ holds.

In this study, applying Theorem 2, we prove the following infinite dimensional analogue of Theorem 3. The following theorem is main results.

**Theorem4(Asakura)** Let $\mathcal{H}$ and $\mathcal{K}$ be infinite dimensional Hilbert spaces, and let $\psi$, $\phi \in \mathcal{H} \otimes \mathcal{K}$ be full rank unit vectors. Then, the followings are equivalent.

- There exist a Borel set $I$ of a certain of metric space, a probability mesure $\mu$ on $I$, a set of densely defined (not necessarily bounded) operators $\{M_i\}_{i\in I}$ on $\mathcal{H}$, a dense subspace $\mathcal{H}_0 \subset \mathcal{H}$ and a set of unitary operators $\{U_i\}_{i\in I}$ on $\mathcal{K}$ such that
$$|\psi\rangle \in \mathrm{D}(M_i \otimes U_i),\ i \in I, \quad (2)$$
$$(\mathrm{Tr}_\mathcal{K}|\psi\rangle\langle\psi|)\mathcal{H}_0 \subset \mathcal{H}_0, \quad (3)$$
$$\mathrm{D}(M_i) \supset \mathcal{H}_0,\ i \in I \quad (4)$$
$$\int_I \langle\eta|M_i{}^* M_i|\xi\rangle d\mu(i) = \langle\eta|\xi\rangle, \text{ for } \eta, \xi \in \mathcal{H}_0, \quad (5)$$
$$I \ni i \mapsto (M_i \otimes U_i)|\psi\rangle\langle\psi|(M_i^* \otimes U_i^*) \in \mathfrak{C}_1(\mathcal{H}) \text{ is integrable,} \quad (6)$$
$$|\phi\rangle\langle\phi| = \int_I (M_i \otimes U_i)|\psi\rangle\langle\psi|(M_i^* \otimes U_i^*) d\mu(i),$$
where the integral convergesges in $\mathfrak{C}_1(H)$. (7)
- $\mathrm{Tr}_\mathcal{K} |\psi\rangle\langle\psi| \prec \mathrm{Tr}_\mathcal{K} |\phi\rangle\langle\phi|$ holds.

In general case, Theorem 4 becomes the following theorem, which immediately follows from Theorem 4.

**Theorem6(Asakura)** Let $\mathcal{H}$ and $\mathcal{K}$ be infinite dimensional Hilbert spaces, and let $\psi$, $\phi \in \mathcal{H} \otimes \mathcal{K}$ be unit vectors.

- There exist $(I,\ \mu,\ \{M_i\}_{i\in I},\ \mathcal{H}_0,\ \{U_i\}_{i\in I})$ in Theorem 4 and infinite rank partial isometries $V_\mathcal{H}$, $V_\mathcal{K}$ such that
$$|\phi\rangle\langle\phi| = (V_\mathcal{H} \otimes V_\mathcal{K})\Big(\int_I (M_i \otimes U_i)|\psi\rangle\langle\psi| (M_i^* \otimes U_i^*) d\mu(i)\Big)(V_\mathcal{H}{}^* \otimes V_\mathcal{K}{}^*) \quad (8)$$
- $\mathrm{Tr}_\mathcal{K} |\psi\rangle\langle\psi| \prec \mathrm{Tr}_\mathcal{K} |\phi\rangle\langle\phi|$ holds.

Moreover, by Theorem 6, we can construct a sequence of LOCC-quantum channel $\{\Lambda_n\}_n$ such that $\Lambda_n(|\psi\rangle\langle\psi|)$ converges (8) in the trace norm. Namely, we reprove the following result as a corollary of Theorem 6:

**Theorem7(Owari*et al.* [3])**

Let $\mathcal{H}$ and $\mathcal{K}$ be infinite dimensional Hilbert spaces, and let $\psi$, $\phi \in \mathcal{H} \otimes \mathcal{K}$ be unit vectors. If $\mathrm{Tr}_\mathcal{K} |\psi\rangle\langle\psi| \prec \mathrm{Tr}_\mathcal{K} |\phi\rangle\langle\phi|$ holds, then, for any $\epsilon > 0$, there exists a LOCC quantum channel $\Lambda_\epsilon$ such that

$$\|\Lambda_\epsilon(|\psi\rangle\langle\psi|) - |\phi\rangle\langle\phi|\|_1 < \epsilon.$$

## References

[1] M.A.Nielsen, "Condition for a class of entanglement transformations", Physical Review Letters, Vol.83, Issue2 :436-439(1999)

[2] M.A.Nielesen, I.L.Chuang, *Quantum Computation and Quantum Information*, Cambridge University Press, Cambridge, 2000.

[3] M. Owari, S. L. Braunstein, K. Nemoto, M. Murao, " ε -convertibility of entangled states and extension of Schmidt rank in infinite dimensional systems", Quantum Information and Computation, Vol.8 :30-52(2008)

[4] G. Birkhoff. "Three observations on linear algebra".(Spanish) Univ. Nac. Tucuman. Revista A. 5 :147-151(1946)

[5] R. Bhatia, *Matrix Analysis*, Springer, New York, 1997.

[6] G. Birkhoff. *Lattice Theory*, revised ed., Amer. Math. Soc. Colloquium Pub., vol 25, 1948

[7] G. Birkhoff. *Lattice Theory*, third ed., Amer. Math. Soc. Colloquium Pub., vol 25, 1967

[8] Y. Safarov, "Birkoff's theorem and multidimensional spectra", Journal of Functional Analysis 222 :61-97(2005)

[9] J.R,Isbell, "Infinite Doubly Stochastic Matrices", Canada. Math .Bull. Vol.5, no.1 :1-4(1961)

[10] D.G.Kendall, "On Infinite Doubly Stochastic Matrices and Birkoff's problem". J. London Math. Soc.35 :81-84(1960)

[11] B. A. Rattray, J. E. L. Peck, "Infinite stochastic matrices", Trans. Roy. Soc. Canada. Sect. III. (3) 49 :55-57(1955)

[12] R. Grzaślewicz. "On extreme infinite doubly stochastic matrices". Illinois Journal of Mathematics 31, no. 4 :529-543(1987)

# How local is the information in MPS/PEPS tensor networks? (extended abstract)

Anurag Anshu[1] * Itai Arad[1] † Aditya Jain[2] ‡

[1] *Centre for Quantum Technologies, National University of Singapore, Singapore*
[2] *Center for Computational Natural Sciences and Bioinformatics, International Institute of Information Technology-Hyderabad, India*

**Abstract.** We introduce a new approach for approximating the expectation value of a local observable in ground states of local Hamiltonians that are represented as PEPS tensor-networks. Instead of contracting the full tensor-network, we estimate the expectation value using only a local patch of the tensor-network around the observable. Surprisingly, we demonstrate that this is often easier to do when the system is frustrated. We test our approach in 1D systems, where we show how the expectation value can be calculated up to at least 3 or 4 digits of precision, even when the patch radius is smaller than the correlation length.

**Keywords:** Local Hamiltonians, Ground states, Tensor networks, MPS, PEPS, SDP

## 1 Introduction

Variational tensor-network methods [1] provide a promising way for understanding the low-temperature physics of many-body condensed matter systems. In particular, they seem suitable for studying the ground states of highly frustrated systems, where the sign problem hinders many of the quantum Monte Carlo approaches. The best-known and by far the most successful tensor-network method is the Density Matrix Renormalization Group (DMRG) algorithm [2, 3]. It can be viewed as a variational algorithm for minimizing the energy of the system over the manifold of *Matrix Product States* (MPS) [4, 5], which are special types of tensor-network states a with linear 1D structure. In 2D and beyond the most natural generalization of MPS are the so-called *Projected Entangled Pairs States* (PEPS) tensor-network states [6, 7, 8, 9, 10]. PEPS have proven useful for understanding the physics of 2D lattice systems and in particular their entanglement structure. However, as a numerical method for studying 2D quantum systems, they still face substantial challenges which limit their applicability. In most cases, the best results are still obtained either by DMRG, in which a 1D MPS wraps around the 2D surface, or by quantum Monte Carlo methods.

There are several reasons for this qualitative difference between 1D and 2D systems. The most important one is the computational cost of *contracting* the 2D tensor network. While in 1D this cost scales linearly in the system size, it is exponential for 2D and above. Formally, contracting a PEPS is #P-hard [11], which is at least NP-hard. To overcome this exponential barrier, many approximation schemes have been devised [9, 10, 12, 13, 14, 15, 16, 17, 18, 19, 20]. However, while being physically motivated, none of them is rigorous, and to some extent they all produce uncontrolled approximations, even when dealing with the ground state itself. Moreover, while their computational cost is linear in PEPS size, it scales badly in the so-called 'bond-dimension' of the tensor-network, which limits their practical use to small systems/resolutions.

In this work we introduce a new approach for approximating the expectation value of a local observable in a 2D PEPS tensor-network. Our starting point is a simple observation that while the contraction of a general 2D PEPS is #P-hard, this is not necessarily the case if the PEPS describes a ground state of a gapped local Hamiltonian. Gapped ground states exhibit strong properties of locality, such as exponential decay of correlations [21] and are therefore subject to many constraints to which arbitrary PEPS are not. This enables us to use only a *local patch* of the PEPS tensor-network around the local observable to approximate its expectation value, which therefore leads to an efficient algorithm.

We identify two novel methods that provide *rigorous* upper- and lower- bounds on the expectation value. While we usually cannot give rigorous bound on the distance between these bounds, we demonstrate numerically that this distance – and hence the error in our approximation – can be surprisingly small.

The first method, which we call the 'basic method', is expected to give good results in the case of frustration-free gapped systems. The second one, which we call the 'commutator gauge optimization' (CGO) method, works only for frustrated systems by utilizing the many inter-constraints that the solutions of these systems have to satisfy. We show that it can be essentially reduced to a SDP program, which can be efficiently solved. In addition, it does not rely directly on the existence of a gap, and may work even when considering patches of the PEPS that are much smaller than the correlation length.

To test the validity of the two methods, we performed some numerical tests on 1D systems whose ground states are described by MPS. The main purpose of these tests was *not* to suggest a *practical* numerical method for estimating $\langle B\rangle$, but to demonstrate that a surprisingly large amount of information is found locally in a tensor network that represents a ground state, in particular if the system is frustrated – which is counter-intuitive.

*`henrikabel.27@gmail.com`
†`arad.itai@fastmail.com`
‡`aditya.jain@research.iiit.ac.in`

Our numerical experiments demonstrate that in the frustrated case, one can easily obtain 3-4 digits of $\langle B \rangle$ by accessing only a ball of radius $\ell \sim 3, 4$ around $B$ — smaller than the correlation lengths of these models! Moreover, as we indicated above, this is better than the frustration-free case, where we could only recover 1-2 digits of $\langle B \rangle$. The full details of these numerical experiments can be found in the arXiv version of this paper at http://arxiv.org/abs/1603.06049.

While a *direct* implementation of the above methods for 2D systems is *not* numerically practical for 2D, we are confident that the observations underlying these algorithms can be turned into practical heuristics for the 2D problem.

## References

[1] R. Orús, "A practical introduction to tensor networks: Matrix product states and projected entangled pair states," *Annals of Physics*, vol. 349, pp. 117 – 158, 2014.

[2] S. R. White, "Density matrix formulation for quantum renormalization groups," *Phys. Rev. Lett.*, vol. 69, pp. 2863–2866, Nov 1992.

[3] S. R. White, "Density-matrix algorithms for quantum renormalization groups," *Phys. Rev. B*, vol. 48, pp. 10345–10356, Oct 1993.

[4] S. Östlund and S. Rommer, "Thermodynamic limit of density matrix renormalization," *Physical review letters*, vol. 75, no. 19, p. 3537, 1995.

[5] S. Rommer and S. Östlund, "Class of ansatz wave functions for one-dimensional spin systems and their relation to the density matrix renormalization group," *Physical Review B*, vol. 55, no. 4, p. 2164, 1997.

[6] G. Sierra and M. A. Martin-Delgado, "The Density Matrix Renormalization Group, Quantum Groups and Conformal Field Theory," *arXiv preprint cond-mat/9811170*, 1998.

[7] Y. Hieida, K. Okunishi, and Y. Akutsu, "Numerical renormalization approach to two-dimensional quantum antiferromagnets with valence-bond-solid type ground state," *New Journal of Physics*, vol. 1, no. 1, p. 7, 1999.

[8] T. Nishino, Y. Hieida, K. Okunishi, N. Maeshima, Y. Akutsu, and A. Gendiar, "Two-Dimensional Tensor Product Variational Formulation," *Progress of Theoretical Physics*, vol. 105, no. 3, pp. 409–417, 2001.

[9] F. Verstraete and J. I. Cirac, "Renormalization algorithms for Quantum-Many Body Systems in two and higher dimensions," *eprint arXiv:cond-mat/0407066*, July 2004.

[10] F. Verstraete, V. Murg, and J. I. Cirac, "Matrix product states, projected entangled pair states, and variational renormalization group methods for quantum spin systems," *Advances in Physics*, vol. 57, no. 2, pp. 143–224, 2008.

[11] N. Schuch, M. M. Wolf, F. Verstraete, and J. I. Cirac, "Computational complexity of projected entangled pair states," *Phys. Rev. Lett.*, vol. 98, p. 140506, Apr 2007.

[12] T. Nishino and K. Okunishi, "Corner transfer matrix renormalization group method," *Journal of the Physical Society of Japan*, vol. 65, no. 4, pp. 891–894, 1996.

[13] R. Orús and G. Vidal, "Simulation of two-dimensional quantum systems on an infinite lattice revisited: Corner transfer matrix for tensor contraction," *Phys. Rev. B*, vol. 80, p. 094403, Sep 2009.

[14] R. Orús, "Exploring corner transfer matrices and corner tensors for the classical simulation of quantum lattice systems," *Phys. Rev. B*, vol. 85, p. 205117, May 2012.

[15] L. Vanderstraeten, M. Mariën, F. Verstraete, and J. Haegeman, "Excitations and the tangent space of projected entangled-pair states," *Phys. Rev. B*, vol. 92, p. 201111, Nov 2015.

[16] M. Levin and C. P. Nave, "Tensor renormalization group approach to two-dimensional classical lattice models," *Phys. Rev. Lett.*, vol. 99, p. 120601, Sep 2007.

[17] Z. Y. Xie, H. C. Jiang, Q. N. Chen, Z. Y. Weng, and T. Xiang, "Second renormalization of tensor-network states," *Phys. Rev. Lett.*, vol. 103, p. 160601, Oct 2009.

[18] H. H. Zhao, Z. Y. Xie, Q. N. Chen, Z. C. Wei, J. W. Cai, and T. Xiang, "Renormalization of tensor-network states," *Phys. Rev. B*, vol. 81, p. 174411, May 2010.

[19] Z. Y. Xie, J. Chen, M. P. Qin, J. W. Zhu, L. P. Yang, and T. Xiang, "Coarse-graining renormalization by higher-order singular value decomposition," *Phys. Rev. B*, vol. 86, p. 045139, Jul 2012.

[20] I. Pižorn, L. Wang, and F. Verstraete, "Time evolution of projected entangled pair states in the single-layer picture," *Phys. Rev. A*, vol. 83, p. 052321, May 2011.

[21] M. B. Hastings, "Lieb-Schultz-Mattis in higher dimensions," *Phys. Rev. B*, vol. 69, p. 104431, Mar 2004.

# Information-theoretical analysis of topological entanglement entropy and multipartite correlations

Kohtaro Kato[1] * Fabian Furrer[1 2] † Mio Murao[1 3] ‡

[1] *Department of Physics, Graduate School of Science, The University of Tokyo, Tokyo, Japan*
[2] *NTT Basic Research Laboratories, NTT Corporation, 3-1 Morinosato Wakamiya, Kanagawa, Japan*
[3] *Institute for Nano Quantum Information Electronics, The University of Tokyo, Tokyo, Japan*

**Abstract.** A special feature of the ground state in a topologically ordered phase is the existence of large-scale correlations depending only on the topology of the regions. These correlations can be detected by the topological entanglement entropy or by a measure called irreducible correlation. We show that these two measures coincide for states obeying an area law and having zero-correlation length. Moreover, we provide an operational meaning for these measures by proving its equivalence to the optimal rate of a particular class of secret sharing protocols. This establishes an information-theoretical approach to multipartite correlations in topologically ordered systems.

**Keywords:** topological order, multipartite correlations, conditional mutual information, maximum entropy method, secret sharing

## 1 Introduction

Topologically ordered phase is an exotic quantum phase that cannot be explained by conventional models based on *local* order parameters and symmetry-breaking. One way to classify the ground states with topological orders is by identifying characteristic large-scale global multipartite correlations (topological correlations). A possible measure to detect such topological correlations is the topological entanglement entropy (TEE) [1, 2], which also appears as the universal constant term in the area law [1]. The definition of the TEE is based on the idea that topological correlations reduce the entropy of ring-like regions compared to what is expected by considering the entropy of just local regions [2]. More precisely, the TEE quantifies the entropy reduction by subtracting the contributions of local correlations using a Venn-diagram calculation. Such a quantity of multipartite correlations is known in classical information theory [3]. However, the information-theoretical meaning of the function in both classical and quantum settings is not clear, since it lacks basic properties such as, e.g., positivity and it is always zero for any pure state in quantum settings.

The *irreducible correlation* [4] is an alternative measure of topological correlations which employs the maximum entropy method to quantify the genuinely tripartite correlations. The irreducible correlation is always non-negative, and it has a clear geometrical interpretation as the quantum analog of a correlation measure called the $k$th-order effect [5] in classical information-geometry. It has been conjectured that the 3rd-order irreducible correlation and the TEE coincide in the thermodynamic limit for gapped ground states [6].

Here, we partly resolve this conjecture and show that when the ground state obeys an area law and has zero-correlation length, the TEE and the 3rd-order irreducible correlation are equivalent. This sufficient condition holds for a wide class of exactly solvable spin models which describe non-chiral topological ordered phases. To show the equivalence, we calculate the 3rd-order irreducible correlation by explicitly constructing the maximum entropy state on region $ABC$ that is consistent with all reduced density matrices (RDMs) of the ground state on $AB$, $BC$ and $AC$. In general, calculating the maximum entropy state is a computationally hard problem. We overcome this challenge by employing the properties of *quantum Markov states* which saturate the strong subsdditivity [7].

We further show that under the same assumptions the irreducible correlation is equal to the optimal asymptotic rate of a secret sharing protocol as suggested in [4]. This leads to an operational interpretation of the TEE as the number of bits that can be hidden in global regions from any party that only has access to local regions.

## 2 Summary of results

Let us consider the RDMs of the ground state of a gapped spin lattice system on circle or ring-like regions $ABC$ given in Fig. 1. We then define the TEE by

$$S_{\text{topo}} \equiv S_\rho(AB) + S_\rho(BC) + S_\rho(CA) - S_\rho(A) - S_\rho(B) - S_\rho(C) - S_\rho(ABC)\,, \quad (1)$$

which is in accordance with the one considered by Kitaev and Preskill [1]. Here, $S_\rho(A)$ represents the von Neumann entropy of the RDM $\rho_A$ of region $A$. For regions as given in Fig. 1$(c)$ , the above definition is consistent

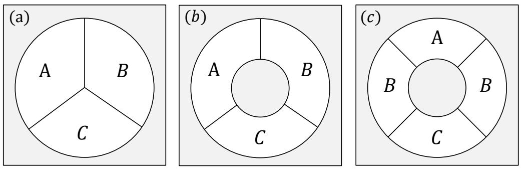

Figure 1: Examples of the region $ABC$ for the calculation of TEE. The value of TEE of $(a)$ is a half of others for a topologically ordered ground state due to the difference of the topology of the whole region $ABC$.

[*] kato@eve.phys.s.u-tokyo.ac.jp
[†] furrer@eve.phys.s.u-tokyo.ac.jp
[‡] murao@phys.s.u-tokyo.ac.jp

with the one by Levin and Wen [2] if it is possible to assume that there is no correlation between $A$ and $C$, i.e., $\rho_{AC} = \rho_A \otimes \rho_C$. The TEE is interpreted as the difference between the entropy of $ABC$ and the expected entropy of $ABC$ by considering the entropy of just local regions [2].

Let us consider the closed convex set $R^2_\rho$ of states which is consistent with all bipartite RDMs of $\rho_{ABC}$

$$R^2_\rho \equiv \{\sigma_{ABC} \mid \sigma_{AB} = \rho_{AB}, \sigma_{BC} = \rho_{BC}, \sigma_{AC} = \rho_{AC}\} \, . \tag{2}$$

We define the maximum entropy state by the state in $R^2_\rho$ which maximizes the von Neumann entropy, i.e.,

$$\tilde{\rho}^{(2)}_{ABC} \equiv \underset{\sigma_{ABC} \in R^2_\rho}{\arg\max} \, S_\sigma(ABC) \, . \tag{3}$$

According to the maximum entropy principle, the maximum entropy state is the most "unbiased" inference of $\rho_{ABC}$ if all of the bipartite marginals are known.

We define the 3rd-order irreducible correlation $C^{(3)}(\rho_{ABC})$ as [4]

$$C^{(3)}(\rho_{ABC}) \equiv S_{\tilde{\rho}^{(2)}}(ABC) - S_\rho(ABC) \, . \tag{4}$$

Note that the irreducible correlation has a clear information-geometric meaning as the distance from the closure of the set of all Gibbs states of 2-local Hamiltonians [8].

Our main result is that if the ground state satisfy the two properties in the following, the TEE is equivalent to the 3rd-order irreducible correlation.

(I) If two regions $A$ and $B$ are separated, $I_\rho(A:B) \equiv S_\rho(A) + S_\rho(B) - S_\rho(AB) = 0$.

(II) If region $A$ and $C$ are indirectly connected through $B$ and $ABC$ has no holes, $\rho_{ABC}$ has zero conditional mutual infromation $I_\rho(A:C|B) \equiv I_\rho(A:BC) - I_\rho(A:B) = 0$.

**Theorem 2.1** *If a ground state on a 2D spin lattice satisfies properties $(I)$ and $(II)$, the equality*

$$S_{\rm topo} = C^{(3)}(\rho_{ABC}) \tag{5}$$

*holds for all choices of regions depicted in Fig. 1.*

It is widely accepted that a ground state in a gapped system obeys an area law of entanglement entropy for any connected region $A$ with smooth boundaries, that is,

$$S_\rho(A) = \alpha|\partial A| - \gamma + \mathcal{O}(|\partial A|^{-1}) \, , \tag{6}$$

where $\alpha$ denotes a non-universal constant, $|\partial A|$ denotes the size of the boundary of region $A$. $\gamma$ is another definition of the TEE and is equivalent to $S_{\rm topo}$ for the configuration in Fig. 1(a). In models with zero-correlation length, $\mathcal{O}(|\partial A|^{-1})$ can be negligible and the ground state satisfy both properties $(I)$ and $(II)$.

The key idea of the proof is to divide each region shown in Fig.1 so that each RDM is a quantum Markov state (QMS). A QMS conditioned on $B$ is a tripartite state that satisfies property $(II)$, i.e., $I_\rho(A:C|B) = 0$ [7]. We develop a technique of merging overlapping marginal QMS to construct the maximum entropy state $\tilde{\rho}^{(2)}_{ABC}$ by using the equivalence condition revealed in Ref. [7].

The equivalence of the TEE to the 3rd-order irreducible correlation also provides an operational interpretation of the TEE. Recall that if $C^{(3)}(\rho_{ABC})$ is nonzero, the global state in region $ABC$ contains information that cannot be determined only from the marginals on $AB$, $BC$ or $AC$. A similar situation is encountered in secret sharing protocols. It has been shown [4, 9] that for stabilizer states, the $k$th-order irreducible correlation of a $n$-partite state represents the difference between the asymptotic bit rate that can be hidden from $k$ and from $k-1$ parties, where secrets are encoded by global unitaries which preserves all $k$ ( or $k-1$) RDMs. We show that this also holds true in our setting for $n=3$ and $k=2$.

**Theorem 2.2** *For a tripartite state $\rho_{ABC}$ satisfying properties (I) and (II), the equality*

$$r(\rho_{ABC}) = C^{(3)}(\rho_{ABC}) \tag{7}$$

*holds for all choices of regions depicted in Fig. 1, where $r(\rho_{ABC})$ is the optimal secret sharing rate.*

Thus, we provide new geometrical and operational meanings of the TEE. Our results motivate us to investigate the relationships between characteristic properties of topological orders by utilizing these information-theoretical meanings.

## Acknowledgment

This work is supported by ALPS, the Project for Developing Innovation Systems of MEXT, Japan, and JSPS KAKENHI (Grant No. 26330006, No.24-02793 and No.15H01677). We also gratefully acknowledge the ELC project (Grant-in-Aid for Scientific Research on Innovative Areas MEXT KAKENHI (Grant No. 24106009)).

## References

[1] A. Kitaev and J. Preskill. *Phys. Rev. Lett.*, 96:110404, 2006.

[2] M. A. Levin and X.-G. Wen. *Phys. Rev. Lett.*, 96:110405, 2006.

[3] W. J. McGill. *Psychometrika*, 19(2):97–116, 1954.

[4] D. L. Zhou. *Phys. Rev. Lett.*, 101:180505, Oct 2008.

[5] S.-I. Amari. *IEEE Trans. Inf. Theory*, 47(5):1701–1711, Jul 2001.

[6] J. Chen, et al. *New Journal of Physics*, 17(8):083019, 2015.

[7] P. Hayden, et al. *Comm. Math. Phys.*, 246(2):359–374, 2004.

[8] S. Weis. *AIP Conference Proceedings*, 1641, 2015.

[9] D. L. Zhou and L. You. *arXiv:quant-ph/0701029*, 2007.

# Phase-like transitions in low-number quantum dots Bayesian magnetometry

Paweł Mazurek[1] * Michał Horodecki[1] Łukasz Czekaj[1] Paweł Horodecki[2] [3]

[1] *Institute of Theoretical Physics and Astrophysics, National Quantum Information Centre, Faculty of Mathematics, Physics and Informatics, University of Gdańsk, Wita Stwosza 57, 80-308 Gdańsk, Poland*
[2] *Faculty of Applied Physics and Mathematics, Gdańsk University of Technology, Narutowicza 11/12, 80-233 Gdańsk, Poland*
[3] *National Quantum Information Centre in Gdańsk, Andersa 27, 81-824 Sopot, Poland*

**Abstract.** We investigate metrological properties of systems of quantum dot electron spin qubits. Optimal strategies for probing the value of an external, static magnetic field are provided within Bayesian approach, with initial knowledge about the magnetic field described by its a priori Gaussian probability distribution. We report phase-like transitions between optimal protocols occurring during the system evolution. We show that optimal scenario requires initial entanglement and point out benefits of classical strategies for longer evolution times. We observe that non-Markovian effects, stemming from the interaction with environment, can provide limited metrological advantage for small magnetic fields. The full version of the paper is available at arXiv:1605.04279.

**Keywords:** quantum metrology, quantum dots, noise

## 1 Introduction

Quantum metrology relies on the fact that quantum correlations make state evolution more sensitive to dynamics which depends on some parameter that is supposed to be revealed. It is known that, in the so called frequentist approach, for estimating small variations of a deterministic parameter, for locally unbiased estimators dependent on its value and $N$ systems undergoing independent evolution, quantum mechanics can offer a $1/N$ (so called Heisenberg scaling) improvement of the precision (defined by the deviation from the precise value) in the asymptotic limit. This should be compared to a scaling $1/\sqrt{N}$, available for classical resources, and referred to as quantum shot-noise limit. Generally it is known that in a situation when the parameter is a phase generated by some Hamiltonian evolution, then the local noise usually destroys the quantum effect (both in atomic spectroscopy and quantum optics), leading to at most constant improvement over classical scaling.

In the so-called Bayesian approach this scenario is altered so that the parameter to be estimated is a random variable with some a priori probability distribution. In many cases, this framework is more justified than the frequentist approach: it does not assume perfect knowledge about a system under consideration before an experiment and it outputs optimal estimators even for small $N$. We apply Bayesian metrology to a physical scenario where the form of the noise depends on the parameter. Specifically, we analyze a system of independent quantum dots interacting via hyperfine interaction with their local, maximally mixed spin environments [1], under a so called box model approximation. Spins of the electron dots are subject to external time independent magnetic field $B$ with the random value characterized by the Gaussian probability distribution with a variance $\Delta^2 B_{prior}$ and mean $B_0$. The Bayesian approach allows to diminish the average mean square error of magnetic field estimator. It relies on measurements that may depend on time.

Our aim was to find the optimal initial state and measurement scheme which results in the smallest relative mean square error $\frac{\Delta^2 B_{est}}{\Delta^2 B_{prior}}$ of the estimator – a signature of the gain of information about the field. It is achieved by numerical optimization [2] yielding optimal strategies for given time of the evolution and initial probability distribution. The system evolution was solved analytically within the ,,box model" of hyperfine interaction, applicable in time regime that encompasses small times, where metrologicalally important effects occur.

## 2 Main results

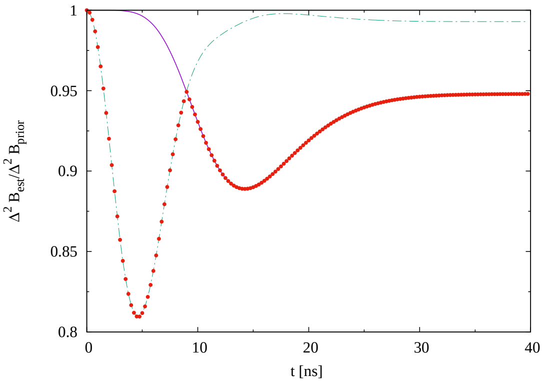

Figure 1: Comparison between 'perpendicular' (green dashed line) and 'parallel' (solid purple line) strategies for 1 quantum dot and prior Gaussian distribution with $B_0 = 7$ mT, $\Delta B_{prior} = 4$ mT. Red points represent the optimal strategy.

In order to sketch the action of noise on the evolution of the system, we start with a single qubit and com-

*pawel.mazurek@ug.edu.pl

pare two strategies, each optimal in different time regime (Fig. 1). The perpendicular strategy relies on preparing the state in Bloch sphere perpendicular to the field direction, and performing measurements of an observable represented by a Bloch sphere vector perpendicular to both field and state vectors. The parallel strategy relies on preparing the state in the direction of the magnetic field, and performing projective measurements along this direction. For large fields, the dynamics does not change populations of the system, hence the estimating of magnetic field can be done only through the phase, and perpendicular strategy is the optimal one, as in a case of a simple unitary evolution. The single minimum in the strategy comes from a trade-off between the damping of phase (resulting both from statistical averaging over prior field probability distribution and physical noise), and the rotation of the phase by magnetic field. For times long enough so that the coherences are nearly completely damped, the state ceases to depend on the magnetic field, hence there is no information gain. For intermediate magnetic fields, the populations of the system start to be effected by the magnetic field, and measurements of the occupation levels lead to information gain dominant in longer times. One should note that for small magnetic fields the ,,perpendicular" strategy proves to be effective even in the long time regime. This can be explained by the fact that, due to the memory effects stemming from the interaction with the environment, the coherences experience a revival to the value dependent on $B$ and remain unaffected by the phase factors of the type $\exp[ig\mu_B Bt]$, which for non-zero $\Delta^2 B_{prior}$ would lead to their decay. Clearly, apart from the mentioned minor memory effects, the long time regime is entirely classical, as the estimation there is purely statistical, while in the short time regime, quantum coherences are crucial. For this reason, for more particles in non-negligible magnetic field, only for low times entanglement will lead to enhancement of estimation.

Indeed, by performing similar studies for systems of $N = 2, \ldots, 5$ dots, as well as Monte Carlo simulations, we showed that entanglement is the necessary resource for achieving the global optimum. In description of these systems below, we use the notation in which magnetic field is directed along $z$ axis, and eigenstates of $z$-component of electron spin operator are given by $\hat{S}^z|0\rangle = \frac{\hbar}{2}|0\rangle$, $\hat{S}^z|1\rangle = -\frac{\hbar}{2}|1\rangle$, and $|+\rangle = \frac{1}{\sqrt{2}}(|0\rangle + |1\rangle)$. We denote GHZ(N)= $\frac{1}{\sqrt{2}}\left(|0\rangle^{\otimes N} + |1\rangle^{\otimes N}\right)$.

A feature characteristic for transition into larger systems is the growing structural complexity of the region that relies on product coherence states. We showed that the general sequence of optimal states for small number $N$ of quantum dots is the following: (1) regime of initially entangled states, with (1a) regime of GHZ(N) and (1b) regime of GHZ(N) superposed with $|+\rangle^{\otimes N}$; (2) intermediate regime of optimal product coherent states $|+\rangle^{\otimes N-1}|0\rangle$, followed by $|+\rangle^{\otimes N-2}|0\rangle|0\rangle$, end so on; (3) regime of product states without coherences $|0\rangle^{\otimes N}$.

Transitions within the region (1) are characterized by a continuous change of the optimal initial state, while transitions inside (2) region, as well transitions (1)-(2) and (2)-(3), signalize a non-continuous change of the optimal initial state. One should note that the precision of field estimation grows with increasing $N$ for all possible times of performing the measurements, with time of optimal information gain not strongly depending on $N$. We stress that for the regimes (2) and (3), in contrast with the entanglement regime (1), the effects associated with lack of initial knowledge described by a non-zero $\Delta^2 B_{prior}$ play a secondary role and the physical noise for longer times is solely beneficial for magnetometric purposes. Note that the whole regime is absent for a unitary evolution, which implies lack of discontinuous transitions in the optimal state space.

## 3 Discussion

The presented physical model enables the structure of the measurement strategy, involving measurement of occupation levels, to partially recover information that, due to noise, becomes inaccessible for phase-based measurements. Nevertheless, it does not enable to win over the noisless case, which for all investigated a priori Gaussian probability distributions achieve better information gains optimized over initial state, measurement strategy and time of performing the measurement.

The standard situation considered in the literature is when the parameter under consideration (here the magnetic field) is encoded into the system *directly* and the noise can only destroy that information. Here the dynamics makes the parameter imprinted both on the system and environment or - strictly speaking - into a global state of both. Despite the fact that the initial ancillas are maximally noisy and that the final noisy dynamics acts here completely locally, the corresponding noise is unavoidably ,,convoluted" with the original dynamics and the final result is such that we get the product noisy dynamics which has the parameter imprinted in a *nonstandard*, nonlinear way. On the other hand the imprinting the magnetic field by unitary dynamics is restricted to the Bloch sphere. Effectively we have then the two scenarios. In the latter the parameter is imprinted in the states on the sphere, while in the former, it is imprinted in the mixed states that in general belong to the interior of the sphere. It seems that this is *the geometry* of the two sets out of which only the one has the nonzero volume, that in general might make the difference in favor of the noisy scenario.

## References

[1] Mazurek, P., Roszak, K., Chhajlany, R. W. & Horodecki, P. Sensitivity of entanglement decay of quantum-dot spin qubits to the external magnetic field. *Phys. Rev. A* **89**, 062318 (2014).

[2] Macieszczak, K., Fraas, M. & Demkowicz-Dobrzański, R. Bayesian quantum frequency estimation in presence of collective dephasing. *New Journal of Physics* **16**, 113002 (2014)

# Separation between quantum Lovász number and entanglement-assisted zero-error classical capacity

Xin Wang[1] *　　Runyao Duan[1] [2] †

[1] *Centre for Quantum Computation and Intelligent Systems (QCIS),*
*Faculty of Engineering and Information Technology,*
*University of Technology Sydney (UTS), NSW 2007, Australia*
[2] *UTS-AMSS Joint Research Laboratory for Quantum Computation and Quantum Information Processing,*
*Academy of Mathematics and Systems Science,*
*Chinese Academy of Sciences, Beijing 100190, China*

**Abstract.** Before our work, it was unknown that whether the quantum Lovász number always coincides with the entanglement-assisted zero-error classical capacity of a quantum channel. In this paper, we resolve this open problem by explicitly constructing a class of qutrit-to-qutrit channels whose quantum Lovász number is strictly larger than its entanglement-assisted zero-error classical capacity. Interestingly, this class of channels is reversible in the presence of quantum no-signalling correlations.

**Keywords:** Zero-error classical capacity, Quantum Lovász number, Non-commutative graph

**Introduction** A fundamental problem of information theory is to determine the capability of a communication channel for delivering messages from the sender to the receiver. Shannon first investigated this problem in the zero-error setting and described the zero-error capacity of a channel as the maximum rate at which it can be used to transmit information with zero probability of confusion [1]. Recently the zero-error information theory has been studied in the quantum setting and many new phenomena were observed. One of the most remarkable results is that entanglement can be used to improve the zero-error capacity of a classical channel [2, 3]. Furthermore, there are more kinds of capacities when considering auxiliary resources, such as shared entanglement [2, 3, 4, 5] and no-signalling correlations [2, 6].

For the zero-error communication via quantum channels, the non-commutative graph associated with a quantum channel captures the zero-error communication properties of this channel [5], thus the non-commutative graph plays a similar role to confusability graph of a classical channel. It is well-known that the zero-error capacity is extremely difficult to compute for both classical and quantum channels. In Ref. [7], it was proved that computing the one-shot zero-error capacity of a quantum channel is QMA-complete and the calculation of the asymptotic zero-error capacity is even not known to be computable. Nevertheless, the zero-error capacities of classical channels and quantum channels are upper bounded by the the famous Lovász number of a confusability graph [8] and the quantum Lovász number [5] of a non-commutative graph, respectively. Furthermore, the entanglement-assisted zero-error capacity $C_{0E}$ of a classical channel is also upper-bounded by the Lovász number [5, 9], and this notable result can be generalized to quantum channels by using the quantum Lovász number [5].

One of the most important and intriguing open problems in zero-error information theory is whether there is a gap between the entanglement-assisted zero-error capacity and the quantum Lovász number of a classical or quantum channel, which is frequently mentioned in Refs. [3, 5, 9, 10, 11, 12]. If they are equal, it would imply that $C_{0E}$ is additive while the unassisted case is not [13].

In this paper, we show the answer to the open problem above is negative for quantum channels. We construct a class of qutrit-to-qutrit channels whose quantum Lovász number is strictly larger than its entanglement-assisted zero-error capacity. In particular, this class of channels is reversible under quantum no-signalling correlations (QNSC).

**Main results** The entanglement-assisted zero-error capacity $C_{0E}$ of a channel is the optimal rate at which it is possible to transmit information perfectly while the sender and receiver share free entanglement. Since $C_{0E}$ is not known to be computable, it is difficult to compare $C_{0E}$ to the quantum Lovász

*xin.wang-8@student.uts.edu.au
†runyao.duan@uts.edu.au

number. The problem whether there exists a gap between them remained open for almost six years. Our approach to answer this problem is based on the class of channels $\mathcal{N}_\alpha(\rho) = C_\alpha \rho C_\alpha^\dagger + D_\alpha \rho D_\alpha^\dagger$ $(0 < \alpha \leq \pi/4)$ with

$$C_\alpha = \sin\alpha|0\rangle\langle 1| + |1\rangle\langle 2|, D_\alpha = \cos\alpha|2\rangle\langle 1| + |1\rangle\langle 0|.$$

We first consider the QNSC assisted zero-error capacity [6], which is potentially larger than the entanglement-assisted case. We also use the QNSC assisted zero-error classical simulation cost $S_{0,NS}$ [6] during the proof, which is the minimum noiseless bits required to simulate a channel under QNSC. It holds that $C_{0E} \leq C_{0,NS} \leq S_{0,NS}$.

**Proposition 1** *For* $\mathcal{N}_\alpha$ $(0 < \alpha \leq \pi/4)$*,*

$$C_{0,NS}(\mathcal{N}_\alpha) = S_{0,NS}(\mathcal{N}_\alpha) = 2.$$

We then show the exact value of the quantum Lovász number of $\mathcal{N}_\alpha$.

**Proposition 2** *For* $\mathcal{N}_\alpha$ $(0 < \alpha \leq \pi/4)$*,*

$$\widetilde{\vartheta}(\mathcal{N}_\alpha) = 2 + \cos^2\alpha + \cos^{-2}\alpha > 4. \qquad (1)$$

Combining Propositions 1 and 2, we can conclude that there is a separation between quantum Lovász number and entanglement-assisted zero-error classical capacity. This is based on the fact that $C_{0E}$ is upper bounded by the QNSC assisted zero-error capacity $C_{0,NS}$. Our main result is presented as follows.

**Theorem 3** *For the class of quantum channels* $\mathcal{N}_\alpha$ $(0 < \alpha \leq \pi/4)$*,*

$$\log_2 \widetilde{\vartheta}(\mathcal{N}_\alpha) > C_{0,NS}(\mathcal{N}_\alpha) \geq C_{0E}(\mathcal{N}_\alpha). \qquad (2)$$

**Conclusions and discussions** In summary, we construct a class of quantum channels whose quantum Lovász number is strictly larger than its entanglement-assisted zero-error capacity. This resolves a well-known open problem in zero-error quantum information. There are still several unsolved problems left. For instance, it is of great interest to study the case of classical channel. For the confusability graph $G$, a variant of Lovász number called Schrijver number [14, 15] was proved to be an tighter upper bound for the entanglement-assisted independence number than Lovász number [16] . However, it remains unknown whether Schrijver number will converge to Lovász number in the asymptotic setting. A gap between the regularized Schrijver number and Lovász number would imply a separation between $C_{0E}(G)$ and $\vartheta(G)$.

We would like to thank Andreas Winter for helpful suggestions. This work was partly supported by the Australian Research Council (Grant No. DP120103776 and No. FT120100449).

## References

[1] C. E. Shannon, *IRE Trans. Inf. Theory* **2**, 8 (1956).

[2] T. S. Cubitt, D. Leung, W. Matthews, and A. Winter, *Phys. Rev. Lett.* **104**, 230503 (2010).

[3] D. Leung, L. Mancinska, W. Matthews, M. Ozols, and A. Roy, *Commun. Math. Phys.* **311**, 97 (2012).

[4] R. Duan and Y. Shi, *Phys. Rev. Lett.* **101**, 20501 (2008).

[5] R. Duan, S. Severini, and A. Winter, *IEEE Trans. Inf. Theory* **59**, 1164 (2013).

[6] R. Duan and A. Winter, *IEEE Trans. Inf. Theory* **62**, 891 (2016).

[7] S. Beigi and P. W. Shor, *arXiv:0709.2090.*

[8] L. Lovász, *IEEE Trans. Inf. Theory* **25**, 1 (1979).

[9] S. Beigi, *Phys. Rev. A*, vol. 82, no. 1, p. 10303, (2010).

[10] T. Cubitt, L. Mancinska, D. E. Roberson, S. Severini, D. Stahlke, and A. Winter, *IEEE Trans. Inf. Theory* **60**, 7330 (2014).

[11] T. S. Cubitt, D. Leung, W. Matthews, and A. Winter, *IEEE Trans. Inf. Theory* **57**, 5509 (2011).

[12] L. Mancinska, G. Scarpa, and S. Severini, *IEEE Trans. Inf. Theory* **59**, 4025 (2013).

[13] N. Alon, *Combinatorica* **18**, 301 (1998).

[14] A. Schrijver, *IEEE Trans. Inf. Theory*, **25**, 4, 1979.

[15] R. J. McEliece, E. R. Rodemich, and H. C. Rumsey Jr, *J. Comb. Inform. Syst. Sci*, **3**, 3, 1978.

[16] T. Cubitt, L. Mancinska, D. E. Roberson, S. Severini, D. Stahlke, and A. Winter,
*IEEE Trans. Inf. Theory*, **60**, 11, 2014.

# Maximum privacy without coherence, zero-error

Debbie Leung[1] * Nengkun Yu[2 1 3] †

[1] *Institute for Quantum Computing and Department of Combinatorics and Optimization, University of Waterloo, Waterloo, Ontario, Canada*
[2] *Centre for Quantum Computation & Intelligent Systems, Faculty of Engineering and Information Technology, University of Technology Sydney, NSW 2007, Australia*
[3] *Department of Mathematics & Statistics, University of Guelph, Guelph, Ontario, Canada*

**Abstract.** We study the possible difference between the quantum and the private capacities of a quantum channel in the zero-error setting. For a family of channels introduced by [LLSS14], we demonstrate an extreme difference: the zero-error quantum capacity is zero, whereas the zero-error private capacity is maximum given the quantum output dimension.

**Keywords:** Private Capacity, Zero-error, Quantum Capacity, Coherence

The quantum capacity $Q(\mathcal{N})$, measured in qubits per channel use, establishes the maximum rate for transmitting quantum information and how well we can perform quantum error correction. The private capacity $\mathcal{P}(\mathcal{N})$, in bits per channel use, gives the maximum rate of *private* classical communication. Errors that become negligible as the number of channel uses increases are allowed in the above definitions.

Understanding the relation between the quantum and the private capacities is an essential task in quantum Shannon theory. In [HHHO05], some channels $\mathcal{N}$ are found for which $Q(\mathcal{N}) = 0$ but $P(\mathcal{N}) > 0$, breaking a long-held intuition that coherence is necessary for privacy. In [LLSS14], a class of channels with $Q(\mathcal{N}) \leq 1$ and $P(\mathcal{N}) = \log d$ is presented, where $d^2$ is the input dimension and log is taken base 2. As $d$ increases, these channels saturate an upper bound for $P(\mathcal{N}) - Q(\mathcal{N})$ thus approximately realizing the largest possible separation between the two capacities.

Quite recently, the notion of zero-error capacity has been introduced for quantum channels [MA05]. We denote the zero-error quantum and private capacities for a quantum channel $\mathcal{N}$ as $Q_0(\mathcal{N})$ and $P_0(\mathcal{N})$ respectively. Zero-error private classical communication requires perfect data transmission such that no one but the receiver gains any information on the data. Clearly $Q_0(\mathcal{N}) \leq Q(\mathcal{N}) \leq \mathcal{P}(\mathcal{N})$ and $Q_0(\mathcal{N}) \leq P_0(\mathcal{N}) \leq \mathcal{P}(\mathcal{N})$.

In this paper, we study the zero-error quantum capacity of the channels introduced in [LLSS14], and demonstrate an exact extreme separation. For these channels, $P_0(\mathcal{N}) = \log d$ and $Q_0(\mathcal{N}) = 0$. In other words, each of these channels has no capacity to transmit quantum information perfectly, even it has full ability to distribute private information perfectly.

The notion of zero-error quantum capacity can be introduced as follows. Let $\alpha^q(\mathcal{N})$ be the maximum integer $k$ such that there is a $k$-dimensional subspace $\mathcal{H}'_A$ of $\mathcal{H}_A$ that can be perfectly transmitted through $\mathcal{N}$. That is, there is a recovery quantum channel $\mathcal{R}$ from $\mathcal{D}(\mathcal{H}_B)$ to $\mathcal{D}(\mathcal{H}_{A'})$ so that $(\mathcal{R} \circ \mathcal{N})(\psi) = \psi$ for any $|\psi\rangle \in \mathcal{H}_{A'}$ (recall $\psi = |\psi\rangle\langle\psi|$). Then, $\log_2 \alpha^q(\mathcal{N})$ represents the maximum number of qubits one can send perfectly by one use of $\mathcal{N}$. The *zero-error quantum capacity* of $\mathcal{N}$, $Q_0(\mathcal{N})$, is defined as:

$$Q_0(\mathcal{N}) = \sup_{n \geq 1} \frac{\log_2 \alpha^q(\mathcal{N}^{\otimes n})}{n}. \tag{1}$$

we can invoke the following lemma from [CS12].

**Lemma 1** *Let $\mathcal{N} : \mathcal{D}(\mathcal{H}_A) \to \mathcal{D}(\mathcal{H}_B)$ be a quantum channel. One can transmit quantum information without error through a single use of $\mathcal{N}$ if and only if there are orthogonal states $|\alpha\rangle$ and $|\beta\rangle$ such that*

$$\mathrm{tr}\,[\mathcal{N}(|\alpha\rangle\langle\alpha|)\,\mathcal{N}(|\beta\rangle\langle\beta|)] = 0 \tag{2}$$

*and*

$$\mathrm{tr}\,[\mathcal{N}(|\alpha+\beta\rangle\langle\alpha+\beta|)\,\mathcal{N}(|\alpha-\beta\rangle\langle\alpha-\beta|)] = 0. \tag{3}$$

where $|\alpha \pm \beta\rangle = 1/\sqrt{2}(|\alpha\rangle \pm |\beta\rangle)$.

Private communication via a memoryless classical channel and quantum key distribution are well established subjects. Private classical communication of a quantum channel has more recently been formally introduced in [Dev05]. The private capacity of $\mathcal{N}$ measures the maximum rate of reliable classical data transmission via $\mathcal{N}$ while keeping the output of the complementary channel independent of the data.

The family of channels $\mathcal{N}_d$ introduced in [LLSS14] can be schematically summarized as follows:

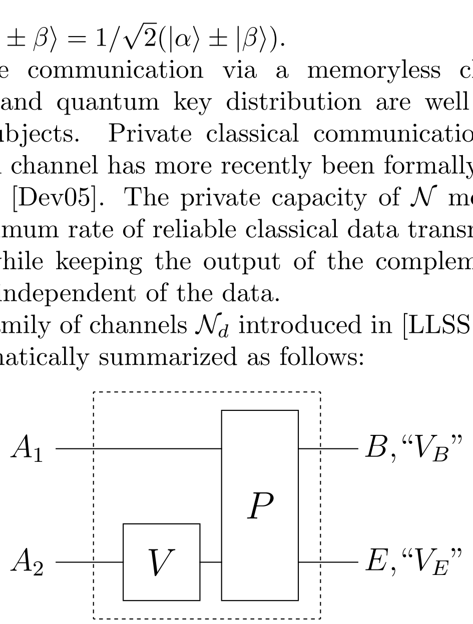

(4)

For each integer $d \geq 2$, we define the channel $\mathcal{N}_d$ which has two input registers $A_1$ and $A_2$, each of dimension $d$. A unitary operation $V$ is applied to $A_2$, followed by a controlled phase gate $P = \sum_{i,j} \omega^{ij} |i\rangle\langle i| \otimes |j\rangle\langle j|$ acting on $A_1 A_2$, where $\omega$ is a primitive $d^{\text{th}}$ root of unity. Bob

*wcleung@uwaterloo.ca

†nengkunyu@gmail.com

receives only $A_1$ (now relabeled as $B$) and "$V_B$", which denotes a classical register with a description of $V$. The $A_2$ register is discarded. The complementary channel has outputs $A_2$ (relabeled as $E$) and "$V_E$" which also contains a description of $V$. The isometric extension is given by

$$U_d \left|\psi\right\rangle_{A_1A_2} = \sum_V \sqrt{\mathrm{pr}(V)}\ \left(P\left(I\otimes V\right)\left|\psi\right\rangle_{A_1A_2}\right)\otimes|V\rangle_{V_B}\otimes|V\rangle_{V_E}.$$

Here, $V$ is drawn from any exact unitary 2-design $\mathcal{G} = \{g_1, g_2, \cdots, g_m\}$.

It was shown in [LLSS14] that $P(\mathcal{N}_d) = \log d$. The method given by [LLSS14] to transmit private classical data has no error and has perfect secrecy so $P_0(\mathcal{N}_d) = \log d$. To be self-contained, we provide a quick argument here. Suppose the input into $A_2$ is half of a maximally entangled state $|\Phi\rangle = \frac{1}{\sqrt{d}}\sum_i |i\rangle_{A_2}|i\rangle_{A_3}$ where $A_3$ stays in Alice's possession. By the transpose trick, the unitary operations $V$ and $P$ can be replaced by unitary operations acting on $A_1$ and $A_3$ without changing the final state on $B, E, A_3, V_B, V_E$. So, the output of the complementary channel $(E, V_E)$ is independent of the input. Moreover, $\mathcal{N}_d(|i\rangle\langle i| \otimes I/d) = |i\rangle\langle i|$. So $\log d$ bits can be transmitted perfectly and secretly.

Furthermore, [LLSS14] also shows that $Q(\mathcal{N}_d) \leq 1$. Intuitively, superposition of states in system $A_1$ will be heavily decohered by the $P$ gate, because error correction is ineffective due to the random unitary $V$. However, [LLSS14] finds that $Q(\mathcal{N}_d) \geq 0.61$ for large $d$.

This motivates the current study, to demonstrate an extreme separation of $P_0$ and $Q_0$ using the channels $\mathcal{N}_d$. Our main result is that, no finite number of uses of $\mathcal{N}_d$ can be used to transmit one qubit with zero error. This implies in particular $Q_0(\mathcal{N}_d) = 0$, while $P_0(\mathcal{N}_d) = \log d$, attaining the extremes allowed by the quantum output dimension.

Our main technical result is a characterization of pairs of input states whose orthogonality is preserved by $n$ uses of the channel.

**Theorem 2** Let $n$ be any positive integer, $|\psi_1\rangle = \sum_{i_1,\cdots,i_n} |i_1,\cdots,i_n\rangle\,|\alpha_{i_1,\cdots,i_n}\rangle$, and $|\psi_2\rangle = \sum_{i_1,\cdots,i_n} |i_1,\cdots,i_n\rangle\,|\beta_{i_1,\cdots,i_n}\rangle$ be two arbitrary pure state inputs for $\mathcal{N}_d^{\otimes n}$. Then, $\mathrm{tr}[\mathcal{N}_d^{\otimes n}(\psi_1)\mathcal{N}_d^{\otimes n}(\psi_2)] = 0$ if and only if at most one of $|\alpha_{i_1,\cdots,i_n}\rangle$ and $|\beta_{i_1,\cdots,i_n}\rangle$ is nonzero for each tuple $(i_1,\cdots,i_n)$.

In other words, states suitable for transmitting classical information through $\mathcal{N}_d^{\otimes n}$ without any error have no "overlap" in the computational basis of $A_1^{\otimes n}$.

As a consequence, we have

**Theorem 3** For any positive integer $n$, $\mathcal{N}_d^{\otimes n}$ cannot transmit a qubit with zero error. In particular, this implies $Q_0(\mathcal{N}_d) = 0$.

To prove Theorem 2, the following two lemmas are needed,

**Lemma 4** Let $|\psi_1\rangle = \sum_i |i\rangle\,|\alpha_i\rangle$ and $|\psi_2\rangle = \sum_i |i\rangle\,|\beta_i\rangle$ be two possible pure input states for $\mathcal{N}_d$. Then, $\mathrm{tr}[\mathcal{N}_d(\psi_1)\mathcal{N}_d(\psi_2)] = 0$ if and only if at most one of $|\alpha_i\rangle$ and $|\beta_i\rangle$ is nonzero for each $i$.

**Lemma 5** [YDY14] For all positive integer $n$, there is no non-zero bipartite matrix $M$ satisfying $M \geq 0$, $M^\Gamma \geq 0$, and $\mathrm{tr}(M(I-\Phi)^{\otimes n}) = 0$, where $M^\Gamma$ denotes the partial transpose of bipartite matrix $M$.

In this paper, we show an extreme separation between zero-error quantum capacity and the private capacity by demonstrating for a class of channels that the private capacity is maximum given the output dimension, while there is no ability to transmit even one-qubit with any finite number of channel uses, when no error can be tolerated. We hope techniques from our work can be used to study the zero-error capacity of other channels.

## References

[LLSS14] D. Leung, K. Li, G. Smith, and J. A. Smolin. Maximal Privacy without Coherence. *Physical Review Letters*, 113:030512, 2014.

[HHHO05] K. Horodecki, M. Horodecki, P. Horodecki, and J. Oppenheim. Secure key from bound entanglement. *Phys. Rev. Lett.*, 94, 160502 (2005).

[MA05] R. A. C. Medeiros, F. M. de Assis. Zero-error capacity of a quantum channel. IJQI, 3(1):135-139, 2005.

[CS12] T. S. Cubitt and G. Smith. An Extreme Form of Superactivation for Quantum Zero-Error Capacities. *IEEE Transactions on Information Theory*, 58(3):1953–1961, 2012.

[Dev05] I. Devetak. The private classical capacity and quantum capacity of a quantum channel. IEEE Trans. Inf. Theory 51, 44 (2005) (quant-ph/0304127v6).

[YDY14] N. Yu, R. Duan and M. Ying. Distinguishability of Quantum States by Positive Operator-Valued Measures with Positive Partial Transpose. *IEEE Transactions on Information Theory*, 60(4):2069-2079, 2014.

# Unconstrained distillation capacities of a pure-loss bosonic broadcast channel

Masahiro Takeoka[1] Kaushik P. Seshadreesan[2] Mark M. Wilde[3]

[1] *National Institute of Information and Communications Technology, Koganei, Tokyo 184-8795, Japan*
[2] *Max-Planck-Institut für die Physik des Lichts, 91058 Erlangen, Germany*
[3] *Hearne Institute for Theoretical Physics, Department of Physics and Astronomy, Center for Computation and Technology, Louisiana State University, Baton Rouge, Louisiana 70803, USA*

**Abstract.** Bosonic channels are important in practice as they form a simple model for free-space or fiber-optic communication. We consider a single-sender multi-receiver pure-loss bosonic broadcast channel and establish the unconstrained capacity region for the distillation of bipartite entanglement and secret key between the sender and each receiver, where they are allowed arbitrary public classical communication.

Quantum key distribution (QKD) and entanglement distillation (ED) are two cornerstones of quantum communication technology. QKD enables two or more parties to share unconditionally secure random bit sequences whereas ED allows them to distill pure maximal entanglement from a quantum state shared via a noisy communication channel. In both protocols, the parties are allowed to perform (in principle) an unlimited amount of local operations and classical communication (LOCC).

One of the problem in optical quantum communication is the channel loss. For example, all known QKD protocols exhibit an exponential rate-loss tradeoff, in which the secret key rate drops exponentially with increasing fiber distance [1].

Some time after these limitations were observed, Refs. [2] provided a mathematical proof, using the notion of squashed entanglement [3], that the tradeoff is indeed a fundamental limitation even with unconstrained input energy. One of the main results of [2] is an upper bound on the LOCC assisted quantum and secret key agreement capacity of a pure-loss bosonic channel, which is solely a function of the channel transmittance $\eta$ (for finite energy, tighter bounds are also available [2]). Ref. [4] extended the squashed entanglement technique to obtain upper bounds for a variety of phase-insensitive Gaussian channels. Concurrently with [4], Ref. [5] improved the infinite-energy bound from [2] and conclusively established the unconstrained capacity of the pure-loss bosonic channel as $\mathcal{C}(\eta) = -\log_2(1-\eta)$.

Extension of the above point-to-point scenario to the network quantum communication scenarios such as broadcast and multiple access channels is an important direction. Even though various network quantum communication scenarios have been examined, there has been limited work on the LOCC-assisted quantum and private capacities. Only recently in [6] were nontrivial outer bounds on the achievable rates established for the LOCC-assisted capacities in a general $m$-receiver quantum broadcast channel (QBC) (for any $m \geq 1$) based on multipartite generalizations of the squashed entanglement [7] and the methods of [2].

In this paper, we consider a single-sender multiple-receiver pure-loss bosonic QBC and establish the unconstrained LOCC-assisted capacity region for the distillation of bipartite entanglement and secret key between the sender and each receiver. Consider a pure loss bosonic QBC $\mathcal{L}_{A'\to BC}$ where the channel splits the input state into three systems, one to each of Bob, Charlie, and the environment with transmittance $\eta_B$, $\eta_C$, and $1-\eta_B-\eta_C$, respectively, where $\eta_B, \eta_C \in [0, 1], \eta_B + \eta_C \leq 1$. Physically it is modeled by a pair of beam splitters, in both the signal is mixed with a vacuum, where the first one induces pure loss and the second one splits the signal to Bob and Charlie. Alice wants to share the entanglement or secret keys with Bob and Charlie through $n$ channel uses and unlimited amount of LOCC. Let us denote entanglement rates between Alice and Bob (Charlie) as $E_{AB}$ ($E_{AC}$), and the secret key rate as $K_{AB}$ ($K_{AC}$), respectively. Our main theorem is stated as follows:

**Theorem 1** *The LOCC-assisted, unconstrained capacity region of the pure-loss bosonic QBC $\mathcal{L}_{A'\to BC}$ is given by*

$$E_{AB} + K_{AB} \leq \log_2([1-\eta_C]/[1-\eta_B-\eta_C]), \quad (1)$$

$$E_{AC}+K_{AC} \leq \log_2([1-\eta_B]/[1-\eta_B-\eta_C]), \quad (2)$$

$$E_{AB}+K_{AB}+E_{AC}+K_{AC} \leq -\log_2(1-\eta_B-\eta_C). \quad (3)$$

A complete proof is given in [8]. To prove the statement, we establish inner bounds on the achievable rate region by employing the quantum state merging protocol [9]. The converse part relies upon several tools. First, we utilize a teleportation simulation argument originally introduced in [10, Section V]. and recently extended in [5]. Next, it is known that the relative entropy of entanglement is an upper bound on the distillable key of a bipartite state [11]. Then the recent work in [5] stated how these two ideas are combined to upper bound the LOCC-assisted quantum and private capacities for certain class of point-to-point channels.

Also critical for the proof of the converse part is the fact that the physical implementation of $\mathcal{L}_{A'\to BC}$ is not unique. For example, we could have a first beam splitter split system $B$ from $C$ and $E$, and then a second one split $C$ and $E$. It is also possible to split $C$ at the first beam splitter. This observation implies a drastic simplification of the calculation of the relative entropy of entanglement. The obtained outer bounds match the inner bounds in the infinite-energy limit, thereby establishing the unconstrained capacity region. An example fothe rate region is shown in Fig. 1.

The above theorem can be generalized for single-sender multiple-receiver pure-loss broadcast channel $\mathcal{L}_{A'\to B_1\cdots B_m}$ with $m > 2$ which is characterized by a set of transmittances $\{\eta_{B_1}, \cdots, \eta_{B_m}\}$ with $\sum_{i=1}^m \eta_{B_i} \leq 1$ [12]. Let $\mathcal{B} = \{B_1, \cdots, B_m\}$, $\mathcal{T} \subseteq \mathcal{B}$, and $\overline{\mathcal{T}}$ be a complement of set $\mathcal{T}$. We have the following theorem:

**Theorem 2** *The LOCC-assisted unconstrained capacity region of the pure-loss bosonic QBC $\mathcal{L}_{A'\to B_1\cdots B_m}$ is given by*

$$\sum_{B_i\in\mathcal{T}} E_{AB_i}+K_{AB_i} \leq \log_2\left(\frac{1-\eta_{\overline{\mathcal{T}}}}{1-\eta_{\mathcal{B}}}\right), \quad (4)$$

*for all non-empty $\mathcal{T}$, where $\eta_{\mathcal{B}} = \sum_{i=1}^m \eta_{B_i}$ and $\eta_{\overline{\mathcal{T}}} = \sum_{B_i\in\overline{\mathcal{T}}} \eta_{B_i}$.*

A complete proof is given in [8].

Our result could provide a useful benchmark for implementing a broadcasting of entanglement and secret key through linear optics networks which is usually used in real world quantum communications. Important open questions include the distillations of $E_{BC}$ and $K_{BC}$, or even GHZ states through QBC, and determining the capacity region in both this setting and even the single-sender single-receiver case when there is an energy constraint on the transmitter which is practically more relevant.

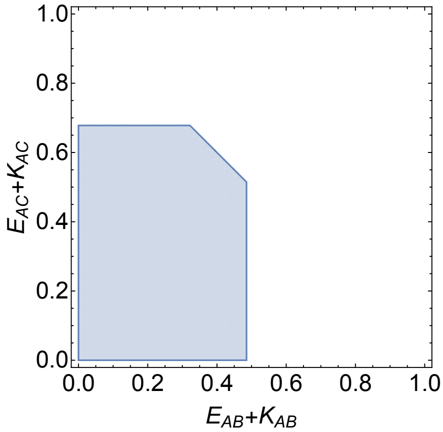

Figure 1: LOCC-assisted capacity region given by (1)–(3), where $(\eta_B, \eta_C) = (0.2, 0.3)$.

## References

[1] V. Scarani et al., *Rev. Mod. Phys.*, 81, 1301 (2009).

[2] M. Takeoka, S. Guha, and M. M. Wilde, *Nat. Commun.*, 5:5235 (2014), *ibid*, *IEEE Trans. Inf. Theory*, 60, 4987 (2014).

[3] M. Christandl and A. Winter, *J. Math. Phys.*, 45, 829 (2004).

[4] K. Goodenough, D. Elkouss, and S. Wehner, *New J. Phys.*, 18, 063005 (2016).

[5] S. Pirandola et al., arXiv:1510.08863.

[6] K. P. Seshadreesan et al., *IEEE Trans. Inf. Theory*, 62, 2849 (2016).

[7] D. Yang et al., *IEEE Trans. Inf. Theory*, 55, 3375 (2009).

[8] M. Takeoka, K. P. Seshadreesan, and M. M. Wilde, arXiv:1601.05563v2.

[9] M. Horodecki, J. Oppenheim, and A. Winter, *Nature*, 436, 673 (2005).

[10] C. H. Bennett et al., *Phys. Rev. A*, 54, 3824 (1996).

[11] K. Horodecki et al., *Phys. Rev. Lett.*, 94, 160502 (2005).

[12] S. Guha, Ph.D. dissertation, MIT, 2008.

# Quantifying Asymmetric Einstein-Podolsky-Rosen Steering

Kai Sun[1 2 *] Xiang-Jun Ye[1 2 †] Jin-Shi Xu[1 2 ‡] Chuan-Feng Li[1 2 §]

[1] *Key Laboratory of Quantum Information, CAS, University of Science and Technology of China, Hefei, Anhui 230026, P. R. China*

[2] *Synergetic Innovation Center of Quantum Information and Quantum Physics, University of Science and Technology of China, Hefei, Anhui 230026, P. R. China*

**Abstract.** Einstein-Podolsky-Rosen (EPR) steering exhibits a unique asymmetric property, i.e., the steerability can differ between observers. This property is inherently different from the symmetric concepts of entanglement and Bell nonlocality, and it has attracted increasing interest. We propose a practical method to quantify the steerability. And we experimentally use it to quantify asymmetric EPR steering in the frame of projective measurements. Furthermore, we then clearly demonstrate one-way EPR steering. Our work provides a new insight into the fundamental asymmetry of quantum nonlocality and has potential applications in asymmetric quantum information processing.

**Keywords:** asymmetry, steering, quantification, one-way

Asymmetric EPR steering is an important open question proposed when EPR steering is reformulated in 2007 [1]. Supposing Alice and Bob share a pair of two-qubit state, it is easy to image that if Alice entangles with Bob, then Bob must also entangle with Alice. Such a symmetric feature holds for both entanglement and Bell nonlocality [2]. However, the situation is dramatically changed when one turns to a novel kind of quantum nonlocality, the EPR steering, which stands between entanglement and Bell nonlocality. It may happen that for some asymmetric bipartite quantum states, Alice can steer Bob but Bob cannot steer Alice. This distinguished feature would be useful for the one-way quantum tasks. The first experimental verification of one-way EPR steering was performed by using two entangled continuous variable systems in 2012 [3]. However, the experiments demonstrating one-way EPR steering [3, 4] are restricted to Gaussian measurements, and for more general measurements, like projective measurements, there is no experiment realizing the asymmetric feature of EPR steering even the theoretical analysis has been proposed [5].

Recently, we for the first time quantify the steerability and demonstrate one-way EPR steering in the simplest entangled system (two qubits) using two-setting projective measurements [6]. The asymmetric two-qubit states in the form of

$$\rho_{AB} = \eta|\Psi(\theta)\rangle\langle\Psi(\theta)| + (1-\eta)|\Phi(\theta)\rangle\langle\Phi(\theta)|, \quad (1)$$

where $0 \leq \eta \leq 1$, $|\Psi(\theta)\rangle = \cos\theta|0_A 0_B\rangle + \sin\theta|1_A 1_B\rangle$, $|\Phi(\theta)\rangle = \cos\theta|1_A 0_B\rangle + \sin\theta|0_A 1_B\rangle$, are prepared based on the setup shown in Figure 1. For all non-trivial $\rho_{AB}$, Alice can steer Bob's state. When $|\cos 2\theta| < |2\eta - 1|$, Bob can also steer Alice's state. If $|\cos 2\theta| \geq |2\eta - 1|$, there always exists a local hidden state model for Alice to reproduce her conditional states when Bob chooses any two directions to measure, which means Bob can *not* steer Alice's state.

Based on the steering robustness [7], we introduce an intuitive criterion $R$ called as steering radius, which is defined as

$$R(\rho_{AB}) = \max_{\{\vec{n}_1,\vec{n}_2\}} \{r(\rho_{AB})_{\{\vec{n}_1,\vec{n}_2\}}\}, \quad (2)$$

to quantify the steerability. Here, $r(\rho_{AB})_{\{\vec{n}_1,\vec{n}_2\}}$ is explained below. In the case of two measurement settings $\{\vec{n}_1, \vec{n}_2\}$, there are at most four local hidden states, $\rho_i$ ($i = a$, $b$, $c$, $d$), reproducing Bob's conditional states if Alice can *not* steer Bob's system. We can expand the hidden

[*] skaikai@mail.ustc.edu.cn

[†] xiangjun@ustc.edu.cn

[‡] jsxu@ustc.edu.cn

[§] cfli@ustc.edu.cn

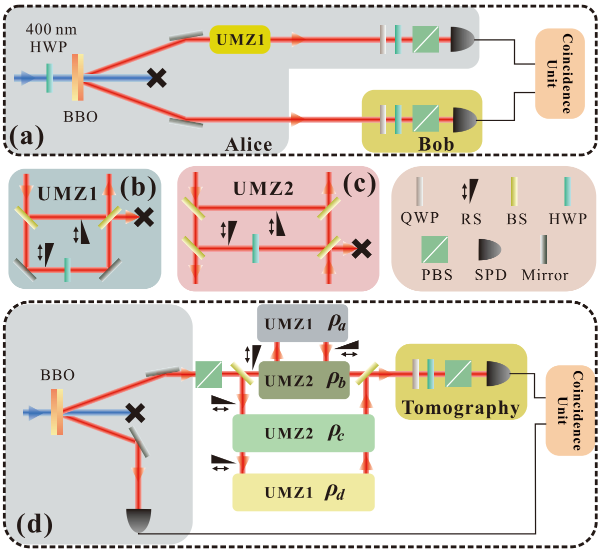

Figure 1: Experimental setup. **(a)**. The entangled photon pairs are prepared through the spontaneous parametric down conversion (SPDC) process by pumping the BBO crystal with ultraviolet pulses. The state's parameters $\eta$ and $\theta$ can be detuned conveniently by employing the setup shown in **(a)** and the unbalanced Mach-Zehnder interferometer (UMZ) with beam splitters (BSs) and removable shutters (RSs) shown in **(b)**. A unit consisting of a quarter-wave plate (QWP) and a half-wave plate (HWP) on Alice's side is used to set the measurement direction. The same unit with an extra polarization beam splitter (PBS) on Bob's side is used to perform state tomography. Photons are collected into a single mode fiber equipped with a 3 $nm$ interference filter and are then detected by a single-photon detector (SPD) on each side. **(d)**. The strategy is for local hidden states to reproduce the conditional states. One of the two photons is used as the trigger for the coincidence unit, and the other is used to prepare the four local hidden states, which can be conveniently prepared by employing the setup of **(b)** and **(c)**. The probabilities are controlled by adjusting the RSs.

states to the super quantum hidden state model (SQHSM), which means there are no physical restrictions on the states $\rho_i$ and $\rho_i$, which can be located outside of the Bloch sphere. In such a case, there is generally more than one set of SQHSM. Thus, $r(\rho_{AB})_{\{\vec{n}_1,\vec{n}_2\}}$ can be defined as the radius of the SQHSM which is written as

$$\min_{SQHSM}\{\max\{L[\rho_a], L[\rho_b], L[\rho_c], L[\rho_d]\}\}, \qquad (3)$$

where $L[\rho_i]$ $(i = a, b, c, d)$ denotes the length of Bloch vectors of the states $\rho_i$. If $r(\rho_{AB})_{\{\vec{n}_1,\vec{n}_2\}} > 1$, at least one of the hidden states is located beyond the Bloch sphere; thus, the model is not physical. The different values of $R$ on two sides clearly illustrate the asymmetric feature of EPR steering. Furthermore, the one-way steering is demonstrated when $R > 1$ on one side and $R < 1$ on the other side (see Figure 2 (b)).

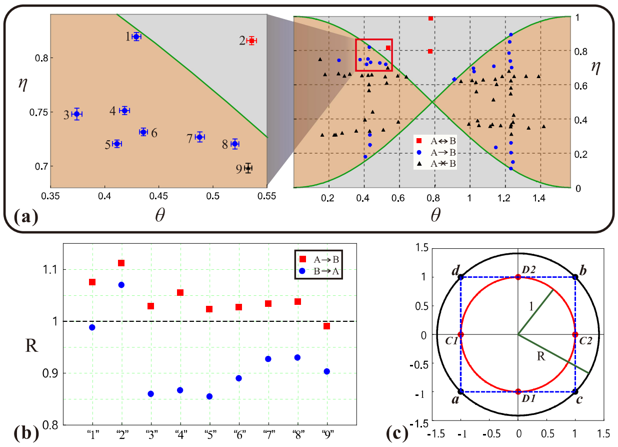

Figure 2: Experimental results for asymmetric EPR steering. **(a)** The distribution of the experimental states. The right column shows the entangled states we prepared, and the left column is a magnification of the corresponding region in the right column. The two green curves represent the cases of $|\cos 2\theta| = |2\eta - 1|$. The blue points and red squares represent the states realizing one-way and two-way EPR steering, respectively. The black triangles represent the states for which EPR steering task fails for both observers. **(b)** The values of $R$ for the states labeled in the left column in **(a)**. The red squares represent the situation where Alice steers Bob's system, and the blue points represent the case where Bob steers Alice's system. **(c)** Geometric illustration of the strategy for local hidden states (black points) to construct the four normalized conditional states (red points) obtained from the maximally entangled state.

For the failing EPR steering process, the local hidden state model, which provides a direct and convinced contradiction between the nonlocal EPR steering and classical physics, is prepared experimentally to reconstruct the conditional states obtained in the steering process (see Figure 3).

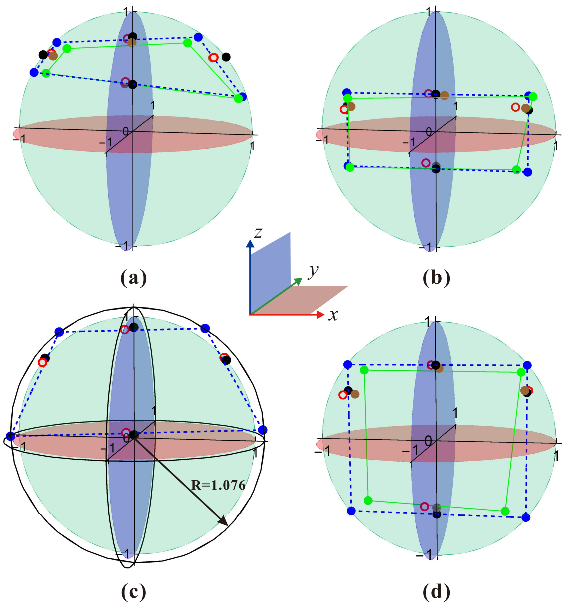

Figure 3: The experimental results of the normalized conditional states and local hidden states shown in the Bloch sphere. The theoretical and experimental results of the normalized conditional states are marked by the black and red points (hollow), respectively. The blue and green points represent the results of the four local hidden states in theory and experiment, respectively. The normalized conditional states constructed by the local hidden states are shown by the brown points. **(a)** and **(c)** Show the case in which Alice steers Bob's system, whereas **(b)** and **(d)** show the case in which Bob steers Alice's system. The parameters of the shared state in **(a)** and **(b)** are $\theta = 0.442$ and $\eta = 0.658$; the parameters of the shared state in **(c)** and **(d)** are $\theta = 0.429$ and $\eta = 0.819$. **(a)**, **(b)** and **(d)** Show that the local hidden state models exist, and the steering tasks fail. **(c)** Shows that no local hidden state model exists for the steering process with the constructed hidden states located beyond the Bloch sphere and $R = 1.076$.

The quantification of EPR steering provides an intuitional and fundamental way to understand the EPR steering. The demonstrated asymmetric EPR steering, especially one-way steering, helps us to investigate the asymmetric feature of quantum nonlocality. This is significant within quantum foundations and quantum information, and shows the potential applications in the tasks of one-way quantum key distribution [8] and the quantum subchannel discrimination [7], even within the frame of two-setting measurements.

## References

[1] H. M. Wiseman, S. J. Jones, and A. C. Doherty. Steering, entanglement, nonlocality, and the Einstein-Podolsky-Rosen paradox. *Phys. Rev. Lett.*, 98, 140402, 2007.

[2] J. S. Bell. On the Einstein Podolsky Rosen paradox. *Physics (Long Island City, N. Y.)*, 1, 195, 1964.

[3] Vitus Händchen *et al.*. Observation of one-way Einstein-Podolsky-Rosen steering. *Nature Photonics*, 6, 596, 2012.

[4] Seiji Armstrong *et al.*. Multipartite Einstein-Podolsky-Rosen steering and genuine tripartite entanglement with optical networks. *Nature Physics*, 11, 167, 2015.

[5] Joseph Bowles, Tamás Vértesi, Marco Túlio Quintino, and Nicolas Brunner. One-way Einstein-Podolsky-Rosen steering. *Phys. Rev. Lett.*, 112, 200402, 2014.

[6] Kai Sun *et al.*. Experimental quantification of asymmetric Einstein-Podolsky-Rosen steering. *Phys. Rev. Lett.*, 116, 160404, 2016.

[7] Marco Piani and John Watrous. Necessary and sufficient quantum information characterization of Einstein-Podolsky-Rosen steering. *Phys. Rev. Lett.*, 114, 060404, 2015.

[8] Cyril Branciard *et al.*. One-sided device-independent quantum key distribution: Security, feasibility, and the connection with steering. *Phys. Rev. A*, 85, 010301, 2012.

# A Quantum Paradox of Choice: More Freedom Makes Summoning a Quantum State Harder

Emily Adlam[1] *            Adrian Kent[1] [2] †

[1] *Centre for Quantum Information and Foundations, DAMTP, Centre for Mathematical Sciences, University of Cambridge, Wilberforce Road, Cambridge, CB3 0WA, U.K.*

[2] *Perimeter Institute for Theoretical Physics, 31 Caroline Street North, Waterloo, ON N2L 2Y5, Canada*

**Abstract.** The properties of quantum information in space-time can be investigated by studying operational tasks. In one such task, summoning, an unknown quantum state is supplied at one point, and a call is made at another for it to be returned at a third. Hayden-May recently proved necessary and sufficient conditions for guaranteeing successful return of a summoned state for finite sets of call and return points when there is a guarantee of at most one summons. We prove necessary and sufficient conditions when there may be several possible summonses and complying with any one constitutes success. We show there is a "quantum paradox of choice" in summoning: the extra freedom in completing the task makes it strictly harder. This intriguing result has practical applications for distributed quantum computing and cryptography and also implications for our understanding of relativistic quantum information and its localization in space-time.

**Keywords:** Relativistic quantum cryptography, distributed quantum computing, summoning

It is well known that the exploitation of quantum effects gives rise to exciting new possibilities for computation, information processing and cryptography[3, 16, 13, 15, 5], but more recently, it has been realized that placing quantum information under relativistic constraints leads to the emergence of further unique effects[11, 9, 7] and since this area has not yet been well explored, it is likely that many useful relativistic quantum phenomena remain to be discovered.

In this project, we have been studying constraints on quantum information processing that arise in the relativistic context, and have uncovered a new and surprising effect: under appropriate circumstances, transmitting a quantum message may be possible if there is only one option for the place of delivery, but impossible if multiple options are offered, so having more freedom can sometimes make a relativistic quantum task more difficult. This apparent paradox has important consequences for our understanding of how quantum states may be propagated in distributed quantum computers, global financial networks and other contexts where relativistic signalling constraints are important.

The starting point for our project is a task known as summoning, in which an agent is given an unknown quantum state and required to produce it at a point in space-time in response to a call made at some earlier point[11]. The combination of the relativistic no-signalling principle[14] and the quantum no-cloning theorem[4, 17] together impose strict constraints on the possible geometric configurations of call and return points. Our work involves a generalization of this task in which calls may be made at any number of call points and the agent is required to return the state at any one of the return points corresponding to one of the calls: we have proved a theorem establishing necessary and sufficient conditions on the possible geometric configurations of call and return points in space-time for which there exists a protocol that guarantees a successful response to this task, and showed that these are strictly stronger conditions than those established by Hayden-May[7] for the original summoning task. Thus, strangely, giving an agent more possible ways to respond to this task actually makes it harder for him to respond successfully.

The resolution of the apparent paradox rests on a previously unappreciated feature of summoning tasks. Prima facie it seems that the guarantee of at most one call plays no special role in a summoning task other than to ensure that Alice is never required to produce two copies of an unknown state, in violation of the no-cloning theorem. It thus initially seems paradoxical that summoning becomes strictly harder if we allow the possibility of more than one call, even though only one valid response is required. However, if Alice knows that no more than one call will occur, learning that a call has been made at one point tells her that there are no calls at any other point, and this allows her to coordinate the behaviour of her agents via the global call distribution. A single call gives Alice less information if multiple calls can occur: she learns nothing about the distribution of calls at other points. She thus cannot use the call distribution to coordinate her agents actions in the same way. In other words, the guarantee of at most one call provides a resource that gives Alice the ability to complete tasks that would be impossible without it.

The effect we describe has important practical applications, because the no-summoning theorem has already been used for the development of new protocols in relativistic quantum cryptography[8, 10, 12, 1, 2], and our stronger results suggest further ways of exploiting summoning as a general way of controlling the flow of quantum information. For example, our result is a useful way of characterizing possible distributed parallel quantum computations in which the output of a sub-protocol is routed to one of several parallel computations which call

*ea385@cam.ac.uk

†apak@cam.ac.uk

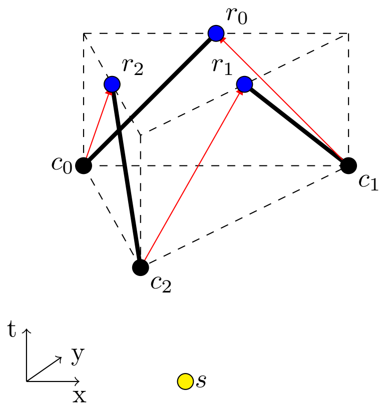

Figure 1: A $2+1$ dimensional example of a spacetime configuration of call and repsonse points where summoning is possible if it is guaranteed that there will be only one call, but not if more than one call may arrive.

for the output when they reach a certain state[6]. We thus expect this result to find application in future cryptographic protocols as well as in quantum network algorithms.

Our result also has interesting theoretical implications: there is a long-standing tradition of using apparent paradoxes to refine our understanding of quantum theory[3, 16, 13, 15, 5], but this new effect is perhaps the first intrinsically relativistic quantum paradox, in the sense that the effect can be exhibited only in the framework of relativistic quantum theory. Our project thus offers a useful starting point for probing intuitions about the nature of quantum states as spatiotemporal entities - an area which has received comparatively little attention in recent debates over the reality of the quantum state.

## References

[1] E. Adlam and A. Kent. Deterministic relativistic quantum bit commitment. *International Journal of Quantum Information*, 13:1550029, June 2015.

[2] E. Adlam and A. Kent. Device-independent relativistic quantum bit commitment. *Physical Review A*, 92(2):022315, August 2015.

[3] M. L. Almeida, J.-D. Bancal, N. Brunner, A. Acín, N. Gisin, and S. Pironio. Guess Your Neighbor's Input: A Multipartite Nonlocal Game with No Quantum Advantage. *Physical Review Letters*, 104(23):230404, June 2010.

[4] D. Dieks. Communication by EPR Devices. *Phys. Lett.*, A92:271–272, 1982.

[5] P. Gawron, J. A. Miszczak, and J. Sladkowski. Noise Effects in Quantum Magic Squares Game. *ArXiv e-prints*, January 2008.

[6] D. Gottesman and I. L. Chuang. Demonstrating the viability of universal quantum computation using teleportation and single-qubit operations. *Nature*, 402:390–393, November 1999.

[7] P. Hayden and A. May. Summoning Information in Spacetime, or Where and When Can a Qubit Be? *Journal of Physics A*, March 2016.

[8] A. Kent. Unconditionally secure bit commitment with flying qudits. *New Journal of Physics*, 13(11):113015, 2011.

[9] A Kent. Quantum Tasks in Minkowski Space. *Class. Quantum Grav.*, 29, 2012.

[10] A. Kent. Unconditionally Secure Bit Commitment by Transmitting Measurement Outcomes. *Physical Review Letters*, 109(13):130501, September 2012.

[11] A. Kent. A no-summoning theorem in relativistic quantum theory. *Quantum Information Processing*, 12(2):1023–1032, 2013.

[12] T. Lunghi, J. Kaniewski, F. Bussières, R. Houlmann, M. Tomamichel, A. Kent, N. Gisin, S. Wehner, and H. Zbinden. Experimental Bit Commitment Based on Quantum Communication and Special Relativity. *Phys. Rev. Lett.*, 111:180504, Nov 2013.

[13] L. Mančinska, D. E. Roberson, and A. Varvitsiotis. Deciding the existence of perfect entangled strategies for nonlocal games. *ArXiv e-prints*, June 2015.

[14] L. Sartori. *Understanding Relativity: A Simplified Approach to Einstein's Theories*. University of California Press, 1996.

[15] Marco Tomamichel, Serge Fehr, Jdrzej Kaniewski, and Stephanie Wehner. One-sided device-independent qkd and position-based cryptography from monogamy games. In Thomas Johansson and PhongQ. Nguyen, editors, *Advances in Cryptology EUROCRYPT 2013*, volume 7881 of *Lecture Notes in Computer Science*, pages 609–625. Springer Berlin Heidelberg, 2013.

[16] Thomas Vidick. The complexity of entangled games. *Phd thesis, University of California, Berkeley*, 2011.

[17] W. K. Wootters and W. H. Zurek. A single quantum cannot be cloned. *Nature*, 299:802, October 1982.

# Dimension Witnesses Beyond Non-Classicality Tests

Edgar A. Aguilar[1] * Máté Farkas[1] † Marcin Pawłowski[1] ‡

[1] *Faculty of Mathematics, Physics and Informatics, University of Gdańsk, 80-952 Gdańsk, Poland,*
*National Quantum Information Centre in Gdańsk, 81-824 Sopot, Poland*

**Abstract.** Current experimental tests of non-classicality are binary in their conclusions, regardless of the dimension. Either a physical information carrier is considered to be classical in nature, or else it is said to be quantum. Nevertheless, this does not imply straight away that the experimental setup can produce any desired quantum state of the desired dimension. In this work, we provide a refined dimension witness based on Quantum Random Access Codes, which is able to distinguish between fully classical states, classical-quantum states, separable quantum states, and arbitrary high-dimensional quantum states. These results will be useful to the community, in order to correctly characterize the power of existing experimental setups, to know which quantum information and computation protocols are within our grasp.

**Keywords:** Dimension Witness, QRACs, Classical-Quantum States

The dimension, or degrees of freedom, of physical information carriers is crucial. In order for quantum computers to show a true practical advantage over their classical counterparts, they must operate on systems of large dimension. That is why we are increasingly striving to coherently control systems of large dimensions [1, 2, 3, 4]. Another promising area is that of quantum information processing, where the dimension of the system is also regarded as a resource. Not only do higher dimensional systems offer more computational and communication power, but they are also useful in e.g. Bell experiments [5, 6] Hence, the quantum information community has come up with the brilliant idea of a dimension witness, originally based on the violation of some particular Bell inequalities [7], and then extended to the prepare and measure scenario [8].

Dimension witnesses can be understood in slightly different ways, depending on the underlying assumptions, but in general refer to some linear function on measurement outcome probabilities. For example, in [7] the systems are assumed to be quantum in nature, and the dimension witness is a Bell inequality which cannot be violated without using quantum systems of at least a specific size. The other example to compare is [8], where they use ideas from state discrimination theory to make a dimension witness that can distinguish between a classical and a quantum system.

While dimension witnesses have been of great help for experimentalists, there is a subtle issue that has been missing in the analysis thus far, which we illustrate with an example. Imagine an experimentalist has complete control over photonic qubit systems but can only create these systems independently (e.g. one at a time), and she does this 20 times. Surely, if done correctly, it's possible to find a dimension witness that makes 20 qubits in a product state perform better than 20 classical bits and then make a claim like "*I work with Hilbert Spaces of Dimension 1 Million*". While, this is strictly not a lie, it is very misleading! Hence, we look for a dimension witness that can signal whether the experimentalist has full (coherent) control of the Hilbert space, in the previous example this would imply arbitrary entanglement between said photons.

This work provides a simple tool for experimental teams to determine up to which dimension they have full control of their Hilbert space (i.e. they can create all states of said dimension). This is very important for the community, as a benchmark tool to check our progress on building quantum computers, and also for experimentalists to know which protocols they can feasibly execute. We focus on the prepare and measure scenario, which is the most general case. Since the point is to show that there is complete coherent control of a particular dimension, it doesn't matter if the physical information carriers are divided as entangled particles, or just one system in an arbitrary state. In particular, we focus on Random Access Codes (RACs), where we call the preparation part of the experiment Alice, and the measurement part Bob.

A $n^d \to 1$ *Random Access Code* (RAC) is a strategy in which Alice tries to compress a $n$-dit string into 1 dit, such that Bob can recover any of the $n$ dits with high probability [10]. Specifically, Alice receives an input string $X = x_0 x_1 \cdots x_{n-1}$ where $x_i \in [d]$, and we write $[d] \equiv \{0, 1, 2, \dots, d-1\}$. She is allowed to send one dit $a = E_c(X)$ to Bob. On the other side, Bob receives an input $y \in [n]$, and together with Alice's message $a$, outputs $b = D_c(a, y)$ as a guess for $x_y$. If Bob's guess is correct (i.e. $b = x_y$) then we say that they *win*, otherwise we say that they *lose*. Since both encoding and decoding functions are in general probabilistic, we in fact quantify the probability of success $p(b = x_y)$. As a figure of merit for the encoding-decoding strategy, we use the average success probability $P = \frac{1}{nd^n} \sum_X \sum_y p(b = x_y)$.

Similarly, we may define $n^d \to 1$ Quantum Random Access Codes (QRACs) with the only change being that Alice tries to compress her input string into a $d$-dimensional quantum system. The decoding function is nothing more than a quantum measurement, i.e. he outputs his guess $b$ with probability $\mathrm{tr}[\rho_a M_b^y]$. It can be shown that the maximum average success probability can be achieved with pure states ($\rho_a = |a\rangle\langle a|$) [10].

*ed.alex.aguilar@gmail.com
†mate.frks@gmail.com
‡dokmpa@univ.gda.pl

Similarly, it is possible to argue that this maximum is achieved when the operators $M_b^y$ are projective measurements, which is what we shall henceforth be assuming.

Assume the dimension factorizes as $d = ab$ (with $a \geq b$), then in general we are interested in the following 5 cases: $C_{ab}, C_aQ_b, C_bQ_a, Q_aQ_b, Q_{ab}$. In the same order, these are to be understood as: a classical system of dimension $ab$, a classical system of dimension $a$ and a quantum system of dimension $b$, a classical system of dimension $b$ and a quantum system of dimension $a$, a quantum system of dimension $a$ in a separable state with a quantum system of dimension $b$, and a quantum system of dimension $ab$. This is trivially generalized. The **Main Result** of our work deals with constructing explicit dimension witnesses which are able to differentiate the above cases. The explicit construction is technical, but an example of how our tools can be used is provided, as well as the main ideas regarding the proof.

**Example.** For a classical $2^d \rightarrow 1$ RAC the average success probability is $P_{C_d} = \frac{1}{2} + \frac{1}{d}$, while for the quantum case the $2^d \rightarrow 1$ QRAC has an average success probability of $P_{Q_d} = \frac{1}{2} + \frac{1}{2\sqrt{d}}$. We look at dimension 4, with $P_{C_4} = 0.625$ and $P_{Q_4} = 0.75$, and with our main result we are able to calculate $P_{C_2Q_2} = 0.6546$ and $P_{Q_2Q_2} \approx 0.7286$. This means that, it is not enough for the experimentalist to obtain an average success probability greater than $P_{C4}$, to claim that she has complete control over 4-dimensional Hilbert space. Surely, this would imply immediately that her states are not entirely classical, but the big prize in this example would be to obtain an experimental result above the $P_{Q_2Q_2}$ value.

Now we briefly present the key ideas of our proof. First, we prove that an identity decoding function (where Bob's outcome measurements are directly used in the output without further post-processing) cannot be worse than the optimal decoding function. Second, adaptive measurements cannot outperform non-adaptive ones. By this we mean, Bob's measurement strategy only depends on his input $y$, and in the optimal case does not depend on the measurement results of the first systems. These two points, make it so that essentially Alice and Bob are playing two parallel QRACs at the same time. Finally, for a given $2^d \rightarrow 1$ QRAC, we derive "maximal quantum curves" which relate the probability of guessing dit 1, as a function of the probability of guessing dit 2 when using the optimal quantum mechanical strategy - which involves using Mutually Unbiased Bases [11].

Up to this point, we need to assume that the system is a specific dimension $d$, and then we are able to provide the tools necessary for distinguishing the nature of said system. This is problematic, because sometimes experimentalists don't even know what is the effective dimension of their system. Hence, we propose a very simple $1^{d_0} \rightarrow 1$ QRAC (which is just state discrimination in disguise), where $d_0$ is a guess of the dimension size. If the average success probability is less than 1, then we express it as $\frac{d}{d_0}$, and $d$ is the effective system size the experimentalist should be working with. Specifically, the experimentalist would know that his system is at least dimension $d$, and if if it were this dimension, then she could say how classical or quantum it is.

Finally, we conclude by saying that our main result can be used to prove that for some cases $P_{Q_a} > P_{Q_bQ_c}$ even if $a < bc$. This just shows that indeed having access to the full Hilbert space is a great resource, and it is this what we should be checking when developing new quantum technologies.

## References

[1] M. Krenn, M. Huber, R. Fickler, R. Lapkiewicz, S. Ramelow, and A. Zeilinger, "Generation and confirmation of a (100 100)-dimensional entangled quantum system," vol. 111, no. 17, pp. 6243–6247, 2014.

[2] M. Malik, M. Mirhosseini, M. Lavery, J. Leach, M. Padgett, and R. Boyd, "Direct measurement of a 27-dimensional orbital-angular-momentum state vector," vol. 5, p. 3115, 2014.

[3] M. McLaren, F. S. Roux, and A. Forbes, "Realising high-dimensional quantum entanglement with orbital angular momentum," *ArXiv e-prints*, May 2013.

[4] V. D'Ambrosio, F. Bisesto, F. Sciarrino, J. F. Barra, G. Lima, and A. Cabello, "Device-independent certification of high-dimensional quantum systems," *Phys. Rev. Lett.*, vol. 112, p. 140503, Apr 2014.

[5] S. Massar, "Nonlocality, closing the detection loophole, and communication complexity," *Phys. Rev. A*, vol. 65, p. 032121, Mar 2002.

[6] T. Vértesi, S. Pironio, and N. Brunner, "Closing the detection loophole in bell experiments using qudits," *Phys. Rev. Lett.*, vol. 104, p. 060401, Feb 2010.

[7] N. Brunner, S. Pironio, A. Acin, N. Gisin, A. A. Méthot, and V. Scarani, "Testing the dimension of hilbert spaces," *Phys. Rev. Lett.*, vol. 100, p. 210503, May 2008.

[8] N. Brunner, M. Navascués, and T. Vértesi, "Dimension witnesses and quantum state discrimination," *Phys. Rev. Lett.*, vol. 110, p. 150501, Apr 2013.

[9] S. Wehner, M. Christandl, and A. C. Doherty, "Lower bound on the dimension of a quantum system given measured data," *Phys. Rev. A*, vol. 78, p. 062112, Dec 2008.

[10] A. Ambainis, D. Leung, L. Mancinska, and M. Ozols, "Quantum Random Access Codes with Shared Randomness," *ArXiv e-prints*, Oct. 2008.

[11] E. Aguilar, J. Borkała, P. Mironowicz, and M. Pawłowski, "Using Quantum Random Access Codes to Understand Mutually Unbiased Bases," *in preparation.*

# A Reconciliation Protocol Based on Polar Codes for CVQKD

Shengmei Zhao[1] * Le Wang[1] Hanwu Chen[2]

[1] *Institute of Signal Processing and Transmission, Nanjing University of Posts and Telecommunications(NUPT), Nanjing 210003, China*

[2] *School of Computer Science and Engineering, Southeast University, Nanjing, 210096, China*

**Abstract.** This paper proposes a multidimensional reconciliation protocol for continuous variable quantum key distribution based on Polar codes. This protocol consists of two components, one is the multidimensional algorithm, and the other is Polar coding. In the first component, the continuous sifted key at Alice is first normalized then transformed to a binary data by a sphere and rotation transform operation. Then the continuous sifted key at Bob is also operated by normalization and the same rotation above. A virtual binary additive white Gaussian-like channel between Alice and Bob is established. In the second component, a specific decoding scheme with side information for Polar codes is presented, where the frozen bits locations are used as the reconciliation information. Simulation results show that the bit error rate performance and the efficiency of the proposed protocol are improved.

**Keywords:** Multidimensional Reconciliation, Continuous Variable Quantum Key Distribution, Polar Code

## 1 Introduction

Quantum key distribution (QKD) allows two remote parties (Alice and Bob) to share a secret key, even in the presence of an eavesdropper (Eve) with unlimited computational power [1]. Continuous-variable quantum key distribution (CVQKD) [2] attracts a lot of attention recently for its high rate of key generation and no limitations of single photon source and single photon detectors. But the quantum channel for the CVQKD system is not perfect one, the errors in the secret key is unavoidable. Moreover, the CVQKD quantum transmission process can only provide continuously distributed raw keys [3], they have been converted to binary ones. Thus, a reconciliation protocol [4] is crucial to extract the errorless secret keys in a CVQKD system. Furthermore, a high efficient reconciliation protocol would provide a promising way to achieve the long distance CVQKD protocol at low signal-to-noise ratio (SNR). In this paper, we propose a multidimensional reconciliation protocol for CVQKD using Polar codes. The proposed protocol includes multidimensional reconciliation component and polar coding component. In the multidimensional reconciliation component, the continuous Gaussian variables are normalized and transferred to binary without quantization. In the polar coding component, a novel construction is designed. The numerical simulation shows that the bit error rate performance and the efficiency of the proposed protocol are higher than that protocol in [5] with the same condition.

## 2 Multidimensional Reconciliation Protocol of CVQKD using Polar Codes

Figure 1 shows the schematic diagram of the proposed protocol. There are two components in the proposed protocol. One is multidimensional reconciliation component (named MR), the other is error correction component using polar coding.

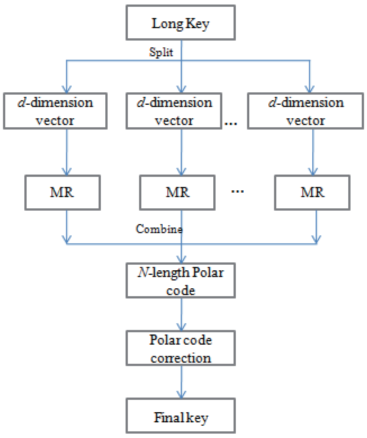

Figure 1: The schematic diagram of Multidimensional Reconciliation protocol using Polar code.

In a CVQKD system, the continuous variable carriers for the key is usually modulated with Gaussian distribution. The raw keys $X$ and $Y$ for Alice and Bob are continuous Gaussian distribution random variables, and it is always assumed that $Y = X + N$, where $N$ is an Additive White Gaussian Noise.

In the multidimensional reconciliation component, Alice and Bob first separately normalize their own raw keys, which are generated from the quantum process. Both Alice and Bob first divide their key variables which generated from the quantum process into a set of shorter ones, $X$ and $Y$, in the size of the dimension $d$, where $Y = X + Z$, $X \sim N(0, \Sigma^2)$ and $Z \sim N(0, \sigma^2)$. Then Alice and Bob normalize their key variables $X$ and $Y$ to get $x$ and $y$ separately. Alice generates a random binary string $u$ as her final key for $x$ and obtains the transformation matrix $\mathbf{M}(x, u)$ with the constraints $\mathbf{M}(x, u)x = u$. She sends the transformation matrix $\mathbf{M}(x, u)$ to Bob. Bob makes the same transformation on his own key information $y$ to get $v$, where $v = \mathbf{M}(x, u)y$. Subsequently, a virtual bi-

*zhaosm@njupt.edu.cn

nary additive white Gaussian-like channel between Bob and Alice is established. Therefore, Alice and Bob hold a pair of key ($u$ and $v$) without quantization, where $u$ is a binary string, and $v$ is a Gaussian distribution. It should be noted that that $v$ is also the error version of $u$, that is $v = u + e$, the final noise $e$ is just a rotated version of the noise $N$ Bob has, in particular, both noises are Gaussian with the same variance. This is true because the Gaussian distribution of the noise is invariant under orthogonal transformations. In Polar coding component, the frozen bits information are used as the side information to correct errors $e$. Alice constructs a Polar code with the code rate $R$ and code length $N$, and shares the frozen bits information to Alice. With the frozen bits information, Bob decodes $v$ with BP decoding algorithm. Finally, they get a pair of common binary key.

## 3 Discussion and Conclusion

In this section, numerical simulation results are presented to discuss the proposed reconciliation protocol. The simulations are done with CPU of Intel Core i5-3230M. For simulation, the dimension $d$ is set to 4. The variance of signal is set to 1. Belief propagation decoding algorithm is adopted for Polar codes. The maximum value for the frame number is set to be 500.

The efficiency is an important parameter for reconciliation protocol, which is defined as,

$$\beta = \frac{D_{eccOutput}}{D_{eccInput}}(1 - FER), \tag{1}$$

where $D_{eccOutput}$ denotes the error-correction output rate, $D_{eccInput}$ denotes for the data output rate of the system used as an input for the error-correction, and $FER$ is frame error rate. The bigger $\beta$ is, the higher efficiency the protocol has.

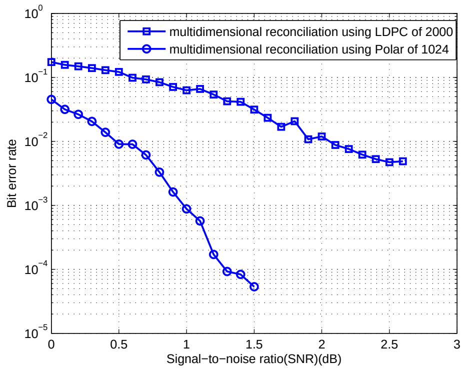

Figure 2: The bit error rate (BER) performance of the proposed reconciliation protocol, together with the BER performance of the protocol in [5].

Fig.2 shows the bit error rate (BER) performance of the proposed reconciliation protocol, together with the BER performance of the protocol in [5]. For the comparison, the code length for Polar code is 1024, the code length for low density parity check (LDPC) code in [5] is set to 2000. The code rate is set to 0.375. The results show that the BER performance of the proposed protocol is better than that using the protocol in [5]. When SNR=1, the BER for the proposed protocol is $10^{-3}$, while it is $5 \times 10^{-1}$ for the protocol in [5]. It is indicated that the proposed reconciliation protocol is better for CVQKD systems.

Table 1: Efficiency of the proposed reconciliation protocol, in comparison with the efficiency with the protocol in [5].

| SNR | Proposed protocol | Protocol in [5] |
|---|---|---|
| 0.8 | 63.75 | 49.54 |
| 0.9 | 66.90 | 57.60 |
| 1.0 | 73.16 | 62.22 |
| 1.1 | 78.16 | 64.00 |

Table 1 further presents the efficiency of the proposed reconciliation protocol, in comparison with the efficiency with the protocol in [5]. The results show that the efficiency of the proposed protocol is higher than that using protocol in [5]. Although the proposed reconciliation protocol with code length of 1024 and code rate of 0.375 doesnt get the required efficiency, the length of practical key in CVQKD is much longer than 1024. It is believable that the efficiency of the proposed protocol can be up to 90% because the performance of Polar code is increasingly improved with a longer code length at low SNRs.

In this paper, we have presented a protocol of multi-dimensional reconciliation using Polar codes for CVQKD system. It has been shown that the protocol can correct the error without the need to discrete the continuous variable, it can be implemented only by constructing a special kind of side information. It is more adaptable for a long distance CVQKD system.

## References

[1] P. Jouguet. High performance error correction for quantum key distribution using polar codes. *Quantum Inf. Comput.*, 14, 329-338, 2014.

[2] A. Leverrier, P. Grangier. Unconditional security proof of long -distance continuous-variable quantum key distribution with discrete modulation. *Phys. Rev. Lett.*, 102, 180504, 2009.

[3] P. Jouguet. Long-distance continuous-variable quantum key distribution with a Gaussian modulation. *Phys. Rev. A*, 84, 062317, 2011.

[4] F. Grosshans, V. A. Gilles, W. Jerome, et al. Quantum key distribution using gaussian-modulated coherent states. *Nature*, 421, 238-241, 2003.

[5] A. Leverrier, R. Alleaume, J. Boutros, et. al. Multidimensional reconciliation for a continuous-variable quantum key distribution. *Phys. Rev. A*, 77, 042325, 2008.

# ABC's of bosonic non-Gaussian channels: photon-added Gaussian channels

Krishna Kumar Sabapathy[1, *]

[1] *Física Teòrica: Informació i Fenòmens Quàntics,*
*Universitat Autònoma de Barcelona, ES-08193 Bellaterra (Barcelona), Spain.*

We present a framework for systematically studying linear bosonic non-Gaussian channels. A strong motivation being that it is compulsory to go beyond the Gaussian regime for numerous tasks in continuous-variable quantum information protocols. Our emphasis is on a class of channels that we call photon-added Gaussian channels and these are experimentally viable with current quantum-optical technologies. These channels are obtained by extending Gaussian channels with photon addition applied to the ancilla ports (in its respective Stinespring unitary representation) giving rise to a one-parameter family of non-Gaussian channels indexed by photon number $n \geq 1$ with $n = 0$ corresponding to the underlying Gaussian channel. We then derive the corresponding operator-sum representation which becomes indispensable since the phase-space framework has limited usefulness in the present context. We observe that these channels are Fock-preserving, i.e., coherence non-generating on incoherent states in the Fock basis. Furthermore, noisy Gaussian channels can be expressed as a convex mixture of these non-Gaussian channels analogous to the Fock basis representation of a thermal state. We then report examples of activation of nonclassicality, using this method of photon-addition, at outputs of channels that would otherwise output only classical states, and present a classicality no-go theorem. We also derive many structure theorems for these channels. Finally, we observe that there exists an environment-assisted error-correction scheme for transmitting classical information through these channels.

**Keywords:** non-Gaussianity, non-Gaussian channels, photon-addition, Gaussian channels, Stinespring dilation, continuous-variable systems

Non-Gaussian states and operations have recently received much attention with respect to theoretical and experimental schemes in continuous-variable quantum information theory. Commonly used non-Gaussian operations include photon addition [1, 2], photon subtraction [3–5], photon counting [6], cubic phase gates[7], and Kerr nonlinearities [8]. Experimentally realizable non-Gaussian states include Fock states [9–11], noon states [12], cat states [13, 14], and photon-added coherent states [15, 16], among other examples [17–19].

There are various motivations and uses for going beyond the Gaussian regime for implementing quantum information protocols. These include no-go theorems against Gaussian-

[*] Electronic address: `krishnakumar.sabapathy@gmail.com`

Photon-addition (environment)
+
Gaussian channels
=
Photon-added Gaussian channels

FIG. 1: Showing a schematic diagram for the construction of a class of non-Gaussian channels by using two constituent elements of photon-addition and bosonic Gaussian channels.

only toolbox like distillation of entanglement from Gaussian states [20–22], use as quantum repeaters [23], and for other quantum information protocols like cloning [24], error-correction [25], bit-commitment [26], and computing with cluster states [27], to list a few examples. Also non-Gaussian resources have proven advantageous in many scenarios like parameter estimation [28], generation of entangled states [29–32], teleportation [33–35], and universal quantum computation [36–38].

In this article we generate non-Gaussian operations using two main ingredients, the commonly used photon-addition and the ubiquitous class of bosonic Gaussian channels[39]. We call the resulting non-Gaussian operations as photon-added Gaussian channels and this is schematically represented in Fig. 1. Here the photon-addition will be applied to the environment state in the Stinespring dilation of the underlying Gaussian channel. As a consequence we generate non-Gaussian operations on the initial system when the environment system is ignored.

The method can also be thought of as being one example of the many protocols and implementations which concern manipulating the environment state in the Stinespring representation of a channel that have been considered in literature. Some illustrative examples include implementation of general gates [40], using mixed environment states for channel simulation [41], manipulating the environment to generate additional capacities either as a helper or adversary [42–44], and using feedback from the environment to correct for transmission of information through the channel [45–47].

## I. SUMMARY OF MAIN RESULTS

Our main contribution is to formulate and present a systematic framework to study non-Gaussian channels. We focus on a special class of channels we call as photon-added Gaussian channels. These channels are realized by extending quantum-limited Gaussian channels with photon-addition applied to the environment state in the Stinespring dilation of these channels. The resulting channels are linear and non-Gaussian in nature. We consider the case of photon-added attenuator, amplifier, and phase conjugator as our main examples.

We then obtain the operator-sum representation[39] of the photon-added channels and study various implications. We find that for each of the three families of channels there exists an operator-sum representation in which the Kraus operators are real. Furthermore, the positive quadratic operators associated with the Kraus operators can all be taken to be simultaneously diagonal in the Fock basis. This allows for environment-assisted classical information transmission through these channels.

We derive a series of structure theorems for these channels. The photon-added amplifier, attenuator, and phase-conjugation channels take incoherent states in the Fock basis to incoherent states showing that they belong to the class of the so-called maximally incoherent operations from a resource-theoretic point of view for coherence in the Fock basis. We also see that the photon-added channels are complementary to the photon-added amplifier channels leading to a trivial implication on the minimum output entropy for these channels.

We show that the output nonclassicality of the phase conjugation channel can be activated by a non-trivial photon-addition leading to a classicality no-go theorem concerning the nonclassicality-breaking nature of the channel [48–50]. We also provide a decomposition of noisy Gaussian channels in terms of their respective photon-added quantum-limited channels analogous to the Fock basis representation of a thermal state.

The present study is one approach contributing to the systematic study of non-Gaussian operations that have not only proved advantageous for many quantum information protocols but are also necessary due to many Gaussian no-go theorems as mentioned earlier. The non-Gaussian channels that we introduce are arguably the simplest class of channels that go beyond the Gaussian scenario.

Furthermore, our method allows for tuning between the Gaussian and non-Gaussian regime in the space of channels through photon-addition where $n$ plays the role of the tuning parameter, with $n = 0$ corresponding to a Gaussian channel and $n > 0$ corresponding to a non-Gaussian channel. Also the photon-added channels considered in the article [51] are experimentally realizable. We believe that there are many applications of the present work in light of the increasing use of non-Gaussian resources in continuous-variable quantum computing, cryptography, and communications tasks.

For technical details please refer **arXiv:1604.07859 [quant-ph]** [51].

[1] V. Parigi, A. Zavatta, M. S. Kim, and M. Bellini, Probing quantum commutation rules by addition and subtraction of single photons to/from a light field, Science **317**, 1890 (2007).

[2] J. Fiurášek, Engineering quantum operations on traveling light beams by multiple photon addition and subtraction, Phys. Rev. A **80**, 052822 (2009).

[3] A. Kitagawa, M. Takeoka, M. Sasaki, and A. Chefles, Entanglement evaluation of non-Gaussian states generated by photon subtraction from squeezed states, Phys. Rev. A **73**, 042310 (2006).

[4] N. Namekata, Y. Takahashi, G. Fujii, D. Fukuda, S. Kurimura and S. Inoue, Non-Gaussian operation based on photon subtraction using a photon-number-resolving detector at a telecommunications wavelength, Nat. Photonics **4**, 655 (2010).

[5] K. Wakui, H. Takahashi, A. Furusawa, and M. Sasaki, Photon subtracted squeezed states generated with periodically poled $KTiOPO_4$, Opt. Exp. **15**, 3568 (2007).

[6] C. Guerlin et. al., Progressive field-state collapse and quantum non-demolition photon counting, Nature **448**, 889 (2007).

[7] K. Miyata et. al., Implementation of a quantum cubic gate by an adaptive non-Gaussian measurement, Phys. Rev. A **93**, 022301 (2016).

[8] T. Tyc and N. Korolkova, Highly non-Gaussian states created via cross-Kerr nonlinearity, New J. Phys. **10**, 023041 (2008).

[9] M. Hofheinz et. al., Generation of Fock states in a superconducting quantum circuit, Nature **454**, 310 (2008).

[10] C. Sayrin et. al., Real-time quantum feedback prepares and stabilizes photon number states, Nature **477**, 73 (2011).

[11] K. R. Motes et. al., Efficient recycling strategies for preparing large Fock states from single-photon sources — Applications to quantum metrology, arXiv:1603.00533[quant-ph].

[12] I. Afek, O. Ambar, and Y. Silberberg, High-NOON states by mixing quantum and classical light, Science **328**, 879 (2010).

[13] M. Sasaki and M. Suzuki, Multimode theory of measurement-induced non-Gaussian operation on wideband squeezed light: Analytical formula, Phys. Rev. A **73**, 043807 (2006).

[14] A, Ourjoumtsev, H. Jeong, R. Tualle-Brouri, and P. Grangier, Generation of optical 'Schrödinger cats' from photon number states, Nature **448**, 784 (2007).

[15] G. S. Agarwal and K. Tara, Nonclassical properties of states generated by the excitations on a coherent state, Phys. Rev. A **43**, 492 (1991).

[16] A. Zavatta, S. Viciani, and M. Bellini, Quantum-to-Classical Transition with Single-Photon-Added Coherent States of Light, Science **306**, 660 (2004).

[17] J. Wenger, R. Tualle-Brouri, and P. Grangier, Non-Gaussian Statistics from Individual Pulses of Squeezed Light, Phys. Rev. Lett. **92**, 153601 (2004).

[18] J. S. Neergaard-Nielsen, B. M. Nielsen, C. Hettich, K. Mølmer, and E. S. Polzik, Generation of a Superposition of Odd Photon Number States for Quantum Information Networks, Phys. Rev. Lett. **97**, 083604 (2006).

[19] J. Stanojevic et. al., Generating non-Gaussian states using collisions between Rydberg polaritons, Phys. Rev. A **86**, 021403(R) (2012).

[20] J. Eisert, S. Scheel, and M. B. Plenio, Distilling Gaussian states with Gaussian operations is impossible, Phys. Rev. Lett. **89**, 137903 (2002).

[21] J. Fiurášek, Gaussian transformations and distillation of entangled Gaussian states, Phys. Rev. Lett. **89**, 137904 (2002).

[22] G. Giedke and J. I. Cirac, Characterization of Gaussian operations and distillation of Gaussian states, Phys. Rev. A **66**, 032316 (2002).

[23] R. Namiki, O. Gittsovich, S. Guha, and N. Lütkenhaus, Gaussian-only regenerative stations cannot act as quantum repeaters, Phys. Rev. A **90**, 062316 (2014).

[24] N. J. Cerf, O. Krüger, P. Navez, R. F. Werner, and M. M. Wolf, Non-Gaussian Cloning of Quantum Coherent States is Optimal, Phys. Rev. Lett. **95**, 070501 (2005).

[25] J. Niset, J. Fiurášek, and N. J. Cerf, No-Go Theorem for Gaussian Quantum Error Correction, Phys. Rev. Lett. **102**, 120501 (2009).

[26] L. Magnin, F. Magniez, A. Leverrier, and N. J. Cerf, Strong no-go theorem for Gaussian quantum bit commitment, Phys. Rev. A **81**, 010302(R) (2010).

[27] M. Ohliger, K. Kieling, and J. Eisert, Limitations of quantum computing with Gaussian cluster states, Phys. Rev. A **82**, 042336 (2010).

[28] G. Adesso, F. Dell'Anno, S. De Siena, F. Illuminati, and L. A. M. Souza, Optimal estimation of losses at the ultimate quantum limit with non-Gaussian states, Phys. Rev. A **79**, 040305(R) (2009).

[29] A. Ourjoumtsev, A. Dantan, R. Tualle-Brouri, and P. Grangier, Increasing Entanglement between Gaussian States by Coherent Photon Subtraction, Phys. Rev. Lett. **98**, 030502 (2007).

[30] H. Yakahashi, J. S. Neergaard-Nielsen, M. Takeuchi, M. Takeoka, K. Hayasaka, A. Furusawa, and M. Sasaki, Entanglement distillation from Gaussian input states, Nat. Photonics **4**, 178 (2010).

[31] K. K. Sabapathy, J. S. Ivan, and R. Simon, Robustness of Non-Gaussian Entanglement against Noisy Amplifier and Attenuator Environments, Phys. Rev. Lett. **107**, 130501 (2011).

[32] C. Navarrete-Benlloch, R. García-Patrón, J. H. Shapiro, and N. J. Cerf, Enhancing quantum entanglement by photon addition and subtraction, Phys. Rev. A **86**, 012328 (2012).

[33] S. Olivares, M. G. A. Paris, and R. Bonifacio, Teleportation improvement by inconclusive photon subtraction, Phys. Rev. A **67**, 032314 (2003).

[34] T. Opatrný, G. Kurizki, and D.-G. Welsch, Improvement on teleportation of continuous variables by photon subtraction via conditional measurement, Phys. Rev. A **61**, 032302 (2000).

[35] F. Dell'Anno, S. De Siena, L. Albano, and F. Illuminati, Continuous-variable quantum teleportation with non-Gaussian resources, Phys. Rev. A **76**, 022301 (2007).

[36] S. Lloyd and S. L. Braunstein, Quantum Computation over Continuous Variables, prl **82**, 1784 (1999).

[37] S. D. Bartlett and B. C. Sanders, Universal continuous-variable quantum computation: Requirement of optical nonlinearity for photon counting, Phys. Rev. A **65**, 042304 (2002).

[38] N. C. Menicucci *et al.*, Universal Quantum Computation with Continuous-Variable Cluster States, Phys. Rev. Lett. **97**, 110501 (2006).

[39] J. S. Ivan, K. K. Sabapathy, and R. Simon, Operator-sum representation for bosonic Gaussian channels, Phys. Rev. A **84**, 042311 (2011).

[40] S. Ghose and B. C. Sanders, Non-Gaussian ancilla states for continuous variable quantum computation via Gaussian maps, J. Mod. Opt. **54**, 855 (2007).

[41] B. M. Terhal, I. L. Chuang, D. P. DiVincenzo, M. Grassl, and J. A. Smolin, Simulating quantum operations with mixed environments, Phys. Rev. A **60**, 881 (1999).

[42] S. Karumanchi, S. Mancini, A. Winter, and D. Yang, Quantum Channel Capacities with Passive Environment Assistance, IEEE Trans. Inf. Theory **62**, 1733 (2016).

[43] S. Karumanchi, S. Mancini, A. Winter, and D. Yang, Classical capacities of quantum channels with environment assistance, arXiv:1602.02036 [quant-ph].

[44] J. A. Smolin, F. Verstraete, A. Winter, Entanglement of assistance and multipartite state distillation, Phys. Rev. A **72**, 052317, 2005.

[45] M. Gregoratti and R. F. Werner, Quantum lost and found, J. Mod. Opt. **50**, 915 (2003).

[46] M. Gregoratti and R. F. Werner, On quantum error-correction by classical feedback in discrete time, J. Math. Phys. **45**, 2600 (2004).

[47] P. Hayden and C. King, Correcting quantum channels by measuring the environment, Quantum Inf. Comput. **5**, 156 (2005).

[48] J. S. Ivan, K. K. Sabapathy, R. Simon, Nonclassicality breaking is the same as entanglement breaking for bosonic Gaussian channels, Phys. Rev. A **88**, 032302 (2013).

[49] K. K. Sabapathy, Quantum-optical channels that output only classical states, Phys. Rev. A **92**, 052301 (2015).

[50] K. K. Sabapathy, Process output nonclassicality and nonclassicality depth of quantum-optical channels, Phys. Rev. A **93**, 042103 (2016).

[51] K. K. Sabapathy, On bosonic non-Gaussian processes: photon-added Gaussian channels, arXiv:1604.07859 [quant-ph].

# An explicit classical strategy for winning a $\mathrm{CHSH}_q$ game

Martin Plesch *[1] [2]  Matej Pivoluska †[1] [2]

[1] *Faculty of Informatics, Masaryk University, Botanická 68a, 602 00 Brno, Czech Republic*
[2] *Institute of Physics, Slovak Academy of Sciences, Bratislava, Slovakia*

**Abstract.** A $\mathrm{CHSH}_q$ game is a generalization of the standard two player CHSH game, having $q$ different input and output options. In contrast to the binary game, the best classical and quantum winning strategies are not known exactly. In our work [8] we provide a constructive classical strategy for winning a $\mathrm{CHSH}_q$ game, with $q$ being a prime. Our construction achieves a winning probability better than $\frac{1}{22}q^{-\frac{2}{3}}$, which is in contrast with the previously known constructive strategies achieving only the winning probability of $O(q^{-1})$.

**Keywords:** Non-locality, CHSH game

## 1 Introduction

Non-locality is one of the defining features of quantum mechanics qualitatively differentiating it from classical physics [4]. Apart from its foundational importance, scientists have recently realized that quantum non-locality is also an extremely valuable resource enabling various tasks, such as quantum key distribution [1] or randomness expansion and amplification [9]. All these applications use a unifying feature of quantum mechanics – namely its possibility to provide the experimentalist results that exhibit super-classical correlations. Measurements on distant parts of a quantum system can, if performed in a specific way, produce results that are not reproducible by any classical system, even with the help of pre-shared information. Since the seminal work of Bell [3], who first realized this fact, a long line of research was devoted both to experimental realization of different tests of quantumness and its theoretical implications.

Arguably the simplest and most studied generalization of the original Bell setting is the Clauser-Horne-Shimony-Holt (CHSH) setting [5], where two experimentalists choose one out of two possible binary measurements on their part of the system. The setting can be rephrased into a language of games, where two non-communicating players, Alice and Bob, both receive a uniformly chosen single bit input $x$ and $y$ respectively and their goal is to produce single bit outputs $a$ and $b$, such that $a + b \equiv xy \mod 2$ (see Fig. 1a).

It is well known that classical players can win this game with probability no more than 75%. Utilizing quantum mechanics, players can share a maximally entangled state of two qubits and perform a suitable measurement (dependent on the input) on their respective qubit. In such a way they can increase the probability of wining the game up to $\frac{2+\sqrt{2}}{4} \approx 85\%$.

A straightforward generalization is a $\mathrm{CHSH}_q$ game, where the dimensionality of both inputs and outputs is limited to a prime $q$ (see Fig. 1b). In this case, the winning condition states $a + b \equiv xy \mod q$. However, in order for this game to be interesting, the probability of winning the game with a quantum strategy must be higher than the probability with purely classical systems. Therefore, bounds for these probabilities are of utmost importance for its possible use.

Contrary to the binary CHSH game, neither the exact value of the probability of winning the game with a quantum strategy $\omega^*(\mathrm{CHSH}_q)$, nor a strategy obtaining the optimal value is known. The only existing result due to [2] introduces an upper bound for the quantum probability

$$\omega^*(\mathrm{CHSH}_q) \leq \frac{1}{q} + \frac{q-1}{q}\frac{1}{\sqrt{q}} = \frac{1}{\sqrt{q}} + \frac{1}{q} - \frac{1}{q\sqrt{q}}.$$

For classical strategies [2], there exists an upper bound in the form

$$\omega(\mathrm{CHSH}_q) = \ O\left(q^{-\frac{1}{2}-\varepsilon}\right) \qquad \text{for } q = p^{2k+1},$$

where $p$ is a prime, $k \geq 1$ and $\varepsilon > 0$ is a constant. It is only valid for the case of an odd prime power, but still could serve for a proof of a classical – quantum gap if the quantum bound would be proven tight.

There also exists a set of lower bounds (also proven in [2]) in the form

$$\omega(\mathrm{CHSH}_q) = \begin{cases} \Omega\left(q^{-\frac{1}{2}}\right) & \text{for } q = p^{2k} \\ \Omega\left(q^{-\frac{2}{3}}\right) & \text{for } q = p^{2k+1} \end{cases}.$$

We see that for $q$ being an even power prime the lower bound is higher than for odd powers and thus for all values of $q$ there is a significant gap between the lower or upper (partly non-existent) bounds.

Even more importantly and perhaps surprisingly, these lower bounds are not connected with any concrete strategy. Quantum strategies existing so far are limited to different heuristics (*e.g.* trying to maximize the winning probability over all measurements of the maximally entangled bipartite state), random searches and numerics [6, 7]. Best known classical strategies so far obtained only $\omega(\mathrm{CHSH}_q) = \Omega\left(\frac{1}{q}\right)$ [7], which corresponds to a trivial strategy (both Alice and Bob output 0 irrespective on

*plesch@savba.sk
†mpivoluska@mail.muni.cz

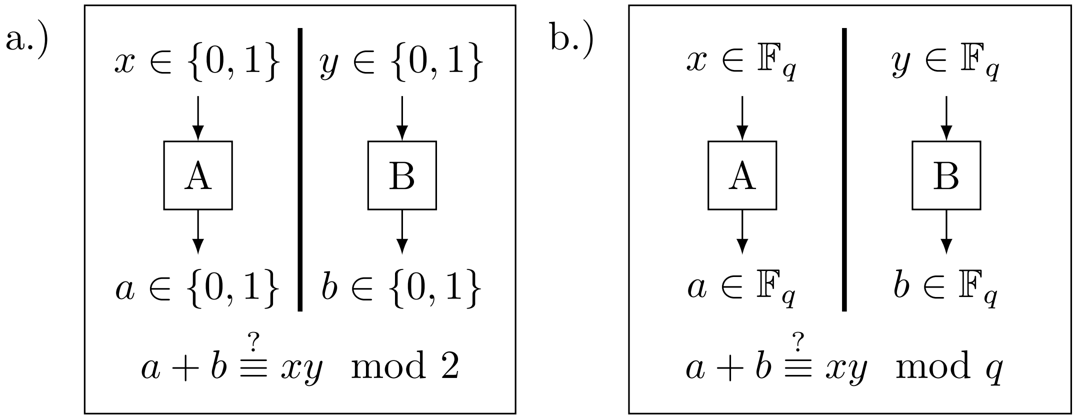

Figure 1: a.) Two non-communicating players Alice ($A$) and Bob ($B$) get one bit inputs $x$ and $y$ each, chosen at random. Their goal is to produce two outputs $a$ and $b$ such that $a + b \equiv xy \mod 2$. b.) The same situation with inputs $x$ and $y$ chosen at random from a finite field $\mathbb{F}_q$ with prime $q$. Goal of the players it to produce two outputs $a, b \in \mathbb{F}_q$ respectively, such that $a + b \equiv xy \mod q$.

their input and win if either $x = 0$ or $y = 0$, thus in $2q - 1$ out of $q^2$ cases).

In our paper [8] we presented the first constructive classical strategy for the CHSH$_q$ game with the probability of winning $\Omega\left(q^{-\frac{2}{3}}\right)$ for $q$ being a prime. With this strategy we close the gap between constructive strategies and existence bounds. To be able to prove this result, we first related the problem of classical CHSH$_q$ game strategies to a well-known problem of point-line incidences. Doing that we were able to construct an explicit strategy for winning a generalized CHSH$_q$ game with a winning probability lower bounded by $\frac{p^{-2/3}}{22}$, what perfectly mimics the non-constructive existence bound known so far.

This result is useful for potential design of device independent algorithms based on higher alphabet CHSH games in different aspects. First, it closes the gap between existing explicit strategies and proven existence bounds, which helps the understanding of the nature of the problem. Second, and most importantly, the presented result provides the first non-trivial classical strategy for a CHSH game, where Alice and Bob need to act in a way that depends on their input and their output is a result of a non-trivial calculation.

There is also a set of open questions that remain. The obvious one is, how one could generalize the result presented in this paper for prime power fields. This is not easy, as the nature of the proof relays on the relation between addition and multiplication, which is unique for prime fields. Also the fact that known existence bounds crucially depend on whether they are deployed on even or odd power prime field suggests that any possible generalization will not be straightforward.

More ambitious goals include the aim of finding tight bounds on classical strategies. This might, in accordance with suitable heuristic results for quantum strategies, lead to the possibility of direct use of higher-order CHSH$_q$ games in experiments. The ultimate goal, naturally, remains to directly prove a gap between classical and quantum strategies.

## References

[1] A. Acín, *et. al.* Device-independent security of quantum cryptography against collective attacks. *Phys. Rev. Lett.*, 98:230501, 2007.

[2] M. Bavarian and P. W. Shor. Information causality, szemerédi-trotter and algebraic variants of chsh. ITCS '15, pages 123–132, New York, NY, USA, 2015. ACM.

[3] John S. Bell. On the Einstein-Podolsky-Rosen paradox. *Physics*, 1:195–200, 1964.

[4] N. Brunner,*et. al.* Bell nonlocality. *Rev. Mod. Phys.*, 86:419–478, Apr 2014.

[5] John F. Clauser, *et. al.* Proposed experiment to test local hidden-variable theories. *Phys. Rev. Lett.*, 23:880–884, Oct 1969.

[6] Se-Wan Ji, *et. al.* Multisetting bell inequality for qudits. *Phys. Rev. A*, 78:052103, Nov 2008.

[7] Y.-C. Liang, C.-W. Lim, and D.-L. Deng. Reexamination of a multisetting bell inequality for qudits. *Phys. Rev. A*, 80:052116, Nov 2009.

[8] M. Pivoluska and M. Plesch. An explicit classical strategy for winning a *chsh*$_q$ game. *New Journal of Physics*, 18, 2016.

[9] M. Pivoluska and M. Plesch. Device independent random number generation. *Acta Physica Slovaca*, 64(6):600 – 663, 2014.

# Cache-Aware Quantum Circuit Simulation on a GPGPU

Masaki Nakanishi[1] * Naohiro Morioka[1] † Kenta Shoji[1] ‡

[1] *Department of Education, Art and Science, Yamagata University, Yamagata 990–8560, Japan*

**Abstract.** Quantum computer simulators play an important role when we develop and evaluate quantum algorithms. Quantum computation can be regarded as parallel computation in some sense, and thus, it is suitable to implement a simulator on a device that can process many operations in parallel. In this research, we propose a GPGPU-based quantum computer simulator. The proposed simulator recursively decomposes the state space so that the sizes of the subspaces will fit the sizes of hierarchical caches. This makes cache hit rates higher. We also developed the method that can avoid bank conflicts. We implemented the proposed simulator on an NVIDIA GeForce GTX 970. Experimental results show that the proposed simulator has better performance.

**Keywords:** quantum circuit simulation, GPGPU, cache-aware simulation

## 1 Introduction

Development of quantum algorithms is a difficult task and sometimes needs analysis based on simulation as well as theoretical analysis. For this purpose, simulation of quantum computers is highly demanded. However, simulation of quantum computers is a time-consuming task, and thus, various kinds of simulation methods have been investigated intensively[1, 2, 3, 4, 5, 6, 7, 8, 9, 10, 11, 12, 13, 14].

Since quantum computation is parallel computation in some sense, which is called *quantum parallelism*, it is suitable to implement simulators on parallel computation devices such as GPGPUs, many-core CPUs, and ASICs. In this research, we focus on simulators on GPGPUs. In [5], a GPGPU-based simulator was proposed. The simulator is designed so that it can access data in a coalesced manner since coalesced memory access is crucial for high performance in GPGPU computing. The simulator generates coalesced access patterns by decomposing the state space into subspaces so that each subspace may have consecutive computational basis vectors as its basis.

In GPGPU computing, memory access often becomes a bottleneck, and so is the case of quantum circuit simulation. Thus, reducing memory access overhead is the main concern in this research field. One of the solutions for this problem is to make efficient use of L2-cache. A GPGPU has an L2-cache between shared memory and global memory, and by achieving high L2-cache hit rate we can improve the performance of the simulator. In GPGPU computing, shared memory is used as a user-controllable cache. Shared memory is divided into memory banks. Data stored in different banks can be accessed in parallel. On the other hand, data stored in the same bank must be accessed sequentially, which is called a bank conflict. Thus, generating memory access patterns that avoids bank conflicts also improves the performance.

In this research, we extended the method in [5] and developed a GPGPU-based quantum circuit simulator that achieves high L2-cache hit rate. We also developed a method that can avoid bank conflicts in shared memory. We implemented our simulator on an NVIDIA GeForce GTX 970. Experimental results show that the proposed simulator has better performance.

## 2 GPGPU Programming Model

The programming model of the target GPGPU is so-called SIMT (Single Instruction, Multiple Thread) model. A bunch of threads (32 threads for our target architecture), called a *warp*, executes the same instruction on different data. Threads are grouped into *thread-blocks*. Threads in a thread-block share on-chip shared memory. The shared memory can be used to communicate between threads in the same thread-block. On the other hand, communication across thread-blocks needs to transfer data to the off-chip global memory. The global memory has an L2-cache, and the L2-cache can be used to boost inter-block communication. The shared memory can be used as a user-controllable L1-cache. Thus, the shared memory together with the L2-cache forms a hierarchical cache architecture.

## 3 Cache-Aware Quantum Circuit Simulation

We use the linearity of matrix-vector multiplication to simulate quantum gates efficiently, which is commonly used in quantum circuit simulations[5, 7, 8, 12]. Let $Q = \{q_0, \ldots, q_{n-1}\}$ be a set of qubits, and also let $v = (\alpha_0, \ldots, \alpha_{2^n-1})^T$ be a state vector of the $n$-qubit system. For $m < n$, we divide $Q$ into two disjoint subsets, $S_1 = \{q_{i_1}, \ldots, q_{i_m}\}$, $S_2 = \{q_{j_1}, \ldots, q_{j_{n-m}}\}$ where $i_1 < \cdots < i_m$ and $j_1 < \cdots < j_{n-m}$. We fix the values of the qubits in $S_2$ as $x_{j_1}, x_{j_2}, \ldots, x_{j_{n-m}}$ ($x_{j_k} \in \{0, 1\}$), respectively. Then, $v_{x_{j_1}x_{j_2}\cdots x_{j_{n-m}}}$ denotes the projection of $v$ onto the subspace where the qubits in $S_2$ are fixed to $x_{j_1}x_{j_2}\cdots x_{j_{n-m}}$. Note that the following holds:

$$\sum_{x_{j_1}x_{j_2}\cdots x_{j_{n-m}}=00\cdots0}^{11\cdots1} v_{x_{j_1}x_{j_2}\cdots x_{j_{n-m}}} = v, \text{ and}$$

$$v_x \cdot v_y = 0 \text{ for } x \neq y (x, y \in \{0,1\}^{n-m}).$$

[*] masaki@cs.e.yamagata-u.ac.jp

[†] n-morioka@cs.e.yamagata-u.ac.jp

[‡] k-shoji@cs.e.yamagata-u.ac.jp

We consider a sequence of quantum gates, $(g_1, g_2, \ldots, g_k)$. We restrict each of $g_i$'s to be a one-qubit gate or a controlled-unitary gate. We identify each of the quantum gates $g_i$ with the corresponding transformation. Then by linearity, the following holds:

$$g_k \circ \cdots \circ g_2 \circ g_1(v) = \sum_i g_k \circ \cdots \circ g_2 \circ g_1(v_i),$$

where $g_j \circ g_i$ is a composite transformation of $g_i$ and $g_j$. This means that we may apply quantum gates to each $v_i$ independently, and then sum up the resulting vectors $v'_i = g_k \circ \cdots \circ g_2 \circ g_1(v_i)$ $(0 \leq i < 2^{n-m})$ to obtain a complete result. Note that if the target bits of $g_j$'s $(1 \leq j \leq k)$ are placed on the qubits in $S_1$, $v'_i$ is in the same subspace as $v_i$.

In order to make L2-cache hit rate higher, we apply the above method recursively. That is, we decompose the state space into subspaces whose size fits in the L2-cache. Then, we recursively decompose each of the subspaces into smaller subspaces whose size fits in the shared memory. Then, by simulating quantum gate operations within each subspace, we can achieve high memory access locality. The simulation can be done for each subspace one by one. However, in order to achieve high memory access locality for L2-cache, it is needed to appropriately schedule the order of the subspaces to be simulated. The proposed method does this without spoiling the parallel computation of a GPGPU.

## 4 Avoiding Bank Conflicts

When simulating a quantum gate sequence for a subspace, the amplitudes of the basis vectors that lies in the target subspace are in the shared memory. Let the number of memory banks be $2^k$. Also, let the shared memory have amplitudes of the basis vectors $|00\ldots0\rangle, \ldots, |11\ldots1\rangle$ where the amplitude of $|x\rangle$ is stored at address $x$. When simulating a quantum gate whose target bit is on the $i$-th qubit, each thread fetches from the shared memory a pair of amplitudes whose corresponding computational basis state differs only on the $i$-th bit. When $i \leq k$, the $j$-th thread and the $(j + 2^{k-1})$-th thread access to the same bank, which causes a bank conflict.

To avoid the bank conflict, we modified the access patterns so that the $(j + 2^{k-1})$-th thread may access to the other amplitude of the pair first. By this, the $j$-th to the $(j + 2^k - 1)$-th threads access to mutually distinct banks, and we can improve memory access performance.

## 5 Implementation and Experiments

We implemented our method on an NVIDIA GeForce GTX 970. The CUDA runtime version used for the implementation is 7.0. We used 25-qubit quantum circuits as benchmarks. The experimental results show that the proposed method can achieve from 4.3% to 10% improvement of the performance.

**Acknowledgement.** This work was partially supported by JSPS KAKENHI Grant Numbers 16K00007, 24500003 and 24106009, and also by the Asahi Glass Foundation.

## References

[1] M. Aminian, M. Saeedi, M.S. Zamani, and M. Sedighi. FPGA-based circuit model emulation of quantum algorithms. In *IEEE Computer Society Annual Symposium on VLSI, ISVLSI '08*, pages 399–404, April 2008.

[2] K. De Raedt, K. Michielsen, H De Raedt, B. Trieu, G. Arnold, M. Richter, Th Lippert, H. Watanabe, and N. Ito. Massively parallel quantum computer simulator. *Computer Physics Communications*, 176(2):121 – 136, 2007.

[3] Michael P. Frank, Uwe H. Meyer-Baese, Irinel Chiorescu, Liviu Oniciuc, and Robert A. van Engelen. Space-efficient simulation of quantum computers. In *Proceedings of the 47th Annual Southeast Regional Conference*, ACM-SE 47, pages 83:1–83:6, New York, NY, USA, 2009. ACM.

[4] M. Fujishima. FPGA-based high-speed emulator of quantum computing. In *Proceedings of IEEE International Conference on Field-Programmable Technology, FPT 2003*, pages 21–26, Dec 2003.

[5] Eladio Gutiérrez, Sergio Romero, María A. Trenas, and Emilio L. Zapata. Quantum computer simulation using the CUDA programming model. *Computer Physics Communications*, 181(2):283–300, 2010.

[6] A.U. Khalid, Z. Zilic, and K. Radecka. FPGA emulation of quantum circuits. In *Proceedings of IEEE International Conference on Computer Design: VLSI in Computers and Processors, ICCD 2004.*, pages 310–315, Oct 2004.

[7] Masaki Nakanishi, Miki Matsuyama, and Yumi Yokoo. A fast quantum computer simulator based on register reordering. *IEICE Trans. Inf. & Syst.*, E99-D(2):332–340, 2016.

[8] Jumpei Niwa, Keiji Matsumoto, and Hiroshi Imai. General-purpose parallel simulator for quantum computing. In *Proceedings of the Third International Conference on Unconventional Models of Computation, UMC '02*, pages 230–251, 2002.

[9] Kevin M. Obenland and Alvin M. Despain. A parallel quantum computer simulator. quant-ph/9804039, 1998.

[10] S. O'uchi, M. Fujishima, and K. Hoh. An 8-qubit quantum-circuit processor. In *Proceedings of IEEE International Symposium on Circuits and Systems, ISCAS 2002.*, pages 209–212, 2002.

[11] G. Patz. *A parallel environment for simulating quantum computation.* PhD thesis, MIT, 2003.

[12] A. Shibata, T. Nakada, M. Nakanishi, S. Yamashita, and Y. Nakashima. A method of reducing communication costs for parallel simulations of quantum computation. *IEICE Transactions on Information and Systems (Japanese Edition)*, 93(3):253–264, mar 2010.

[13] Frank Tabakin and Bruno Juliá-Díaz. Qcmpi: A parallel environment for quantum computing. *Computer Physics Communications*, 180(6):948 – 964, 2009.

[14] George F. Viamontes, Igor L. Markov, and John P. Hayes. Graph-based simulation of quantum computation in the density matrix representation. *Quantum Info. Comput.*, 5(2):113–130, March 2005.

# Clauser-Horne Bell test with imperfect random inputs

Xiao Yuan[1] Qi Zhao[1] Xiongfeng Ma[1] *

[1] *Center for Quantum Information, Institute for Interdisciplinary Information Sciences, Tsinghua University, Beijing 100084, China*

**Abstract.** Bell test is one of the most important tools in quantum information science. In practice, loopholes existing in experimental demonstrations of Bell tests may affect the validity of the conclusions. In this work, we focus on the randomness (freewill) loophole and investigate the randomness requirement in a well-known Bell test, the Clauser-Horne test, under various conditions. Our result thus provides input randomness requirements on the Clauser-Horne test under varieties of practical scenarios. The employed analysis technique can also be generalized to other Bell inequalities.

**Keywords:** Bell test, Clauser-Horne test, randomness (freewill) loophole

## 1 Introduction

Since the inception of quantum mechanics, whether the law of nature is deterministic or truly random has been long debated.During this debate, Einstein, Podolsky, and Rosen (EPR) proposed a paradox [1] that eventually leaded to a counterintuitive phenomenon — quantum nonlocality. Later, Bell put the EPR paradox in an experimentally testable framework, known as Bell test [2]. In the bipartite scenario, a Bell test involves two remotely separated parties, Alice and Bob, who receive random inputs $x$ and $y$ and produce outputs $a$ and $b$, respectively. Based on the probability distribution $\tilde{p}_{AB}(a,b|x,y)$ of the outputs conditioned on the inputs, Bell's inequality can be defined by a linear combination of $\tilde{p}_{AB}(a,b|x,y)$ according to

$$J=\sum_{a,b,x,y}\beta_{a,b}^{x,y}\tilde{p}_{AB}(a,b|x,y)\le J_C, \tag{1}$$

where $J_C$ is a bound for all local hidden variable models (LHVMs), meaning that, any LHVM cannot violate any Bell's inequality.

There are three main inherent loopholes. The first one is the locality loophole and the second one is the detection efficiency loophole. These two loopholes can be closed by separating the two parties sufficiently apart with regard to the synchronization precision of different measurements in the tests. Third, the randomness (freewill) loophole refers to the underlying assumption in Bell tests that different measurement settings can be chosen randomly (freely). Generally, a Bell test requires the input of each party to be fully random in order to avoid information leakage between different parties. If there is a local hidden variable that shares information about the random inputs, where in the worst scenario, the inputs are all predetermined such that each party knows exactly the input of the other party, it is possible to violate Bell inequalities just with LHVM strategies. Yet, it is still meaningful to discuss the randomness requirement of Bell tests in a practical scenario. This is especially meaningful when considering a loophole free Bell test [3, 4] and its applications to practical tasks in the presence of an eavesdropper.

## 2 Randomness Requirement

In this work, we consider Bell's inequalities with input settings not chosen fully randomly. That is, the inputs $x$ and $y$ depend on some local hidden variable, denoted as $\lambda$. The input randomness can be quantified by the dependence of the inputs conditioned on $\lambda$. Suppose the inputs $x$ and $y$ are chosen according to *a priori* probability $p(x,y|\lambda)$, the input randomness can be measured by its upper and lower bounds,

$$\begin{aligned}P&=\max_{x,y,\lambda}p(x,y|\lambda),\\ Q&=\min_{x,y,\lambda}p(x,y|\lambda).\end{aligned} \tag{2}$$

When the input settings are determined by $p(x,y|\lambda)$, the observed probability $\tilde{p}_{AB}(a,b|x,y)$ of outputs conditioned on inputs is given by

$$\tilde{p}_{AB}(a,b|x,y)=\frac{\sum_\lambda \tilde{p}_{AB}(a,b|x,y,\lambda)p(x,y|\lambda)q(\lambda)}{p(x,y)}, \tag{3}$$

where $q(\lambda)$ is the priori probability of $\lambda$, $p(x,y)=\sum_\lambda p(x,y|\lambda)q(\lambda)$ is the averaged probability of choosing $x$ and $y$, and $\tilde{p}_{AB}(a,b|x,y,\lambda)$ is the strategy of Alice and Bob conditioned on $\lambda$. Then, the Bell's inequality defined in Eq. (1) should be rephrased by

$$\begin{aligned}J=&\sum_{x,y}\frac{1}{p(x,y)}\sum_\lambda\sum_{a,b}\beta_{a,b}^{x,y}\tilde{p}_{AB}(a,b|x,y,\lambda)p(x,y|\lambda)q(\lambda)\\ &\le J_C.\end{aligned} \tag{4}$$

## 3 CH inequality

In this section, we will investigate the randomness requirement of the CH inequality under different conditions, including whether $\tilde{p}_{AB}(a,b|x,y)$ is signaling or NS, and whether the factorizable condition is satisfied or not.

### 3.1 CH inequality with LHVMs

The CH inequality is defined in the bipartite scenario, where the input settings $x$ and $y$ and the outputs $a$ and $b$ are all bits. Based on the probability distribution that

*xma@tsinghua.edu.cn

obtains a specific measurement outcome, for instance 00, the CH inequality is defined according to

$$\begin{aligned} J_{\mathrm{CH}} = \tilde{p}_{AB}(0,0) + \tilde{p}_{AB}(0,1) + \tilde{p}_{AB}(1,0) \\ - \tilde{p}_{AB}(1,1) - \tilde{p}_A(0) - \tilde{p}_B(0) \leq 0, \end{aligned} \tag{5}$$

where we omit the outputs $a$ and $b$ and define $\tilde{p}_A(x)$ ($\tilde{p}_B(y)$) to be the probability of detecting 0 with input setting $x$ ($y$) by Alice (Bob), and $\tilde{p}_{AB}(x,y)$ the probability of coincidence detection 00 for both sides with input settings $x$ and $y$ for Alice and Bob, respectively.

In real experiments, the input probability can be arbitrary, where our result can still apply with certain modifications on normalization. With the normalization condition, the CH value with LHVMs strategies is given by

$$J_{\mathrm{CH}}^{\mathrm{LHVM}} = 4 \sum_{\lambda} q(\lambda) J_{\lambda} \tag{6}$$

with $J_\lambda$ defined by

$$\begin{aligned} J_\lambda = & \tilde{p}_A(0,\lambda)\tilde{p}_B(0,\lambda)p(0,0|\lambda) + \tilde{p}_A(0,\lambda)\tilde{p}_B(1,\lambda)p(0,1|\lambda) \\ & + \tilde{p}_A(1,\lambda)\tilde{p}_B(0,\lambda)p(1,0|\lambda) - \tilde{p}_A(1,\lambda)\tilde{p}_B(1,\lambda)p(1,1|\lambda) \\ & - \tilde{p}_A(0,\lambda)(p(0,0|\lambda) + p(0,1|\lambda))/2 \\ & - \tilde{p}_B(0,\lambda)(p(0,0|\lambda) + p(1,0|\lambda))/2. \end{aligned} \tag{7}$$

With the randomness parameter defined in Eq. (2), our target is to maximize $J_{\mathrm{CH}}^{\mathrm{LHVM}}$ defined in Eq. (6).

### 3.2 General strategy (attack)

In this part, we consider a general strategy (attack) where no additional assumption is imposed. Note that the optimization of Eq. (6) requires to optimize over the strategy of Alice and Bob, $\tilde{p}_A(x,\lambda)$ and $\tilde{p}_B(y,\lambda)$, and also the strategy of deciding the inputs, $p(x,y|\lambda)$. Here, we first analyze how to optimize the strategy of Alice and Bob.

Because all probabilistic LHVM strategies can be realized with a convex combination of deterministic strategies, it is sufficient to just consider deterministic strategies, i.e., $\tilde{p}_A(x), \tilde{p}_B(y) \in \{0,1\}$ for the optimization. Conditioned on different values of $\tilde{p}_A(x)$ and $\tilde{p}_B(y)$, we should choose the optimal strategy of $\tilde{p}_A(x)$ and $\tilde{p}_B(y)$ that maximize $J_\lambda$.

| $(\tilde{p}_A(0), \tilde{p}_A(1), \tilde{p}_B(0), \tilde{p}_B(1))$ | $J_\lambda$ |
|---|---|
| (0,1,1,0) | $(p(1,0) - p(0,0))/2$ |
| (0,1,1,1) | $(p(1,0) - p(0,0))/2 - p(1,1)$ |
| (1,0,0,1) | $(p(0,1) - p(0,0))/2$ |
| (1,0,1,1) | $(p(0,1) - p(1,0))/2$ |
| (1,1,0,1) | $(p(0,1) - p(0,0))/2 - p(1,1)$ |
| (1,1,1,0) | $(p(1,0) - p(0,1))/2$ |
| (1,1,1,1) | $(p(1,0) + p(0,1))/2 - p(1,1)$ |

Table 1: Possible strategies for letting $J_\lambda$ be positive.

For simple notation, we denote $p(i,j)$ by $p_{2*i+j}$ hereafter, thus the possible deterministic strategies for $J_\lambda$ are in the following set

$$\left\{ \frac{p_2 - p_0}{2}, \frac{p_1 - p_0}{2}, \frac{p_1 - p_2}{2}, \frac{p_2 - p_1}{2}, \frac{p_2 + p_1}{2} - p_3 \right\}. \tag{8}$$

Because there are only five possible strategies of Alice and Bob, we can also consider that there are only five different strategies of choosing the input settings. Therefore, we label $\lambda_j$ to be the $j$th strategy of choosing the input settings and $J_{\mathrm{CH}}^{\mathrm{LHVM}}$ can be rewritten in the following way,

$$\begin{aligned} & J_{\mathrm{CH}}^{\mathrm{LHVM}}/4 \\ & = q(\lambda_1)(p_2(\lambda_1) - p_0(\lambda_1))/2 + q(\lambda_2)(p_1(\lambda_2) - p_0(\lambda_2))/2 \\ & + q(\lambda_3)(p_1(\lambda_3) - p_2(\lambda_3))/2 + q(\lambda_4)(p_2(\lambda_4) - p_1(\lambda_4))/2 \\ & + q(\lambda_5)[(p_2(\lambda_5) + p_1(\lambda_5))/2 - p_3(\lambda_5)]. \end{aligned} \tag{9}$$

Then $J_{\mathrm{CH}}^{\mathrm{LHVM}}$ can be expressed by

$$J_{\mathrm{CH}}^{\mathrm{LHVM}} = 4 \sum_{ij} \beta_{ij} q(\lambda_j) p_i(\lambda_j), \tag{10}$$

Based on the value of $P$ and $Q$, we give the optimal CH value $J_{\mathrm{CH}}^{\mathrm{LHVM}}$ with LHVMs by

$$J_{\mathrm{CH}}^{\mathrm{LHVM}}(P,Q) = \begin{cases} \frac{5}{2}(4P-1) & 3P+Q \leq 1, \\ 1-4Q & 2P+Q \geq \frac{3}{4}, \\ 4P-2Q-\frac{1}{2} & \text{else}, \end{cases} \tag{11}$$

Note that when $P$ is greater than 3/8, the value of $J_{\mathrm{CH}}^{\mathrm{LHVM}}$ is independent of $P$.

### 3.3 Results

Let us compare the results of the CH values $J_{\mathrm{CH}}^{\mathrm{LHVM}}$ under different conditions. For the maximal quantum violation $J_Q = (\sqrt{2}-1)/2$, we calculate the critical values of $Q$ and $P$ such that $J_{\mathrm{CH}}^{\mathrm{LHVM}}(P,Q) = J_Q$. When $Q$ is small, the optimal CH value $J_{\mathrm{CH}}^{\mathrm{LHVM}}(P,Q)$ depends only on $P$. In this case, the critical values of $P$ for the signaling, signaling+fac, NS, and NS+fac are 0.207, 0.302, 0.285, 0.354, respectively. On the other hand, when $Q$ is large, the optimal CH value $J_{\mathrm{CH}}^{\mathrm{LHVM}}(P,Q)$ depends only on $Q$ instead. In this case, the critical values of $Q$ for the signaling and NS condition are 0.198 and 0.146, respectively.

## References

[1] Einstein, A. and Podolsky, B. and Rosen, N. Can Quantum-Mechanical Description of Physical Reality Be Considered Complete? Phys. Rev.47.777

[2] Bell, John Stuart. On the Einstein-Podolsky-Rosen Paradox. Physics 1, 195–200 (1964).

[3] Larsson, J.-Å. Loopholes in Bell inequality tests of local realism. Journal of Physics A Mathematical General, 2014.

[4] Kofler, J. and Giustina, M. Requirements for a loophole-free Bell test using imperfect setting generators. ArXiv e-prints.1411.4787.

# Creating cat states in one-dimensional quantum walks using delocalized initial states

Wei-Wei Zhang,[1, 2, *] Sandeep K. Goyal,[2, †] Fei Gao,[1, ‡] Barry C. Sanders,[2, 3, 4, 5, §] and Christoph Simon[2, ¶]

[1] *State Key Laboratory of Networking and Switching Technology, Beijing University of Posts and Telecommunications, Beijing 100876, China*

[2] *Institute for Quantum Science and Technology, and Department of Physics and Astronomy, University of Calgary, Canada, T2N 1N4*

[3] *Hefei National Laboratory for Physical Sciences at Microscale, University of Science and Technology of China, Hefei, Anhui 230026, China*

[4] *Shanghai Branch, CAS Center for Excellence and Synergetic Innovation Center in Quantum Information and Quantum Physics, University of Science and Technology of China, Shanghai 201315, China*

[5] *Program in Quantum Information Science, Canadian Institute for Advanced Research, Toronto, Ontario M5G 1Z8, Canada*

Cat states are coherent quantum superpositions of macroscopically distinct states and are useful for understanding the boundary between the classical and the quantum world. Due to their macroscopic nature, cat states are difficult to prepare in physical systems. We propose a method to create cat states in one-dimensional quantum walks using delocalized initial states of the walker. Since the quantum walks can be performed on any quantum system, our proposal enables a platform-independent realization of the cat states. We further show that the linear dispersion relation of the effective quantum walk Hamiltonian, which governs the dynamics of the delocalized states, is responsible for the formation of the cat states. We analyze the robustness of these states against the environmental interactions and present methods to control and manipulate the cat states in the photonic implementation of quantum walks.

## I. INTRODUCTION

Schrödinger cat states can be defined as quantum superpositions of macroscopically distinct states of a quantum system [1–4]. Due to their macroscopic nature, the cat states play an important role in fundamental tests of quantum theory and precision measurements [5–8]. Numerous attempts are being made to prepare the cat states in various physical systems [9–27].

The macroscopic superposition, which makes the cat states interesting also makes them hard to create in physical systems. This is because of the difficulty in controlling the evolution of macroscopic quantum systems while preserving the coherence in the state. Quantum walks inherently involve the coherent evolution of a macroscopic system.

In a quantum walk process, a quantum walker propagates on a lattice where the propagation is conditioned over its internal states (the coin states) [28, 29]. The quantum walker, unlike its classical counterpart, preserves the coherence during the propagation which results in a faster spread of the walker over the lattice as compared to the classical random walks. Quantum walks have been extensively studied to devise quantum algorithms [30–34] and to simulate various quantum phenomena [35–55].

Here we propose a method to prepare the cat states in a one-dimensional discrete time quantum walk (DTQW) using delocalized initial states of the walker. The quantum walks can be implemented on virtually any quantum system that meets the requirements (a lattice and a coin). Thus, our proposal provides a platform-independent method to create cat states, which enables us to test the fundamental theories on more accessible systems.

In Ref. [56], Cardano et al. implemented a one-dimensional quantum walk on the orbital angular momentum (OAM) space of a single photon, following the proposal of Refs. [57, 58]. In this experiment, they demonstrated that the state of the walker, which is delocalized initially, evolves to form a bimodal distribution that resembles a cat state. Their experimental finding, which is consistent with their numerical calculations, motivates the research to find the cause of the formation of cat states and analysis of the stability of these states against the decoherence in quantum walks.

Here we start with a Gaussian (delocalized) initial state and prove that it evolves to form a cat state. We clarify the conditions for the formation of the cat states for the entire range of the parameter $\theta$, which characterizes the bias in the coin flip in the quantum walk. The linearity of the dispersion relation of the low-momentum effective Hamiltonian, which governs the dynamics of the delocalized states, is shown to be the reason for the formation of the cat states in the one-dimensional quantum walks. Furthermore, experimentally viable methods are proposed to demonstrate the coherence in the presence of environmental interactions. Our analysis of the effects of decoherence on the quality of the cat states show that large separations in the cat states are possible even in the presence of noise. Finally, we provide a method to stabilize and manipulate the cat states over the OAM of light.

[*] weiwei.zhang@ucalgary.ca
[†] sandeep.goyal@ucalgary.ca
[‡] gaofei_bupt@hotmail.com
[§] sandersb@ucalgary.ca
[¶] csimo@ucalgary.ca

The structure of the article is as follows: we provide the relevant background regarding the one-dimensional quantum walks in Sec. II. In Sec. III and IV we present our numerical and analytical findings. We discuss the effect of decoherence on the cat states in Sec. V. Method to control and manipulate the cat states are presented in Sec. VI. We conclude in Sec. VII.

## II. BACKGROUND

In this section, we present the relevant background of the one-dimensional quantum walks. We describe the regular coined quantum walks on a one-dimensional lattice, its generalization and the Hamiltonian, which governs the dynamics of the quantum walks. We conclude the section with an optical implementation scheme where the walk is performed over the OAM of a light beam.

### A. One-dimensional Discrete time quantum walks

In a one-dimensional DTQW the walker propagates on a one-dimensional lattice. The movements of the walker on the lattice are conditioned over the state of a two-state quantum coin. Each step in the walk consists of a coin-flip ($C$) followed by the conditional propagation ($S$). If $\{|\uparrow\rangle, |\downarrow\rangle\}$ represents a set of two orthogonal states of the coin then the coin-flip operator $C$ reads [59]

$$C = \big(\cos\theta\,|\uparrow\rangle + \sin\theta\,|\downarrow\rangle\big)\langle\uparrow| + \big(\sin\theta\,|\uparrow\rangle - \cos\theta\,|\downarrow\rangle\big)\langle\downarrow|, \tag{1}$$

where the parameter $\theta \in [0, 2\pi)$. The conditional propagator $S$ instructs the walker to move forward ($F = \sum_x |x+1\rangle\langle x|$) or backward ($F^\dagger$) on the lattice conditioned over the states of the coin,

$$S = F \otimes |\uparrow\rangle\langle\uparrow| + F^\dagger \otimes |\downarrow\rangle\langle\downarrow|. \tag{2}$$

Here $x$ is the index for the lattice sites. Thus, the quantum walk propagator $Z$ reads

$$Z = S(\mathbb{1} \otimes C). \tag{3}$$

Repeated action of the propagator $Z$ gives rise to the quantum walk dynamics.

One-dimensional DTQW has been generalized to simulate various dynamics. One of the most interesting generalizations is where a phase, which is linear in the position, is introduced after every step of the quantum walk [60, 61]. The operator $F_\mathrm{m}$ which gives the site-dependent phase reads

$$F_\mathrm{m} = \sum_x \exp(i\Phi x)\,|x\rangle\langle x|, \tag{4}$$

where $\Phi$ is an independent parameter. The subscript m in the operator $F_\mathrm{m}$ is just a reminder that the operator $F_\mathrm{m}$ is a shift operator in the momentum space. The propagator for the generalized quantum walk reads

$$\bar{Z} = F_\mathrm{m} Z. \tag{5}$$

This generalized quantum walk demonstrates various interesting properties such as Bloch oscillations and quasi-periodic dynamics [61]. If the strength of the parameter $\Phi$ is set to be $\Phi = 2\pi/p$, where $p$ is a positive integer, then the walker recovers its original state after $2p$ number of steps for odd $p$ and after $p$ number of steps for even $p$. This feature can be used to restrict the spread of the walker on the lattice.

### B. Quantum walk Hamiltonian

The Hamiltonian $H$ that governs the quantum walk dynamics can be calculated by substituting

$$Z = \exp(-iH\delta t), \tag{6}$$

where $\delta t$ is the duration of a single step in the quantum walk. Here we have taken $\hbar \equiv 1$.

From the definition of the conditional propagator $S$ in (2) and the operator $F$, we can assert that the propagator $Z$ and the Hamiltonian $H$ are translation invariant. Thus, the Hamiltonian $H$ can be block diagonalized in the momentum (or Fourier transform) basis $\{|k\rangle\}$

$$H = \bigoplus_{k\in[-\pi,\pi)} H(k). \tag{7}$$

Here we have considered a lattice of size $N$ with periodic boundary condition, where $N$ is taken to be much larger than the number of quantum walk steps. The variable $k$ represents the (quasi-) momentum that can take discrete values between $-\pi$ and $\pi$ in the integer multiples of $2\pi/N$.

The Hamiltonian $H(k)$ in the momentum basis can be calculated by expanding the position eigenstates $\{|x\rangle\}$ in the momentum basis $\{|k\rangle\}$ as

$$|x\rangle = \frac{1}{\sqrt{N}} \sum_k \exp(ikx)\,|k\rangle. \tag{8}$$

By substituting Eq. (8) into the definition of the propagator $Z$ and using Eq. (6) we arrive at

$$H(k) = \boldsymbol{h}(k) \cdot \boldsymbol{\sigma}. \tag{9}$$

Here $\boldsymbol{\sigma}$ is the vector $(\sigma_x, \sigma_y, \sigma_z)$ of Pauli spin matrices and $\boldsymbol{h}(k) = (h_1(k), h_2(k), h_3(k))$ is a three dimensional real vector, which reads

$$h_1(k) = -R(k)\sin\theta\cos k, \tag{10}$$

$$h_2(k) = R(k)\sin\theta\sin k, \tag{11}$$

$$h_3(k) = -R(k)\cos\theta\cos k, \tag{12}$$

$$R(k) = \frac{\cos^{-1}(-\cos\theta\sin k)}{\sqrt{\sin^2\theta\sin^2 k + \cos^2 k}}. \tag{13}$$

Interestingly, for small values of the parameter $\theta$ and small $k$, the Hamiltonian $H(k)$ takes a special form that resembles a two-component Dirac Hamiltonian (see Appendix A). In this limit the effective Hamiltonian, which we represent by $H_{\rm d}$, reads

$$H_{\rm d}(k) = -\left(k + \frac{\pi}{2}\right)\sigma_z - \theta\frac{\pi}{2}\sigma_x. \tag{14}$$

In the Hamiltonian $H_{\rm d}(k)$ the parameter $\theta$ characterizes the mass of the particle.

### C. Implementing quantum walks in optical system

In this section, we describe an implementation scheme to realize a one-dimensional quantum walk on the OAM of light. This scheme was proposed in [58] and experimentally demonstrated in [56]. The purpose of this section is to familiarize the readers with an implementation scheme for the cat states in the quantum walks. Using this implementation for the one-dimensional quantum walks we will propose a method to manipulate and control the cat states.

In this implementation scheme, the OAM of light serves as the lattice and the polarization is used as the coin. The conditional propagator $S$ (2) is constructed by means of a q-plate which is a device that couples the OAM of light with its spin angular momentum (polarization) [62]. The action of a q-plate on the combined state of the OAM and the polarization is given by

$$|L, \ell\rangle \to |R, \ell - 2q\rangle\,, \tag{15}$$
$$|R, \ell\rangle \to |L, \ell + 2q\rangle\,, \tag{16}$$

where $|L\rangle$ and $|R\rangle$ are the left- and right-handed circular polarization of light, and $|\ell\rangle$ is the OAM state that has angular momentum proportional to $\ell\hbar$. The half-integer parameter $q$ characterizes the q-plate.

A half-wave plate with its fast axis parallel to the horizontal axis interchange the left- and right-handed circular polarization. Therefore, a q-plate with $q = 1/2$ followed by a half-wave plate give rise to the conditional propagator $S$ (2).

The coin-flip operator $C$ (1) can be implemented using the Simon-Mukunda polarization gadget [63]. This gadget is a combination of one half-wave plate and two quarter-wave plates, and can be used to realize an arbitrary SU(2) operation on the polarization of light. Hence, the quantum walk propagator $Z$ can be simulated using a q-plate, a half-wave plate, and a Simon-Mukunda polarization gadget in series. Placing these three components in a loop can realize a one-dimensional quantum walk on the OAM of light.

## III. CAT STATES IN QUANTUM WALKS

In this section, we demonstrate the formation of the cat states in the one-dimensional DTQW. We show that the walker in a delocalized (Gaussian) initial state evolves to form a cat state. We present methods to analyze the cat nature of the evolved state of the walker.

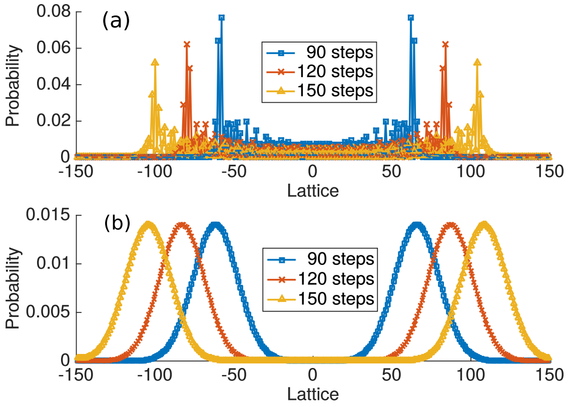

FIG. 1. The evolution of the walker on a one-dimensional lattice for (a) localized and (b) delocalized initial states. Here, the parameter $\theta = \pi/4$, and the width of the Gaussian for the figure (b) is $\sigma \approx 10$.

Quantum walk evolution, typically, results in a bimodal distribution of the walker on the lattice. In Fig. 1, we plot the probability distribution of the walker at time $t$ = 90, 120, 150 steps for a localized and a delocalized initial states. In Fig. 1a, the initial state of the walker is localized at the origin. The state of the walker evolves to a bimodal distribution with a residual probability between the two components of the distribution. The residual probability signifies the overlap between the two components of the distribution. Hence, the evolved state is not a cat state.

In Fig. 1b, we start with a delocalized initial state $|\Psi(0)\rangle_{\rm de}$ of the walker

$$|\Psi(0)\rangle_{\rm de} = \frac{1}{\mathcal{N}}\sum_n \exp\left(-\frac{n^2}{4\sigma^2}\right)|n\rangle \otimes |\chi\rangle_c\,, \tag{17}$$

which has a Gaussian probability distribution. We find that the delocalized state $|\Psi(0)\rangle_{\rm de}$ evolves to a state $|\Psi(t)\rangle_{\rm de}$ after time $t$ that has the bimodal probability distribution with vanishing residual probability between the two components of the bimodal distribution. Here we have chosen the width $\sigma$ of the Gaussian to be sufficiently large (about 10 lattice sites). $|\chi\rangle_c$ is a normalized initial state of the coin, and $\mathcal{N}$ is the normalization constant. The two components of the bimodal distribution can represent macroscopically distinct states of the walker. Hence, the evolved state can be seen as a cat state. In the remainder of this section, we analyze the conditions required for the evolved state to be a cat state.

### A. Small $\theta$ case

We start with a simple case when the parameter $\theta$ is small. In this limit, the quantum walk Hamiltonian can be approximated to a two-component Dirac Hamiltonian $H_{\rm d}$ (14). In this limit, the quantum walk can be used to simulate quantum relativistic effects such as Klein paradox and Zitterbewegung [38, 43]. Thus, this limit can be considered as the relativistic limit of the quantum walk.

The parameter $\theta$ in the Dirac Hamiltonian $H_{\rm d}$ characterizes the mass of the particle. For $\theta = 0$ the Hamiltonian $H_{\rm d}$ represents a massless particle. If the initial state of the walker in the momentum space is

$$|\Psi(0)\rangle = \sum_k |\psi_k\rangle \otimes (a\,|\uparrow\rangle + b\,|\downarrow\rangle)\,, \tag{18}$$

then the evolved state, for the case $\theta = 0$, reads

$$\begin{aligned}|\Psi(t)\rangle &= \exp(-iH_{\rm d}t)\,|\Psi(0)\rangle\,,\\ &= \sum_k \left(iae^{ikt}\,|\psi_k\rangle \otimes |\uparrow\rangle - ibe^{-ikt}\,|\psi_k\rangle \otimes |\downarrow\rangle\right).\end{aligned} \tag{19}$$

Here, the two orthogonal spin components of the particle propagate in the opposite directions independent of each other. Due to the linear dispersion relation in the Dirac Hamiltonian, the evolution does not result in the spreading of the wave function of the particle, which results in the formation of cat states.

The same feature, namely, the non-dispersive behaviour of the wave function, persists for non-zero values of $\theta$ as long as $\theta$ is small. Thus, cat states can be formed in the relativistic limit of the one-dimensional quantum walks.

### B. Arbitrary $\theta$ case

In the limit when $\theta$ is large, the Dirac description of the quantum walk breaks down, therefore, one might not expect to observe the cat states. In Fig. 2, we plot the probability distribution of the walker over the lattice at different times. Here we have considered two different dynamics for the walker, one where we use the exact quantum walk evolution to propagate the walker on the lattice and other where we use Dirac Hamiltonian to propagate the walker. We have chosen $\theta = \pi/2.4$, i.e., a large value of $\theta$. From this figure, we see that the Dirac Hamiltonian and the exact quantum walk dynamics result in strikingly different evolutions. The cat-state-like distribution persists for large $\theta$ in the exact quantum walk evolution where Dirac description predicts only dispersed wave function.

In the following, we show that the evolved states achieved for an arbitrary $\theta$ and the state $|\Psi(t)\rangle$ (19) achieved in the small $\theta$ limit are qualitatively the same. In order to see that, first, we notice that the state $|\Psi(t)\rangle$ in Eq. (19) is highly entangled and the wave-packets corresponding to the orthogonal states of the coin propagate in the opposite directions.

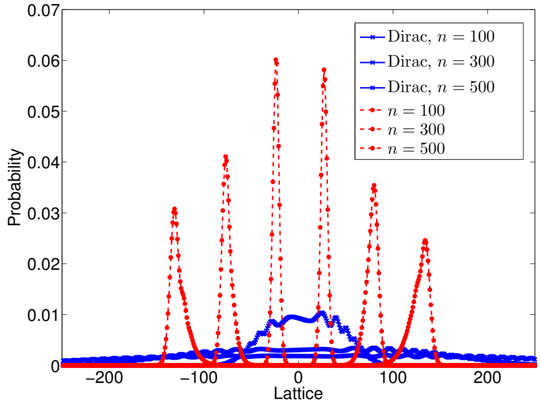

FIG. 2. The comparison between the exact quantum walk evolution (the dashed line) and the evolution using the Dirac Hamiltonian (the solid line) for large values of $\theta$ ($\theta = \pi/2.4 = 75°$). This figure shows the spread in the width of the Gaussian in the case of the Dirac evolution but almost no spread in the exact quantum walks evolution.

In Fig. 3a we plot the entanglement in the state $|\Psi(t)\rangle_{\rm de}$ between the coin and the walker. The entanglement is calculated by first calculating the reduced density matrix of the coin (or the walker) and then calculating the von-Neumann entropy of the reduce density matrix [64]. In this figure, we can see that the entanglement approaches the maximum value after sufficiently long time. In Fig. 3b we plot the distribution for the states of the walker corresponding to the two orthogonal states of the coin, which are calculated by diagonalizing the reduced density matrix of the coin. Clearly the two wave-packets are moving in the opposite directions. The maximum entanglement along with the purity show that the state $|\Psi(t)\rangle_{\rm de}$ must have the form

$$|\Psi(t)\rangle_{\rm de} = \frac{1}{\sqrt{2}}\left(|X(t)\rangle \otimes |\phi(t)\rangle + |X_\perp(t)\rangle \otimes |\phi_\perp(t)\rangle\right), \tag{20}$$

where the states $|X(t)\rangle$ and $|X_\perp(t)\rangle$ represent the two non-overlapping wave-packets and $|\phi(t)\rangle$ and $|\phi_\perp(t)\rangle$ are the orthogonal states of the coin.

Another method to verify the coherence in the two wave-packets in the evolved state $|\Psi(t)\rangle_{\rm de}$ is by studying the probability distribution of the walker in the momentum space after projecting over an appropriate state of the coin. This can be done as follows: if the states $|X(t)\rangle$ and $|X_\perp(t)\rangle$ are coherent Gaussian states that have the form

$$|G(\pm n_t, \sigma)\rangle = \frac{1}{\mathcal{M}}\sum_n \exp\left(-\frac{(n \pm n_t)^2}{4\sigma^2}\right)|n\rangle\,, \tag{21}$$

with the mean at $\pm n_t$ and the width $\sigma$, then the Fourier transform of these states read

$$|G(\pm n_t, \sigma)\rangle \rightarrow \frac{1}{\mathcal{M}}\sum_k e^{\mp i n_t k} e^{-\sigma^2 k^2/2}\,|k\rangle\,. \tag{22}$$

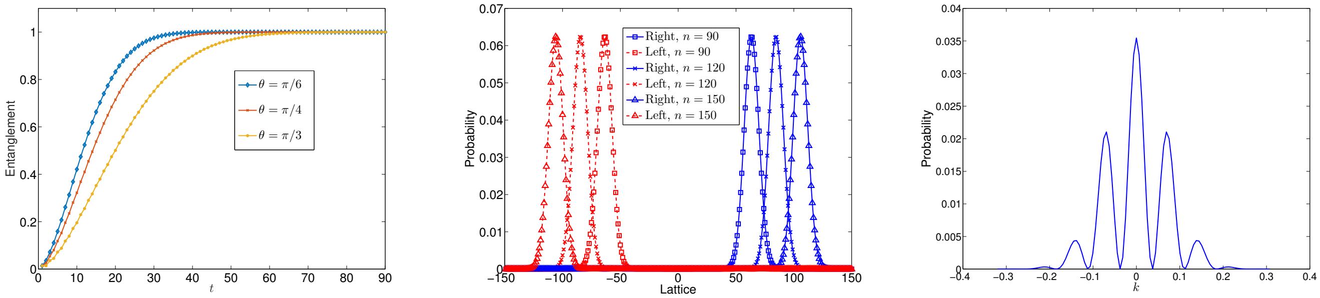

(a) (b) (c)

FIG. 3. In this figure we summarize the numerical evidence in favour of the cat states in one dimensional DTQW. Here we have chosen the parameter $\theta = \pi/4$ and the width of the Gaussian $\sigma \approx 10$, unless specified explicitly. In Fig. (a) we plot the entanglement between the coin and the lattice as a function of time for different values of $\theta$. The entanglement is calculated by calculating the von-Neumann entropy of the reduced density matrix of the coin. In Fig. (b) we show the macroscopically distinct states of the walker propagating in the opposite directions. The two macroscopically distinct states correspond to the states $|X\rangle$ and $|X_\perp\rangle$ introduced in Eq. (20). Here the solid curves are the Gaussian moving towards the right and the dashed curves are the Gaussian moving towards the left. (c) The probability distribution in the momentum space after projecting the evolved state on a chosen coin state. Here we have chosen the coin states $|\chi\rangle_c = |\chi'\rangle_c = |u_-(0)\rangle + i\,|u_+(0)\rangle$, where $|u_\pm(0)\rangle$ are the eigenvectors of the quantum walk Hamiltonian corresponding to $k = 0$. The occurrence of the fringes in this distribution signifies the coherence between the two macroscopic states $|X\rangle$ and $|X_\perp\rangle$ of the walker.

Thus, the state $|\Psi(t)\rangle_{\rm de}$ in the momentum basis reads

$$\left|\tilde{\Psi}_t\right\rangle = \frac{1}{\sqrt{2\mathcal{M}}}\sum_k e^{-\sigma^2k^2/2}\,|k\rangle\otimes\left(e^{-in_tk}\,|\phi\rangle + e^{in_tk}\,|\phi_\perp\rangle\right). \tag{23}$$

After projecting the state $\left|\tilde{\Psi}_t\right\rangle$ on the coin state $|\chi'\rangle_c$, the state of the walker reads

$$|\Psi\rangle = \frac{1}{\sqrt{2\mathcal{M}}}\sum_k e^{-\sigma^2k^2/2}\left(\alpha e^{-in_tk} + \beta e^{in_tk}\right)|k\rangle\,, \tag{24}$$

where

$$\alpha = {}_c\langle\chi'\,|\,\phi(t)\rangle, \quad \beta = {}_c\langle\chi'\,|\,\phi_\perp(t)\rangle. \tag{25}$$

Note that, $|\Psi\rangle$ in (24) represents a state of the walker which is a superposition of two Gaussians in the position space centred around $\pm n_t$. Thus, the state $|\Psi\rangle$ itself is a cat state as it contains a coherent superposition of two macroscopically distinct states.

For $\alpha = \beta$, the probability distribution corresponding to $|\Psi\rangle$ in the momentum space will be a product of a Gaussian and $\cos^2 n_tk$. For an appropriate choice of $|\chi'\rangle_c$ one can acquire $\alpha = \beta$. Thus, the presence of the fringes in the momentum space probability distribution signifies the coherence in the two Gaussian probability distributions in the evolved state of the quantum walk. In Fig. 3c we plot the probability distribution for the state $|\Psi\rangle$ in the momentum space. The clear presence of the fringes in the plot ensures that the two Gaussian probability distributions in the evolved state of the walker are coherent, thus, the evolved state is a cat state.

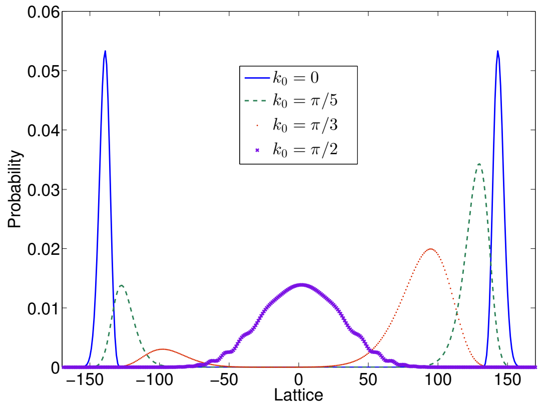

FIG. 4. The plot for the probability distribution of the evolved state for different values of the mean momentum $k_0$. Here we have set $\theta = \pi/4$ and the width of the Gaussian $\sigma = 10$.

Until now we have considered only those cases when the initial state of the walker is centred around $k = 0$; therefore, the average momentum of the walker is small. What happens when the initial state is a Gaussian but not centred at $k = 0$? In Fig. 4 we plot the probability distribution for different initial states. Here we consider the initial state of the walker to have a Gaussian probability distribution and the mean value of the momentum to be $0 \le k_0 \le \pi/2$. From Fig. 4 it can be seen that we get perfect cat states only when $k_0 \approx 0$.

In this section, we have shown that the delocalized initial states of a quantum walker evolve to form the cat states. This result is independent of the coin parameter $\theta$. However, the formation of the cat states strongly depends on the mean value of the momentum in the initial state. So far our analysis was based only on numerical results. In the following section, we present the analytic description for the formation of the cat states in quantum walks for the entire range of $\theta$ including the large $\theta$ regime where Dirac Hamiltonian does not comply.

## IV. ANALYTIC APPROACH TO THE CAT STATES IN QUANTUM WALKS

The numerical results, although compelling, do not give us the real physics behind the formation of the cat states in the quantum walks. In this section, we present the reasons behind the formation of the cat states in the quantum walk.

An important result in the previous section is that the cat states are formed due to the delocalized initial states that are centred around zero momentum. It suggests that the low-momentum behaviour of the quantum walks is responsible for the formation of the cat states. Furthermore, from the small $\theta$ limit of the quantum walk Hamiltonian, i.e., Dirac Hamiltonian, we can see that the linear dispersion relation and the momentum-independent eigenvectors of the Hamiltonian cause the formation of the cat states.

Interestingly, for small values of the momentum $k$ the Hamiltonian $H(k)$ in Eq. (9) also has linear dispersion even though the Hamiltonian $H(k)$ itself is non-linear in $k$ (see Appendix A for detailed calculations)

$$E_{\pm}(k) = \pm\left(k\cos\theta + \frac{\pi}{2}\right) + O(k^3). \tag{26}$$

In other words, the energy $E_{\pm}(k)$ does not have second order terms in $k$ and for small values of $k$ (say $k < \pi/20$) the $k^3$ terms can be neglected, hence, giving rise to linear dispersion relation.

Furthermore, the eigenvectors $|u_{\pm}(k)\rangle$ of the Hamiltonian $H(k)$ depend weakly on the momentum $k$ for small values of $k$ (see Appendix A)

$$|\langle u_i(0)\,|\,u_j(k)\rangle|^2 = \delta_{ij} + O(k^2). \tag{27}$$

Eq. (27) along with the linear dispersion relation is responsible for the formation of the cat states. This can be understood as follows: if we start with a delocalized state $\left|\tilde{\Psi}(0)\right\rangle_{\rm de}$ of the walker

$$\left|\tilde{\Psi}(0)\right\rangle_{\rm de} = \frac{1}{\mathcal{N}'}\sum_k \exp\left(-\frac{k^2}{4\delta^2}\right)|k\rangle\otimes|\chi\rangle_c\,, \tag{28}$$

which has a Gaussian spread in the momentum space, centred around $k=0$ and having the width $\delta < \pi/20$, and the coin state $|\chi\rangle_c$, then the evolved state at time $t$ reads

$$\left|\tilde{\Psi}(t)\right\rangle = \frac{1}{\mathcal{N}'}\sum_k \exp\left(-\frac{k^2}{4\delta^2}\right)|k\rangle\otimes \left(e^{-iE_-(k)t}a_-(k)\,|u_-(k)\rangle + e^{-iE_+(k)t}a_+(k)\,|u_+(k)\rangle\right), \tag{29}$$

where $a_{\pm}(k) = \langle u_{\pm}(k)\,|\,\chi\rangle_c$. Now projecting the state $\left|\tilde{\Psi}(t)\right\rangle$ on the coin state $|\chi\rangle_c$ results in state of the walker

$$|\Psi\rangle_{\rm mom} = \frac{1}{\mathcal{N}'}\sum_k \exp\left(-\frac{k^2}{4\delta^2}\right)\left(e^{-iE_-(k)t}|a_-(k)|^2 + e^{-iE_+(k)t}|a_+(k)|^2\right)|k\rangle\,. \tag{30}$$

The state $|\Psi\rangle_{\rm mom}$ in (30) is same as the state $|\Psi\rangle$ in (24) with $\alpha = |a_-|^2$, $\beta = |a_+|^2$ and $\delta = 1/\sigma$, and in the position space $|\Psi\rangle_{\rm mom}$ represents a state which is in a superposition of two Gaussians centred around $\pm t\cos\theta$. Hence, $|\Psi\rangle_{\rm mom}$ represents a cat state.

Alternatively, if $|a_-(k)|^2 = |a_+(k)|^2$ and independent of $k$ then the probability distribution corresponding to the state $|\Psi\rangle_{\rm mom}$ in the momentum space is a product of a Gaussian and $\cos^2 E_-(k)t$. This means the probability distribution corresponding to the state $|\Psi\rangle_{\rm mom}$ has fringes exactly like the one in Fig. 3c. In that case the state $\left|\tilde{\Psi}(t)\right\rangle_{\rm de}$ represents a cat state.

For appropriate choices for the state $|\chi\rangle_c$ we can get $|a_-(k)|^2 \approx |a_+(k)|^2$ which, for small values of $k$, is $k$-independent. Using Eq. (27) we can construct one such class of state which reads

$$|\chi\rangle_c = \frac{1}{\sqrt{2}}\left(|u_-(0)\rangle + e^{i\varphi}\,|u_+(0)\rangle\right), \tag{31}$$

where $\varphi$ is a free parameter. This class satisfies the relation

$$|a_-(k)|^2 \approx |a_+(k)|^2 \approx \frac{1}{2}. \tag{32}$$

This completes our proof that the Hamiltonian $H(k)$, and hence the one-dimensional DTQW, gives rise to the cat states.

Let us emphasize that the linear dispersion (26) does not mean that the Hamiltonian is linear. In fact in our case, if we truncate the Hamiltonian $H(k)$ to the first order in $k$, then we will not get the linear dispersion relation for large values of the parameter $\theta$. The $O(k^2)$ terms in the Hamiltonian $H(k)$ make the dispersion relation linear.

To summarize, we have shown that the formation of the cat states is due to the linear dispersion relation and the weak dependence of the eigenvectors of the quantum walk Hamiltonian on the momentum $k$. In the following section, we analyze the effect of decoherence on the cat states in quantum walks.

## V. EFFECT OF DEPHASING ON THE CAT STATES

The discussion of the cat states is incomplete without considering the effects of the environmental interactions with the quantum system. Cat states are highly susceptible to their surroundings. Therefore, establishing the feasibility of forming a cat states in a quantum system interacting with a bath is important. In this section, we study the effect of pure dephasing type bath interactions on the quality of the cat states. We consider three different scenarios, (i) the bath is acting only on the walker, (ii) the bath is acting only on the coin, and (iii) the bath is acting on both, the walker and the coin.

The action of a pure dephasing type bath on a given density matrix $\rho$ can be defined by the relation [65–67]

$$\rho \to \tilde{\rho} = e^{-\eta t}\rho + (1 - e^{-\eta t})\mathrm{diag}(\rho) = \hat{V}(\rho). \qquad (33)$$

Here $\eta$ characterizes the strength of the bath, $\eta = 0$ implies no interaction with the bath. The function diag$(\rho)$ keeps the diagonal elements of the matrix $\rho$ and discard all the off-diagonal elements. Formally, the action of the pure dephasing bath can be represented by the superoperator $\hat{V}$.

We incorporate the effect of the dephasing in our evolution by applying the superoperator $\hat{V}$ after every step of the quantum walk on either the walker or the coin or on both. In Fig. 5, we plot the spread of the walker over the lattice in the presence of dephasing. Interestingly, we still get the bimodal distribution with an additional residual probability between the two peaks.

Although the evolved state in the presence of dephasing has a similar bimodal distribution as in the case of pure states (without dephasing), the coherence in the two cases can be very different. To quantify the coherence in the evolved state of the walker we can calculate the revival fidelity of the evolved state upon reversing the dynamics using a physical operation [18, 68]. If the state of the walker remains pure in the evolution then the walker can regain its original state by reversing the dynamics. However, if the walker loses the purity in the evolution then the revival is not perfect.

To quantify the coherence, first, we need to devise an operation that can reverse the dynamics of the quantum walk. In our numerical calculations, we find that the Pauli spin operator $\sigma_y$ acting on the coin state of the walker can be used to reverse the direction of propagation of the walker if the initial state of the walker is delocalized.

Using the $\sigma_y$ operator we can calculate the revival fidelity as follows: we first evolve the initial delocalized state of the walker for time $T$ in the presence of the bath. At this point, we reverse the dynamics by applying the $\sigma_y$ operator on the coin. We again evolve the state for time $T$ in the presence of the bath followed by $\sigma_y$ operation. Now we can calculate the fidelity between the evolved state $\rho(2T)$ and the initial state $|\Psi(0)\rangle_{\mathrm{de}}$ as

$$r = {}_{\mathrm{de}}\langle\Psi(0)\,|\,(\mathbb{1}\otimes\sigma_y)\rho(2T)(\mathbb{1}\otimes\sigma_y)\,|\,\Psi(0)\rangle_{\mathrm{de}}. \qquad (34)$$

High values of the revival fidelity $r$ signifies high amount of coherence in the state.

In Fig. 6 we plot the revival fidelity in the quantum walk evolution for various values of $\theta$ in the absence of the dephasing. Here we apply the $\sigma_y$ operation after $n$ number of steps. Till then the fidelity between the evolved state and the initial state decreases monotonically. After we apply the dynamic-reversing operation, the fidelity start increasing which acquire the maximum value 1 at $2n$ steps. From this plot it is clear that the system regains its initial state with high fidelity, thus, confirming the high coherence in the state.

In Fig. 7 we plot the revival fidelity as a function of the bath strength $\eta$. Here we have chosen $T = 250$ steps, thus, the total evolution is for $2T = 500$ steps. This figure shows that we can achieve a very high revival fidelity for small $\eta$ ($\eta \approx 0.001$). If we choose $T$ to be smaller then the revival fidelity can be high even for stronger bath interactions. This suggests that the cat states with significant separation between the two components in the bimodal distribution should be possible in the physical implementations of quantum walks.

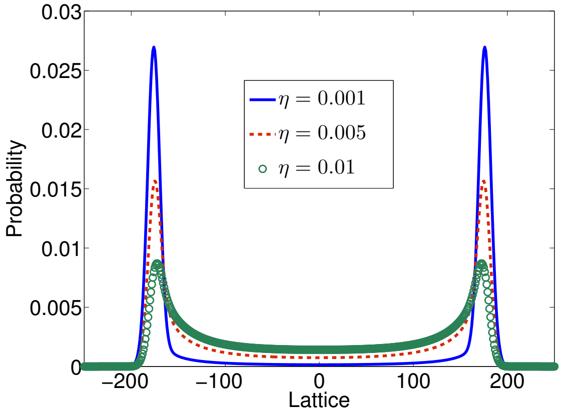

FIG. 5. Spread of the walker on the lattice in the presence of dephasing after 250 steps.

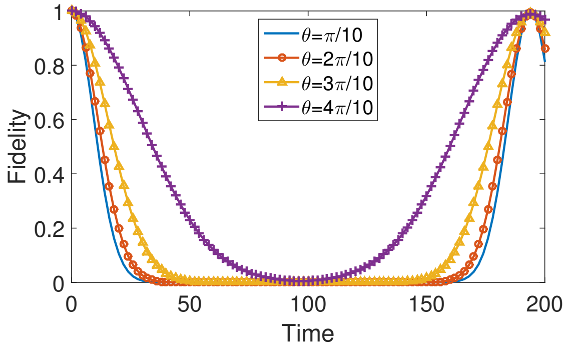

FIG. 6. Plot for the revival fidelity between the evolved state and the initial state for different values of $\theta$ in the absence of the dephasing. For first $n = 97$ steps the walk is uninterrupted at which point we apply the $\sigma_y$ operation. The application of $\sigma_y$ causes the walker to retrace its footsteps resulting in a rise in the fidelity reaching the maximum at $n = 194$ steps. Here we have plotted the values of the fidelity only for the even number of steps as the fidelity for the odd number of steps is zero.

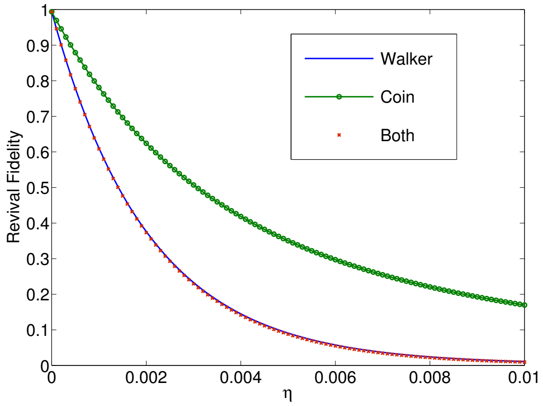

FIG. 7. Revival fidelity of the quantum walk under the action of different baths

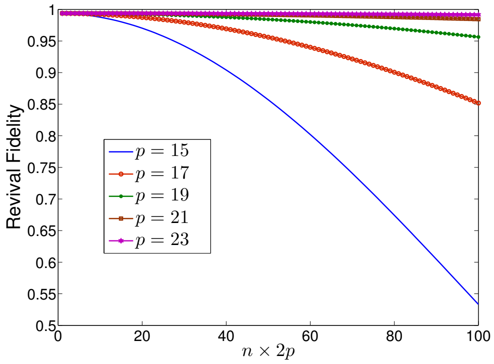

FIG. 8. Here we plot the revival fidelity of the cat state after the experiencing electric field for $n \times 2p$. Here the width of the delocalized initial state is $\sigma = 9$ and the time of evolution is $t = 100$ steps.

## VI. CONTROLLING THE CAT STATES IN OAM IMPLEMENTATION OF QUANTUM WALKS

In this section, we consider the optical implementation of the one-dimensional quantum walk which we introduced in Sec. II C. In this implementation, the quantum walk is performed over the OAM space of light. Here we propose a method to manipulate and control the separation between the two distinct components in the cat state.

The first requirement to realize a cat state in a one-dimensional quantum walk is the delocalized (Gaussian) initial state. The Gaussian initial state in the OAM implementation of the quantum walk can be constructed, simply, by using a spatial light modulators [56]. Thus, by using a spatial light modulator and using the scheme presented in Ref. [56, 58] we can form the cat states in the optical quantum walks.

After realizing the cat state, the next step is to control the separation between the macroscopic states of the walker. In Sec. II A we have seen that the application of the momentum shift operator $F_{\mathrm{m}}$ in a one-dimensional DTQW causes a periodic revival of the initial state of the walker. The walker regains its initial state after $2p$ number of steps where the number $p = 2\pi/\Phi$ is related to the parameter of the operator $F_{\mathrm{m}}$.

We use the same $F_{\mathrm{m}}$ to stabilize the cat state in the quantum walks. In order to stabilize the cat state at time $t$, first, we evolve the initial Gaussian state of the walker for time $t$ using the quantum walk propagator $Z$ (3). The evolved state $|\Psi(t)\rangle$ reads

$$|\Psi(t)\rangle \approx \frac{1}{\sqrt{2}} \left( |G(-n_t, \sigma)\rangle \otimes |u_-\rangle + |G(n_t, \sigma)\rangle \otimes |u_+\rangle \right). \tag{35}$$

At time $t$ we introduce the momentum shift operator $F_{\mathrm{m}}$ in the quantum walk with a certain value of $p$. Due to the momentum shift operator the state of the walker start oscillating, recovering the state $|\Psi(t)\rangle$ periodically after the time period $2p$. Hence, we can preserve the cat state $|\Psi(t)\rangle$ for a long time. The only obstacle in preserving the cat states in the decoherence.

Now if we want to increase the separation between the two Gaussian wave-packets of the cat state $|\Psi(t)\rangle$, then we remove the operator $F_{\mathrm{m}}$ after a time period which is a multiple of $2p$. On the other hand, if we want to decrease the separation between the two Gaussian wave-packets we remove $F_{\mathrm{m}}$ after $2np$ followed immediately by one-time application of $\sigma_y$ operation. Hence, by introducing the $F_{\mathrm{m}}$ and the reversal operation $\sigma_y$ we can control and manipulate the cat states in the quantum walks.

In Fig. 8 we show the numerically calculated revival fidelity of the cat states. Here we have evolved the delocalized initial state for 100 steps. Then we apply $F_{\mathrm{m}}$ for $n \times 2p$ number of steps. We remove the operator $F_{\mathrm{m}}$ and apply the quantum walk reversal operation $\sigma_y$ and evolve the system for 100 steps and calculate the fidelity with the initial state. Here $n$ is an integer between 1 and 100. We can see that for sufficiently large values of $p$ the revival fidelity converges to the value 1.

The action of the operator $F_{\mathrm{m}}$ can be implemented in the OAM quantum walk by means of a Dove prism [69]. The action of the dove prism on the OAM states of light can be written as

$$|\ell\rangle \to \exp(i2\varphi\ell)\,|-\ell\rangle\,, \tag{36}$$

where $\varphi$ is the angle of rotation of the dove prism along the propagation axis of the light beam. Thus, two dove prisms in a sequence with angles $\varphi/4$ and $-\varphi/4$ can implement the action of the operator $F_{\mathrm{m}}$ (4) with $\Phi = \varphi$.

The final component required to achieve the complete control over the cat states in one-dimensional quantum walks is the reversal operation $\sigma_y$. In the current scheme, this operation can be achieved by simply using a half-wave plate that has the fast axis parallel to the horizontal axis.

To summarize, we have discussed an optical scheme to manipulate and control the cat state in OAM quantum walks using linear optical devices half-wave plates and dove prisms.

## VII. CONCLUSION

In conclusion, we have proposed a method to prepare the cat states in the quantum walk setup using delocalized initial states. Our method is system-independent and works for the entire range of the parameter $\theta$. We have also studied the effects of environmental interactions on the cat states and demonstrated that the large separation in the cat states is possible even in the presence of noise. Finally, we presented a method to control and manipulate the cat states in the optical systems.

The formation of the cat states in one-dimensional DTQW yields an interesting class of low-momentum Hamiltonians that, despite being non-linear in the momentum, possess linear dispersion relation. Both quantum walks and the cat states have been used to describe the coherent energy transfer in the photosynthesis process [35, 36, 40–42, 70]. The current proposal of preparing cat states using quantum walks threads the two concepts together, which might also contribute to a better understanding of the underlying physics of photosynthesis.

## ACKNOWLEDGMENTS

SKG and CS acknowledge the support from NSERC. BCS thanks NSERC, Alberta Innovates, and China's 1000 Talent Plan for financial support. WZ appreciates the financial support from the BUPT Excellent Ph.D. Students Foundation (Grant No. CX201325), the China Scholarship Council (Grant No. 201406470022), and NSERC. FG acknowledges the financial support from NSFC (Grants No. 61272057 and No. 61572081).

### Appendix A: Hamiltonian for the one-dimensional discrete time quantum walk

The low-momentum expansion of the Hamiltonian $H(k)$ in (9) can be calculated by using the Taylor series expansion of the Hamiltonian $H(k)$ and discarding the $O(k^3)$ and higher order terms. The truncated 2nd-order Hamiltonians read

$$H^{(2)} = \begin{pmatrix} -\cos\theta\left(k\cos\theta + \frac{\pi}{2} - \frac{1}{4}\pi k^2 \sin^2\theta\right) & \begin{pmatrix} -\sin\theta\left(k\cos\theta + \frac{\pi}{2} - \frac{1}{4}\pi k^2\sin^2\theta\right) \\ -ik\sin\theta\left(k\cos\theta + \frac{\pi}{2}\right) \end{pmatrix} \\ \begin{pmatrix} -\sin\theta\left(k\cos\theta + \frac{\pi}{2} - \frac{1}{4}\pi k^2\sin^2\theta\right) \\ +ik\sin\theta\left(k\cos\theta + \frac{\pi}{2}\right) \end{pmatrix} & \cos\theta\left(k\cos\theta + \frac{\pi}{2} - \frac{1}{4}\pi k^2\sin^2\theta\right) \end{pmatrix}. \tag{A1}$$

The eigenvalues $E_\pm(k)$ of the Hamiltonian (A1) read

$$E_\pm(k) = \pm\left(k\cos\theta + \frac{\pi}{2}\right) + O(k^3), \tag{A2}$$

and the corresponding eigenvectors read

$$|u_-(k)\rangle = \frac{1}{N_1}\begin{pmatrix} \left(-\frac{1}{2}k^2\cos\theta + k^2 - 2ik - 2\right)\cos\frac{\theta}{2} \\ \sin\frac{\theta}{2} \end{pmatrix}, \tag{A3}$$

$$|u_+(k)\rangle = \frac{1}{N_2}\begin{pmatrix} \left(-\frac{1}{2}k^2\cos\theta - k^2 + 2ik + 2\right)\sin\frac{\theta}{2} \\ \cos\frac{\theta}{2} \end{pmatrix}. \tag{A4}$$

Here, $N_1$ and $N_2$ are normalization factors which read

$$N_1 = \sqrt{\sin^2\frac{\theta}{2} + \left|-\frac{k^2}{2}\cos\theta + k^2 - 2ik - 2\right|^2\cos^2\frac{\theta}{2}}, \tag{A5}$$

$$N_2 = \sqrt{\cos^2\frac{\theta}{2} + \left|\frac{k^2}{2}\cos\theta + k^2 - 2ik - 2\right|^2\sin^2\frac{\theta}{2}}. \tag{A6}$$

With these eigenvectors and eigenvalues we can rewrite the Hamiltonian $H^{(2)}(k)$ as

$$H^{(2)}(k) = E_+(k)\left|u_+(k)\right\rangle\left\langle u_+(k)\right| + E_-\left|u_-(k)\right\rangle\left\langle u_-(k)\right|. \tag{A7}$$

For the small values of the parameter $\theta$ and small $k$, the Hamiltonian $H(k)$ reduces to a simpler form $H_\mathrm{d}$ that reads [37, 48]

$$H_\mathrm{d}(k) = -\left(k + \frac{\pi}{2}\right)\sigma_z - \theta\frac{\pi}{2}\sigma_x. \tag{A8}$$

The Hamiltonian $H_\mathrm{d}$ is linear in $k$; hence, it corresponds to a two-component Dirac Hamiltonian. From Eq. (A8) it is clear that the parameter $\theta$ characterizes the mass and the velocity of the walker. For small values of $\theta$ the walker behaves like a quantum relativistic particle with energy

$$E_d(k) = \pm\sqrt{\left(k + \frac{\pi}{2}\right)^2 + \frac{\pi^2}{4}\theta^2} = \pm\left(k + \frac{\pi}{2}\right) + O(\theta^2). \tag{A9}$$

The Hamiltonian $H_\mathrm{d}$ is valid only for the small values of the parameter $\theta$. For large values of $\theta$ (but still small $k$) the effective quantum walk Hamiltonian takes a slightly more complicated form which is the truncated 1st-order Hamiltonian $H^{(1)}$ for quantum walks

$$H^{(1)} = \begin{pmatrix} -\cos\theta\left(k\cos\theta+\frac{\pi}{2}\right) & -\sin\theta\left(k\cos\theta+\frac{\pi}{2}\right)-ik\frac{\pi}{2}\sin\theta \\ -\sin\theta\left(k\cos\theta+\frac{\pi}{2}\right)+ik\frac{\pi}{2}\sin\theta & \cos\theta\left(k\cos\theta+\frac{\pi}{2}\right) \end{pmatrix}, \tag{A10}$$

The eigenvalues for this Hamiltonian are

$$E_{\pm}^{(1)} = \pm\sqrt{\left(k\cos\theta+\frac{\pi}{2}\right)^2+\left(k\frac{\pi}{2}\sin\theta\right)^2}, \tag{A11}$$

which are, in general, not linear in $k$. However, one can recover the linear dispersion relation (A9) from (A11) by restricting the parameter $\theta$ to small values or introducing $O(k^2)$ terms in the Hamiltonian.

[1] E. Schrödinger, Naturwissenschaften **23**, 807 (1935).

[2] G. J. Milburn, Phys. Rev. A **33**, 674 (1986).

[3] B. Yurke and D. Stoler, Phys. Rev. Lett. **57**, 13 (1986).

[4] V. Bužek and P. L. Knight, Prog. Opt. **34**, 1 (1995).

[5] B. C. Sanders, Phys. Rev. A **45**, 6811 (1992).

[6] W. J. Munro, K. Nemoto, G. J. Milburn, and S. L. Braunstein, Phys. Rev. A **66**, 023819 (2002).

[7] J. Wenger, M. Hafezi, F. Grosshans, R. Tualle-Brouri, and P. Grangier, Phys. Rev. A **67**, 012105 (2003).

[8] M. Stobińska, H. Jeong, and T. C. Ralph, Phys. Rev. A **75**, 052105 (2007).

[9] C. Monroe, D. M. Meekhof, B. E. King, and D. J. Wineland, Science **272**, 1131 (1996).

[10] M. Brune, E. Hagley, J. Dreyer, X. Maître, A. Maali, C. Wunderlich, J. M. Raimond, and S. Haroche, Phys. Rev. Lett. **77**, 4887 (1996).

[11] J. J. Slosser and G. J. Milburn, Phys. Rev. Lett. **75**, 418 (1995).

[12] H. Jeong, M. S. Kim, T. C. Ralph, and B. S. Ham, Phys. Rev. A **70**, 061801 (2004).

[13] Y. P. Huang and M. G. Moore, Phys. Rev. A **73**, 023606 (2006).

[14] D. D. Bhaktavatsala Rao, N. Bar-Gill, and G. Kurizki, Phys. Rev. Lett. **106**, 010404 (2011).

[15] G. Csire and B. Apagyi, Phys. Rev. A **85**, 033613 (2012).

[16] C.-W. Lee, J. Lee, H. Nha, and H. Jeong, Phys. Rev. A **85**, 063815 (2012).

[17] B. Wu and J. Zhang, Sci. China Phys. Mech. Astron. **56**, 1810 (2013).

[18] H. W. Lau, Z. Dutton, T. Wang, and C. Simon, Phys. Rev. Lett. **113**, 090401 (2014).

[19] U. R. Fischer and M.-K. Kang, Phys. Rev. Lett. **115**, 260404 (2015).

[20] T. Wang, H. W. Lau, H. Kaviani, R. Ghobadi, and C. Simon, Phys. Rev. A **92**, 012316 (2015).

[21] J. R. Friedman, V. Patel, W. Chen, S. K. Tolpygo, and J. E. Lukens, Nature **406**, 43 (2000).

[22] D. Leibfried, E. Knill, S. Seidelin, J. Britton, R. B. Blakestad, J. Chiaverini, D. B. Hume, W. M. Itano, J. D. Jost, C. Langer, R. Ozeri1, R. Reichle1, and D. J. Wineland, Nature **438**, 639 (2005).

[23] A. Ourjoumtsev, H. Jeong, R. Tualle-Brouri, and P. Grangier, Nature **448**, 784 (2007).

[24] A. I. Lvovsky, R. Ghobadi, A. Chandra, A. S. Prasad, and C. Simon, Nat. Phys. **9**, 541 (2013).

[25] N. Bruno, A. Martin, P. Sekatski, N. Sangouard, R. T. Thew, and N. Gisin, Nat. Phys. **9**, 545 (2013).

[26] B. Vlastakis, G. Kirchmair, Z. Leghtas, S. E. Nigg, L. Frunzio, S. M. Girvin, M. Mirrahimi, M. H. Devoret, and R. J. Schoelkopf, Science **342**, 607 (2013).

[27] C. Wang, Y. Y. Gao, P. Reinhold, R. W. Heeres, N. Ofek, K. Chou, C. Axline, M. Reagor, J. Blumoff, K. M. Sliwa, and et al., Science **352**, 1087 (2016).

[28] S. E. Venegas-Andraca, Quantum Inf. Process. **11**, 1015 (2012).

[29] J. Kempe, Contemp. Phys. **44**, 307 (2003).

[30] A. Ambainis, Int. J. Quantum Inf. **01**, 507518 (2003).

[31] N. Shenvi, J. Kempe, and K. B. Whaley, Phys. Rev. A **67**, 052307 (2003).

[32] A. M. Childs and J. Goldstone, Phys. Rev. A **70**, 022314 (2004).

[33] A. M. Childs, Phys. Rev. Lett. **102**, 180501 (2009).

[34] N. B. Lovett, S. Cooper, M. Everitt, M. Trevers, and V. Kendon, Phys. Rev. A **81**, 042330 (2010).

[35] J. Klafter and R. Silbey, Phys. Lett. **125**, 339 (1980).

[36] I. Barvík and V. Szöcs, Phys. Lett. A **125**, 339 (1987).

[37] F. W. Strauch, Phys. Rev. A **73**, 054302 (2006).

[38] F. W. Strauch, J. Math. Phys. **48**, 082102 (2007).

[39] A. J. Bracken, D. Ellinas, and I. Smyrnakis, Phys. Rev. A **75**, 022322 (2007).

[40] G. S. Engel, T. R. Calhoun, E. L. Read, T.-K. Ahn, T. Mančal, Y.-C. Cheng, R. E. Blankenship, and G. R. Fleming, Nature **446**, 782 (2007).

[41] H. Lee, Y.-C. Cheng, and G. R. Fleming, Science **316**, 1462 (2007).

[42] M. Mohseni, P. Rebentrost, S. Lloyd, and A. Aspuru-Guzik, J. Chem. Phys. **129**, 174106 (2008).

[43] P. Kurzyński, Phys. Lett. A **372**, 6125 (2008).

[44] A. M. Childs, Commun. Math. Phys. **294**, 581 (2009).

[45] T. Kitagawa, M. S. Rudner, E. Berg, and E. Demler, Phys. Rev. A **82**, 033429 (2010).

[46] A. Schreiber, K. N. Cassemiro, V. Potoček, A. Gábris, P. J. Mosley, E. Andersson, I. Jex, and C. Silberhorn, Phys. Rev. Lett. **104**, 050502 (2010).

[47] A. Schreiber, A. Gábris, P. P. Rohde, K. Laiho, M. Štefaňak, V. Potoček, C. Hamilton, I. Jex, and C. Silberhorn, Science **336**, 55 (2012).

[48] C. M. Chandrashekar, S. Banerjee, and R. Srikanth, Phys. Rev. A **81**, 062340 (2010).

[49] D. W. Berry and A. M. Childs, Q. Info. Comp. **12**, 29 (2012).

[50] T. Kitagawa, Quantum Inf. Process. **11**, 1107 (2012).

[51] T. Kitagawa, M. A. Broome, A. Fedrizzi, M. S. Rudner, E. Berg, I. Kassal, A. Aspuru-Guzik, E. Demler, and A. G. White, Nat. Commun. **3**, 882 (2012).

[52] J. K. Asbóth, Phys. Rev. B **86**, 195414 (2012).

[53] S. Moulieras, M. Lewenstein, and G. Puentes, J. Phys. B: At. Mol. Opt. Phys. **46**, 104005 (2013).

[54] H. Obuse, J. K. Asbóth, Y. Nishimura, and N. Kawakami, Phys. Rev. B **92**, 045424 (2015).

[55] J. M. Edge and J. K. Asbóth, Phys. Rev. B **91**, 104202 (2015).

[56] F. Cardano, F. Massa, H. Qassim, E. Karimi, S. Slussarenko, D. Paparo, C. de Lisio, F. Sciarrino, E. Santamato, R. W. Boyd, and L. Marrucci, Sci. Adv. **1**, 1500087 (2015).

[57] P. Zhang, B.-H. Liu, R.-F. Liu, H.-R. Li, F.-L. Li, and G.-C. Guo, Phys. Rev. A **81**, 052322 (2010).

[58] S. K. Goyal, F. S. Roux, A. Forbes, and T. Konrad, Phys. Rev. Lett. **110**, 263602 (2013).

[59] S. K. Goyal, T. Konrad, and L. Diósi, Phys. Lett. A **379**, 100 (2015).

[60] M. Genske, W. Alt, A. Steffen, A. H. Werner, R. F. Werner, D. Meschede, and A. Alberti, Phys. Rev. Lett. **110**, 190601 (2013).

[61] C. Cedzich, T. Rybár, A. H. Werner, A. Alberti, M. Genske, and R. F. Werner, Phys. Rev. Lett. **111**, 160601 (2013).

[62] L. Marrucci, C. Manzo, and D. Paparo, Phys. Rev. Lett. **96**, 163905 (2006).

[63] R. Simon and N. Mukunda, Phys. Lett. A **138**, 474 (1989).

[64] M. A. Nielsen and I. L. Chuang, *Quantum Computation and Quantum Information* (Cambridge University Press, Cambridge, 2010).

[65] V. Kendon and B. Tregenna, Phys. Rev. A **67**, 042315 (2003).

[66] V. Kendon, Math. Struct. Comput. Sci. **17**, 1169 (2007).

[67] M. A. Broome, A. Fedrizzi, B. P. Lanyon, I. Kassal, A. Aspuru-Guzik, and A. G. White, Phys. Rev. Lett. **104**, 153602 (2010).

[68] D. A. R. Dalvit, J. Dziarmaga, and W. H. Zurek, Phys. Rev. A **62**, 013607 (2000).

[69] M. J. Padgett and J. P. Lesso, J. Mod. Opt. **46**, 175 (1999).

[70] P. Nalbach, D. Braun, and M. Thorwart, Phys. Rev. E **84**, 041926 (2011).

# Entropic uncertainty relations for successive generalized measurements

Kyunghyun Baek[1] Gwangil Bae[1] Wonmin Son[1 2]

[1] *Department of Physics, Sogang University, Mapo-gu, Shinsu-dong, Seoul 121-742, Korea*
[2] *Department of Physics, University of Oxford, Parks Road, Oxford OX1 3PU, UK*

**Abstract.** We derive entropic uncertainty relations for successive generalized measurements by using general descriptions of quantum measurement within two distinctive operational scenarios. In the first scenario, by merging two successive measurements into one we consider successive measurement scheme as a method to perform an overall composite measurement. In the second scenario, on the other hand, we consider it as a method to measure a pair of jointly measurable observables by marginalizing over the distribution obtained in this scheme. Entropic uncertainty relations derived in both scenarios are examined in specific examples of spin-1/2 systems.

**Keywords:** Entropic uncertainty relations, Successive measurements, Unsharpness, Disturbance

## 1 Introduction

Uncertainty principle has been considered as one of the most important concepts in quantum physics, since Heisenberg suggested a trade-off between imprecision of instrument measuring a particle's position and disturbance of its momentum. From the Heisenberg's viewpoint, the uncertainty principle is actively discussed recently with increasing abilities to control quantum systems, and successive measurement(SM) scheme plays key roles in clarifying meanings of imprecision and disturbance of measurements.

In this work, we investigate statistical properties of probability distributions obtained via SM scheme, and derive entropic uncertainty relations(URs) for successive generalized measurements, by generalizing the previous work [1] for the concept of positive-operator-valued measures(POVMs). We refer to [2] for detailed discussions and references of this manuscript.

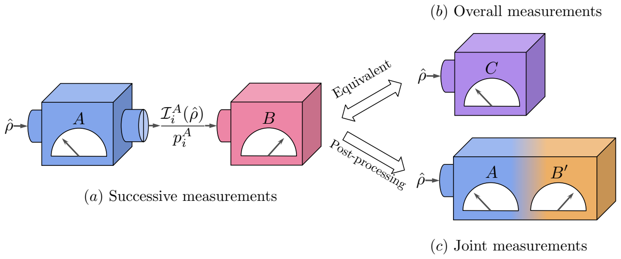

Figure 1: Relations among measurement schemes. (**a**) SM of observables $A$ and $B$, where the first measurement $A$ gives rise to output state $\mathcal{I}_i^A(\rho)/p_A(i)$ conditioned on its outcome $i$; (**b**) Overall measurement of $C$, (**c**) Joint measurements of $A$ and $B'$.

### 1.1 Measure of unsharpness

To begin with, let us clarify notations and terminologies as follows. For a finite $d$-dimensional Hilbert space $\mathcal{H}_d$, we denote the vector space of all linear operators on $\mathcal{H}_d$ by $\mathcal{L}(\mathcal{H}_d)$. Any observable $A$ then is described by POVM $\{\hat{A}_i\}$ which is a set of positive operators $\hat{A}_i \in \mathcal{L}(\mathcal{H}_d)$ obeying $\sum_{i=1}^{n_A} \hat{A}_i = \hat{I}$ with the number of elements $n_A$. In a particular case that all POVM elements are given as projections, $A$ is a projection-valued measure (PVM). In this case, A is called a *sharp observable*. On the other hand, if A is not a PVM, it is called an *unsharp observable*.

To characterize the unsharpness, we consider $\hat{A}_i$ in the form of spectral decomposition $\hat{A}_i = \sum_{k=1}^{d} a_i^k |a_i^k\rangle\langle a_i^k|$, where $0 \le a_i^k \le 1$ is an eigenvalue corresponding to an eigenvector $|a_i^k\rangle$. Then the measure of unsharpness is defined as

$$D_\rho(A) = \sum_{i=1}^{n_A} \sum_{k=1}^{d} \langle a_i^k|\hat{\rho}|a_i^k\rangle h(a_i^k) \tag{1}$$

for $\hat{\rho}$ with $h(a_i^k) = -a_i^k \log a_i^k$, which is so-called *device uncertainty* (see [3] for details). This quantity has an important property that a nontrivial lower bound of entropy is given by itself such that

$$H_\rho(A) \ge D_\rho(A) \ge \min_\rho D_\rho(A) \ge -\log \max_i \|\hat{A}_i\| \tag{2}$$

due to the concavity of entropy. The minimal device uncertainty can be obtained by diagonalizing $\sum_{i=1}^{n_A} \sum_{k=1}^{d} h(a_i^k)|a_i^k\rangle\langle a_i^k|$ and taking the lowest eigenvalue, which is stronger than $-\log \max_i \|\hat{A}_i\|$ proposed in [4].

### 1.2 General description of successive measurement

In the present work, by a *successive measurement(SM)*, we mean a scheme where two measurements are performed one after the other successively as the second one is performed immediately on an output state conditionally transformed according to an outcome of the first one. To describe SM, we need the concept of an *A-compatible instrument*, which is a mapping $\mathcal{I}^A : i \to \mathcal{I}_i^A$ such that each $\mathcal{I}_i^A$ is a completely positive linear map on $\mathcal{L}(\mathcal{H}_d)$ satisfying $\mathrm{tr}[\mathcal{I}_i^A(\hat{\rho})] = \mathrm{tr}[\hat{A}_i\hat{\rho}]$ for all states $\hat{\rho}$. Accordingly, the instrument illustrates that a measurement outcome $i$ is obtained with the probability $p_i^A = \mathrm{tr}[\hat{A}_i\hat{\rho}]$ for a state $\hat{\rho}$, and a normalized output state $\mathcal{I}_i^A(\hat{\rho})/p_i^A$ is generated as depicted in Fig. 1-(a).

Now, let us consider the first scenario as depicted in Figure 1-(b) that can be seen as a method to obtain the

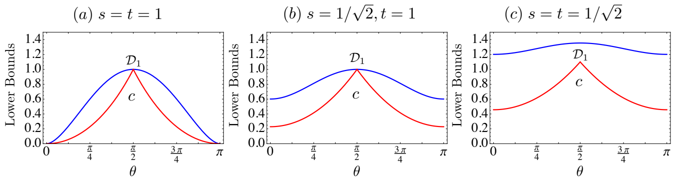

Figure 2: Graphs illustrate the lower bounds in Equation (5) for SM of $Z$ and $X(\theta)$ with respect to angle $\theta$ and the unsharpness parameters $s$ and $t$.

*overall observable* $C$ described by POVM $\{\hat{C}_{ij}\}$ obeying

$$\mathrm{tr}[\hat{C}_{ij}\hat{\rho}] = \mathrm{tr}[\mathcal{I}_i^A(\hat{\rho})\hat{B}_j] = p_{AB}(i,j) \tag{3}$$

for all $i, j$ and all states $\hat{\rho}$. In the Heisenberg picture, equivalently, it can be rewritten as $\hat{C}_{ij} = \mathcal{I}_i^{A*}(\hat{B}_j)$ where $\mathcal{I}_i^{A*}$ denotes the adjoint map of $\mathcal{I}_i^A$. Namely, the SM of $A$, $B$ are merged into $C$ having $n_A n_B$ outcomes.

On the other hand, in the second scenario the scheme is considered as a strategy to perform a joint measurement of $A$ and $B'$ as depicted in Fig. 1-(c), where $A$ and $B'$ are described by

$$\hat{A}_i = \sum_{j=1}^{n_B} \hat{C}_{ij} \qquad \text{and} \qquad \hat{B}'_j = \sum_{i=1}^{n_A} \hat{C}_{ij} \tag{4}$$

for all $i$, $j$, respectively.

## 2 Overall observables obtained via SM

In the first scenario, we can consider performing SM of $A$ and $B$ as a method to implement the overall measurement of $C$. This fact implies $H_\rho(A,B) = H_\rho(C)$, since $p_{AB}(i,j) = p_C(i,j)$ for all $i$, $j$. Thus, our goal to analyze uncertainty existing in the first scenario can be achieved under consideration of the overall observable $C$. By using the fact that uncertainty of a measurement does not vanish due to its unsharpness, as described in Eq. (2), we obtain entropic form of UR lower bounded by device uncertainty characterizing unsharpness of $C$ such that

$$H_\rho(A,B) \geq D_\rho(C) \geq \min_\rho D_\rho(C) \equiv \mathcal{D}_1. \tag{5}$$

Let us take an example of successively measuring two qubit observables $Z$ at first and $X(\theta)$ later in $\mathcal{H}_2$ described by $\hat{Z}_\pm = (\hat{I} \pm s\hat{\sigma}_z)/2$ and $\hat{X}_\pm(\theta) = \{\hat{I} \pm t(\sin\theta\hat{\sigma}_x + \cos\theta\hat{\sigma}_z)\}/2$ respectively, where unsharp parameters are denoted by $0 \leq s, t \leq 1$. Additionally, we assume the Lüders instrument for $Z$, which means the overall observable $S$ is described by $\hat{S}_{\mu\nu} = \sqrt{\hat{Z}_\mu}\hat{X}_\nu(\theta)\sqrt{\hat{Z}_\mu}$ for $\mu, \nu = \pm 1$. In this case, we plot the lower bounds $\mathcal{D}_1$ and the incompatibility $c = -\log\max_{\mu,\nu}\|\sqrt{\hat{Z}_\mu}\sqrt{\hat{X}_\nu(\theta)}\|$ versus the angle $\theta$ in Fig.2.

## 3 Joint observables obtained via SM

Both observables $A$ and $B'$ obtained via the second scenario may have their own unsharpness, so that an amount of uncertainties about $A$ and $B'$ may not vanish due to the unsharpness of them. As formulating this fact, we obtain entropic URs in the form of

$$\begin{aligned} H_\rho(A) + H_\rho(B') &\geq D_\rho(A) + D_\rho(B') \\ &\geq \min_\rho\,[D_\rho(A) + D_\rho(B')] \equiv \mathcal{D}_2. \end{aligned} \tag{6}$$

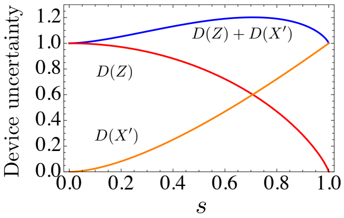

Figure 3: Graph illustrates device uncertainties $D(Z)$, $D(X')$ and their summation $D(Z) + D(X')$ with respect to the unsharp parameter $s$.

Here, an important point is that the second measurement $B$ may be perturbed to be $B'$ because of disturbance caused by the first measurement $A$, while $A$ is preserved.

We assume to implement the Lüders instrument for $Z$ and a measurement of $X$ successively in $\mathcal{H}_2$ described by $\hat{Z}_\pm = (\hat{I} \pm s\hat{\sigma}_z)/2$ and $\hat{X}_\pm = (\hat{I} \pm \hat{\sigma}_x)/2$ respectively. In this case, the SM is equivalent to measure a pair of jointly measurable observables $Z$ and $X'$, where $X'$ is given as $\hat{X}'_\pm = (\hat{I} \pm t\hat{\sigma}_x)2$ with the unsharp parameter $t = \sqrt{1-s^2}$. Thus, we cannot avoid unsharpness, and there is the trade-off between the unsharpness of $Z$ and $X'$ such that the more sharpness of $Z$, the more unsharpness of $X'$. This behavior can be found in Fig. 3

## 4 Conclusion

In the present work we have suggested entropic URs for successive generalized measurement within two distinctive scenarios. In both scenarios, it is identified that measuring incompatible observables via SM scheme imposes unavoidable uncertainty, as illustrated in Figs. 2 and 3. Additionally, we note that the entropic UR (6) derived in the second scenario is applicable to any pair of jointly measurable observables, since Heinosaari *et al.* have proved that we can obtain any pair of jointly measurable observables via SM scheme.

## References

[1] K. Baek; T. Farrow; W. Son, Optimized entropic uncertainty for successive projective measurements *Phys. Rev. A*, 89, 032108, 2016.

[2] K. Baek, W. Son, Unsharpness of generalized measurement and its effects in entropic uncertainty relations. *Sci. Rep.*, 6, 30228, 2016.

[3] K. Baek, W. Son, Entropic uncertainty relations for successive generalized measurements *Mathematics*, 4, 41, 2016.

[4] M. Krishna, K.R. Parthasarathy, An entropic uncertainty principle for quantum measurements, *Indian J. Stat. Ser. A*, *64*, 842, 2002.

# Fault-tolerant quantum computation using a maximum-likelihood decoder with the GKP code states

Kosuke Fukui[1] * Akihisa Tomita[1] † Atsushi Okamoto[1] ‡

[1] *Graduate School of Information Science and Technology, Hokkaido University, Kita14-Nishi9, Kita-ku, Sapporo 060-0814, Japan*

**Abstract.** In this paper, utilizing continuous variable nature of the GKP code states effectively, we propose a decoder using maximum-likelihood for concatenated Calderbank-Shor-Steane codes. In particular, we perform numerical simulation with the C4/C6 code proposed by Knill. A numerical calculations for a decoding of C4/C6 confirmed the effectiveness of our method in terms of error-tolerance and the threshold for concatenation.

**Keywords:** GKP code states, continuous variables, maximum-likelihood decoder

## 1 Introduction

Quantum computers have a great deal of potential, but to realize that potential, they need some sort of protection from noise to construct a large scale quantum computation. Optical continuous variable states are promising candidates for building blocks to implement scalable quantum computation and communication [1,2]. However, the finite squeezing limits the scale of the quantum computation by inducing noise, which destroys the quantum information even with the perfect experimental apparatus[3]. Nevertheless, it has been shown that an infinite length fault-tolerant quantum computation is possible using qubit encoding of an oscillator introduced by Gottesman, Kitaev, and Preskill (so called the GKP code states) in 2014 [4]. In this paper, we propose a maximum-likelihood scheme for concatenated Calderbank-Shor-Steane (CSS) codes with the GKP code states. In particular, we perform numerical simulation with the C4/C6 code proposed by Knill [5].

## 2 Likelihood for the GKP code states

We start by explaining the GKP code states where the qubit is protected against small shifts in phase space [6]. GKP proposed to use states whose $q$ quadrature wave function is composed of a series of Gaussian peaks of width $\Delta$ contained in a larger Gaussian envelope of width $1/\Delta$. The approximated logical states $|\widetilde{0}\rangle$ and $|\widetilde{1}\rangle$ are given by

$$\begin{aligned} |\widetilde{0}\rangle &\propto \sum_{t=-\infty}^{\infty} \int \mathrm{e}^{-2\pi\Delta^2 t^2} \mathrm{e}^{-(q-2t\sqrt{\pi})^2/(2\Delta^2)} \, |q\rangle \, dq \\ |\widetilde{1}\rangle &\propto \sum_{t=-\infty}^{\infty} \int \mathrm{e}^{-\pi\Delta^2(2t+1)^2/2} \mathrm{e}^{-(q-(2t+1)\sqrt{\pi})^2/(2\Delta^2)} \, |q\rangle \, dq. \end{aligned} \tag{1}$$

The bit values 0 and 1 of the GKP code states can be determined by measurement of the variable $q$. Although in case of $\Delta \rightarrow 0$ (infinite squeezing) the state becomes the perfect code states, the approximate states are not orthogonal, and there are some probability of misidentify a 0 state $|\widetilde{0}\rangle$ as a 1 state $|\widetilde{1}\rangle$ and vise versa. Measurement on the approximated states $|\widetilde{0}\rangle$ ($|\widetilde{1}\rangle$) yields an outcome $q_m$ around the nearest bit value $q_k = (2t + k)$ ($t = 0, \pm 1, \pm 2, \cdots .\ k = 0, 1$). In practice, because we don't know the true state, we need to guess the true bit value is k from the measurement result $q_m$. We define the measurement shift by $\Delta q_m = \mid q_m - q_k \mid$ for the logical state $|\widetilde{k}\rangle$. If $\Delta q_m$ is less than$\sqrt{\pi}/2$, the true shift $\overline{\Delta}$ is equal to $\Delta q_m$ . On the other hand, if $\Delta q_m$ is between$\sqrt{\pi}/2$ and$\sqrt{\pi}$, the true shift $\overline{\Delta}$ is equal to $-\Delta q_m$. We notice that $\Delta$ obeys the following Gaussian probability distribution $f(\overline{\Delta})$ with the average 0 and the variance $\Delta^2$,

$$f(\overline{\Delta}) = \frac{1}{\sqrt{2\pi\Delta^2}} \mathrm{e}^{-\overline{\Delta}^2/(2\Delta^2)} \tag{2}$$

In our method we regard the function$f(\overline{\Delta})$as a likelihood function and combine the discrete variables $k$, which refer to the degree of freedom for the logical level, with the continuous variables $\overline{\Delta}$, the degree of freedom for the physical level to improve our guess on $k$.

## 3 Maximum-likelihood decoder

To give the idea of our maximum-likelihood method, we briefly describe our method by three-qubit bit flip error code. The three-qubit code encodes a single logical qubit into three physical qubits to correct a single bit flip error. Suppose the three physical qubits are labeled by 1, 2, and 3. The two logical states $|0\rangle$ L and $|1\rangle$L are defined as $|0\rangle_{\mathrm{L}} = |000\rangle_{123}$ and $|1\rangle_{\mathrm{L}}=|111\rangle_{123}$, so that an arbitrary single qubit state $|\mathit{\Psi}\rangle = \alpha|0\rangle + \beta|0\rangle$ is mapped to $\alpha|0\rangle_{\mathrm{L}} + \beta|0\rangle_{\mathrm{L}} = \alpha|000\rangle_{123} + \beta|0\rangle_{123} = |\mathit{\Psi}\rangle_{\mathrm{L}}$. In a conventional manner, the three-qubit code will correct a state such as $|100\rangle_{123}$ ($|011\rangle_{123}$) to $|000\rangle_{123}$ ($|111\rangle_{123}$) by a majority voting. In our maximum-likelihood manner, we compare two maximum-likelihood functions which are corresponding to the case with a single error and double errors. If the error syndrome shows that the first qubit is 0 (or1) and other two qubits are 11(or 00), we compare the function $F_1 = f(\Delta_{m1}) \times f(-\Delta_{m2}) \times f(-\Delta_{m3})$ with $F_2 = f(-\Delta_{m1}) \times f(\Delta_{m2}) \times f(\Delta_{m3})$, where the $\Delta_{mi}$ is

*fukui.opt@gmail.com

†tomita@ist.hokudai.ac.jp

‡ao@optnet.ist.hokudai.ac.jp

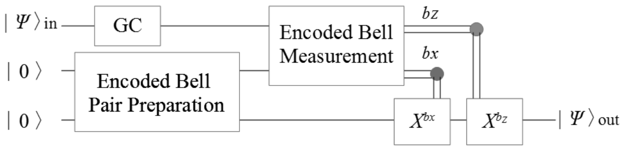

Figure 1: Error-correcting teleportation with the maximum-likelihood decoding for C4/C6 code.

the measurement shift of $i$-th qubit. Because the function $F_1(F_2)$ is a likelihood, in the case of $F_1 > F_2$, we decide that a single error occurs on the first qubit. In the case of $F_1 < F_2$, we decide that two error occur on the second and third qubits. In our method the three-qubit code can correct two errors, whereas in the conventional method the code corrects only a single error.

We apply the likelihood function to our maximum-likelihood method for concatenated CSS codes and confirm the validity of our method by a numerical calculation for the specific case of C4/C6 code based on teleportation. As in the figure.1, which shows the decoder of the C4/C6 code, the encoded data qubit $|\Psi\rangle_{\rm in}$ is teleported to the fresh encoded qubit of the ancilla Bell state $|\Psi\rangle_{\rm out}$ using maximum-likelihood decoding (MLD). The outcome of the encoded Bell measurement, b$_x$ and b$_z$, provides the syndrome information and error-detecting or error-correcting operation is performed by teleportation. The C4/C6 code is composed of a concatenation of two codes, C4 and C6. At level-1, a qubit pair is encoded into four physical qubits, which refers to C4. At more than level-1, a level-$l$ qubit pair is encoded into three level-($l$-1) qubit pairs ($l$= 2,3,4 $\cdots$). To evaluate the performance of the proposed decoder, we examined the error-tolerance for a Gaussian channel which leads to errors of displacements in the $q$ and $p$ quadrature, which is dipicted as GC in figure.1. By considering the displacement which follows Gaussian distribution, we evaluate the influence as the decreasing of the squeezing level of the encoded data qubit. In this simulation, we assumed that errors occur only on the channel and the other operations (encoding, Bell-state preparation, decoding, and Bell measurement) are performed without any errors. In figure. 2, the error probabilities are plotted as a function of the squeezing level of the encoded data qubit for the levels $l$ = 1,2,3 after the channel for 11 dB of the encoded Bell pair's squeezing level. In figure.2, for example, the error probability is improved from about 0.25 to 0.05 at squeezing level of 6.7 dB for level-3, by use of our maximum-likelihood method. Moreover, the threshold for concatenation of C4/C6 by use of the proposal are improved by a little less than 1 dB. The simulation results show our method improves the error rate and the thresholds effectively.

## 4 Conclusion

Towards efficient fault-tolerant quantum computation with the GKP code states, we introduced a maximum-likelihood method for concatenated Calderbank-Shor-Steane codes and applied for the C4/C6 code proposed by Knill. In our method, we use a hybrid quantum information processing, where discrete degree of freedom of a bit value are combined with continuous degree of freedom of a shift value for enhancing noise resistance. A numerical calculations for a decoding of C4/C6 confirmed the effectiveness of our method in terms of error-tolerance and the threshold for concatenation. Moreover, the method will reduce resources required for fault-tolerant quantum computation. The enhanced power results from the continuous variable nature of the oscillators combined with discretization on decoding.

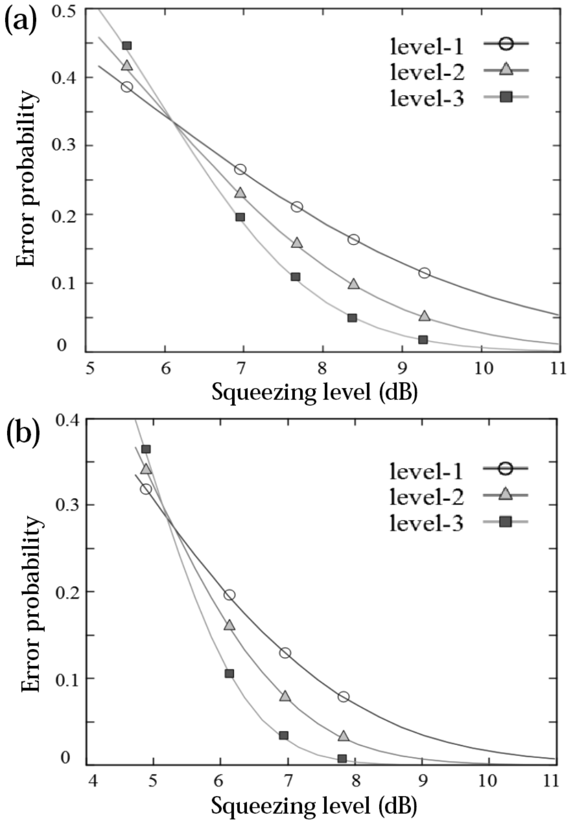

Figure 2: The error probabilities of the decoding with (a) Knill's conventional method, and (b) our maximum-likelihood method for the levels $l$ = 1,2,3.

**Acknowledgement** : This work was partly supported by ImPACT "Advanced Information Society Infrastructure Linking Quantum Artificial Brains in Quantum Network".

## References

[1] M. Pysher, Y. Miwa, R. Shahrokhshahi, R. Bloomer and O. Pfister, In *Phys. Rev. Lett.* 107, 030505, 2011.

[2] M. Chen, N. C. Menicucci and O. Pfister, *Phys. Rev. Lett.*. 112, 120505, 2014 McGraw-Hill, 1999.

[3] M. Ohliger, K. Kieling and J. Eisert, *Phys. Rev. A* 82, 042336, 2010.

[4] N. C. Menicucci, *Phys. Rev. Lett.*, 112, 120504, 2014.

[5] E, Knill, *Nature*, 434, 39-44, 2005.

[6] D. Gottesman, A. Kitaev and J. Preskill, *Phys. Rev. A*, 64, 012310, 2001.

# Generation and Characterization of Quantum Cluster States using Surface Acoustic Waves

MG Majumdar, CHW Barnes

(Dated: April 15, 2016)

**Abstract.** Cluster State Generation and Use

**Keywords.** Cluster State, GHZ States, Entanglement Monogamy

We describe a method of generation of four-qubit and six-qubit cluster states using electrons in Quantum One-Dimensional Channels (Q1DC), driven by Surface Acoustic Waves (SAWs).

Section 1 is on the generation of the cluster state using electrons in quantum one-dimensional channels, driven by Surface Acoustic Waves. Section 2 is on measures for characterization of N-particle entanglement. Section 3 is on the results and discussion of the entanglement generation and characterization.

## I. INTRODUCTION

One-way quantum computation, also known as Cluster State Quantum Computation, provides a robust and efficient tool to perform universal quantum computation using only single-qubit projective measurements, given a highly entangled cluster state. The cluster-state approach to quantum computation also leads to certain practical advantages such as robustness against errors.

The cluster state is generated on a basis defined by electrons in Quantum One-Dimensional Channels (Q1DCs), driven by Surface Acoustic Waves [1]. The setup for the generation consists of Copper interdigitated transducers on a Silicon substrate with layers of Silicon Dioxide and Zinc Oxide, to reinforce the piezoelectric effect on the substrate. The transducers are placed on either sides of a centrally-placed etched region with an Electron Gas. When a high frequency AC signal is applied, Surface Acoustic Waves are generated, by the principle of piezoelectricity. As the SAW propagates through the etched region, the travelling potential it creates carries the electrons from the electron gas with it.

A typical SAW frequency of 3 GHz and an applied power of 10 dBm produces a measurable current in the nano-ampere range, as shown by *Barnes, et al* [1]. One-qubit rotations and controlled two-qubit gates can be implemented on this system. The primary gate in our generation-protocol is the Root of Swap gate.

Interchannel and intra-channel, two-instance swap operations form the primary building blocks of the given generation-protocol. *Owen et al* [2] demonstrated how two particles that are interacting in a harmonic potential generate maximally entangled states, which are created simply through the quantum dynamics of the system and possessing a high entanglement fidelity (F > 0.98). The underlying operation is essentially a root-of-SWAP operation. *Bayer et al* [3] demonstrated coupling and entanglement of quantum states in a pair of vertically aligned quantum dots by studying the emission of an interacting exciton in a single dot molecule as a function of the separation between the dots. The electron-hole complex was shown to be equivalent to entangled states of two interacting spins.

## II. SURFACE ACOUSTIC WAVES

Surface-acoustic waves (SAWs) are sound waves that travel parallel to the surface of an elastic material. The displacement amplitude decays into the material and therefore these waves are confined to within roughly a wavelength of the surface. In a piezoelectric material, mechanical deformations associated with the SAW produce electric fields.

For non-piezoelectric materials, Hooke's law states that the mechanical stress field experienced by a body is proportional to the strain field:

$$\sigma_{ij} = c_{ijkl}\epsilon_{kl}$$

where $\sigma_{ij}$ and $\epsilon_{kl}$ are components of the stress and strain fields respectively, and $c_{ijkl}$ is a component of the 4th rank 'elastic' tensor. The electric displacement for non-piezoelectric materials is proportional to components of the electric field, with components of the permittivity tensor being the proportionality constants.

For piezoelectric materials, the electric displacement depends on the applied electric field and mechanical strain, and the stresses depend on both the applied mechanical strain and the electric field.

$$D_i = \epsilon^S_{ij} + e_{ijk}\epsilon_{jk}$$
$$\sigma_{ij} = \text{-}e_{kij}E_k + c^E_{ijkl}\epsilon_{kl}$$

Here superscripts S and E denote that the quantities are measured under constant strain and electric field respectively.

A SAW can be generated by applying an oscillating signal to a suitably designed set of interdigitated transducer based surface gates on a piezoelectric substrate. Small localized displacements of the fluid will propagate as an acoustic wave, also known as a compressional wave. When a SAW passes beneath a SAW transducer of the appropriate pitch, an alternating potential is generated across the transducer.

## III. THE SETUP

In our setup, by bringing the channels close to each other, we allow for Coulombic interaction to take place between the electrons travelling in the channels. As seen, with a high fidelity, this generates an entangled state using the 'Root-of-Swap' operation. One can also use a magnetic field, oriented in a certain direction to implement single qubit rotations, which constitute an essential part of the Universal Quantum Gates set.

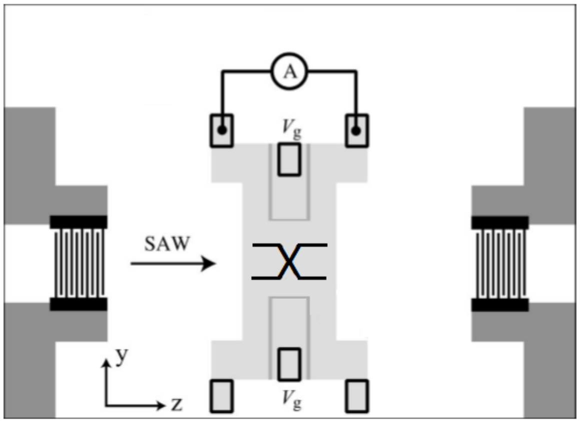

**Figure 1**: *Setup, comprising of Quantum One-Dimensional Channels with electrons driven by Surface Acoustic Waves (SAWs)*

## IV. CHARACTERIZATION OF ENTANGLEMENT

We wish to characterize the entanglement in multipartite qubit states. A pure n-qubit state is called unentangled if its wave function may be written as an n-fold tensor product of individual qubits. A state is globally entangled if it cannot be written as a tensor product of any set of subsystems.

There are several ways of quantifying entanglement. Measures of entanglement can be been used that are constant on locally equivalent states. These must be entanglement monotones i.e. they must be non-increasing under Local Operations and Classical Communication (LOCC).

One can also have observables whose expectation values are positive (negative) on unentangled states and negative (positive) on entangled states.

### Partial Density Matrices

The density operator $\rho$ for the ensemble or mixture of states $|\psi_i\rangle$ with probabilities $p_i$ is given by

$$\rho = \textstyle\sum_i p_i |\psi_i\rangle\langle\psi_i|$$

The reduced density operator describes the properties of measurements of a sub-system A, when the other subsystem(s) is(are) left unobserved, by tracing them out.

Peres [4] showed that a necessary condition for seperability in a system is that a matrix obtained using partial transposition of the density matrix of the system has only non-negative eigenvalues.

### Concurrence

As defined by *Carvalho et al* [5], for an N-partite quantum system, one can define $2^N - 2$ reduced density matrices and an associated concurrence measure:

$$C_N = 2^{1-\frac{N}{2}}\sqrt{(2^N-2)(\langle\psi|\psi\rangle)^2 - \sum_\alpha Tr{\rho_\alpha}^2}$$

where $\alpha$ labels all the reduced density matrices.

## V. RESULTS AND DISCUSSION

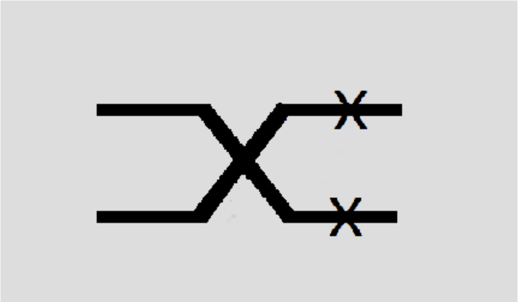

**Figure 2**: *Gate Combination with interchannel and intrachannel Root-of-Swap Operations*

For this setup, we consider the various input states and the concurrence measures for the entanglement generated by the setup in the process.

**Case 1**: Input comprises of $|00\rangle$ and $|00\rangle$

$$C_4 = 0$$

**Case 2**: Input comprises of $|11\rangle$ and $|11\rangle$

$$C_4 = 0$$

Both these cases are expected to have vanishing entanglement concurrence-measures, as the Root-of-Swap operation leaves the $|11\rangle/|00\rangle$ combinations unaltered. In this case, a seperable input composite state is unaffected by the *setup-entanglers*.

**Case 3**:
Input comprises of $|00\rangle$ and $|01\rangle$
Input comprises of $|00\rangle$ and $|10\rangle$
Input comprises of $|01\rangle$ and $|00\rangle$
Input comprises of $|10\rangle$ and $|00\rangle$
Input comprises of $|11\rangle$ and $|10\rangle$
Input comprises of $|11\rangle$ and $|01\rangle$
Input comprises of $|10\rangle$ and $|11\rangle$
Input comprises of $|01\rangle$ and $|11\rangle$

$$C_4 = 1.479$$

In these cases, there is one flipped spin, with respect to the remaining qubit subsystem. As a result, the entanglement capacity for each of these systems is equal.

**Case 4**:
Input comprises of $|00\rangle$ and $|11\rangle$
Input comprises of $|11\rangle$ and $|00\rangle$

$$C_4 = 1.458$$

The first inter-channel entangling Root-of-Swap operation has no effect on the input state since they are $|11\rangle/|00\rangle$ combinations. However, the subsequent intra-channel entanglers give rise to entanglement in the state.

**Case 5**:
Input comprises of $|01\rangle$ and $|01\rangle$
Input comprises of $|10\rangle$ and $|10\rangle$

$$C_4 = 1.620$$

This is the case when both interchannel and intrachannel entanglers contribute to the generation of entanglement.

**Case 6**:
Input comprises of $|01\rangle$ and $|10\rangle$
Input comprises of $|10\rangle$ and $|01\rangle$

$$C_4 = 1.225$$

This is an interesting case wherein the entanglers contribute to the generation of entanglement, much like in *Case 5*. However, the concurrence measure is much lower in this case.

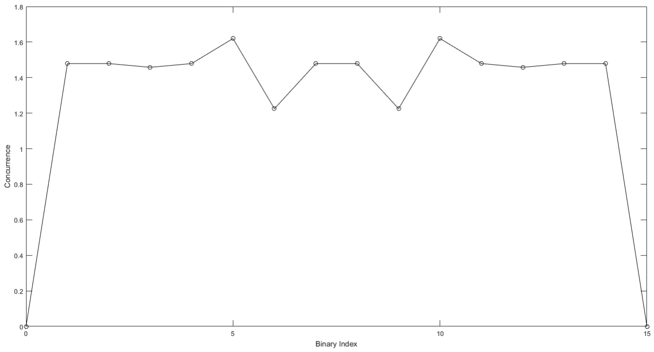

**Figure 3**: *Concurrence Plot*

We hypothize that the dip in the plot (*Case 6*) is because of the concept of *Entanglement Monogamy*. Once the entanglement is generated by the interchannel entanglers, the intrachannel entanglers entangle the states further, though this essentially reduces entanglement between subsystems and we obtain a cluster state.

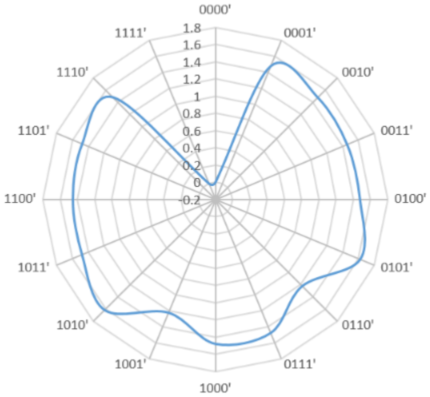

**Figure 4**: *Polar Plot of Concurrence Measures*

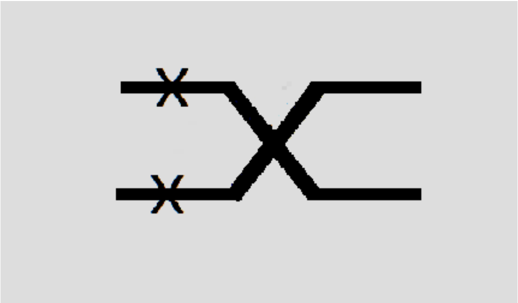

**Figure 5**: *Gate Combination with intrachannel and interchannel Root-of-Swap Operations*

In this case, we have vanishing concurrence (implying seperability) for input comprising of $|00\rangle|00\rangle$ and $|11\rangle|11\rangle$, as in the previous setup.

This is due to the entanglers not generating entanglement for this particular input state, given a Root-of-Swap based generator setup, irrespective of the order of the entanglers: first intra- and then inter-channel entanglers, or first inter- and then intra-channel entanglers.

For the case with one spin flipped, with respect to other qubits in the system, we have the same result as for the previous setup. The concurrence remains at 1.479. The concurrence measure and the amount of entanglement remains unchanged due to the fact that after the first entangler operation in both circuits, entanglement is generated only in a single two-qubit subsystem while the remaining two-qubit subsystem remains in a composite state. This step remains unchanged due to the symmetry of this particular kind of four-qubit input state. Eventually, the second entangler generates entanglement in the entire system by generating quantum correlations between one part of the entangled two-qubit subsytem and one half of the composite subsystem of qubits.

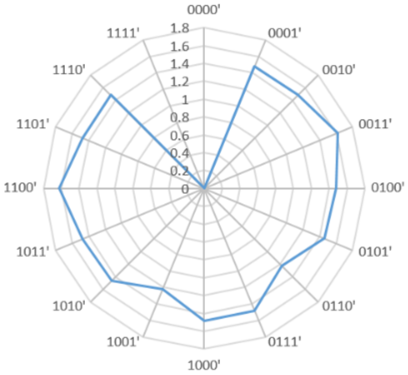

**Figure 6**: *Polar Plot of Concurrence Measures*

The concurrence for the $|00\rangle|11\rangle/|11\rangle|00\rangle$ and the $|01\rangle|01\rangle/|10\rangle|10\rangle$ states are interchanged, with respect to the case for the inter-intrachannel combination. The former has a concurrence of 1.620 while the latter has a concurrence of 1.458. This is because the switch in the entangler combination and sequence is countered by the rearrangement of input qubits for the respective matching concurrence measures in the two setup-cases. For the $|01\rangle|10\rangle/|10\rangle|01\rangle$, the concurrence remains at 1.225.

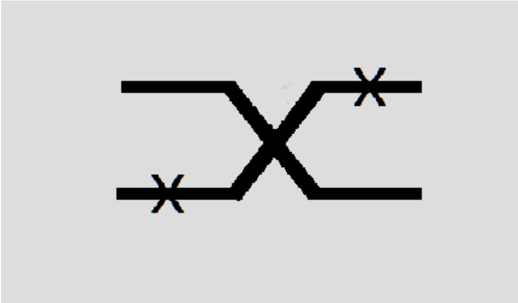

**Figure 7**: *Special Gate Combination ('Cross-Arm Mobius')*

In this case, for same-spin qubit input, concurrence vanishes, while for the case with one spin flipped, with respect to other qubits in the system, we have a higher concurrence than the previous case. The value of concurrence for this input combination and the setup (Figure 7) is 1.571.

The concurrence for the $|00\rangle|11\rangle/|11\rangle|00\rangle$ and the $|01\rangle|01\rangle/|10\rangle|10\rangle$ states are higher or equal to the previous setup-cases. The former has a concurrence of 1.894 while the latter has a concurrence of 1.620.

For the $|01\rangle|10\rangle/|10\rangle|01\rangle$, the concurrence value is 1.785. The possible cause for higher concurrence for all input combinations is viewed in the entanglement within the various subsystem partitions. Previously, there was a trade-off between the contribution of an entangled partition-class and the seperability of remaining subsystem partition-classes. In this setup, the entanglement is present across the various partitions and subsystems. Thus this setup, named as the 'Cross-Arm Mobius', is a good generator of entanglement in SAW-driven electrons.

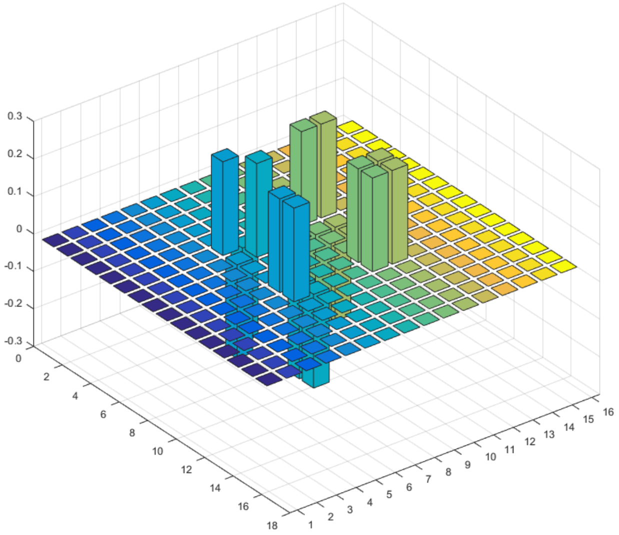

**Figure 8**: *Density Matrix for* $|0110\rangle$ *case and inter-intrachannel setup)*

## VI. CONCLUSION

We have developed a scheme for the generation of entanglement and cluster states on a basis defined by electrons in Quantum One Dimensional Channels (Q1DCs), driven by Surface Acoustic Waves (SAWs).

## VII. ACKNOWLEDGEMENTS

We would like to thank the Nehru Trust for Cambridge University (NTCU), Trinity College - Cambridge, the Hitachi Cambridge Laboratory and the Thin Film

Magnetism group of Cavendish Laboratory, University of Cambridge for their support in the pursuit of this project.

## VIII. REFERENCES

[1] Barnes, C. H. W., J. M. Shilton, and A. M. Robinson. "Quantum computation using electrons trapped by surface acoustic waves." Physical Review B 62.12 (2000): 8410.

[2] Owen, E. T., M. C. Dean, and C. H. W. Barnes. "Generation of entanglement between qubits in a one-dimensional harmonic oscillator." Physical Review A 85.2 (2012): 022319.

[3] Bayer, M., et al. "Coupling and entangling of quantum states in quantum dot molecules." Science 291.5503 (2001): 451-453.

[4] Peres, Asher. "Separability criterion for density matrices." Physical Review Letters 77.8 (1996): 1413.

[5] Carvalho, Andr RR, Florian Mintert, and Andreas Buchleitner. "Decoherence and multipartite entanglement." Physical review letters 93.23 (2004): 230501.

[6] Rungta, Pranaw, et al. "Universal state inversion and concurrence in arbitrary dimensions." Physical Review A 64.4 (2001): 042315.

[7] Hill, Scott, and William K. Wootters. "Entanglement of a pair of quantum bits." Physical review letters 78.26 (1997): 5022.

[8] Bennett, Charles H., et al. "Mixed-state entanglement and quantum error correction." Physical Review A 54.5 (1996): 3824.

[9] Horodecki, Micha, Pawe Horodecki, and Ryszard Horodecki. "Limits for entanglement measures." Physical Review Letters 84.9 (2000): 2014.

[10] Wong, Alexander, and Nelson Christensen. "Potential multiparticle entanglement measure." Physical Review A 63.4 (2001): 044301.

# Generation and evaluation of entanglement using multiple single photon sources and linear optics

Jun-Yi Wu[1] Holger F. Hofmann[1]

[1] *Graduate School of Advanced Sciences of Matter, Hiroshima University, Japan*

**Abstract.** We study the experimentally accessible properties of multi-photon entanglement generated by single photon sources and beam splitters. As the photon number increases, it is possible to observe a rich variety of structures in the photon distributions obtained after linear optics transformations. In this presentation, we focus on the patterns obtained from the unbiased interference of all modes that is described by a discrete Fourier transformation of the light field amplitudes and show how the entanglement can be characterized using the correlations of photon statistics observed in the two multi-mode outputs.

**Keywords:** Multi-photon entanglement, entanglement generation, entanglement evaluation

## 1 Introduction

Nowadays, the development of reliable single photon sources opens up new possibilities of quantum information processing using an increasing number of single photon inputs. It is well-known that splitting a single photon into two output modes by a beam splitter can generate a Bell state with entanglement between the modes (single-rail encoded entanglement). Although the single-rail encoded entanglement of single photon Bell states can be accessed by linear optics and photon detection with extra ancillary photons [1, 2, 3], we restrict ourself on the Fock spaces of the entangled states themselves without any ancilla. Under this constraint, the single-rail encoded entanglement of two modes is not more accessible. By scaling up the single photon entanglement between a pair of modes to multi-photon entanglement between pairs of multiple modes, more possible local unitaries are implementable by linear optics and photon number detection, such that the multi-photon entanglement is then accessible without ancillas. An entanglement criterion for a specific type of multi-photon entangled states which can be implemented by discrete Fourier transformations and photon number detection without ancillas will be derived.

## 2 Generation and evaluation of multi-photon entanglement

To tackle the limits on the unitary transformations in the Fock space of a single mode, we scale the system up to multiple single photon sources. As it is shown in Fig. 1, $M$ photons in $M$ input modes are split by $M$ beam splitters and redistributed into two separate output ports $A$ and $B$. In this manner, one obtains a state represented by a coherent superposition of all possible photon number states satisfying the condition that here is only one photon in each mode $m$, and this photon is found either in port $A$ or in port $B$, i.e.

$$|\psi_M\rangle = \sum_{n_m \leq 1} |\boldsymbol{n}\rangle_A \, |\bar{\boldsymbol{n}}\rangle_B \,, \tag{1}$$

Since we only consider linear optics and photon detection, the local measurements will not be sensitive to quantum coherence between different total photon numbers.

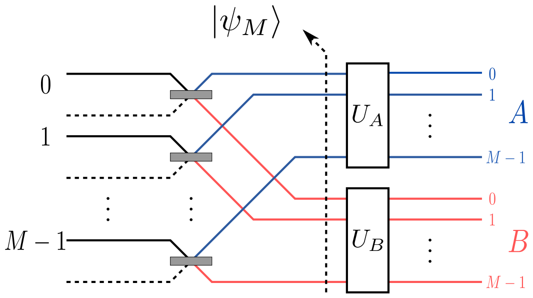

Figure 1: Entanglement generation from $M$ single photons. The modes are indexed by $0, ..., M-1$.

Therefore, we should consider the different partitions of photon number between $A$ and $B$ separately, assigning a different entangled state to each. Post-selecting the output states $|\psi_M\rangle$ with fixed photon number partitions $(1_A : M-1_B), ..., (M-1_A : 1_B)$ between $A$ and $B$, one can obtain $(M-1)$ entangled states $|\phi_{N,M-N}\rangle$ which are the binomially distributed components of the coherent superposition of the total output state given by Eq. (1), i.e.

$$|\psi_M\rangle = \frac{1}{2^{M/2}} \sum_{N=0}^{M} \sqrt{\binom{M}{N}} \, |\phi_{N,M-N}\rangle \tag{2}$$

with

$$|\phi_{N,M-N}\rangle = \frac{1}{\sqrt{\binom{M}{N}}} \sum_{n_m \leq 1, |\boldsymbol{n}|=N} |\boldsymbol{n}\rangle \, |\bar{\boldsymbol{n}}\rangle \,. \tag{3}$$

Here the sum in Eq. (3) runs over all patterns of $N$ photons that have zero or one photon in each mode and the bar over the photon number distribution in $B$ indicates the complementary correlation $\boldsymbol{n}^{(A)} + \boldsymbol{n}^{(B)} = (1, ..., 1)$. Increasing total photon number $M$, one can generate an increasing number of entangled states $|\phi_{N,M-N}\rangle$, all of which have their own entanglement structures.

To access this multi-photon entanglement by photon detection, one needs to implement certain local unitaries $U_A$ and $U_B$ to transform the photon number state basis $\mathcal{E}$ to another basis system $\mathcal{K}$ on the subsystems $A$

and $B$, such that one can perform measurements sensitive to the quantum coherences between the complementarily correlated Fock states (Fig. 1). The best unitary transformation for entanglement evaluation would be the one that maps the photon number state basis $\mathcal{E}$ into its MUB. However, due to the large number of possible photon distributions compared to the much lower number of modes, such a unitary cannot be implemented via linear optics transformations of modes at photon numbers greater than one. Instead of the perfect MUBs-mapping in the whole post-selected Fock space, the next best choice is the discrete Fourier transformation (DFT) $U_F$, which transforms a single optical input mode into a mutually unbiased superposition of all $M$ output modes, i.e.

$$b_k^\dagger = \hat{U}_F a_k^\dagger \hat{U}_F^\dagger = \sum_{m=0}^{M-1} \frac{1}{\sqrt{M}} e^{i\frac{2\pi}{M}km} a_m^\dagger. \qquad (4)$$

In general, the combinations of creation operators in the multi-photon statistics results in a non-trivial bias in the statistics of the multi-photon output distributions. However, we can identify specific translational patterns $\boldsymbol{p}$, such that the DFT transforms each input pattern into a superposition of mutually unbiased output patterns related to each other by cyclic mode shifts $\hat{S}$. The pattern class $\mathcal{E}_{\boldsymbol{p}}$ of $\boldsymbol{p}$ are generated from the cyclic mode shifts $\hat{S}$ from the origin photon number state $\boldsymbol{p}$, i.e.

$$\mathcal{E}_{\boldsymbol{p}} = \{\hat{S}^m |\boldsymbol{p}\rangle\}_{m=0,\dots,M-1}. \qquad (5)$$

The MUB $\mathcal{K}_{\boldsymbol{p}} = \{|k_{\boldsymbol{p}}\rangle\}_k$ of the translational pattern class $\mathcal{E}_{\boldsymbol{p}}$ is then given by

$$|k_{\boldsymbol{p}}\rangle := \frac{1}{\sqrt{d_{\boldsymbol{p}}}} \sum_{m=0}^{M-1} e^{-i\frac{2\pi}{M}km} \hat{S}^m |\boldsymbol{p}\rangle. \qquad (6)$$

where $d_{\boldsymbol{p}}$ is the cardinality of the $\boldsymbol{p}$-pattern class $\mathcal{E}_{\boldsymbol{p}}$. In the $\mathcal{K}_{\boldsymbol{p}}$ basis the the state $|\phi_{N,M-N}\rangle$ is correlated by $(k^{(A)}, -k^{(B)})$, i.e.

$$|\phi_{N,M-N}\rangle = \frac{1}{\sqrt{\binom{M}{N}}} \sum_{\boldsymbol{p},k} |k_{\boldsymbol{p}}\rangle |{-k_{\bar{\boldsymbol{p}}}}\rangle. \qquad (7)$$

The $k$-values of $|k_{\boldsymbol{p}}\rangle$ states can be displaced by DFTs in the output patterns $\boldsymbol{n}$ of photon number detections. We call this property the $K$-readout rule of DFTs, which says

$$\langle \boldsymbol{n}|U_F|k_{\boldsymbol{p}}\rangle = 0, \text{ for all } K(\boldsymbol{n}) \neq k \qquad (8)$$

with

$$K(\boldsymbol{n}) = \sum_{m=0,\dots,M-1} n_m m \pmod{M} \qquad (9)$$

being the $M$-modulus total mode index of the photon number state $|\boldsymbol{n}\rangle$, which we call the displacement of the output pattern $\boldsymbol{n}$. The $K$-readout rule implies that the correlations of $k$-values of in the $k_{\boldsymbol{p}}$-basis will be displaced in the correlations of $K$-values in the photon number detection after local DFTs. According to Eq. (7), the output patterns of photon number detection after local DFTs of the target entangled state $|\phi_{N,M-N}\rangle$ exhibits therefore perfect $(K,-K)$-correlations. That means for the state $|\phi_{N,M-N}\rangle$, the probability $\mathcal{P}(K,-K)$ of $(K,-K)$-correlations in the output patterns of photon number detection after local DFTs is 100%. In the naturally photon number state basis, the probability $\mathcal{P}(\boldsymbol{n},\bar{\boldsymbol{n}})$ of the complementary correlations $(\boldsymbol{n},\bar{\boldsymbol{n}})$ is also 100% for the state $|\phi_{N,M-N}\rangle$. In general, the sum of the two probabilities for correct correlations ($(\boldsymbol{n},\bar{\boldsymbol{n}})$- and $(K,-K)$-correlations) has an upper bound for separable states, which is smaller than 2. The upper bound can be derived with the help of the separable inequality of correlation functions in MUBs [4]. As a result, we can then derive a separability inequality as follows.

$$\mathcal{P}(\boldsymbol{n},\bar{\boldsymbol{n}}|\rho_{\text{sep.}}) + \mathcal{P}(K,-K|U_F^{\otimes 2}\rho_{\text{sep.}}U_F^{\dagger\otimes 2}) \leq \frac{3}{2}. \qquad (10)$$

Note that, while this is by no means the optimal bound for DFTs, it does provides a sufficient criterion for the experimental verification of multi-photon entanglement in our system. We have therefore demonstrated the possibility of detecting the multi-photon entanglement of the post-selected state $|\phi_{N,M-N}\rangle$ using linear optics (specifically the DFTs) and photon detection.

## 3 Conclusion

We consider the generation of entangled multi-photon states using multiple single photon sources and linear optics. The resulting state exhibit a highly non-trivial structure in their photon number statistics. After post-selection of fixed photon number partitions with respect to the subsystems $A$ and $B$ the entanglement of each output state can be evaluated by linear optics and photon detection. Specifically, we show that the mode transformation known as the discrete Fourier transformation (DFT) can be used to evaluate the correlations in two different photon number bases, where the identification of mutually unbiased subspaces permits us to formulate a criterion for entanglement detection based on the sum of the probabilities of measuring the correct correlations in both photon detection measurements. For separable states, the bound of this sum of two probabilities is 3/2, while the entangled state generated by beam splitting ideally exhibits both correlations with probability 1. Experimentally, it should therefore be possible to verify this entanglement using DFTs by observing correlations that exceed this bound.

## References

[1] E. Knill. *Phys. Rev. A*, 66:052306, 2002.

[2] A. P. Lund and T. C. Ralph. *Phys. Rev. A*, 66:032307, 2002.

[3] T. C. Ralph, A. P. Lund, and H. M. Wiseman. *Journal of Optics B: Quantum and Semiclassical Optics*, 7(10):S245, 2005.

[4] C. Spengler, M. Huber, S. Brierley, et al. *Phys. Rev. A*, 86:022311, 2012.

# Geometrical distance on quantum channels

Haidong Yuan
*Department of Mechanical and Automation Engineering,*
*The Chinese University of Hong Kong, Shatin, Hong Kong*[*]

Chi-Hang Fred Fung
*Canada Research Centre, Huawei Technologies Canada, Ontario, Canada*[†]

(Dated: July 21, 2016)

We propose a metric on the space of quantum channels and show how this metric determines the prefect discrimination between quantum channels and the ultimate precision limit for quantum parameter estimation, it thus provides a unified framework for these two related, but so far largely separated fields. New insights can then be gained for studies in both fields, which we demonstrate with two examples: first we derive a lower bound on the minimum number of uses needed for perfect discrimination of two quantum channels, which can be seen as the counterpart of the Heisenberg limit in quantum parameter estimation; second we show that sequential strategy has advantage over parallel strategy in quantum parameter estimation by providing an example inspired by quantum channel discrimination. We remark that our metric is efficiently computable using semi-definite programming.

PACS numbers:

Quantum channel discrimination and quantum parameter estimation are two active fields in quantum information science, quantum channel discrimination studies how to identify a quantum channel among a discrete set of channels[4–9] whereas quantum parameter estimation focus on identifying a channel among a continuous set of channels that characterized by some parameters[10–28]. Intuitively they are all related to the distinguishability of quantum channels, which are determined by the distance between the channels. Despite their similar nature, studies in these two fields are largely separated, as it lacks of a common measure of the distances on quantum channels.

We propose a distance measure on general quantum channels which can be seen as an extension of Bures metric on quantum states to quantum channels. We first show how this distance measure provide a general framework for quantum parameter estimation which relates the ultimate precision limit directly to the underlying dynamics, this provides efficient methods for computing the ultimate precision limit. It also provides an analytical formula of the precision limit with arbitrary pure input states, which does not need any optimization over equivalent Kraus operators as required in previous studies[20, 21]. We further demonstrate the power of the framework by deriving a sufficient condition on when ancillary systems are not useful for improving the precision limit. We then show this distance measure bridges the studies in quantum channel discrimination and quantum parameter estimation, and show how new insights can be gained on studies of both fields through two examples: first we derive a lower bound on the minimum number of evaluations needed for perfect discrimination between two quantum channels, this lower bound is a counterpart of the Heisenberg limit in quantum parameter estimation; second we show sequential strategy can outperform parallel strategy in quantum parameter estimation by providing an example inspired by quantum channel discrimination, which sheds light on a conjecture in quantum parameter estimation.

[1] H.D. Yuan, & C.-H. F. Fung, arXiv: 1506.01909 (2015).
[2] H.D. Yuan, & C.-H. F. Fung, arXiv: 1506.00819 (2015).
[3] H.D. Yuan, & C.-H. F. Fung, Phys. Rev. Lett. 115, 110401 (2015).
[4] A. Acín. Statistical distinguishability between unitary operations. *Physical Review Letters*, 87(17):177901, 2001.
[5] R. Y. Duan, Y. Feng, and M. S. Ying, "Entanglement is Not Necessary for Perfect Discrimination between Unitary Operations", Phys. Rev. Lett. 98, 100503 (2007).
[6] R. Y. Duan, Y. Feng, and M. S. Ying, Phys. Rev. Lett. 100, 020503 (2008).
[7] G. Chiribella, G. D'Ariano, and P. Perinotti. Memory effects in quantum channel discrimination. *Physical Review Letters*, 101, 180501, 2008.

[*] Electronic address: hdyuan@mae.cuhk.edu.hk
[†] Electronic address: chffung.app@gmail.com

[8] R. Duan, Y. Feng, and M. Ying. Perfect distinguishability of quantum operations. Phys. Rev. Lett. 103, 210501 (2009).

[9] Aram W. Harrow, Avinatan Hassidim, Debbie W. Leung, and John Watrous, Phys. Rev. A 81, 032339 (2010).

[10] Helstrom, C. W., Quantum Detection and Estimation Theory. (Academic Press, New York, 1976).

[11] Holevo, A. S., Probabilistic and Statistical Aspect of Quantum Theory. (North-Holland, Amsterdam, 1982).

[12] Giovannetti, V., Lloyd, S. & Maccone, L. *Nature Photonics.* **5**, 222 (2011).

[13] Giovannetti, V., Lloyd, S. & Maccone, L., Quantum metrology. *Phys. Rev. Lett.* **96**, 010401 (2006).

[14] Wineland, D. J., Bollinger J. J., Itano, W. M. & Moore, F.L., *Phys. Rev. A* **46**, R6797-R6800 (1992).

[15] Caves, C. M., *Phys. Rev. D* **23**, 1693-1708 (1981).

[16] Lee H., Kok P. & Dowling, J.P., *J. Mod. Opt.* **49**, 2325-2338 (2002).

[17] Braunstein, S. L., *Phys. Rev. Lett.* **69**, 3598 (1992).

[18] Braunstein, S. L. & Caves, C. M., Statistical distance and the geometry of quantum states. *Phys. Rev. Lett.* **72**, 3439 (1994).

[19] Braunstein, S. L., Caves, M. C. & Milburn, G. J., Generalized Uncertainty Relations: Theory, Examples, and Lorentz Invariance. *Annals of Physics* **247**, 135-173 (1996).

[20] Fujiwara, A.& Imai, H., *J. Phys. A: Math. Theor.* **41**, 255304 (2008).

[21] Escher,B.M., de Matos Filho, R.L. & Davidovich, L., *Nature Phys.* **7**, 406 (2011).

[22] M. Tsang, Quantum metrology with open dynamical systems. *New J. Phys.* **15**, 073005 (2013)

[23] Demkowicz-Dobrzański, R., Kołodyński, J. & Guta, M. *Nature Comm.* **3**, 1063 (2012).

[24] Knysh, S., Smelyanskiy, V. N., & Durkin, G. A., *Phys. Rev. A.* **83**, 021804 (2011).

[25] Knysh, S., Chen, E. & Durkin, G., arxiv:1402.0495 (2014).

[26] Kołodyński, J. & Demkowicz-Dobrzański, R., *New Journal of Physics* **15**, 073043 (2013).

[27] Demkowicz-Dobrzański, R. & Maccone, L., *Phys. Rev. Lett.* **113**, 250801 (2014).

[28] Alipour,S., Mehboudi,M.,& Rezakhani, A.T. *Phys. Rev. Lett.* **112**, 120405 (2014).

[29] Chau, H. F., *Quant. Inf. Compu.* **11**, 0721 (2011).

[30] Fung, C.-H. F. & Chau, H. F., *Phys. Rev. A* **88**, 012307 (2013).

[31] Fung, C.-H. F. & Chau, H. F., *Phys. Rev. A* **90**, 022333 (2014).

[32] Fung, C.-H. F., Chau, H. F., Li, C.K. & Sze, N.S., Quantum Information and Computation, Vol. 15, No. 7&8, 0685-0693 (2015).

[33] A. Childs, J. Preskill, and J. Renes. Quantum information and precision measurement. *Journal of Modern Optics*, 47(2–3):155–176, 2000.

[34] Uhlmann, A., *Rep. Math. Phys.* **9**, 273-279 (1976).

[35] M.A. Nielsen, I.L. Chuang, Quantum Information and Quantum Computation, (Cambridge Univeristy Press, 2000).

[36] Masahito Hayashi, Communications in Mathematical Physics, Vol. 304, No. 3, 689-709 (2011);

[37] Masahito Hayashi, Progress of Informatics, No.8 81-87 2011

[38] Masahito Hayashi, Sai Vinjanampathy, L. C. Kwek, arXiv:1602.07131 (2016).

# Group covariance of $q$-ary PSK coherent-state signals coded by codes over extension field $\mathbb{F}_q$

Minami TANAKA[1] * Asuka OHASHI[2] † Tsuyoshi Sasaki USUDA[1] ‡

[1] *School of Information Science and Technology, Aichi Prefectural University,*
*1522-3 Ibaragabasama, Nagakute-shi, Aichi, 480-1198, Japan*
[2] *College of Science and Engineering, Ritsumeikan University,*
*1-1-1 Noji-Higashi, Kusatsu-shi, Shiga, 525-8577, Japan*

**Abstract.** The formula of the channel matrix for group covariant signals in classical-quantum communication has been studied to calculate the channel matrix analytically. However, the derived formula cannot be applied to coded $q$-ary phase shift keing (PSK) signals by the codes over extension field $\mathbb{F}_q$ despite its importance. In this study, using coding by group codes over $\mathbb{F}_4$ and $\mathbb{F}_8$, we demonstrate that coded 4PSK and 8PSK signal sets can be narrow sense group covariant with respect to $\mathbb{F}_4$ and $\mathbb{F}_8$, respectively.

**Keywords:** Quantum information theory, Extension field, Gram matrix, Channel matrix

## 1 Introduction

In classical-quantum communication[1], the computation of the channel capacity in finite codeword length is difficult even though finite codeword length is used in actual communication. For example, when Square-Root Measurement (SRM)[2] is used, the channel matrix is calculated by the square root of the Gram matrix of the quantum signal set. However, due to computational complexity, it is difficult to calculate using a universal algorithm if there are many signals.

Therefore, we have studied formulas to calculate the channel matrix analytically, and formula of channel matrix for narrow sense group covariant signals[4] has been derived[3]. However, the formula cannot be applied to quantum signal sets coded by codes over extension field $\mathbb{F}_{p^k} = \mathbb{F}_q$ despite its importance. Here, $p$ is a prime number and $k$ is a natural number. Thus, we now focus on the group covariance of $q$-ary Phase Shift Keying (PSK) coherent-state signals coded by codes over $\mathbb{F}_q$.

In this paper, with coding by codes over $\mathbb{F}_4$ and $\mathbb{F}_8$, we show that coded 4PSK and 8PSK signal sets can be narrow sense group covariant with respect to $\mathbb{F}_4$ and $\mathbb{F}_8$ respectively.

## 2 Group covariant signals

**Definition 1 ([5])** *Let $(G;\circ)$ be a finite group and a set of parameters that characterize pure quantum-state signals $\{|\psi_i\rangle \mid i \in G\}$. The set of signals is called $(G;\circ,\hat{\chi})$-* covariant *if there exist unitary operators $U_k (k \in G)$ such that*

$$U_k|\psi_i\rangle = \hat{\chi}(k,i)|\psi_{k\circ i}\rangle,\ \forall i,k \in G, \tag{1}$$

*where $\hat{\chi}$ is a map from $G \times G$ into $\mathbb{U} = \{x \in \mathbb{C} \mid |x| = 1\}$.*

If $\hat{\chi}(i,j) = 1\ (\forall i,j \in G)$, the set of signals is referred to as narrow sense group covariant.

**Proposition 2 ([3])** *A set of pure quantum-state signals $\{|\psi_i\rangle \mid i \in G\}$ is $(G;\circ,\hat{\chi})$-covariant if and only if, for any $i,j \in G$,*

$$\langle\psi_{k\circ i}|\psi_{k\circ j}\rangle = \hat{\chi}(k,i)\hat{\chi}(k,j)\langle\psi_i|\psi_j\rangle, \tag{2}$$

*for all $k \in G$.*

Next, we give another proposition for $(G;\circ,\hat{\chi})$-covariant signals, which is used in Section 3.

**Proposition 3 ([6])** *Let $G$ be an additive group. A set $\{\boldsymbol{v} \mid \boldsymbol{v} \in C\}$ of coded $(G;+,\hat{\chi})$-covariant signals by a group code $C(\subseteq G^n)$ over $G$ is $(C;+,\hat{\chi}')$-covariant. Here, $\hat{\chi}'$ is defined as follows:*

$$\hat{\chi}'(\boldsymbol{v},\boldsymbol{w}) = \prod_{i=1}^{n} \hat{\chi}(v_i,w_i), \tag{3}$$

*for $\boldsymbol{v} = (v_1,\ldots,v_n)$, $\boldsymbol{w} = (w_1,\ldots,w_n) \in C$.*

## 3 Group covariance of coded PSK signals

### 3.1 Coded 4PSK signals by codes over $\mathbb{F}_4$

We show an example wherein 4PSK signals can be narrow sense group covariant with respect to $\mathbb{F}_4$ by coding, and a construction method of narrow sense group covariant codes of length $2n$ over $\mathbb{F}_{2^2} = \mathbb{F}_4$ from arbitrary group codes over $\mathbb{F}_4$.

In the following, we use quaternary vector representation $\{0,1,2,3\}$ for elements of $\mathbb{F}_4$ rather than$\{0,1,\omega,\omega+1\}(\omega^2+\omega+1=0)$.

**Proposition 4** *The set of coded 4PSK signals by the (2,1) code*

$$C_{(2,1)} := \{00, 13, 22, 31\}$$

*over $\mathbb{F}_4$ is narrow sense group covariant with respect to $C_{(2,1)}$ (and $\mathbb{F}_4$).*

This proposition is proven using Proposition 2.

To prepare to demonstrate the method, we define a map $f_4 : \mathbb{F}_4 \to \mathbb{F}_4$ as follows:

$$f_4(a) = \begin{cases} a & \text{if } a \in \{0,2\}, \\ a+2 & \text{if } a \in \{1,3\}. \end{cases} \tag{4}$$

*im153006@cis.aichi-pu.ac.jp
†a-ohashi@fc.ritsumei.ac.jp
‡usuda@ist.aichi-pu.ac.jp

**Definition 5** *For code $C$ over $\mathbb{F}_4$ of length $n$, consider the codes $C^{\mathrm{ex}}_{(2,1)}(C) \subset \mathbb{F}_4^{2n}$ constructed by adding redundant symbols as follows:*

$$C^{\mathrm{ex}}_{(2,1)}(C) := \big\{ (\boldsymbol{a}|\boldsymbol{b}) \mid \boldsymbol{a} = (a_1, \ldots, a_n) \in C \\ \boldsymbol{b} = (f_4(a_1), \ldots, f_4(a_n)) \in \mathbb{F}_4^n \big\}. \quad (5)$$

*We refer to $C^{\mathrm{ex}}_{(2,1)}$ as the extended code of $C$ by $C_{(2,1)}$.*

From Proposition 3, we obtain the following proposition for codes $C^{\mathrm{ex}}_{(2,1)}$.

**Proposition 6** *A set of coded 4PSK signals $\{|\boldsymbol{w}_i\rangle \mid \boldsymbol{w}_i \in C^{\mathrm{ex}}_{(2,1)}\}$ is narrow sense group covariant with respect to $C^{\mathrm{ex}}_{(2,1)}$ if $C$ is a group.*

### 3.2 Coded 8PSK signals by codes over $\mathbb{F}_8$

Here, we show an example of symmetrization of 8PSK signals by coding and a construction method of narrow sense group covariant codes of length $8n$ over $\mathbb{F}_{2^3} = \mathbb{F}_8$ from arbitrary group codes over $\mathbb{F}_8$.

In the following, we use an octonary vector representation $\{0, 1, 2, 3, 4, 5, 6, 7\}$ for elements of $\mathbb{F}_8$ rather than $\{0, 1, \omega, \omega{+}1, \omega^2, \omega^2{+}1, \omega^2{+}\omega, \omega^2{+}\omega{+}1\} (\omega^3{+}\omega{+}1 = 0)$. Furthermore, note that the eight letters correspond to 8PSK signals in the order 0, 4, 1, 6, 2, 7, 3 from the first signal.

**Proposition 7** *The set of coded 8PSK signals by the (8,1) code*

$$C_{(8,1)} := \{00000000, 13131313, 22222222, 31313131 \\ 44576675, 57447566, 66754457, 75665744\}$$

*over $\mathbb{F}_8$ is narrow sense group covariant with respect to $C_{(8,1)}$ (and $\mathbb{F}_8$).*

This proposition is proven using Proposition 2.

To demonstrate the method, we define a map $f_8 : \mathbb{F}_8 \to \mathbb{F}_8^7$ as follows:

$$f_8(a) = \begin{cases} (0,0,0,0,0,0,0) & \text{if } a = 0, \\ (3,1,3,1,3,1,3) & \text{if } a = 1, \\ (2,2,2,2,2,2,2) & \text{if } a = 2, \\ (1,2,1,2,1,2,1) & \text{if } a = 3, \\ (4,5,7,6,6,7,5) & \text{if } a = 4, \\ (7,4,4,7,5,6,6) & \text{if } a = 5, \\ (6,7,5,4,4,5,7) & \text{if } a = 6, \\ (5,6,6,5,7,4,4) & \text{if } a = 7. \end{cases} \quad (6)$$

**Definition 8** *For code $C$ over $\mathbb{F}_8$ of length $n$, consider the code $C^{\mathrm{ex}}_{(8,1)}(C) \subset \mathbb{F}_8^{8n}$ constructed by adding redundant symbols as follows:*

$$C^{\mathrm{ex}}_{(8,1)}(C) := \big\{ (\boldsymbol{a}|\boldsymbol{b}) \mid \boldsymbol{a} = (a_1, \ldots, a_n) \in C \\ \boldsymbol{b} = (f_8(a_1), \ldots, f_8(a_n)) \in \mathbb{F}_8^{7n} \big\}. \quad (7)$$

*We refer to $C^{\mathrm{ex}}_{(8,1)}$ as the extended code of $C$ by $C_{(8,1)}$.*

From Proposition 3, we obtain following proposition for the codes $C^{\mathrm{ex}}_{(8,1)}$.

**Proposition 9** *A set of coded 8PSK signals $\{|\boldsymbol{w}_i\rangle \mid \boldsymbol{w}_i \in C^{\mathrm{ex}}_{(8,1)}\}$ is narrow sense group covariant with respect to $C^{\mathrm{ex}}_{(8,1)}$ if $C$ is a group.*

## 4 Example

Here, we give an example of our method. Let $C = \{000, 121, 232, 313\}$. Gram matrix of the coded 4PSK signals by $C$ is

$$\Gamma_C = \begin{pmatrix} 1 & \mathrm{e}^{(-4+2\mathbf{i})N_{\mathrm{S}}} & \mathrm{e}^{(-5-\mathbf{i})N_{\mathrm{S}}} & \mathrm{e}^{(-3-\mathbf{i})N_{\mathrm{S}}} \\ \mathrm{e}^{(-4-2\mathbf{i})N_{\mathrm{S}}} & 1 & \mathrm{e}^{(-3+3\mathbf{i})N_{\mathrm{S}}} & \mathrm{e}^{(-5-\mathbf{i})N_{\mathrm{S}}} \\ \mathrm{e}^{(-5+\mathbf{i})N_{\mathrm{S}}} & \mathrm{e}^{(-3-3\mathbf{i})N_{\mathrm{S}}} & 1 & \mathrm{e}^{(-4+2\mathbf{i})N_{\mathrm{S}}} \\ \mathrm{e}^{(-3+\mathbf{i})N_{\mathrm{S}}} & \mathrm{e}^{(-5+\mathbf{i})N_{\mathrm{S}}} & \mathrm{e}^{(-4-2\mathbf{i})N_{\mathrm{S}}} & 1 \end{pmatrix}, \quad (8)$$

and it is obvious that this code does not comprise group covariant signals. However, the Gram matrix of the coded 4PSK signals by the code

$$C^{\mathrm{ex}}_{(2,1)}(C) = \{000000, 132213, 223122, 311331\} \quad (9)$$

which is a group code over $\mathbb{F}_4$ but is not a group code over $\mathbb{Z}_4$ is

$$\Gamma_{C^{\mathrm{ex}}_{(2,1)}(C)} = \begin{pmatrix} 1 & \mathrm{e}^{-8N_{\mathrm{S}}} & \mathrm{e}^{-10N_{\mathrm{S}}} & \mathrm{e}^{-6N_{\mathrm{S}}} \\ \mathrm{e}^{-8N_{\mathrm{S}}} & 1 & \mathrm{e}^{-6N_{\mathrm{S}}} & \mathrm{e}^{-10N_{\mathrm{S}}} \\ \mathrm{e}^{-10N_{\mathrm{S}}} & \mathrm{e}^{-6N_{\mathrm{S}}} & 1 & \mathrm{e}^{-8N_{\mathrm{S}}} \\ \mathrm{e}^{-6N_{\mathrm{S}}} & \mathrm{e}^{-10N_{\mathrm{S}}} & \mathrm{e}^{-8N_{\mathrm{S}}} & 1 \end{pmatrix}. \quad (10)$$

This signal set is narrow sense group covariant with respect to $C_{(2,1)}$ (and $\mathbb{F}_4$) from Proposition 3.

## 5 Conclusion

We have shown codes over extension fields $\mathbb{F}_4$ and $\mathbb{F}_8$ with which coded 4PSK signal sets and coded 8PSK signal sets are applicable to the channel matrix formula.

Our method is simple; however we think it proposes a type of symmetrization method of non-symmetric signals using "coding". Therefore, in future study, we will consider symmetrization of quadrature-amplitude modulation (QAM) signals by coding. Note that QAM signals are important but are not group covariant in any sense.

**Acknowledgment:** This work has been supported in part by KAKENHI (Grant Numbers 24360151 and 16H04367).

## References

[1] C.W. Helstrom, *Quantum Detection and Estimation Theory*, Academic Press, New York, (1976).

[2] P. Hausladen, R. Jozsa, B. Schumacher, M. Westmoreland, and W.K. Wootters, Phys. Rev. **A54**, pp.1869-1876, (1996).

[3] T.S. Usuda and K. Shiromoto, AIP Conf. Proc. **1363**, T. Ralph and P.K. Lam (Eds.), pp.97-100, (2011).

[4] T.S. Usuda and I. Takumi, QCMC2, Plenum Press, New York, pp.37-43, (2000).

[5] T.S. Usuda, Y. Ishikawa, and K. Shiromoto, AIP Conf. Proc. **1633**, H.-J. Schmiedmayer and P. Walther (Eds.), pp.201-203, (2014).

[6] M. Tanaka, T. Sogabe, K. Shiromoto, and T.S. Usuda, Proc. of ISITA2014, p.348, (2014).

# Intensity fluctuation suppression in a decoy-state quantum key distribution transmitter

Kensuke Nakata[1] * Akihisa Tomita[1] Yu Kadosawa[1] † Kazuhisa Ogawa[1] Atsushi Okamoto[1]

[1] *Graduate School of Information Science and Technology, Hokkaido University, Kita14-Nishi9, Kita-ku, Sapporo 060-0814, Japan*

**Abstract.** In decoy-BB84 quantum key distribution (QKD) protocol, intensity fluctuation of the transmitted optical pulses reduce secure key rate. The main factors of intensity fluctuation are a light source and an intensity modulator (IM). In this study, we focus an IM and show that fluctuation of modulation signals affect intensity fluctuation. Furthermore, we propose a robust IM with Nested Modulator (NM) for suppressing influence of fluctuation of modulation signals and experimentally confirm that the influence is greatly suppressed by NM

**Keywords:** Quantum key distribution, security certification

## 1 Introduction

It is rather recent that quantum key distribution (QKD) systems have shown enough performances for practical use, in terms of key generation speed and stability. Currently, state-of-arts QKD systems generate key at several hundred kb/s through an installed fiber of more than 10-dB loss[1]. The automatic control on the QKD systems enables unmanned operation for months without severe disruption. People are now seriously considering deployment of QKD systems. Still, there are a number of obsessions on the social deployment, one of which is the lack of security certification on a working system. In fact, security of the QKD protocol, particularly decoy-BB84, has been fully established in theory. However, such security proofs would be of no use without the certification that QKD equipment works properly under the practical conditions. In terms of security certification, " working properly" refers that the system satisfies the assumptions of the security proof.

An important issue for the decoy protocol is that the intensities of the transmitted pulses should be set precisely and kept stable. Since the estimation of the leakage information to the eavesdropper (Eve) depends on the intensities of the pulses, errors in the pulse intensities prevent us from accurate calculation of the amount of sacrifice bits, and thus affect the security of the final key. Recent studies suggested that the error of the pulse intensity should be kept smaller than 5 % [2, 3]. Therefore, it is necessary for the transmitters to stabilize the intensity within this range.

Experimentally, the intensity varies by several reasons, such as fluctuation of laser intensity, drift and fluctuation in the intensity modulation, and alteration of the loss in the passive components. Among these mechanisms, the effects from passive components would be smaller than others. We here focus on the intensity modulator, and propose a novel intensity modulator to reduce the intensity fluctuation.

We consider a $\mathrm{LiNbO_3}$ (LN) based intensity modulator (IM) used for high speed QKD systems. Since decoy method requires to change the intensity pulse by pulse, the IM should operate as fast as the clock frequency. The LN modulators are often employed for decoy method, because high speed modulators up to 20 GHz band width are commercially available. The intensity fluctuation originates from the fluctuation of the drive voltage. Actually, the drive voltage may fluctuate for high frequency operation. As well-known, the band width of the drivers should be much larger than the clock frequency to conserve the rectangular pulse shape. Otherwise, the waveform of the pulse is deformed and the signal varies by timing. The pulse jitter then results in the fluctuation of the applied voltage to alter the modulation.

## 2 Intensity fluctuation in a conventional modulator

Dual-drive Modulators (DDM) are often used for IM in QKD systems [4]. Figure 1(a) shows the schematic structure of the DDM. The intensity of the output is given by the phase shifts $\theta_1$ and $\theta_2$ through the upper and lower arms, as

$$I_{out}(\theta_1, \theta_2) = \frac{1}{2}\left(1 + \cos(\theta_1 - \theta_2)\right) I_{in}. \tag{1}$$

For two-decoy method, three different intensities $I_S$, $I_D$, and $I_0$ are used, where the phases are set to $(\theta_1, \theta_2) = (0, 0), (\theta, 0), and (0, \pi)$ for $I_S$, $I_D$, and $I_0$, respectively. If the applied voltage deviates from the designed value, the phase shift error results in the intensity error. Suppose the phase shift error appears in the upper arm $\theta_1 \to \theta_1 + \Delta$, the intensity error $I(\Delta) = \left[I(\theta_1 + \Delta, \theta_2) - I(\theta_1, \theta_2)\right] / I(\theta_1, \theta_2)$ grows proportionally to $\Delta^2$ for $I_S$ and $I_0$, but to $\Delta$ for $I_D$. Therefore, decoy intensity is more sensitive to the phase error than other intensities $I_S$ and $I_0$. We measured the fluctuation of the decoy intensity for $(\theta_1 = \pi?2, \theta_2 = 0)$. As shown in Fig. 1(b), intensity distribution is broaden at the DDM output. If we evaluate the fluctuation by $3\sigma/\mu$, with the

*nakata@optnet.ist.hokudai.ac.jp

†username3@domainname3

average intensity $\mu$ and the standard deviation $\sigma$, the range of the fluctuation $3\sigma/\mu$ increased from 4.4 % to 7.5 % by the IM.

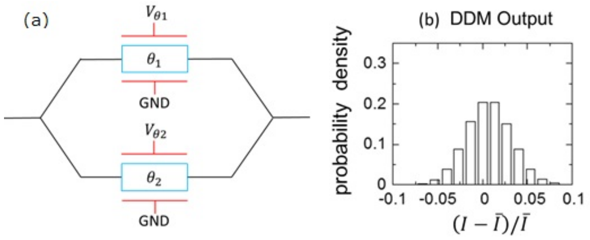

Figure 1: (a) A schematic structure of a Dual-Drive Modulator (DDM,) (b) Intensity distribution of decoy pulses at the DDM output.

## 3 Reduction of the intensity fluctuation by a nested modulator

We observed that the large intensity fluctuation comes from the linear dependence of the intensity on the phase error for the decoy pulses. Therefore, we can reduce the intensity fluctuation by changing the linear dependence to the square dependence. To this end, we introduce a novel intensity modulator structure to the QKD transmitter. This type of the modulator, called a nested modulator (NM) [5] contains two Mach-Zehnder interferometer, as shown in Fig. 2(a). Though the phases $\theta_1$, $\theta_2$, $\theta_3$, and $\theta_4$ can be controlled independently, we fix $\theta_3$ and $\theta_4$ to zero. Then, the output intensity is given by

$$I_{out}(\theta_1, \theta_2) = \frac{1}{8}\left(3 + 2\cos\theta_1 + 2\cos\theta_2 + \cos(\theta_1 - \theta_2)\right) I_{in}. \tag{2}$$

We obtain signal and two decoys by setting $\theta_1$ and $\theta_2$ as $I_S = I_{out}(0,0) = I_{in}$, $I_D = I_{out}(0,\pi) = I_{in}/4$ , and $I_0 = I_{out}(\pi,\pi) = 0$. By applying phase error as in the DDM $\theta_1 \to \theta_1 + \Delta$, we observe the intensity errors grows proportional to $\Delta^2$ for all $I_S$, $I_D$, and $I_0$. Therefore, NM output should be robust to the phase error, i.e., error of the applied voltage. Figure 2 (b) shows the measured intensity distribution of the NM output. The fluctuation was estimated to be $3\sigma/\mu$ =4.9 %, which was almost equal to the input fluctuation.

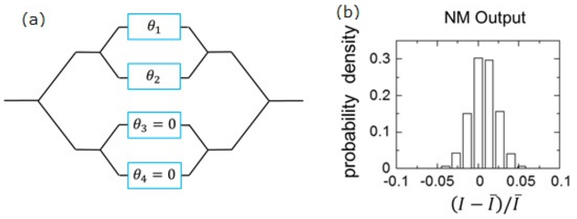

Figure 2: (a) A schematic structure of a Nested Modulator (NM,) (b) Intensity distribution of decoy pulses at the NM output.

## 4 Conclusion

We have shown that the intensity of the modulator output may fluctuate largely by the change of the applied voltage. The change may originate from the deformation of the electric pulses due to the limited band width of the driver, which become serious for the high speed QKD systems. We propose the use of nested modulators (NMs) to decoy-QKD transmitter. The output intensities from the NM vary as a quadratic function of the phase error, so that the intensities are little affected by the drive voltage fluctuation, if the operation point is properly set. The decoy intensity from the nested modulator should be fixed to 0.25 $I_{in}$ to achieve the robustness to the applied voltage fluctuation. However, this value is often used in decoy-BB84 system, so that the effect on the final key rate would be small.

**Acknowledgement** This work was partly supported by NICT contract research project 157-B, and ImPACT "Advanced Information Society Infrastructure Linking Quantum Artificial Brains in Quantum Network."

## References

[1] M. Sasaki, *et al.* *Opt. Express*, 19, 10387–10409 (2011).

[2] M. Hayashi and R. Nakayama. *New J. Phys.* 16, 063009 (2014).

[3] Y. Nagamatsu, A. Mizutani, R. Ikuta, T. Yamamoto, N. Imoto, and K. Tamaki. *Phys. Rev. A* 93, 042325 (2016).

[4] A. Tanaka, *et al.* *IEEE J. Quant. Electron.* 48, 542–550 (2012).

[5] J. Ichikawa, *et al.* U.S. patent US20080212915 A1 (04, September, 2008)

# Measurement based quantum computation and Quantum Error correction codes

**Abhishek Sharma[1], Divyanshi Bhatnagar[2] and Atipriya Bajaj[3]**

[1]SRM University, NCR Campus,
Ghaziabad 201204, India
er.abhishek01@gmail.com

[2] Student, SRM University, NCR Campus,
Ghaziabad 201204, India
divyanshi.db@gmail

[3] Student, SRM University, NCR Campus,
Ghaziabad 201204, India
atipriyabajaj19@gmail.com

***ABSTRACT:*** *Quantum Computing is the new hope in the field of computation. In one way quantum computation, an incredible technological advancement in the field of quantum computation, the previously prepared entangled state is computed via measurements. This article studies the basic concepts of measurement-based quantum computation, error correcting codes and fault tolerant system. Qubits, the building unit of Quantum Computation are prone to errors and are affected by the environment. However, fault tolerant algorithms can be designed for better performance. This paper presents a theoretical schema of large scale quantum computation.*

***Keywords:*** *Measurement based quantum computation, error correcting codes, decoherence, topological code*

## 1. INTRODUCTION

Information processing technology is largely based on the physics of classical electromagnetic dynamics.The processing of computers and networks is based on this principle. This principle has blossomed in 20th century as electronics. Digitalcomputers operate on data including magnitudes, symbols and letters i.e. in the form of binary digits 0 and 1. Each information is encoded in using different combinations of these digits. By comparing, counting and manipulating different combinations of these digits as per instructions digital computers perform tasks. These tasks include controlling industrial processes, regulating operations of machines, stimulating dynamic systems,analyzing and organizing vast business data etc. A new principle of physics is on focus since late 20th century. This new principle of information processing is based on quantum physics. Entering the realms of atoms opens up enormous powerful opportunities where processors work a million times faster than the ones we use today. A quantum computer has a sequence of qubits. A qubit can have any value 0, 1 or any quantum superposition of these two qubit states. If there are n qubits then 2^n states can be represented by it simultaneously. A QC is a step ahead of classical computer in computation of prime Factorization, secure communication, and teleportation of quantum information.However this information processing is not easy to realize because the quantum states are not stable (easily decoherence) for long time and difficult to manipulate. Vigorous efforts are going for the realization quantum information processing.

This article is review on the newcomputational model of quantum computers called measurement based quantum computation. Section 2 describes the basic concepts of Measurement based quantum computation and comparison with conventional computation models i.e. the circuit model. Section 3 describes errors and quantum error correcting codes. Section 4 is about fault tolerant topological quantum computer.

## 2. MEASUREMENT BASED QUANTUM COMPUTATION

From the beginning the realizationof quantum computing has been considered on the basis of circuit model (fig 1). Circuit model has few basic gates such as single qubit rotation gates and two qubit interaction gate: the controlled not gate.Controlled

NOT gate is one of the main difficulty in realization of QC. To obtain proper interaction between the particles is quite difficult.

In 2000s a new paradigm for quantum computers started. Researchers began to re-examine the computational model to utilize the feature of quantum physics. Since classical physics is completely different form quantum physics they thought of a new model for computation. Quantum states can exist in entanglement state. This feature leads to new model described by Gottesman and Chuang. As per their model quantum gates operate by the means of quantum teleportation. In Teleportation, quantum information is transmitted from one location to another with the help of classical computing and quantum entanglement between the sending and receiver location. Output of controlled –NOT is obtained by using entangled state by operating quantum teleportation. (Fig.2). The entangled state can be regarded as a computational resource for the quantum gate. Further modified computation model of teleportation is One way quantum computation. Prepare a cluster state that is entangled.Next stepis to perform single-qubit measurement on the cluster state. After this perform universal quantum computation. Major role is played by entangled cluster state in quantum gate and information flow. Creating an entangled state is a lot easier than measurement because target is already known. We utilize a non deterministic gate that has low success probability in order to generate the entangled resource. Once the resource of entangled state is created it is easy to perform one qubit interaction rather than two qubit interactions gates, so the new computational model decreases the difficulty of realizing quantum computers.

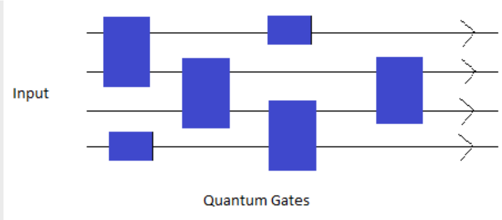

**Figure 1 Circuit Model**

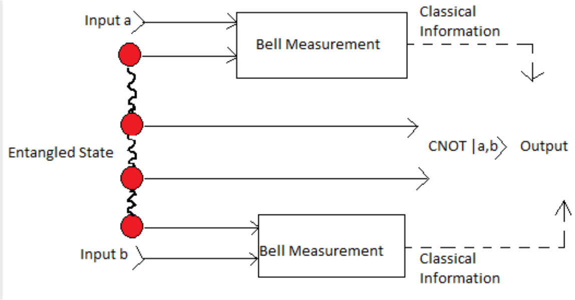

**Figure 2 Teleportation Based Gate**

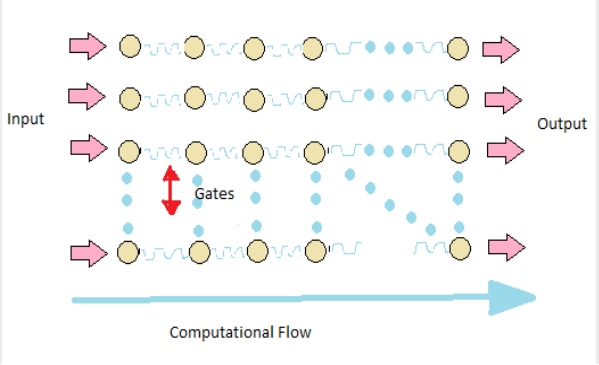

**Figure 3 Measurement based quantum computation**

## 3. ERRORS AND QUANTUM ERROR CORRECTING CODES

Qubits are prone to errors. They can be affected by heat,noise in the environment or by stray electromagnetic couplings. Usually there is bit flip error in classical computing i.e. 0 is mistakenly flipped to 1 or vice versa. Whereas in case of qubits there can be bit flip as well as phase errors. In case of phase error the sign of phase relation between 0 and 1 flips.

There are two main differences between classical error correction and quantum error correction. First is non cloning theorem it states that it is impossible to perfectly copy an unknown quantum state. This means there is no operation that satisfies this U $|\psi\rangle\ |0\rangle = |\psi\rangle|\psi\rangle$ for an unknown $|\psi\rangle$.Therefore, we are unable to protect arbitrary quantum states against errors by simply making multiple copies. It is possible to spread information of one qubit into highly entangled state of several qubits. Peter Shor discovered this methodto formulating a *quantum error correcting code* by storing the information of one qubit onto a highly entangled state of nine qubits.

Secondly, measurement of any unknown quantum state will collapse the wave function describing the state. Quantum information is destroyed while trying to measure certain subset of encoded state.

Classical error correction is the base of quantum error correction but still we need to define codes in slightly different manner. This is due both to the restrictions of what we can theoretically do with quantum information, but also due to the possible errors that can affect qubits. As stated earlier classical bits experience only bit flip but qubits experience both bit flip and phase errors. The errors are mostly continuous .such as rotation around X axis by some phase angle or some incoherent error caused by interaction with the outside world.

We introduce additional measurement qubit or syndrome measurement to diagnose which error corrupts an encoded state. A series of quantum measurement and data combination is used to diagnose. . We then reverse an error by applying a corrective operation based on the syndrome. A syndrome measurement can determine whether a qubit has been corrupted or not. And if it is so thenwhich one had been corrupted. The outcome not only tells which bit was affected but also in which several ways it was affected.The syndrome measurement does not tell us about the value that is stored in the logical qubit as the measurement will destroy soit. It is better to store information in 9 qubits than in 1 qubit.

We only present formalism for coherent errors that can be represented by unitary gate.

Error operator E acting on a qubit$|\psi\rangle$ can be decomposed into linear superposition of X gates, Z gates and Y= iXZ

The detection occurs by redundant encoding with two classical codes. One code will detect X errors and other will detect Z errors without having to necessarily decode the code space. The simplest example is the bit flip code $|0\rangle_L = |0\rangle^{\otimes N}$ and $|1\rangle = |1\rangle^{\otimes N}$ where the $^{\otimes N}$ means N copies of the qubit. The number of physical flips needed to turn |0⟩L ↔ |1⟩L scales linearly with N. In quantum we cannot directly measure the subset of the code block. Therefore we need some different method to spot errors. In bit flip code,there exists a certain property y that for both basis states, pair wise bit-parity in the code block is even (i.e. calculating the parity of any two bits via modulo addition for the |0⟩L and |1⟩L state is even). If the result of comparison is an odd value, we know an error has occurred without actually knowing if we started with the |0iL or |1iL state. This is what we need. Therefore, we need a way to calculate the parity of any two qubits in the code block without directly measuring the qubits themselves. The circuit introduces anancillary bit that interacts with the qubits and measured. The result will determine the parity of the two qubits (even or odd) and also force them to be in one of the parity if it is not beforehand. The principle of codespace is to construct encoded codewords that always have well defined parity regardless of the state of encoded information.

Returning to the example , the two encoded states are of even parity states of any pair wise Z operators. . i.e. applying the operator ZiZj for any i,j∈ N returns the same state, ZiZj |0, 1⟩L = |0, 1⟩L. Bit flip errors result in states which violate this condition. For example, a bit-flip on qubit one of the encoded block will result in Z1Zj |0, 1⟩L = − |0, 1⟩L ,∀j. If we measure the parity of any of these operators and we find an odd result, we know that some type of error has occurred. Location and number of unique errors depend on the size of code block N. The parity of pair wise checks of the $Z_iZ_{i+1}$ operator will help us do so.

In case of quantum phase flip works in same way as bit flip. Therefore a full quantum error correction includes two classical codes one for bit flip and other for phase errors.

In Shor code one redundancy code is embedded into another. The code encodes a single qubit of information into nine physical qubits. The basis states are given by,

$$|0\rangle_L = \frac{1}{\sqrt[2]{2}} (|000\rangle + |111\rangle)(|000\rangle + |111\rangle)(|000\rangle + |111\rangle)$$

$$|1\rangle_L = \frac{1}{\sqrt[2]{2}} (|000\rangle - |111\rangle)(|000\rangle - |111\rangle)(|000\rangle - |111\rangle)$$

We have three blocks of three qubits that effectively act as a distance three redundancy code to correct bit flips. This allows us to correct a single bit flip error in any one of the three blocks.

### 3.1 SUBSYSTEM CODES

3.1.1 Bacon-Shor Codes

A new approach to implement quantum error correction is the quantum subsystem. In subspace codes, The information is encoded ina coding subspace of some large multiqubit system in a subspace code. Subspaces of the multi qubitare identified by the Subsystem and are considered to be equivalent. Bacon-Shor Code is of general nature. It has the ability to perform dynamical code switching in a fault-tolerant manner. The flexibility of BS codes is its strength. BS codes are stabilizer codes and are now defined over a square lattice. The lattice dimensions represent the X and Z error correction properties .Commenting on the size of the lattice in either of these two dimensions dictates the total number of errors the code can correct. In general, a C(n1,n2) BS code is defined over a n1 × n2 square lattice which encodes one logical qubit into n1n2 physical qubits with the ability to correct at least (n1−1)/ 2 Z errors and at least ( n2−1 2) X errors.

3.1.2 Topological Codes

Topological code's structure is defined on a lattice as in the case of subsystem code and the scaling of the code is done in such a way that more errors are corrected. In topological coding schemes the protection afforded to logical information relies on the unlikely application of error chains which define non-trivial topological paths over the code surface. The two ways of approaching areFirst is to treat topological codes as a class of stabilizer codes over qubit system. Second is to construct a physical Hamiltonian model based on the structure of the topological code or choose systems which appear to exhibit topological order. As a result more complicated field on anyonic quantum computation occurs.

Toric code is a topological quantum error correcting code and example to stabilizing code.

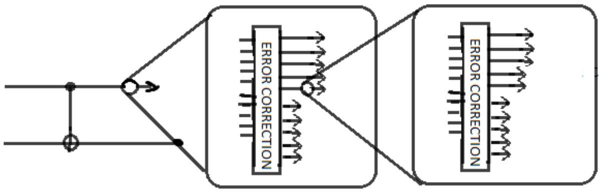

Figure 4 Concatenated Code

## 4. FAULT TOLERANT TOPOLOGICAL QUANTUM COMPUTER

We need to protect quantum computing form decoherence and different kinds of noise.Error correction codes are available for quantum computers and we can perform fault-tolerant quantum computing by applying an error correction procedure appropriately during computation. A fault tolerant system based on circuit model used quantum linear code and concatenated codes. A standard quantum linear encodes a single qubit into several qubits. It can handle single bit flip and phase flip error but if more than one occurs error correction does not work well. Concatenated coding works well for this. It recursively uses linear code . It provides greater error tolerance if the error rate per basic computational unit is less than a certain threshold. By the usage of codeof concatenation of sufficient depth with the error rate below the threshold then reliable computing can be executed. It is assumed here that any quantum gate can be achieved between widely separated particles, but with the increase in distance interaction between particles becomes weak.Code of quantum gate can be rewritten. And is written between spatially separate particles into combinations of quantum gates between nearest-neighbour sites, the number of consumed gates becomes larger in that case and the threshold of the fault-tolerant system becomes significantly small. At some point of time there was shortage of concatenated codes for fault tolerant systems so new topological or surface codes were proposed. Topological code uses the concept of nearest interactions. This is a realistic model than circuit model.A toric code is a quantum error correcting and an example of stabilizer code defined on a 2- D spin lattice.The edges of 2D lattice represents the qubits.The qubits are in entangled state as in topological code. The qubits that are on the endpoints of the 2D lattice are identical/similar to ones that are on the other side. The 2D lattice is on the surface of a torus, which provides us with the degrees of freedom that is used in encoding logical qubits. The entanglement and error correction can be performed on the nearest neighbourinteractions. Theencoding size can be enlarged by expanding the lattice. Toric code can also be rewritten on a square lattice with boundaries by constructing the equivalent for the hole of the torus and introducing the same topology. This makes easier to prepare multiple logical qubits. There exists a special form of 3D cluster state which becomes a resource Error correction. Toric code 0 1 2 3 2' 0' 6 7 6' 5 4 1' In this case, we can perform fault-tolerant quantum computing with only single-qubit measurements after preparing the 3D cluster states. The thresholds can be improved by devising better encoding and decoding methods . Recently, the important realistic case of errors with a high loss rate  and of nondeterministic entangling gates has also been investigated.

## 5. FUTURE OUTLOOK

Having reviewed the concepts and features of measurement based quantum computation and fault tolerant system we would like to mention the outlook for future research. As per theory, we need to find more realistic physical model for realization of measurement based quantum computation.  There have been studies for finding Hamiltonians whose ground states are universal resources for measurement based quantum computation. On experimental sides some demonstrations of MBQC have been performed. However, it is prone to errors. One of the main problems is to obtain scalability in quantum computers. As per further research, optical quantum computation a new high efficiency single photon source is necessary. Ultra cold atomic gas in an optical lattice can be used for preparing large entangled resource for measurement based quantum computation. Another important candidate is the use of solid state artificial atoms such as quantum dots or dopants in solids for stationary qubits and the use of atoms photon interaction with cavity quantum electrodynamics for quantum gates. To conclude, measurement based quantum computation provides great hope towards realising quantum computers.

## REFERENCES

[1] Morimae ,Tomoyuki″Basics and applications of measurement-based quantum computing″ *Information Theory and its Applications (ISITA), 2014 International Symposium on*. IEEE,2014.

[2]Paler, Alexandru, and Simon J. Devitt.″*Proceedings of the 52nd Annual Design Automation Conference.ACM*, 2015.

[3]Feinstein,David Y.,S.S. Nair and Mitchell A.Thornton.″Advances in Quantum Computing Fault Tolerance and Testing.″ *null*.IEEE,2007.

[4]Devitt, Simon. J.,William J. Munro, and KaeNemoto.″Quantumerror correction for beginners.″ *Reports on Progress in Physics* 76.7(2013).

[4]RaussendorfRobert , and Hans J. Briegel.″A one-way quantum computer.″ *Physical Review Letters* 86.22(2001): 5188

[5]https://www.ntt-review.jp/archive/ntttechnical.php?contents=ntr201209fa1.html

[6]https://quantiki.org/wiki/error-correction-0

[7]Duncan,Ross.*Types for quantum computing*. University of Oxford,2006

[8]http://www.mind.ilstu.edu/curriculum/nature/computer_types.php

# Multipartite key distribution in networks

Stefan Bäuml[1] * Koji Azuma[1] †

[1] *NTT Basic Research Laboratories, NTT Corporation, 3-1 Morinosato Wakamiya, Atsugi-shi, Kanagawa 243-0198, Japan*

**Abstract.** The ability to distribute entanglement to be used as cryptographic key over complex quantum networks is an important step towards a quantum version of the Internet. Most attention so far has been given to the distribution of bipartite entanglement. In this work we derive bounds on the rate at which multipartite private states, such as GHZ states, can be distributed using a given network architecture. Our bounds are particular interest for possible applications of multi-receiver cryptography or quantum secret sharing.

**Keywords:** Quantum networks, QKD, Secret sharing

An important prerequisite for the application of quantum protocols such as quantum key distribution (QKD) to real world communication problems is the distribution of entanglement over long distances. The simplest way to do so is to create an entangled state locally and send part of it over a quantum channel. As the channel typically introduces noise, it is usually necessary to send many copies of the state via the channel and perform local operations and classical communication (LOCC) in order to distill the desired resource state.

For point to point communication, it has recently been shown [1] that the rate at which a secret key can be transmitted via asymptotically many uses of a channel assisted by LOCC is upper bounded by the squashed entanglement of the channel. The protocol used here is adaptive in the sense that after each channel use a round of LOCC is performed, determining which state will be inserted into the channel next.

The limitations of point to point transmission of entanglement can be overcome by use of quantum repeaters. While quantum repeaters allow for distribution of entanglement over arbitrarily large distances, the use of quantum protocols in a future version of the Internet will require entanglement to be distributed over complex networks rather than just a chain of nodes. In [2], the upper bound on the bipartite key rate given in [1] has been generalised from only a single quantum channel to an arbitrary network consisting of ancillary nodes and quantum channels. In [3] a lower bound for arbitrary networks is presented.

Another important generalisation towards the quantum Internet is to go beyond a one-sender and one-receiver model. This can be achieved using a GHZ state or a multipartite private state [4]. Another cryptographic protocol involving many parties is secret sharing, where two or more parties have to come together in order to decrypt a message. It has been shown that this can be achieved using a GHZ state [5].

In the present work, we present an upper bound on the rate at which GHZ states and multipartite private states can be distributed between an arbitrary number of parties, who are connected by an arbitrary network consisting of quantum broadcast channels and ancillary nodes. The scenario considered here is a generalisation of [6] in that it contains a network of broadcast channels rather than just a single broadcast channel and it is a generalisation of [2] in that it considers multipartite key distribution rather than bipartite one and broadcast channels rather than single receiver ones. We also discuss how the lower bound presented in [3] can be generalised to the multipartite case.

We consider the following setup: There are $m$ nodes $A_1...A_m$ held by the $m$ parties as well as an arbitrary number of ancillary nodes. The nodes are connected by an arbitrary network of quantum broadcast channels of $\mathcal{N}^e : X^e \rightarrow Y_1^e...Y_{r_e}^e$. The network can be described by a hypergraph with party and ancillary nodes as vertices and broadcast channels $\mathcal{N}^e$ as hyperedges. In addition the nodes are connected by a network of classical communication, such as the conventional Internet. Initially, the quantum state $\rho^0$ of the system is fully separable between all nodes. It is our goal to establish an $m$-partite private state $\gamma_{A_1...A_m}$, as defined in [4], between the parties $A_1...A_m$. A special case of such a private state is the GHZ state.

In order to achieve this goal, an adaptive protocol is performed. The protocol begins with application of broadcast channel $\mathcal{N}^{e_0} : X^{e_0} \rightarrow Y_1^{e_0}...Y_{r_{e_0}}^{e_0}$ followed by a round of (probabilistic) LOCC, the outcome $k_1$ of which determines which broadcast channel $\mathcal{N}^{e_{k_1}} : X^{e_{k_1}} \rightarrow Y_1^{e_{k_1}}...Y_{r_{e_{k_1}}}^{e_{k_1}}$ is used next. Outcome $k_1$ is obtained with probability $p(k_1)$. After the channel use another round of LOCC is performed, resulting in $k_2$. The outcomes $\mathbf{k}_2 = (k_1, k_2)$, which are obtained with probability $p(\mathbf{k}_2) = p(k_2|k_1)p(k_1)$, determine which channel $\mathcal{N}^{e_{\mathbf{k_2}}} : X^{e_{\mathbf{k}_2}} \rightarrow Y_1^{e_{\mathbf{k}_2}}...Y_{r_{e_{\mathbf{k}_2}}}^{e_{\mathbf{k}_2}}$ is used next and so on. After $l$ channel uses we arrive at state $\rho^{\mathbf{k}_l}$ with probability $p(\mathbf{k}_l)$, such that $\left\|\rho_{A_1...A_m}^{\mathbf{k}_l} - \gamma_{A_1...A_m}^{d_{\mathbf{k}_l}}\right\|_1 \leq \epsilon$ for some $m$-partite private state $\gamma^{d_{\mathbf{k}_l}}$.

Our main result is an upper bound on the key dimension $d_{\mathbf{k}_l}$, averaged over all possible outcomes of the $l$-round protocol. Before stating the theorem, let us introduce some notation: We call $\mathcal{P}$ a partition of the nodes

*stefan.bauml@lab.ntt.co.jp

†azuma.koji@lab.ntt.co.jp

into disjoint classes $\mathcal{G}_1...\mathcal{G}_m$ such that each class contains one party node. In general, some branches of a broadcast channel will remain within the class containing the sender whereas some branches cross the boundaries to other classes. Given channel $\mathcal{N}^e : X^e \to Y_1^e...Y_{r_e}^e$, we denote by $\mathcal{G}_X^e \in \{\mathcal{G}_1...\mathcal{G}_m\}$ the class containing the sender node and by $\mathcal{G}_{(1)}^e...\mathcal{G}_{(n_e)}^e \in \{\mathcal{G}_1...\mathcal{G}_m\}$ the other classes containing receiving nodes. Given partition $\mathcal{P}$, we denote by $\text{ext}(\mathcal{P})$ the set of indices $e$, such that channels $\mathcal{N}^e$ crosses at least one boundary between classes. Let us also define $\mathcal{Y}_X^e, \mathcal{Y}_{(1)}^e, ..., \mathcal{Y}_{(n_e)}^e$ as products of all output systems $Y_j^e$ of $\mathcal{N}^e$ going to a node in classes $\mathcal{G}_X^e, \mathcal{G}_{(1)}^e, ..., \mathcal{G}_{(\text{n}_e)}^e$, respectively.

If after $l = \sum_e l^e$ rounds of an adaptive protocol as described above the state of $A_1...A_m$ is $\epsilon$-close to an $m$-partite private state $\gamma_{A_1...A_m}^{d_{\mathbf{k}_l}}$, it holds

$$m \left\langle \log d_{\mathbf{k}_l} \right\rangle_{\mathbf{k}_l} \leq \min_{\mathcal{P}} \frac{1}{1 - c\epsilon} \left( \sum_{e \in \text{ext}(\mathcal{P})} \left\langle l^e \right\rangle_{\mathbf{k}_l} E_{\text{sq}}^{(\mathcal{P})} \left( \mathcal{N}^e \right) + f(\epsilon) \right)$$

where the minimisation is over all partitions $\mathcal{P}$, $l^e$ is the number of uses of channel $\mathcal{N}^e$ and the averaging is over all outcome vectors $\mathbf{k}_l$. Further $c \in \mathbb{Z}^+$ and $f(\epsilon) \to 0$ as $\epsilon \to 0$. $E_{\text{sq}}^{(\mathcal{P})} \left( \mathcal{N}^e \right)$ denotes the multipartite squashed entanglement as introduced in [7], w.r.t. the partitions given by $\mathcal{P}$ and $\mathcal{N}^e$.

Let us now discuss how the lower bound on the key rate presented in [3] can be generalised to the multipartite setting. They have derived a lower bound on the key rate that can be achieved by using each channel $\mathcal{N}^e$ with given frequency $\bar{f}^e$. The bound is achieved by means of a so-called *aggregated quantum repeater protocol.* The protocol involves distribution of $\left\lfloor \bar{f}^e Q^{\leftrightarrow} \left( \mathcal{N}^e \right) \right\rfloor$ copies of Bell states $|\Phi^+\rangle$ via each channel $\mathcal{N}^e$. The resulting network of Bell states is then used to distribute the maximal entanglement between Alice and Bob by means of entanglement swapping. The network of Bell states can be seen as an undirected graph. The amount of key obtainable in this way depends on the number of edge disjoint paths between Alice and Bob. By Menger's theorem [8], this number is equal to the minimum number of edges in any cut between Alice and Bob. In the case of multipartite key distribution the problem of finding an achievable rate becomes more involved. We will restrict ourselves to the simpler case where all channels in the communication network have only a single sender and a single receiver and discuss general broadcast channels in future work.

As in the bipartite case we use an aggregated quantum repeater protocol. We begin by creating a network of Bell states $|\Phi^+\rangle$, that can be described by a graph $\mathcal{G}^{\text{Bell}}$. The Bell state network is then used to establish a number of (qubit) GHZ state among $A_1, ..., A_m$. The number of qubits of the GHZ state then provides us with a lower bound on the multipartite key rate. Finding the maximal number of GHZ-entangled qubits, however, is a more difficult task as in the bipartite case, where we can use Menger's theorem.

In [9] it has been shown that GHZ states can be connected by an operation similar to entanglement swapping: Assuming we have an $n$-partite GHZ state and an $m$-partite GHZ state, application of a projection onto two parties results in an $n + m - 1$ partite GHZ state of the remaining parties. In particular two Bell states can be connected into a 3-partite GHZ state. If necessary, party $A_i$ can also be removed by a measurement in the $\sigma_x$ eigenbasis and a local application of $\sigma_z$ depending on the output, resulting in an $n + m - 2$ partite GHZ state of the remaining parties, which can be seen as a direct generalisation of entanglement swapping to GHZ states. In a general Bell state network we can create a GHZ state between parties $A_1...A_m$ if the corresponding graph contain a *tree* spanning vertices $A_1...A_m$, i.e. if there exists an acyclic subgraph connecting all vertices $A_1...A_m$. A tree that spans a subset of vertices of a graph is referred to as a *Steiner tree.* Hence, in order to determine the number of GHZ states that can be established between $A_1...A_m$ by means of generalised entanglement swapping, we need to compute the number of edge-disjoint Steiner trees spanning $A_1...A_m$ in the graph corresponding to the Bell network, which is another generalisation of Menger's Theorem.

For general graphs the problem of finding the number of edge-disjoint Steiner trees spanning a subset $S$ of vertices, also known as *Steiner tree packing* has been shown to be NP complete [10]. There are, however, polynomial algorithms, that can provide us with lower bounds on the number of edge-disjoint Steiner trees in a graph [11].

## References

[1] M. Takeoka, S. Guha, and M. M. Wilde, Nature communications 5 (2014).

[2] Azuma, A. Mizutani, and H.-K. Lo, arXiv preprint arXiv:1601.02933 (2016).

[3] K. Azuma and G. Kato, arXiv preprint arXiv:1606.00135 (2016)

[4] R. Augusiak and P. Horodecki, Physical Review A 80, 042307 (2009).

[5] M. Hillery, V. Buzek, and A. Berthiaume, Physical Review A 59, 1829 (1999).

[6] K. P. Seshadreesan, M. Takeoka, and M. M. Wilde, arXiv preprint arXiv:1503.08139 (2015).

[7] D. Yang, K. Horodecki, M. Horodecki, P. Horodecki, J. Oppenheim, and W. Song, Information Theory, IEEE Transactions on 55, 3375 (2009).

[8] K. Menger, Fundamenta Mathematicae 10, 96 (1927).

[9] J. Wallnofer, M. Zwerger, C. Muschik, N. Sangouard, and W. Dur, arXiv preprint arXiv:1604.05352 (2016).

[10] Petteri Kaski. Information processing letters, 91(1):1?5, 2004.

[11] Lap Chi Lau, Foundations of Computer Science, 2004. Proceedings. 45th Annual IEEE Symposium on, pages 61-70. IEEE, 2004.

# Permutation-invariant quantum codes from polynomials

Yingkai Ouyang[1] *

[1] *Singapore University of Technology and Design, 8 Somapah Road, Singapore 487372*

**Abstract.** A qudit code is a subspace of the state space of a fixed number of qudits. Such a code is permutation-invariant if it is unchanged under the swapping of any pair of the underlying qudits. Prior permutation-invariant qubit codes encode a single qubit while correcting $t$ arbitrary errors, and their logical codewords have two important properties. First, the Dicke states over which the logical codewords are superposed over have weights spaced a constant number apart. Second, the probability of observing each logical codeword as a given Dicke state is proportional to a binomial coefficient. We design permutation-invariant qudit codes encoding a single qubit with logical codewords that need not have the above two properties, while still allowing the correction of $t$ arbitrary errors. Polynomials govern the structure of the Dicke states and the probabilities in our construction.

The promise offered by the fields of quantum cryptography [1, 2] and quantum computation [3] has fueled recent interest in quantum technologies. To implement such technologies, one needs a way to reliably transmit quantum information, which is inherently fragile and often decoheres because of unwanted physical interactions. If a decoherence-free subspace (DFS) [4] of such interactions were to exist, encoding within it would guarantee the integrity of the quantum information. Indeed, in the case of the spurious exchange couplings [5], the corresponding DFS is just the symmetric subspace of the underlying qubits. In practice, only approximate DFSs are accessible because of small unpredictable perturbations to the dominant physical interaction [6], and using approximate DFSs necessitate a small amount of error correction. When the approximate DFS is the symmetric subspace, permutation-invariant codes can be used to negate the aforementioned errors [7, 8, 9].

Permutation-invariant codes are particularly useful in correcting errors induced by *quantum permutation channels with spontaneous decay errors*, with Kraus decomposition $\mathcal{N}(\rho) = \mathcal{A}(\mathcal{P}(\rho)) = \sum_{\alpha,\beta} A_\beta P_\alpha \rho P_\alpha^\dagger A_\beta$, where $\mathcal{P}$ and $\mathcal{A}$ are quantum channels satisfying the completeness relation $\sum_\alpha P_\alpha^\dagger P_\alpha = \sum_\beta A_\beta^\dagger A_\beta = \mathbb{1}$ and $\mathbb{1}$ is the identity operator on $m$ qubits. The channel $\mathcal{P}$ has each of its Kraus operators $P_\alpha$ proportional to $e^{i\theta_\alpha \hat{a}_\alpha}$, where $\theta_\alpha$ is the infinitesimal parameter and the infinitesimal generator $\hat{a}_\alpha$ is any linear combination of exchange operators. By a judicious choice of $\theta_\alpha$ and $\hat{a}_\alpha$, the channel $\mathcal{P}$ can model the stochastic reordering and coherent exchange of quantum packets as well as out-of-order delivery of classical packets [10]. The channel $\mathcal{A}$ on the other hand models spontaneous decay errors, otherwise also known as amplitude damping errors, where an excited state in each qubit independently relaxes to the ground state with probability $\gamma$. Our permutation-invariant code is inherently robust against the effects of channel $\mathcal{P}$, and can suppress all errors of order $\gamma$ introduced by channel $\mathcal{A}$, and is hence approximately robust against the composite noisy permutation channel $\mathcal{N}$.

The possibility of error correction in permutation-invariant codes [7, 8, 9, 11] is a useful feature, particularly when exchange errors or random permutation errors are the dominant errors afflicting the system. Permutation-invariant codes that can correct even a single qubit error are necessarily non-stabilizer codes, and hence the design of such codes is non-trivial and necessarily uses techniques beyond the stabilizer formalism. Permutation-invariant codes with error correction capabilities are also necessarily highly entangled, and may be of interest to further the theory the entanglement of symmetric states [12, 13, 14, 15, 16, 17].

The first example of a permutation-invariant code which encodes one qubit into 9-qubits while being able to correct any single qubit error was given by Ruskai over a decade ago [7]. A few years later, Ruskai and Pollatshek found 7-qubit permutation invariant codes encoding a single qubit which correct arbitrary single qubit errors [8]. Recently permutation-invariant codes encoding a single qubit into $(2t+1)^2$ qubits that correct arbitrary $t$-qubit errors has been found [9]. In Ref. [11], permutation-invariant codes encoding more than a qubit while correcting spontaneous decay errors to leading order have also been studied. In Ref. [18], the similarity of permutation-invariant quantum codes and bosonic codes has also been explored, and further advance in the theory of either one of these theories might have important implications for the other.

Here, we extend the theory of permutation-invariant quantum codes, while still retaining the ability to correct $t$ arbitrary errors. The full technical details of this submission is available on the arXiv in Ref. [19]. Prior permutation-invariant qubit codes that encode a single qubit while correcting $t$ arbitrary errors, have logical codewords with two important properties. First, the Dicke states over which the logical codewords are superposed over have weights spaced a constant number apart. Second, the probability of observing each logical codeword as a given Dicke state is proportional to a binomial coefficient. We design permutation-invariant qudit codes encoding a single qubit with logical codewords that need not have the above two properties,

*yingkai_ouyang@sutd.edu.sg

while still allowing the correction of $t$ arbitrary errors. Polynomials govern the structure of the Dicke states and the probabilities in our construction.

We also note that unlike prior permutation-invariant quantum codes that have been restricted to systems comprised of solely qubits, we extend our theory to permutation-invariant qudit codes. For $N$-qubit systems, the symmetric subspace is spanned by Dicke states with weights from 0 to $N$. Here, a Dicke state of weight $w$ is a uniform superposition over all computation basis states with exactly $w$ excitations, and we denote it as $|D^N_w\rangle$.

To describe permutation-invariant codes over qudits, we elucidate the basis of the symmetric subspace of $N$ qudits, where each qudit is of dimension $q$. We denote $\mathcal{T}_{N,q}$ to be the set of all $q$-tuples with components that are non-negative integers that sum to $N$. For each $\boldsymbol{\tau} = (\tau_0, \dots, \tau_{q-1}) \in \mathcal{T}_{N,q}$, we necessarily have $\tau_0 + \dots + \tau_{q-1} = N$, and we wish to define a Dicke state of type $\boldsymbol{\tau}$, which we denote as $|D[\boldsymbol{\tau}]\rangle$. Each $|D[\boldsymbol{\tau}]\rangle$ is a superposition over all computational basis states $|\mathbf{x}\rangle = |x_1\rangle \otimes \dots \otimes |x_m\rangle$ such that each $|\mathbf{x}\rangle$ is a tensor product of exactly $p_j$ $|j\rangle$'s for $0 \le j \le q-1$.

We construct permutation-invariant codes encoding a single qubit into $N$ qudits that correct arbitrary $t$ qudit errors using polynomials $p_0, \dots, p_{q-1}$ in the variable $z$ and $f$ in the variable $x$. We assume that the polynomial $f(x) = \sum_{z=0}^{n} f_z x^z$, has real coefficients $f_z$, and $(p_0(z), \dots, p_{q-1}(z)) \in \mathcal{T}_{N,q}$ for every $0 \le z \le n$, with $f_n \neq 0$. Now let

$$\begin{aligned} \mathcal{F}_0 &= \{0 \le z \le n : f_z > 0\}, \\ \mathcal{F}_1 &= \{0 \le z \le n : f_z < 0\}, \end{aligned} \tag{1}$$

denote the index sets for which $f_z$ is positive and negative respectively, and let $|f| = |f_0| + \dots + |f_n|$. Our permutation-invariant codes have basis vectors

$$\begin{aligned} |0_L\rangle &= \sqrt{\frac{2|f_n|}{|f|}} \sum_{z \in \mathcal{F}_0} \sqrt{\frac{|f_z|}{|f_n|}} |D[(p_0(z), \dots, p_{q-1}(z))]\rangle, \\ |1_L\rangle &= \sqrt{\frac{2|f_n|}{|f|}} \sum_{z \in \mathcal{F}_1} \sqrt{\frac{|f_z|}{|f_n|}} |D[p_0(z), \dots, p_{q-1}(z)]\rangle. \end{aligned} \tag{2}$$

Notice that the logical codewords in Eq. (2) are independent of the choice of nonzero $f_n$, and we can without loss of generality consider a constant nonzero $f_n$ such as $f_n = 1$. For all $0 \le z \le n$, we denote the classical codes

$$\mathcal{C}_z = \{\mathbf{x} \in \{0, \dots, N\}^N : \mathrm{wt}_j(\mathbf{x}) = p_j(z), 0 \le j \le q-1\}, \tag{3}$$

and define the pair-wise minimum distance between these codes as

$$\Delta = \min\{d(\mathbf{x}, \mathbf{y}) : \mathbf{x} \in \mathcal{C}_z, \mathbf{y} \in \mathcal{C}_{z'}, 0 \le z < z' \le n\}, \tag{4}$$

where $d(\mathbf{x}, \mathbf{y}) = |\{1 \le i \le N : x_i \neq y_i\}|$ denotes the Hamming distance between the vectors $\mathbf{x}$ and $\mathbf{y}$. Theorem 1 gives sufficient conditions for which the permutation-invariant code spanned by the logical vectors given in Eq. (2) corrects $t$ arbitrary qudit errors.

**Theorem 1** *Let $p_0, \dots, p_{q-1}$ be polynomials of degree at most $\theta$. Let $f(x)$ be a non-zero polynomial with real coefficients having a root at $x = 1$ with multiplicity $m$. Then the code spanned by Eq. (2) corrects at least $t = \min\{\lfloor \frac{\Delta-1}{2} \rfloor, \lfloor \frac{m-1}{2\theta} \rfloor\}$ arbitrary qudit errors.*

Theorem 1 implies that if

$$m \ge (\Delta - 1)\theta + 1, \tag{5}$$

the number of errors that can be corrected is $t = \lfloor \frac{\Delta-1}{2} \rfloor$. In this scenario, evaluating $t$ becomes a combinatorial problem which depends only on $\Delta$.

The amplitudes $\sqrt{\frac{2}{|f|}}\sqrt{|f_z|}$ of our permutation-invariant code that arise in Eq. (2) depend crucially on our choice of the polynomial $f(x)$ with real coefficients. When the degree of $f(x)$ is equal to the multiplicity of its root at $x = 1$, that is when $n = m$, we uniquely have $f(x) = f_n(x-1)^n$ and $f_z = f_n(-1)^{n-z}\binom{n}{z}$. This choice of $f(x)$ gives rise to the amplitudes that are crucial in the specification of certain permutation-invariant codes [7, 9, 11] and certain bosonic codes [18]. When $n > m$, we must have

$$f(x) = f_n(x-1)^m \left( x^{n-m} + \sum_{j=0}^{n-m-1} a_j x^j \right), \tag{6}$$

where $a_j$ are arbitrary real constants for $0 \le j \le n-m-1$. Hence the set of all polynomials of the form in Eq. (6) is isomorphic to $\mathbb{R}^{n-m}$, while the set of all monic polynomials $f(x)$ of degree $n$ with real coefficients is isomorphic to $\mathbb{R}^n$. Random choices of $f_z$ typically yield polynomials $f(x)$ inconsistent with Eq. (6), and the combinatorial identity

$$\sum_{z=0}^{n} f_z z^j = 0, \quad \text{for every } 0 \le j \le m-1, \tag{7}$$

required in the proof of Theorem 1 need not hold. Here we take the convention where $0^0 = 1$. In view of this, requiring $f(x)$ to have a root at $x = 1$ with multiplicity $m$ is non-trivial.

To complete the specification of our code, apart from the polynomial $f(x)$, the polynomials $p_0, \dots, p_{q-1}$ appearing in Eq. (2) are also required. In particular, to correct one error, the Ruskai code [7, 9] has logical codewords

$$\begin{aligned} |0_L\rangle &= \frac{1}{2}(|D^9_0\rangle + \sqrt{3}|D^9_6\rangle) \\ |1_L\rangle &= \frac{1}{2}(|D^9_3\rangle + \sqrt{3}|D^9_9\rangle). \end{aligned} \tag{8}$$

With our current construction, to correct one error we can for example use $p_1(z) = 1 + 3z$, $f(x) = (1+x)(x-1)^5$ and $N = 19$ to obtain a permutation-invariant code with logical codewords

$$\begin{aligned} |0_L\rangle &= \frac{\sqrt{4}|D^{19}_4\rangle + \sqrt{5}|D^{19}_{13}\rangle + |D^{19}_{19}\rangle}{\sqrt{10}} \\ |1_L\rangle &= \frac{|D^{19}_1\rangle + \sqrt{5}|D^{19}_7\rangle + \sqrt{4}|D^{19}_{16}\rangle}{\sqrt{10}}, \end{aligned} \tag{9}$$

where the weight distribution for the Dicke states are linearly shifted, and the square of the amplitudes do not follow the binomial distribution.

Theorem 1 implies that the polynomials $p_0, \dots, p_{q-1}$ can be non-linear. For example for $q = 3$, $f(x) = (1 + x)(x-1)^5$ and $p_1(z) = 3z^2, p_2(z) = 0, p_1(z) = N - p_1(z)$ and $N = 108$, we have

$$|0_L\rangle = \frac{\sqrt{4}|D[105,3,0]\rangle + \sqrt{5}|D[60,48,0]\rangle + |D[0,108,0]\rangle}{\sqrt{10}}$$
$$|1_L\rangle = \frac{|D[108,0,0]\rangle + \sqrt{5}|D[96,12,0]\rangle + \sqrt{4}|D[33,75,0]\rangle}{\sqrt{10}}. \tag{10}$$

The code spanned by Eq. (10) also corrects one error. Clearly many other choices of polynomials $p_0, \dots, p_{q-1}$ are also feasible within the framework of our construction.

To prove Theorem 1, we first state the key lemmas.

**Lemma 2** *Let $P \in \mathcal{P}_q^{\otimes N}$ have weight $w$ where $w \leq 2t$. Let $\tau_0, \dots, \tau_{q-1}$ be polynomials in the variable $z$ of degree at most $\theta$. Let $\boldsymbol{\tau} = (\tau_0, \dots, \tau_{q-1}) \in \mathcal{T}_{N,q}$. Then $\langle D[\boldsymbol{\tau}]|P|D[\boldsymbol{\tau}]\rangle$ is a polynomial of degree at most $2t\theta$ in the variable $z$.*

**Lemma 3** *Let $f(x) = \sum_{z=0}^n f_z x^z$ be a non-zero polynomial with real coefficients $f_z$ and a root at $x = 1$ with multiplicity $m$. Then Eq. (7) holds.*

it then suffices to show for every $N$-qudit Pauli operator of weight at most $2t$ (i) the non-deformation conditions $\langle 0_L|P|0_L\rangle = \langle 1_L|P|1_L\rangle$ and (ii) the orthogonality conditions $\langle 0_L|P|1_L\rangle = 0$ [20]. Having $t \geq \left\lfloor \frac{\Delta - 1}{2} \right\rfloor$ immediately implies that the orthogonality conditions (ii) hold. Hence it remains to prove (i), or equivalently the non-deformation condition

$$\sum_{z=0}^n f_z \langle D[\mathbf{p}(z)]|P|D[\mathbf{p}(z)]\rangle = 0, \tag{11}$$

where we denote $\mathbf{p}(z) = (p_0(z), \dots, p_{q-1}(z))$. The proof of Eq. (11) has two ingredients: (i) the polynomials $\langle D[\mathbf{p}(z)]|P|D[\mathbf{p}(z)]\rangle$ have degree no more than $2t\theta$ in the variable $z$ as given in Lemma 2, and (ii) the combinatorial identity Eq. (7) as given in Lemma 3. Note that condition (i) implies that

$$\langle D[\mathbf{p}(z)]|P|D[\mathbf{p}(z)]\rangle = \sum_{j=0}^{2t\theta} \alpha_j z^j, \tag{12}$$

for some constants $\alpha_j \in \mathbb{C}$. Hence

$$\begin{aligned}\sum_{z=0}^n f_z \langle D[\mathbf{p}(z)]|P|D[\mathbf{p}(z)]\rangle &= \sum_{z=0}^n f_z \sum_{j=0}^{2t\theta} \alpha_j z^j \\ &= \sum_{j=0}^{2t\theta} \alpha_j \left( \sum_{z=0}^n f_z z^j \right).\end{aligned} \tag{13}$$

But the bracketed term in Eq. (13) is always zero because of condition (ii) and $m > 2t\theta$, and this completes the proof of the non-deformation condition Eq. (11). Hence our code can correct at least $t$ arbitrary qudit errors.

## References

[1] C. H. Bennett and G. Brassard, “Quantum cryptography: Public key distribution and coin tossing,” in *Proceedings of IEEE International Conference on Computers, Systems and Signal Processing*, vol. 175, New York, 1984.

[2] A. K. Ekert, “Quantum cryptography based on Bell’s theorem,” *Phys. Rev. Lett.*, vol. 67, pp. 661–663, Aug 1991.

[3] M. A. Nielsen and I. L. Chuang, *Quantum Computation and Quantum Information.* Cambridge University Press, second ed., 2000.

[4] P. Zanardi and M. Rasetti, “Noiseless Quantum Codes,” *Phys. Rev. Lett.*, vol. 79, pp. 3306–3309, Oct. 1997.

[5] S. Blundell, *Magnetism in Condensed Matter.* Great Clarendon Street, Oxford OX2 6DP: Oxford master series in condensed matter physics, first rnote ed., 2003.

[6] D. A. Lidar, D. Bacon, and K. B. Whaley, “Concatenating decoherence-free subspaces with quantum error correcting codes,” *Phys. Rev. Lett.*, vol. 82, pp. 4556–4559, May 1999.

[7] M. B. Ruskai, “Pauli Exchange Errors in Quantum Computation,” *Phys. Rev. Lett.*, vol. 85, pp. 194–197, July 2000.

[8] H. Pollatsek and M. B. Ruskai, “Permutationally invariant codes for quantum error correction,” *Linear Algebra and its Applications*, vol. 392, no. 0, pp. 255–288, 2004.

[9] Y. Ouyang, “Permutation-invariant quantum codes,” *Physical Review A*, vol. 90, no. 6, p. 062317, 2014.

[10] V. Paxson, “End-to-end internet packet dynamics,” *SIGCOMM Comput. Commun. Rev.*, vol. 27, pp. 139–152, Oct. 1997.

[11] Y. Ouyang and J. Fitzsimons *Phys. Rev. A*, vol. 93, p. 042340, Apr 2016.

[12] M. Hayashi, D. Markham, M. Murao, M. Owari, and S. Virmani, “Entanglement of multiparty-stabilizer, symmetric, and antisymmetric states,” *Phys. Rev. A*, vol. 77, p. 012104, Jan 2008.

[13] R. Hübener, M. Kleinmann, T.-C. Wei, C. González-Guillén, and O. Gühne, “Geometric measure of entanglement for symmetric states,” *Physical Review A*, vol. 80, no. 3, p. 032324, 2009.

[14] L. Chen, H. Zhu, and T.-C. Wei, “Connections of geometric measure of entanglement of pure symmetric states to quantum state estimation,” *Physical Review A*, vol. 83, no. 1, p. 012305, 2011.

[15] L. Arnaud and N. J. Cerf, “Exploring pure quantum states with maximally mixed reductions,” *Phys. Rev. A*, vol. 87, p. 012319, Jan 2013.

[16] D. Baguette, T. Bastin, and J. Martin, “Multiqubit symmetric states with maximally mixed one-qubit reductions,” *Phys. Rev. A*, vol. 90, p. 032314, Sep 2014.

[17] K. Feng, L. Jin, C. Xing, and C. Yuan, “Multipartite entangled states, symmetric matrices and error-correcting codes,” 2015. arXiv:1511.07992v1.

[18] M. H. Michael, M. Silveri, R. Brierley, V. V. Albert, J. Salmilehto, L. Jiang, and S. Girvin, “New class of quantum error-correcting codes for a bosonic mode,” *arXiv preprint arXiv:1602.00008*, 2016.

[19] Y. Ouyang, “Permutation-invariant qudit codes from polynomials,” *arXiv preprint arXiv:1604.07925*, 2016.

[20] D. W. Leung, M. A. Nielsen, I. L. Chuang, and Y. Yamamoto, “Approximate quantum error correction can lead to better codes,” *Phys. Rev. A*, vol. 56, p. 2567, 1997.

# Quantum algorithm for association rules mining

Chao-Hua Yu[1 2 *] Fei Gao[1 †] Qiao-Yan Wen[1]

[1] *State Key Laboratory of Networking and Switching Technology, Beijing University of Posts and Telecommunications, Beijing, 100876, China*

[2] *State Key Laboratory of Cryptology, P.O. Box 5159, Beijing, 100878, China*

**Abstract.** Association rules mining (ARM) is one of the most important problems in knowledge discovery and data mining. Given a transaction database that has a large number of transactions and items, the task of ARM is to acquire consumption habits of customers by discovering the relationships between itemsets (sets of items). In this paper, we propose a quantum algorithm for the key procedure of ARM, finding out frequent itemsets from the candidate itemsets and acquiring their supports. Specifically, for the case in which there are $M_f^{(k)}$ frequent $k$-itemsets in the $M_c^{(k)}$ candidate $k$-itemsets ($M_f^{(k)} \leq M_c^{(k)}$), our algorithm can efficiently mine these frequent $k$-itemsets and estimate their supports by using parallel amplitude estimation and amplitude amplification with complexity $\mathcal{O}(\frac{k\sqrt{M_c^{(k)}M_f^{(k)}}}{\epsilon})$, where $\epsilon$ is the error for estimating the supports. Compared with the classical counterpart, classical sampling-based algorithm, whose complexity is $\mathcal{O}(\frac{kM_c^{(k)}}{\epsilon^2})$, our quantum algorithm quadratically improves the dependence on $\epsilon$, and also improves the dependence on $M_c^{(k)}$ to some degree which depends on the practical scale of $M_f^{(k)}$ relative to $M_c^{(k)}$.

**Keywords:** AQIS, template

## 1 Introduction

As one of the most important problems in data mining, association rules mining (ARM) is to discover the consumption habits of customers by finding out relationships between pairs of itemsets (sets of items) from a big transaction database [1]. The transaction database is a large set of a large number of transactions which is denoted by $\mathcal{T} = \{T_0, T_1, \cdots, T_{N-1}\}$ for $N$ transactions, each one being a subset of an overall set of items denoted by $\mathcal{I} = \{I_0, I_1, \cdots, I_{M-1}\}$ for $M$ items, i.e., $T_i \subseteq \mathcal{I}$. It can also be represented by a $N \times M$ binary matrix, denoted by $D$, in which the element $D_{ij} = 1(0)$ means that the item $I_j$ is (not) contained in the transaction $T_i$. The task of ARM can be reduced to that of mining all the frequent itemsets [1]. Here an itemset $X$ is called frequent if its support, defined by the percentage of transactions that contain $X$ and denoted by supp$(X)$, is not less than a preset threshold *min_supp*.

In classical regime, there are various algorithms [1] for mining frequent itemsets, the most famous one being the *Apriori* algorithm [2]. Based on the important *Apriori property* stating that all nonempty subset of a frequent itemset must also be frequent, Apriori algorithm employs an iterative approach known as a level-wise search to discover all the frequent itemsets. In the $k$th iteration of the algorithm, two procedures are executed:

- (P1) Given the set of *candidate* $k$-itemsets $\mathcal{C}^{(k)}$ which is determined by the frequent $(k-1)$-itemsets when $k > 1$ or is just $\mathcal{I}$ when $k = 1$, the supports of all the elements in $\mathcal{C}^{(k)}$ are examined by passing every transaction of database and the frequent elements are pick out to form the set of all frequent $k$-itemsets $\mathcal{F}^{(k)}$.
- (P2) Generate the set of candidate $(k+1)$-itemsets $\mathcal{C}^{(k+1)}$ from $\mathcal{F}^{(k)}$.

In practice, in each iteration (P1) dominant the time complexity of whole process [3]. Therefore, how to efficiently executing (P1) of each iteration, namely finding out frequent itemsets from candidate ones, is of great importance. In the following section, we provide a quantum algorithm to implement (P1) for each iteration that can significantly reduce the time complexity in contrast to the classical algorithms.

## 2 Quantum algorithm

Our quantum algorithm is to find out frequent itemsets from the candidate itemsets in the procedure (P1) of each iteration shown above. Our algorithm is based on the basic quantum oracle $O$ that access the element of the database binary matrix $D$, namely, $O|i\rangle|j\rangle|a\rangle = |i\rangle|j\rangle|a \oplus D_{ij}\rangle$. $\Theta(k)$ basic oracles $O$ together with the generalized CNOT operation [4] can be used to construct the quantum oracle $O^{(k)}$ that can identify whether an arbitrary transaction contain a $k$-itemset in in the way that

$$O^{(k)}|i\rangle|X\rangle = (-1)^{\tau(i,X)}|i\rangle|X\rangle,$$

where $\tau(i, X) = 1$ if $X \subseteq T_i$ and $\tau(i, X) = 0$ otherwise. Corresponding to $O^{(k)}$, we define a "big" Grover operator as

$$G^{(k)} = \big((2|\mathcal{X}_N\rangle\langle\mathcal{X}_N| - \mathbb{I}_N) \otimes \mathbb{I}_{M^k}\big)O^{(k)},$$

where $|\mathcal{X}_N\rangle = \frac{\sum_{i=0}^{N-1}|i\rangle}{\sqrt{N}}$ and $\mathbb{I}_N$ is the identity operator with dimension $N$.

[*] quantum.ych@gmail.com

[†] gaof@bupt.edu.cn

we suppose $\mathcal{C}^{(k)}$ has $M_c^{(k)}$ elements $\mathcal{C}^{(k)} = \{C_j^{(k)} | j = 1, 2, \cdots, M_c^{(k)}\}$ where $C_j^{(k)} = \{I_{c_{jl}^{(k)}} | l = 1, 2, \cdots, k, c_{jl}^{(k)} \in \mathbb{Z}_M\}$, $\mathcal{F}^{(k)}$ has $M_f^{(k)}$ elements and $\mathcal{F}^{(k)} \subseteq \mathcal{C}^{(k)}$. To mine the $M_f^{(k)}$ frequent $k$-itemsets from $M_c^{(k)}$ candidate $k$-itemsets, it requires computing the supports of all the candidate $k$-itemsets and then picking out the frequent $k$-itemsets. Our quantum algorithm will propose a new kind of amplitude estimation [5], *parallel amplitude estimation*, to generate a state approximating

$$\frac{\sum_{j=1}^{M_c^{(k)}} |s_j^{(k)}\rangle\langle s_j^{(k)}| \otimes |C_j^{(k)}\rangle\langle C_j^{(k)}|}{M_c^{(k)}},$$

where $s_j^{(k)}$ denote the supports of $C_j^{(k)}$, and then use the amplitude amplification [5] on the state to search for $s_j^{(k)} \geq min\_supp$. Finally, measuring the state after amplitude amplification reveals the frequent $k$-itemsets and their supports. The details of our algorithm for mining frequent $k$-itemsets are described as follows.

**Algorithm 1** Mining frequent $k$-itemsets $\mathcal{F}^{(k)}$ and their supports from candidate $k$-itemsets $\mathcal{C}^{(k)}$

```
Input:  $\mathcal{C}^{(k)}$,$G^{(k)}$,$k$,$T$;
Output:  $\mathcal{F}^{(k)}$ and the supports of elements in $\mathcal{F}^{(k)}$;
1: Prepare three registers in the state
   $(\frac{\sum_{t=0}^{T-1}|t\rangle}{\sqrt{T}})|\mathcal{X}_N\rangle(\frac{\sum_{j=1}^{M_c^{(k)}}|C_j^{(k)}\rangle}{\sqrt{M_c^{(k)}}})$.
2: Perform the unitary operation $\sum_{y=0}^{T-1}|y\rangle\langle y| \otimes (G^{(k)})^y$
   on the state.
3: Perform the inverse Fourier transformation $F_T^{\dagger}$ on the
   first register. Then the third register encodes all the
   candidate $k$-itemsets, while the first register encoding
   their corresponding supports.
4: Search in the first register of the state for the terms
   $y$ satisfying $\sin^2(\frac{\pi y}{T}) \geq min\_supp$ or $\sin^2(\frac{\pi(T-y)}{T}) \geq$
   $min\_supp$ by using amplitude amplification and then
   the state of the first and third register
   $\sim \frac{\sum_{j=1,\mathrm{supp}(C_j^{(k)})\geq min\_supp}^{M_c^{(k)}} |s_j^{(k)}\rangle\langle s_j^{(k)}| \otimes |C_j^{(k)}\rangle\langle C_j^{(k)}|}{M_f^{(k)}}$.
5: Measure the first and third register for $\mathcal{O}(M_f^{(k)})$ times
   to reveal all the $M_f^{(k)}$ frequent $k$-itemsets (i.e., $\mathcal{F}^{(k)}$)
   and their supports.
```

## 3 Complexity

We take the basic oracle $O$ as the query complexity. The comparison of our quantum algorithm and classical algorithms are given in the TABLE 1. The Apriori algorithm directly calculate the supports of candidate $k$-itemsets by scanning every transaction in a deterministic way, while the classical sampling-based algorithm estimates the supports by sampling the database and thus is non-deterministic. It is shown that our algorithm is significantly faster than the classical algorithms.

Table 1: Comparisons of our quantum algorithm, classical sampling-based algorithm and the classical Apriori algorithm for mining $\mathcal{F}^{(k)}$ from $\mathcal{C}^{(k)}$.

| algorithm | determinacy | query complexity |
|---|---|---|
| Quantum | non-deterministic | $\mathcal{O}(\frac{k\sqrt{M_c^{(k)}M_f^{(k)}}}{\epsilon})$ |
| Sampling-based | non-deterministic | $\mathcal{O}(\frac{kM_c^{(k)}}{\epsilon^2})$ |
| Apriori | deterministic | $\mathcal{O}(kM_c^{(k)}N)$ |

## 4 Conclusions

We provide a quantum algorithm for the core procedure of implementing ARM, mining frequent itemsets from the candidate itemsets. Specifically, by subtly using amplitude estimation and amplitude amplification, our algorithm can efficiently find out the frequent $k$-itemsets from candidate $k$-itemsets and estimate their supports. Complexity analysis shows our algorithm is faster than the classical counterpart, classical sampling-based algorithm, in the sense that the complexity of our algorithm is at least quadratically improved in the dependence on the error. We hope our quantum algorithm for ARM can help better understanding the power of quantum computing and inspire more quantum algorithms for big data mining tasks.

## References

[1] J. W. Han, M. Kamber, and J. Pei, *Data mining: Concepts and Techniques* (Morgan Kaufmann, 2011) 3rd ed..

[2] R Agrawal, R Srikant, Fast algorithms for mining association rules, in *Proceedings of the 1994 international conference on very large data bases (VLDB94)*, Santiago, Chile, 1994, p. 487.

[3] H. Mannila, H. Toivonen, A. I. Verkamo, Efficient algorithms for discovering association rules, in *KDD-94: AAAI workshop on Knowledge Discovery in Databases*, Seattle, Washington, 1994, p. 181.

[4] A. Barenco, C. H. Bennett, R. Cleve, D. P. DiVincenzo, N. Margolus, P Shor, T. Sleator, J. A. Smolin, and H. Weinfurter, Elementary gates for quantum compution, Phys. Rev. A **52**, 3457 (1995).

[5] G. Brassard, P. Høyer, M. Mosca, and A. Tapp, *Quantum Amplitude Aplification and Estimation*, Contemporary Mathematics Series Millenium Volumn **305** (AMS, New York, 2002).

# Quantum Chinese Chess

Chan Ming Shen[1], Jei Wei Chang[1], Wei- Kai Lin[2], Yanlin Chen[2], YiKe Huang[3], and Li-Yi Hsu[1]

[1]*Department of Physics, Chung Yuan Christian University, Chungli 320, Taiwan, Republic of China*
[2]*Institute of Information Science, Academia Sinica*
[3]*Department of Computer Science & Information Engineering, National Taiwan University*

**Abstract.** For the pedagogical and entertaining purposes, we are projecting the quantum Chinese chess. Some additional chess rules are put as simile or metaphor of quantum superposition, entanglement, and measurement. Our short-term goal is to build an online platform for the chess players. As the long-term goal, we want to investigate the effect of the quantum moves on quantum Chinese chess. So far it is still unknown how to evaluate the power quantum moves in the chess play.

**Keywords:** quantum game, quantum entanglement, q

## 1 Introduction

The idea of quantum chess was originally proposed for the study of quantum chromodynamics. Therein, the space-time is pretended as a chessboard [1]. Maybe quantum tic-tac-toe was the first game play developed as a metaphor for the counterintuitive nature in quantum physics [2]. In 2010, Akl and Wismath proposed quantum chess to put "humans and computers on an ostensibly equal footing when faced with the uncertainties of quantum physics" [3]. Early in this year, Chris Cantwell has successfully raised funds for Quantum Chess on the Kickstarter [4]. Now everyone can see Hawking and Rudd playing the quantum chess on YouTube, and there even are apps for quantum chess.

Here we propose the quantum version of Chinese chess, also known as Xiangqi, which is a popular pastime in the Eastern world. For the pedagogical purpose, we eventually hope to propose quantum Chinese chess accessible and understandable for kids and young adult across the Taiwan Strait.

## 2 Rules

Among quantum tic-tac-toe, quantum chess, and Xiangqi, three quantum properties: the superposition, entanglement, and quantum measurement are well exploited. To demonstrate how it can be done, three "quantum" moves are put in addition to the traditional ones. (1) (Superposition) In addition to the regular move, the quantum move can move the regular move twice and make a supposition. Fig. 1 shows the quantum move of the "red Cannon". (2) (Entanglement) Based on (1), one can make entanglement between two or more chess pieces. For example, Fig.2 shows the entanglement between "red Cannon" and "red Chariot". Notably, the entanglement is made because the superposition of Cannon seems to "block" the moving way of Chariot. Fig. 2 (c) and (d) show two possible conditions after the measurement. (3) (Quantum measurement) If one want to capture and remove the opponent piece with the superposition, one has to perform measurement both on this piece and his own. For example, the red Chariot wants to demolish the "black Cannon" in Fig. 3 (a). The probability of this event can occur with the probability 0.25, where the red Chariot and the black Cannon must be collapsed into the position as shown in Fig. 3(b) In addition, one can ask for the measurement on the specific opponent pieces in some circumstance. For example, in Fig. (4), the player with the red pieces can ask for the measurement on the black Canon.

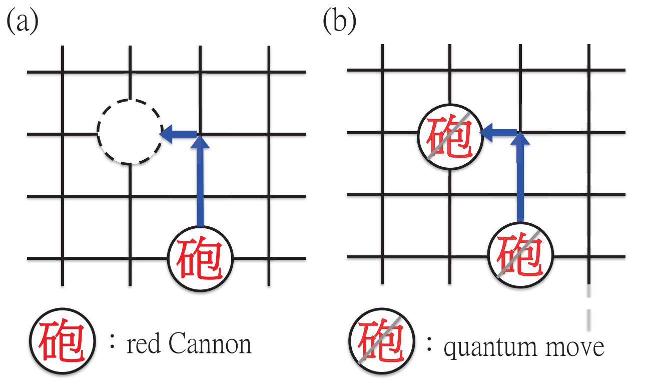

Figure 1: (a) Before the quantum move. The arrows each show the corresponding regular moves. (b) After the quantum move. The slashes indicate that "state" in superposition rather than a "real object" of the piece.

The development of quantum Chinese chess is still in a very early stage. So far, we can play quantum Chinese chess on PC. Our goal is to put quantum Chinese chess on network platform such as twitch. As for the academic study, there are many interesting open questions. One of them is "Do quantum moves really useful?" Based on our chess experience with the low-level strength, we give a very rough answer: It largely depends on how the players recognize the probability on the board.

Traditionally, through the chess play, two players usually seek the balance of terror on the board and start the attacks afterward. Essentially a quantum move can move twice the regular move or make no move with the equal probability. As for the mind-reading, a conserva-

[*] a6a018@yahoo.com.tw
[†] fairycat115@gmail.com
[‡] wklin@iis.sinica.edu.tw
[§] jackervator@gmail.com
[¶] lyhsu@cycu.edu.tw

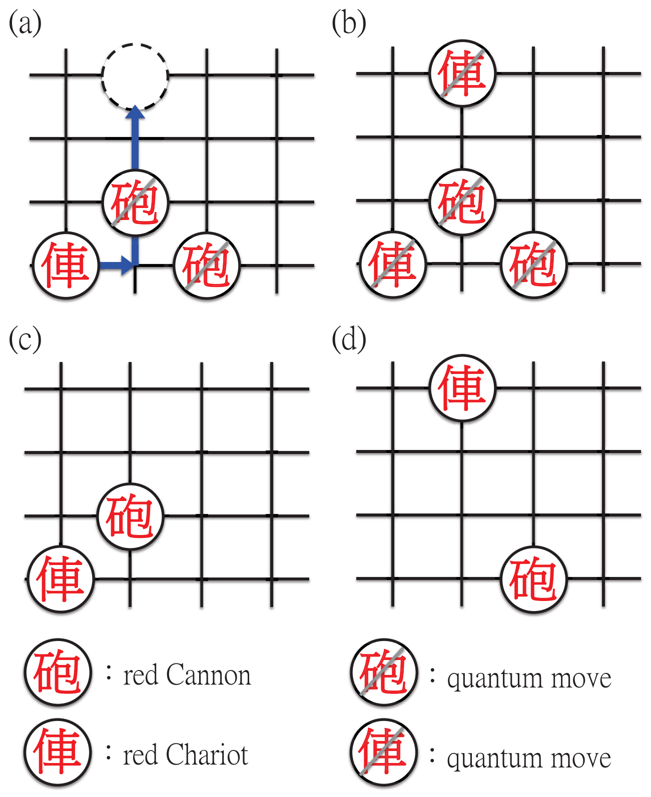

Figure 2: (a) To form the entanglement, the red Chariot make a quantum move. (b) The entanglement between the red Chariot and the red Canon. The quantum measurement on these two pieces results in the cases either (c) or (d).

tive player may recognize the quantum move as a null move, while an aggressive player may recognize it as a quick one. Moreover, if the piece under its superposition can remove the opposite pieces with at most the probability 0.5. In this case, quantum moves are exploited to make a "not-so-real" threaten or a bluff. It is feasible that aggressive quantum moves may not be encouraged for a traditional player.

## 3 Discussion

In the chessboard of Xiangqi, there are 32 chess pieces distributed during 90 standing points. In the setup, the opposite soldiers are divided only a very narrow "river and boundary". The board looks more crowded than that in quantum chess. The legal regular moves are very limited. Moreover, in the initial game play, two players each usually take several regular moves to achieve the layout/ composition for the following defense and offense. In this process, it does not pay to make a quantum move, which will just delay layout completion. Finally, it could be useful that the pieces can escape from be captured and removed using the quantum move. To sum up, quantum Chinese chess is a good game as a metaphor of basic concept in quantum theory. We are looking forward to the collaboration for the further development of quantum Chinese chess.

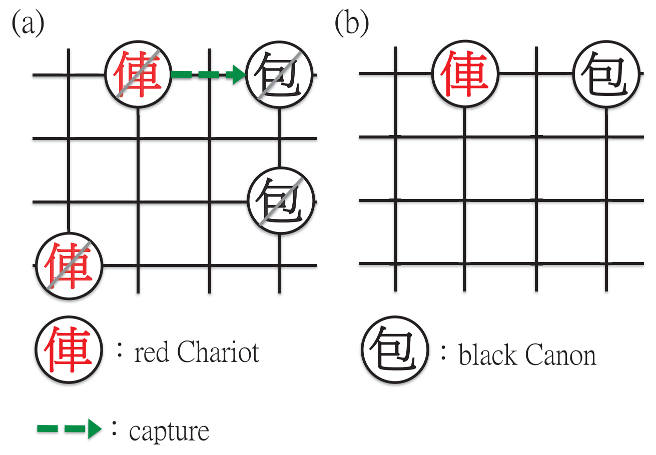

Figure 3: (a) The red Chariot wants to capture the black Canon. To make this happen, the red Chariot ask for the quantum measurement on these two pieces. The capture can become real if the pieces are collapsed into the case (b).

## 4 Acknowledge

The authors acknowledge national support from the Ministry of Science and Technology of the Republic of China under Contract No. 102-2112-M-033 -006 -MY3.

## References

[1] New Scientist, 2137, 32 (1998).

[2] Allan Goff: American Journal of Physics 74, 962 (2006).

[3] S. G. Akl, Parallel Process. Letters, 20, 275 (2010).

[4] http://quantumrealmgames.com/

# Quantum Coherence - Their origin and trade-off relations

R. Chandrashekar[1 2 *] P. Manikandan[3] J. Segar[3 †] Tim Byrnes[1 2 4 5 ‡]

[1] *New York University, 1555 Century Avenue, Pudong, Shanghai 200122, China*
[2] *NYU-ECNU Institute of Physics at NYU Shanghai, 3663 Zhongshan Road North, Shanghai 200062, China*
[3] *Department of Physics, Ramakrishna Mission Vivekananda College, Mylapore, Chennai 600004, India*
[4] *Department of Physics, New York University, New York 10002, USA*
[5] *National Institute of Informatics, 2-1-2 Hitotsubashi, Chiyoda-ku, Tokyo 101-8430, Japan*

**Abstract.** Quantum coherence is investigated using a new measure with metric properties and entropic nature and decomposed into local and intrinsic contributions. The trade-off relation between these contributions as well as their distribution properties are studied for simple tripartite systems and the more complex spin chain model.

**Keywords:** Quantum coherence, Local and Intrinsic coherence, Monogamy of coherence.

## 1 Introduction

Quantifying coherence using methods of quantum information science was introduced in [1]. Apart from the introduction of definitions corresponding to incoherent states, incoherent operations and maximally coherent states, the set of properties a functional should satisfy to be considered as a coherence measure were discussed in [1]. For a coherence measure $C$ they are as follows: *(i)* $\mathcal{C} \geq 0$ and $\mathcal{C} \equiv 0$ iff $\rho \in \mathcal{I}^{(b)}$, where $\mathcal{I}^{(b)}$; is the set of incoherent states. *(ii)* $\mathcal{C}(\rho)$ is invariant under unitary transformations, *(iii)* $\mathcal{C}(\rho)$ is monotonic under incoherent completely positive trace preserving (ICPTP) map, as well as under selective incoherent measurements on average. *(iv)* $\mathcal{C}(\rho)$ is convex i.e., does not increase under mixing of quantum states. Two measures of coherence namely the relative entropy of coherence and the $\ell_1$ norm were introduced in [1]. The former is an entropic measure, whereas the later is a geometric measure with each of them having their own advantages. To be a distance property a function $d$ over a set $X$ should satisfy the following properties: *(i)* $d(x,y) > 0 \; \forall \; x \neq y$ and $d(x,x) = 0$ (Positivity) *(ii)* $d(x,y) = d(y,x)$ (Symmetry). In addition if $d$ satisfies $d(x,y)+d(y,z) \geq d(x,z)$ i.e., the triangle inequality, then $d$ is a metric over the space $X$. We introduce a new coherence measure based on the quantum version of the Jensen-Shannon divergence (QJSD) [2, 3]

$$\mathcal{J}(\rho,\sigma) = \frac{1}{2}[S(\rho\|(\rho+\sigma)/2) + S(\sigma\|(\rho+\sigma)/2)]. \quad (1)$$

which combines the features of both distance property and entropic nature. The QJSD is a distance but it is not a metric i.e., it does not satisfy the triangle inequality. To overcome this we use the square root of the QJSD as our distance measure, since it satisfies the triangle inequality.

## 2 Inter-qubit, Intra-qubit and Total Coherence

The total coherence of a given system is defined using the square root of the QJSD using the following expression

$$\mathcal{C}(\rho) \equiv \min_{\sigma \in \mathcal{I}^{(b)}} \sqrt{\mathcal{J}(\rho,\sigma)}, \quad (2)$$

where $\mathcal{I}^{(b)}$ is the set of incoherent states in a particular basis $b$. This measure (2) satisfies the properties outlined in Ref. [1] and hence qualifies as a coherence quantifier. But coherence can have its origin to intra-qubit and inter-qubit correlations. We propose the following measure of coherence to distinctly measure the intra-qubit and the inter-qubit coherences through the following equations

$$\begin{aligned} \mathcal{C}_I(\rho) &\equiv \min_{\sigma_S \in \mathcal{I}_S} \mathcal{D}(\rho, \sigma_S), & (3)\\ \mathcal{C}_L(\rho) &\equiv \mathcal{D}(\sigma_S^{\min}, \rho^d). & (4) \end{aligned}$$

Here $C_I$ is the inter-qubit coherence and refer to it as intrinsic coherence and $C_L$ is the Local coherence which computes the contribution of the intra-qubit coherence. As an illustrative example we consider a two qubit transverse Ising model which has the Hamiltonian

$$H = \lambda\sigma_1^x\sigma_2^x + J(\sigma_1^x + \sigma_2^x) + \epsilon\lambda(\sigma_1^z + \sigma_2^z). \quad (5)$$

The parameters $J$ and $\lambda$ are the the coupling parameters and $\epsilon$ is a symmetry breaking term. A numerical estimation of the values of $C_L$, $C_I$ and $C$ are given in Fig 1 (a). The local coherence and the intrinsic coherence are complementary. In the limit $J \ll \lambda$ the coherence is intrinsic in nature since the ground state approaches a Bell state in the $J = 0$ and $\epsilon \to 0$ limit. In the limit $J \ll \lambda$ the coherence is localized with each spin since for $\lambda = 0$ the ground state is $(|0\rangle - |1\rangle)(|0\rangle - |1\rangle)$.

## 3 Distribution and Shareability of quantum coherence

The quantum coherence in a tripartite system $\rho_{123}$ may be decomposed in any one of the following forms

$$\begin{aligned} \mathcal{C}_{123} &\leq \mathcal{C}_1 + \mathcal{C}_2 + \mathcal{C}_3 + \mathcal{C}_{1:2:3}, \\ \mathcal{C}_{123} &\leq \mathcal{C}_1 + \mathcal{C}_2 + \mathcal{C}_3 + \mathcal{C}_{2:3} + \mathcal{C}_{1:23}. & (6) \end{aligned}$$

[*] cr2442@nyu.edu
[†] segar@imsc.res.in
[‡] tim.byrnes@nyu.edu

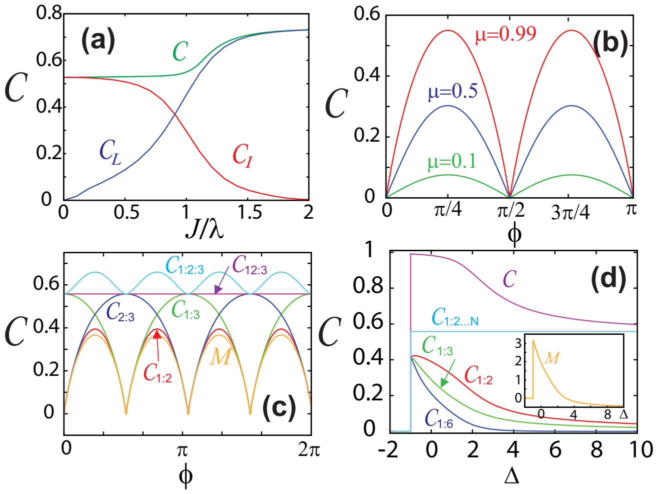

Figure 1: Coherence measured using QJSD for (a) $N = 2$ site Ising model with $\epsilon = 0.2$; (b) Werner GHZ state (c) W state with $\theta = \pi/4$; (d) $N = 10$ site $XXZ$ spin chain model with $J = 1$. Inset: Monogamy of the $XXZ$ spin chain.

where $C_n$ is the local coherence of the n$^{th}$ subsystem obtained from the reduced density matrix $\rho_n$ and $C_{1:2:3}$ is the intrinsic coherence i.e., $C_I(\rho_{123})$. There are many such equivalent decompositions from which can conclude that

$$\mathcal{C}_{1:2:3} \simeq \mathcal{C}_{2:3} + \mathcal{C}_{1:23} \simeq \mathcal{C}_{1:2} + \mathcal{C}_{12:3} \simeq \mathcal{C}_{1:3} + \mathcal{C}_{13:2}. \quad (7)$$

The above decomposition gives us an idea about how coherence is shared between the subsystems of various orders in a composite system. Similar to monogamy of entangled states [4, 5] we define the monogamy of coherence. In a maximally coherent tripartite system $\rho_{123}$, the coherence between the system 1 and the bipartition 23 is related to the coherence between the subsystems 1 and 2 as well the coherence between 1 and 3 through the inequality

$$C_{1:23} \geq C_{1:2} + C_{1:3}. \quad (8)$$

If the inequality is obeyed the system is called monogamous and if not it is referred to as polygamous system. For a multipartite system the inequality is $C_{1:2...N} \geq \sum_{n=1}^{N} C_{1:n}$ and we define the measure

$$M = \sum_{n=2}^{N} C_{1:n} - C_{1:2...N} \quad (9)$$

which is monogamous for $M \leq 0$ and polygamous $M > 0$. Thus from the monogamy concept we get to know whether the coherence is distributed in a bipartite fashion or in a multipartite fashion.

## 4 Investigation of Multipartite systems

The tripartite states can be divided into two classes namely $GHZ$ and the $W$ class. These two classes are unrelated under local operations and classical communication [6]. The Local coherence of the systems in these two kinds of states is zero and hence the intrinsic coherence is equal to the total coherence. For the pure mixed tripartite states the coherence and its distribution is given through Fig 1 (b) and Fig 1 (c).

To understand complex multipartite systems we investigate the Heisenberg $XXZ$ spin chain. The Hamiltonian of the spin chain is

$$H = J \sum_n (\sigma_n^x \sigma_{n+1}^x + \sigma_n^y \sigma_{n+1}^y + \Delta \sigma_n^z \sigma_{n+1}^z), \quad (10)$$

where $J$ is the nearest neighbor spin coupling and $\Delta$ is the anisotropy parameter. The total quantum coherence shown in Fig 1 (d) is found to vary with the anisotropy parameter. The monogamy of coherence is shown in the inset of Fig 1 (d) shows that $\Delta$ switches the coherence from bipartite to multipartite nature.

## 5 Conclusion

A new coherence measure with both distance properties and entropic nature is proposed. The total coherence in the system is decomposed into contributions which arise from Local and Intrinsic contributions. It is found that the coherence transforms from the local to intrinsic nature in a Ising model depending on the interaction parameter. In the case of the Heisenberg spin chain there is a change from the monogamous behavior which is a highly multipartite coherence to the polygamous nature which is more bipartite in nature. Further applications in quantum metrology [7] may lead to interferometric advantages.

## 6 Acknowledgments

The work is supported by the Shanghai Research Challenge Fund, New York University Global seed Grants for Collaborative Research, National Natural Science Foundation of China Grant No. 61571301, and the Thousand Talents Program for Distinguished Young Scholars.

## References

[1] T. Baumgratz, M. Cramer and M.B. Plenio, Phys. Rev. Lett. 113, 140401 (2014).

[2] A.P. Majtey, P.W. Lamberti and D.P. Prato, Phys. Rev. A 72 052310 (2005).

[3] P.W. Lamberti, A.P. Majtey, A. Borras, M. Casas and A. Plastino, Phys. Rev. A 77 052311 (2008).

[4] V. Coffman, J. Kundu and W.K. Wootters, Phys. Rev. A 61, 052306 (2000).

[5] T.J. Osborne and F. Verstraete, Phys. Rev. Lett. 96, 220503 (2006).

[6] W. Dür, G. Vidal and J.I. Cirac, Phys. Rev. A 62, 062314 (2000).

[7] J. Sahota and N. Quesada, Phys. Rev. A 91, 013808 (2015).

# Quantum homomorphic encryption from quantum codes

Yingkai Ouyang and Si-Hui Tan
*Singapore University of Technology and Design, 8 Somapah Road, Singapore*[*]

Joseph Fitzsimons
*Singapore University of Technology and Design, 8 Somapah Road, Singapore*[*] *and*
*Centre for Quantum Technologies, National University of Singapore, 3 Science Drive 2, Singapore*

Homomorphic encryption has been recognised as an important primitive for building secure delegated computation protocols for many decades [1]. It provides a processing functionality for encrypted data which stays secret during the evaluation, and a scheme is *fully-homomorphic* if it allows for arbitrary computation. Despite widespread interest in this problem, it was not until 2009 that the first computationally secure classical scheme for fully homomorphic encryption (FHE) was discovered [2], with many improvements following rapidly from this initial discovery [3, 4], and has recently drawn attention within the quantum information community [5–12]. One might wonder if quantum cryptosystems might offer unconditionally secure homomorphic encryption schemes and whether the privacy homomorphisms could be extended to allow for evaluation of quantum circuits.

Like their classical counterparts, quantum homomorphic encryption (QHE) schemes comprise of four parts: key generation, encryption, evaluation, and decryption. Unlike blind quantum computation [13], in which the computation to be performed forms part of the secret, QHE schemes do not have secret circuit evaluations. They serve to obscure only the information that is contained within the state to be processed using the chosen circuit. The extent to which a scheme is secure depends on its specifics, and in previous work has varied depending on the precise nature of the computation which can be performed on the encrypted input. QHE schemes described in Refs. [9, 10] offer some information theoretic security, but this is only in the form of a gap between the information accessible with and without the secret key, a notion of security which does not imply the stronger notion of security under composition. These schemes are also limited in the set of operations that can be performed on the encrypted data. The scheme in [9] only allows computations in the BosonSampling model, while that in [10] is not known to support encoded universal quantum computing. Broadbent and Jeffrey's scheme [11] enables quantum homomorphic encryption of fixed depth circuits by bootstrapping onto a classical fully homomorphic encryption scheme and as such is only computationally secure. Recently Dulek, Schaffner and Speelman [12] used the garden-hose model of computation with Broadbent and Jeffrey's quantum homomorphic schemes to allow the evaluation of polynomial-depth circuits. Several other schemes for computing on encrypted data have previously been introduced which offer universal quantum computation, but require interactions between the client and evaluator [5–8]. This requirement for interaction places them outside of the formalism of homomorphic encryption, although confusingly several of these schemes use that terminology [5, 6].

The difficulty in creating a perfectly secure quantum fully homomorphic encryption (QFHE) scheme persists, and is in line with the no-go result provided by [14] that perfect information-theoretic security whilst enabling arbitrary processing of encrypted data is impossible, unless the size of the encoding grows exponentially. Nonetheless, given the growing interest in QHE schemes and the multitude of possibilities, Broadbent and Jeffrey set out to provide a rigorous framework for defining QHE schemes [11], basing their security definitions on the requirement for indistinguishability of codewords under chosen plaintext attack with additional computation assumptions. Broadbent and Jeffery also require that a quantum *fully* homomorphic encryption satisfies two properties: correctness and compactness. Perfect correctness occurs when the evaluated output on the cipherstate after decryption is exactly the correct evaluated input.

Here we present a quantum encryption scheme which is homomorphic for arbitrary classical and quantum circuits which have at most some constant number of non-Clifford gates. Unlike classical schemes, the security of the scheme we present is information theoretic, satisfying entropic security definitions, and hence independent of the computational power of an adversary. The QHE scheme we present builds on constructions taken from quantum error correction codes to provide gates for universal quantum computation. The block of qubits that contains the code is embedded in a much larger set of qubits that are initialized in a maximally mixed state. The qubits are then shuffled in a specific but random way to hide the qubits that contain that code. Our protocol guarantees that the trace distance between ciphertexts corresponding to any two quantum inputs is exponentially suppressed. This is a significantly stronger security guarantee than previous homomorphic encryption schemes presented in [9]. Moreover the computation power of our scheme is similar to that of Broadbent and Jeffrey's while avoiding bootstrapping on the classical ho-

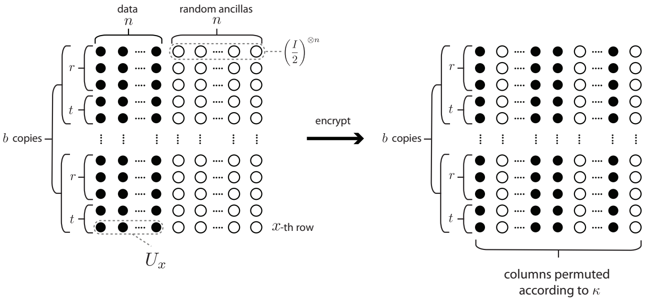
data
$n$
random ancillas
$n$
$\left(\frac{I}{2}\right)^{\otimes n}$
$r$
$t$
$b$ copies
encrypt
$b$ copies
$x$-th row
$U_x$
columns permuted according to $\kappa$

FIG. 1: Figure shows qubits arranged on a grid with shaded circles representing data qubits. Within the $x$-th row, the $n$ data qubits are in a code encoded by $U_x$. The unshaded circles are ancilla qubits which are in the completely mixed state. There are $r$ sets of codes, and $b$ copies of such sets. A random permutation of the columns completes the encryption procedure of our quantum homomorphic encryption scheme.

momorphic encryption scheme.

Our QHE scheme takes as its input a $r$-qubit state $\rho_{\text{input}}$, and $t$ independent copies of the magic state $|T\rangle\langle T| = \frac{I}{2} + \frac{X-Y}{2\sqrt{2}}$, all arranged in a single column (See Figure 1). We then introduce $(2n-1)$ more columns of maximally mixed qubits to obtain a grid of qubits with $r+t$ rows and $2n$ columns. Here, we choose $n$ to such that $\frac{n-1}{4}$ is a non-negative integer. Of the new columns introduced, $n-1$ of them will be incorporated as data qubits while the remaining $n$ columns will be used as ancillae in the encryption. An encoding quantum circuit $U = U_1 \otimes \cdots \otimes U_{r+t}$ is applied row-wise on the first $n$ columns. Applying $U$ spreads the quantum input from just the first column to the first $n$ columns. Since every qubit not residing on the first column is maximally mixed, the encoding circuit on each row encodes the quantum data on the first column into a random quantum code, the resultant quantum information of which resides in a random codespace on the first $n$ columns. Encryption is then achieved via randomly permuting the $2n$ columns with a permutation $\kappa$. Permuting the columns brings the quantum information to be processed from the first $n$ columns to the columns $k_1, \ldots, k_n$, where $1 \leq k_1 < \cdots < k_n \leq 2n$. For the decryption algorithm, one performs the inverse permutation $\kappa^{-1}$ of the columns, followed by the inverse unitary $U^\dagger$ on the first $n$ columns of the grid. Finally every qubit in the rows $r+1$ to $r+t$ are measured in the computation basis. The quantum output of our scheme is then located on the first $r$ rows of the first column of our grid of qubits.

To evaluate the circuit, the evaluator operates independently and identically (i.i.d) on not $n$ but $2n$ columns of qubits, $n$ columns of which are the maximally mixed state. The i.i.d structure of the evaluator's operations allows these operations to commute with any secret permutation of the columns of the qubits on the grid. In addition, the evaluators' operations necessarily leave the $n$ columns of qubits initialized in the maximally mixed state unchanged, thereby implementing i.i.d quantum operations on only the columns containing the encoded quantum data. Hence the evaluator, by applying transversal gates on the $2n$ columns, achieves the application of the corresponding transversal gates on the $n$ columns with the quantum data without requiring knowledge of the location of the columns containing the encoded quantum information.

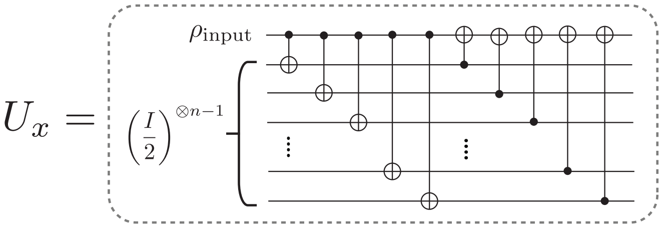

FIG. 2: Figure shows the encoding quantum circuit $U_x$ that is applied on the first $n$ qubits in the $x$-th row. Each line represents one qubit and the gates are applied in the order from left to right.

The circuit to be evaluated can always be written as $V = V_d \ldots V_1$, where the evaluator is to apply privacy homomorphisms of the gates $V_1$ to $V_d$ sequentially. Here, each $V_i$ applies either a Clifford gate or a $T$ gate locally on a single qubit, or applies a CNOT locally on a pair of qubits.

When $V_i$ is a unitary operation that applies a Clifford gate $G$ locally on the $x$-th qubit, the evaluator can apply the logical $G$-gate on our random code on the $x$-th row without any knowledge of the data columns $k_1, \ldots, k_n$. To do so, the evaluator simply applies the unitary $G^{\otimes 2n}$ on the $2n$ qubits located on the $x$-th row on each copy. Since any unitary operation leaves a maximally mixed qubit state unchanged, the evaluator effectively only applies the unitary $G^{\otimes n}$ on the qubits in the encrypted data columns $k_1, \ldots, k_n$ on the $x$-th row, which is the logical $G$-gate on the $x$-th row.

When $V_i$ is a unitary operation that applies a CNOT gate with control on the $x$-th qubit and target on the $y$-th qubit, denoted as $\text{CNOT}_{x,y}$, the evaluator can also apply the corresponding logical CNOT gate on our random code on the $x$-th and $y$-th row without any knowledge of the data columns $k_1, \ldots, k_n$. To do so, the evaluator simply applies a CNOT with control qubit on the $x$-th row and the $j$-th column and target qubit on the $y$-th row and the $j$-th column for every $j = 1, \ldots, 2n$. Since any unitary operation on two qubits leaves a maximally mixed two-qubit state unchanged, the evaluator effectively only applies the unitary $\text{CNOT}^{\otimes n}$ on the qubits in the encrypted data columns $k_1, \ldots, k_n$ with control qubits on the $x$-th row and target qubits on the $y$-th row, which is the correct logical CNOT-gate, which we denote as $\overline{\text{CNOT}}_{x,y}$.

When $V_i$ is a unitary operation that applies the $k$-th non-Clifford gate $T$ on the $x$-th qubit, the evaluator has to perform gate teleportation [15, 16]. Now consider gate teleportation of a single-qubit gate $T$. Omitting the correction operation required by gate teleportation allows this procedure to succeed with probability $\frac{1}{2}$ as depicted in Figure 3. The required measurement can be deferred until decryption due to the principle of deferred measurement [17].

To implement gate teleportation of the logical $T$ operation, the evaluator applies privacy homomorphism for $\mathrm{CNOT}_{x,r+k}$ followed by the privacy homomorphism for $\mathrm{CNOT}_{r+k,x}$. Because of the ancilla columns being in the maximally mixed state, the unitary $\overline{\mathrm{CNOT}}_{x,r+k}$ followed by the the unitary $\overline{\mathrm{CNOT}}_{r+k,x}$ are effectively applied on the data columns $k_1, \ldots, k_n$.

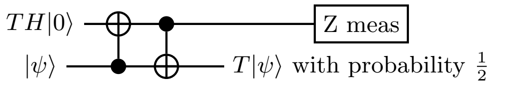

FIG. 3: Gate teleportation of the $T$-gate without correction.

Our scheme satisfies the correctness and compactness condition of Broadbent and Stacey. Each copy of our scheme yields the correct quantum output with constant probability $2^{-t}$. Extra copies simply amplify the probability of success. Thus although each instance of our scheme implements $T$ non-deterministically, it can be said to have *heralded* perfect completeness: namely, $b = \lfloor\sqrt{\frac{\alpha}{2}} + 1\rfloor^2 2^{2t}$ copies of our scheme yields the correct output in at least one copy with probability at least $1 - e^{-\alpha}$, and we know which of the $b$ copies yield the correct output. An arbitrarily large $\alpha$ brings the success probability arbitrarily close to unity. Since $t, b$ are constant, and the total number of gates required for decryption is independent of the depth of the circuit to be evaluated. Hence, our scheme is compact for circuits with a constant maximum number of $T$ gates and unbounded Clifford gates.

Randomly permuting the columns of qubits obfuscates the subset of columns where the quantum information resides, thereby encrypting the quantum data. The maximum trace distance between any two outputs is exponentially suppressed in $n$, with value at most $e\left(\frac{4n}{\pi}\right)^{1/4} 4^{b(r+t)} 2^{-n}$, which is exponentially suppressed in $n$ for constant $r$ and $t$. For full details, see Ref. [18].

This material is based on research supported in part by the Singapore National Research Foundation under NRF Award No. NRF-NRFF2013-01. JFF and ST acknowledges support from the Air Force Office of Scientific Research under AOARD grant FA2386-15-1-4082.

[1] R. L. Rivest, L. Adleman, and M. L. Dertouzos, "On data banks and privacy homomorphisms," *Foundations of secure computation*, vol. 4, no. 11, pp. 169–180, 1978.

[2] C. Gentry, "Fully homomorphic encryption using ideal lattices," in *Proceedings of the Forty-first Annual ACM Symposium on Theory of Computing*, STOC '09, (New York, NY, USA), pp. 169–178, ACM, 2009.

[3] M. Van Dijk, C. Gentry, S. Halevi, and V. Vaikuntanathan, "Fully homomorphic encryption over the integers," in *Advances in cryptology–EUROCRYPT 2010*, pp. 24–43, Springer, 2010.

[4] C. Gentry, S. Halevi, and N. Smart, "Fully homomorphic encryption with polylog overhead," in *Advances in Cryptology EUROCRYPT 2012* (D. Pointcheval and T. Johansson, eds.), vol. 7237 of *Lecture Notes in Computer Science*, pp. 465–482, Springer Berlin Heidelberg, 2012.

[5] M. Liang, "Symmetric quantum fully homomorphic encryption with perfect security," *Quantum Information Processing*, vol. 12, no. 12, pp. 3675–3687, 2013.

[6] M. Liang, "Quantum fully homomorphic encryption scheme based on universal quantum circuit," *Quantum Information Processing*, pp. 1–11, 2015.

[7] K. A. G. Fisher, A. Broadbent, L. K. Shalm, Z. Yan, J. Lavoie, R. Prevedel, T. Jennewein, and K. J. Resch, "Quantum computing on encrypted data," *Nat. Commun.*, vol. 5, 01 2014.

[8] A. M. Childs, "Secure assisted quantum computation," *Quantum Info. Comput.*, vol. 5, pp. 456–466, Sept. 2005.

[9] P. P. Rohde, J. F. Fitzsimons, and A. Gilchrist, "Quantum walks with encrypted data," *Phys. Rev. Lett.*, vol. 109, p. 150501, Oct 2012.

[10] S.-H. Tan, J. A. Kettlewell, Y. Ouyang, L. Chen, and J. F. Fitzsimons, "A quantum approach to fully homomorphic encryption," *arXiv prnote arXiv:1411.5254*, 2014.

[11] A. Broadbent and S. Jeffery, "Quantum homomorphic encryption for circuits of low $T$-gate complexity," *arXiv prnote arXiv:1412.8766*, 2014.

[12] Y. Dulek, C. Schaffner, and F. Speelman, "Quantum homomorphic encryption for polynomial-sized circuits," 2016. arXiv:1603.09717v1.

[13] A. Broadbent, J. Fitzsimons, and E. Kashefi, "Universal blind quantum computation," in *Foundations of Computer Science, 2009. FOCS '09. 50th Annual IEEE Symposium on*, pp. 517–526, Oct 2009.

[14] L. Yu, C. A. Pérez-Delgado, and J. F. Fitzsimons, "Limitations on information-theoretically-secure quantum homomorphic encryption," *Phys. Rev. A*, vol. 90, p. 050303, Nov 2014.

[15] D. Gottesman and I. L. Chuang, "Demonstrating the viability of universal quantum computation using teleportation and single-qubit operations," *Nature*, vol. 402, pp. 390–393, 1999.

[16] X. Zhou, D. W. Leung, and I. L. Chuang, "Methodology for quantum logic gate construction," *Phys. Rev. A*, vol. 62, p. 052316, Oct 2000.

[17] M. A. Nielsen and I. L. Chuang, *Quantum Computation and Quantum Information*. Cambridge University Press, second ed., 2000.

[18] Y. Ouyang, S.-H. Tan, and J. Fitzsimons, "Quantum homomorphic encryption from quantum codes," *arXiv preprint arXiv:1508.00938*, 2015.

[*] Electronic address: yingkai_ouyang@sutd.edu.sg

# Quantum information approach to Bose-Einstein condensation of composite bosons

Su-Yong Lee[1 2 *] Jayne Thompson[2] Sadegh Raeisi[3 2] Paweł Kurzyński[4 2] Dagomir Kaszlikowski[2 5] Jaewan Kim[1]

[1] *School of Computational Sciences, Korea Institute for Advanced Study, Hoegi-ro 85,Dongdaemun-gu, Seoul 02455, Korea*

[2] *Centre for Quantum Technologies, National University of Singapore, 3 Science Drive 2, 117543 Singapore, Singapore*

[3] *Institute for Theoretical Physics II, Friedrich-Alexander-Universitt Erlangen-Nrnberg*

[4] *Faculty of Physics, Adam Mickiewicz University, Umultowska 85, 61-614 Poznań, Poland*

[5] *Department of Physics, National University of Singapore, 2 Science Drive 3, 117542 Singapore, Singapore*

**Abstract.** We consider composite bosons (cobosons) comprised of two elementary particles, fermions or bosons, in an entangled state. First, we show that the effective number of cobosons implies the level of correlation between the two constituent particles. For the maximum level of correlation, the effective number of cobosons is the same as the total number of cobosons, which can exhibit the original Bose-Einstein condensation (BEC). In this context, we study a model of BEC for indistinguishable cobosons with a controllable parameter, i.e., entanglement between the two constituent particles. Furthermore we consider its application in entanglement of macroscopic states.

**Keywords:** BoseEinstein condensation, composite boson, entanglement, macroscopic state

We consider a simple model of BEC with composite bosonic particles. In particular, we assume that neither the composite particles nor their constituents interact, such that the internal structure of composite particles is stable and temperature independent.

Of course, the bound states between constituent particles have to result from their interaction. However, here we assume that once the constituents form a composite particle state, they do not interact anymore. Physically, this may correspond to a dilute gas of composite particles for which energy scales of a binding interaction potential between constituents are much greater than energy scales of the confining trap. As an example, one may think of an atomic hydrogen gas in which ionization temperature is much higher than the standard temperatures required to obtain BEC. Such a simplified model allows us to focus on the fundamental problem of how BEC depends on the internal state of composite particles, while neglecting other physical properties.

Imagine a pair of distinguishable fermionic or bosonic particles. The system is described by the creation operators $\hat{a}_k^\dagger$ and $\hat{b}_l^\dagger$, where the indices $k, l = 0, 1, \ldots, \infty$ label different modes that can be occupied by the two particles. These modes can, for example, correspond to different energy/momentum states. The wave function of the system is of the form

$$\sum_{k,l=0}^{\infty} \alpha_{k,l} \hat{a}_k^\dagger \hat{b}_l^\dagger |0\rangle, \tag{1}$$

where $\alpha_{k,l}$ is the probability amplitude that particle $a$ is in mode $k$ and particle $b$ is in mode $l$, and $|0\rangle$ is the vacuum state. Using insights from entanglement theory, the mathematical procedure known as the Schmidt decomposition allows us to rewrite the above state as [1]

$$\sum_{m=0}^{\infty} \sqrt{\lambda_m} \hat{a}_m^\dagger \hat{b}_m^\dagger |0\rangle \equiv \hat{c}^\dagger |0\rangle, \tag{2}$$

where the modes labeled by $m$ are superpositions of the previous modes $k$ and $l$ and $\sqrt{\lambda_m}$ are probability amplitudes that both particles occupy mode $m$. Note that despite the fact that $\hat{a}_m^\dagger$ and $\hat{b}_m^\dagger$ share the same label, physically these modes might be totally different. What is important is that, the modes labeled by $m$ give rise to the internal structure of a composite particle.

We introduce a composite boson creation operator $\hat{c}^\dagger$, that creates a pair of particles. Note that this operator resembles the one for Cooper pairs [2]. The entanglement between particles is encoded in the amplitudes $\sqrt{\lambda_m}$. In particular, one can introduce a measure of entanglement known as *purity*

$$P = \sum_{m=0}^{\infty} \lambda_m^2, \quad 0 < P \leq 1. \tag{3}$$

For $P = 1$ the particles are disentangled, whereas in the limit $P \to 0$ the entanglement between particles goes to infinity. The degree of entanglement can be also expressed via the so called Schmidt number $K = 1/P$. Intuitively, $K$ estimates the average number of modes that are taken into account in the internal structure of a composite boson.

The bosonic properties of $\hat{c}^\dagger$ can be studied in many ways. For example, the commutation relation gives $[\hat{c}, \hat{c}^\dagger] = 1 + \xi \sum \lambda_m (\hat{a}_m^\dagger \hat{a}_m + \hat{b}_m^\dagger \hat{b}_m)$, where $\xi = -1$ if $a$ and $b$ are fermions, or $\xi = +1$ if they are bosons. On the other hand, following the approach in [1] one may

[*] papercrane79@kias.re.kr

study the ladder properties of this operator

$$|n\rangle \equiv \chi_n^{-1/2}\frac{(\hat{c}^\dagger)^n}{\sqrt{n!}}|0\rangle,$$
$$\hat{c}|n\rangle = \sqrt{\frac{\chi_n}{\chi_{n-1}}}\sqrt{n}|n-1\rangle + |\epsilon_n\rangle,\ \langle n-1|\epsilon_n\rangle = 0,$$
$$\langle\epsilon_n|\epsilon_n\rangle = 1 - n\frac{\chi_n}{\chi_{n-1}} + (n-1)\frac{\chi_{n+1}}{\chi_n}, \qquad (4)$$

where $|n\rangle$ are states of $n$ composite bosons, parameters $\chi_n$ are normalization factors, such that $\langle n|n\rangle = 1$, and $|\epsilon_n\rangle$ are unnormalized states that can result from subtracting a single composite particle from a state $|n\rangle$. The states $|\epsilon_n\rangle$ do not correspond to $n-1$ composite bosons of the same type, but rather to a complicated state of $n-1$ pairs of particles $a$ and $b$. The ladder structure of operators $\hat{c}^\dagger$ and $\hat{c}$ starts to approach those of ideal bosons if $\frac{\chi_{n+1}}{\chi_n} \to 1$ for all $n$.

To simplify our model, we assume BEC in Gaussian states which are represented by a combination of coherent, thermal, and squeezed states. Assuming that composite bosons are in a thermal state or in a harmonic trap, we can describe the composite bosons with a Gaussian state. Thus, the Gaussian formula of the composite bosons is represented by the following modified operator that is based on the one studied in [1]

$$\hat{c}_r^\dagger = \sum_{m=0}^{\infty}\sqrt{(1-x)x^m}\hat{a}_{m,r}^\dagger\hat{b}_{m,r}^\dagger, \qquad (5)$$

where the double indices refer to internal ($m$) and to external degrees of freedom ($r$). The internal index $m$ may represent their position values. In our case $r$ labels the energy levels of the trap in which the BEC takes place. Moreover, as we assumed in the beginning, the internal structure parameters $\lambda_m = (1-x)x^m$ (for $0 \leq x < 1$) are independent of $r$. The internal structure parameter $\lambda_m$ is equivalent to the coefficient of a two-mode squeezed vacuum (TMSV) state, $|TMSV\rangle = \sum_{m=0}^{\infty}\sqrt{(1-r)r^m}|m\rangle_a|m\rangle_b$, which is a typical two-mode Gaussian state. The above operator has desirable properties, since it is possible to analytically evaluate the factors $\chi_n$ and one can control the entanglement between constituents $a$ and $b$ via the parameter $x$ [1]. For $x = 0$ the system is separable and in the limit $x \to 1$ entanglement goes to infinity. In addition

$$0 \leq (\frac{\chi_{n+1}}{\chi_n})_F = \frac{x^n(n+1)(1-x)}{(1-x^{n+1})} < 1 \qquad (6)$$

for a pair of fermions [1] and

$$1 < (\frac{\chi_{n+1}}{\chi_n})_B = \frac{(n+1)(1-x)}{(1-x^{n+1})} \leq n+1 \qquad (7)$$

for a pair of bosons [1].

It is known that the effective number of cobosons is related to the level of correlation between the two constituent particles. For the maximum level of correlation, the effective number of cobosons is the same as the total number of cobosons. For the weak level of correlation, the effective number of cobosons is smaller (larger) than the total number of cobosons while each constituent fermion (boson) exhibits its own property.

We showed how much the coboson BEC deviates from the behavior of a BEC comprised of ideal bosons, using a controllable parameter, i.e., entanglement between the two constituent particles. We specifically considered bi-fermions trapped in a 3D isotropic harmonic system. By the Pauli exclusion principle between bi-fermions, we found that the effective number of bi-fermions can be smaller than the total number of bi-fermions, regardless of system. Thus we demonstrated that the effective number of bi-fermions in the ground state increases with the degree of entanglement between a pair of fermions. *Correspondingly, we found that the transition temperature for the 3D isotropic harmonic system, i.e., the temperature at which all the bi-fermions moved to the excited states, increased with increasing entanglement.*

Moreover, we discussed coboson BEC, where each coboson is a bi-boson. Due to the bunching effect from each constituent boson, the effective number of bi-bosons can be greater than the total number of bi-bosons. Thus it was shown that the effective number of bi-bosons in the ground state decreases with the degree of entanglement between a pair of bosons. *Correspondingly, the transition temperature for the 3D isotropic harmonic system decreased with increasing entanglement. When the entanglement between a pair of bosons becomes sufficiently small, the bi-boson pairs are dissociated, increasing the bunching effect in the effective number of bi-bosons. Consequently the coboson operator is represented by the direct product of each component field operator.*

All the details are given in Ref. [3]. Furthermore, we show that BEC of composite bosons can be applied to quantum indistinguishability using macroscopic states [4].

**Acknowledgments** This research was partly supported by the IT R&D program of MOTIE/KEIT [1004346 (2012)].

## References

[1] C.K. Law. Quantum entanglement as an interpretation of bosonic character in composite two-particle systems. *Phys. Rev. A* 71; 034306, 2005.

[2] M. Combescot. "Commutator formalism" for pairs correlated through Schmidt decomposition as used in Quantum Information. *Europhys. Lett.* 96; 60002, 2011.

[3] S.-Y. Lee, J. Thompson, S. Raeisi, P. Kurzynski, and D. Kaszlikowski. Quantum information approach to BoseEinstein condensation of composite bosons. *New J. Phys.*, 17; 113015, 2015.

[4] S.-Y. Lee, C.-W. Lee, P. Kurzynski, D. Kaszlikowski, and J. Kim. Duality in entanglement of macroscopic states of light. *arXiv* :1606.01613.

# Quantum key distribution without monitoring signal disturbance by using heralded pair-coherent sources

Le Wang[1] Shengmei Zhao[1] *

[1] *Institute of Signal Processing and Transmission, Nanjing University of Posts and Telecommunications(NUPT), Nanjing 210003, China*

**Abstract.** Recently, a new type of quantum key distribution (QKD) without monitoring signal disturbance, named the round-robin differential-phase-shift (RRDPS) QKD, was proposed. However, the current RRDPS-QKD schemes with the weak coherent pulses (WCPs) have low key generation rates and short transmission distances due to the vacuum component of sources of these schemes are significant large. In this paper, we propose to implement the heralded pair-coherent source into the RRDPS-QKD scheme to provide a longer transmission distance comparing with the scheme with WCPs.

**Keywords:** Round-robin differential-phase-shift quantum key distribution, Heralded pair-coherent sources, weak coherent pulses

## 1 Introduction

Quantum key distribution (QKD) allows two remote users, called Alice and Bob, to securely exchange cryptographic keys despite that in the presence of an eavesdropper (Eve), and it has been theoretically proved to be unconditionally secure. However, if there exists the disturbances caused by the imperfect quantum channel or eavesdroppers, the keys might not be identical or secure. Hence, it is essential to guarantee protection against the eavesdropping by monitoring the signal disturbances during the transmission of the quantum signals.

Recently, a new QKD scheme, named the round-robin differential phase-shift (RRDPS) QKD [1], was proposed, which does not need monitoring of disturbances to guarantee the security. Hence, the RRDPS-QKD could tolerate a high bit error rate, up to almost 50%, which is significantly higher than that of the traditional QKD schemes. Since the RRDPS-QKD was proposed, it has been studied from both theoretically [1,2] and experimentally [3,4]. However, the current RRDPS-QKD schemes with the weak coherent pulses (WCPs) have low key generation rate and short transmission distance due to the vacuum component of WCPs is significant large.

On the other hand, the heralded pair-coherent source (HPCS) can remove the shortcomings of the WCPs because the vacuum component of the HPCS is much lower than that of the WCPs. Hence, it shows excellent behaviors when the applications of the HPCS to the traditional QKD schemes [5,6]. In this paper, we propose to implement the HPCS into the RRDPS-QKD scheme. In addition, a tighter and more reasonable bound of the phase error rate proposed by [2] is adopted. By comparing the performances of the current RRDPS-QKD scheme with the WCPs, the transmission distance of the our scheme with HPCS is significantly longer than that of the current scheme with WCPs.

## 2 The RRDPS-QKD scheme with HPCS

The schematic diagram of the RRDPS-QKD with the HPCS is shown in Fig.1, and the proposed scheme runs as follows:

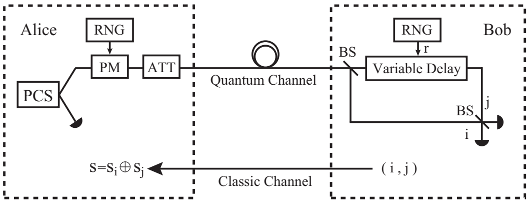

Figure 1: A schematic diagram of the RRDPS-QKD with the HPCS. PCS: pair-coherent source. ATT: attenuator. PM: phase modulator. BS: beam splitter. RNG: random number generator.

Step 1: Alice employs the HPCS to generate a series of pulse trains, where each pulse train contains $L$ pulses. The HPCS is realized by the photon-heralding technique on the pair-coherent source (PCS) [7] that uses one mode of a two-mode correlated coherent state from the PCS as a trigger to encode the behavior of the other mode and the other mode as a carrier to transmit the quantum signals to Bob. Then Alice generates a random $L$-bit sequence, $s_1, s_2, \cdots, s_L$, where $s_i \in \{0, 1\}$ by a random number generator (RNG). Subsequently, Alice encodes the random $L$-bit sequence into the phase of the $L$-pulse train, 0 according by $s_i = 0$ or $\pi$ according by $s_i = 1$, by a phase modulator (PM).

Step 2: Alice uses an attenuator (ATT) to attenuate the pulse trains into the signals with the average intensity $\mu$. Then, Alice sends the pulse trains to Bob through a quantum channel.

Step 3: Upon receiving an $L$-pulse train, Bob splits the pulse train into two pulse trains with a 50:50 beam splitter (BS). Then Bob shifts one of the pulse trains by $r$ pulses with a Variable Delay, which is controlled by a RNG. The RNG is used to generate a number $r \in \{-L+1, \cdots, -2, -1, 1, 2, \cdots, L-1\}$.

Step 4: Bob measures the interference between two $L$-

*zhaosm@njupt.edu.cn

pulse trains. If Bob obtains a detection result on position $i$ and $j$ in the unshifted pulse train and the shifted pulse train, respectively, where $i$ and $j$ satisfy $j = i \pm r \pmod{L}$, Bob records a key bit $s_A$ according to the relative phase $s_B = s_i \oplus s_j$. Otherwise, Bob regards the transmission as a failure.

Step 5: Bob announces the indices $\{i, j\}$ to Alice through a classic channel, and Alice could compute $s_A = s_i \oplus s_j$ to obtain a sifted key $s_A$.

By using the photon-heralding technique on the PCS, one mode of the PCS can be locally triggered and used to encode the behavior of the other mode. Then the $n$-photon number probability of the encoded pulse can be expressed as [5, 6]

$$P_n(\mu) = \frac{1}{\sqrt{I_0(2\mu)}} \frac{\mu^{2n}}{(n!)^2} [1 - (1 - \eta_A)^n + d_A], \qquad (1)$$

where $\mu$ is the average intensity of the pulses, $I_0(x)$ is the modified Bessel's function of the first kind, $\eta_A$ and $d_A$ represent the detection efficiency and the dark count rate of the triggering detector of Alice, respectively.

The key generation rate per pulse for the proposed scheme can be written as the following [2]

$$R = \frac{1}{L} Q_{L\mu} [1 - f H(e_{bit}) - H_{PA}], \qquad (2)$$

where $Q_{L\mu}$ is the overall gain when the average intensity of the pulse trains is $L\mu$, $f$ denotes the efficiency of the error correction, and $H(x) = -x \log_2(x) - (1-x) \log_2(1-x)$ is a binary Shannon entropy. $e_{bit}$ is the bit error rate and $H_{PA}$ is the ratio of the key rate loss in the privacy amplification.

## 3 Results discussion

In this section, we discuss the performance of the proposed protocol by numerical simulations.

Fig.2 shows the key generation rate performance of the RRDPS-QKD with the HPCS against the transmission distance, in comparison with that of the RRDPS-QKD with the WCPs with the same experimental parameters [2] when $L = 32$, $\eta_A = 75\%$ and $d_A = 5 \times 10^{-8}$. The results show that the key generation rate performance of proposed scheme is much better than that of the current scheme with the WCPs. The transmission distance of the our scheme with HPCS is significantly longer than that of the current scheme with WCPs. That is because the vacuum component of the HPCS is significant lower than that of the WCPs.

In this paper, we have presented to implement the HPCS into the RRDPS-QKD scheme. In addition, a tighter and more reasonable bound of the phase error rate proposed by is adopted. It has been shown that the transmission distance of the our scheme with HPCS is significantly longer than that of the current scheme with WCPs.

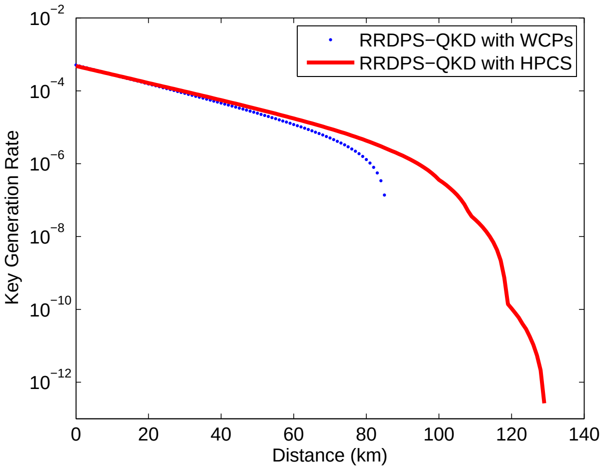

Figure 2: The key generation rate performance of the RRDPS-QKD with the HPCS against the transmission distance, in comparison with that of the RRDPS-QKD with the WCPs.

## References

[1] T. Sasaki et. al. Practical quantum key distribution protocol without monitoring signal disturbance. *Nature*, 509, 475, 2014.

[2] Z. Zhang et. al. Round-robin differential-phase-shift quantum key distribution. *arXiv*, 1505.02481.

[3] J. Y. Guan et. al. Experimental Passive Round-Robin Differential Phase-Shift Quantum Key Distribution. *Phys. Rev. Lett.*, 114, 180502, 2015.

[4] H. Takesue et. al. Experimental quantum key distribution without monitoring signal disturbance. *Nat. Photonics*, 9, 827-831, 2015.

[5] S. L. Zhang et. al. A universal coherent source quantum key distribution. *Chin. Sci. Bull.*, 54, 1863-1871, 2009.

[6] F. Zhu et. al. Enhancing the performance of the measurement-device-independent quantum key distribution with heralded pair-coherent sources. *Phys. Lett. A*, 380, 1408-1413, 2016.

[7] G. S. Agarwal et. al. Generation of pair coherent states and squeezing via the competition of four-wave mixing and amplified spontaneous emission. *Phys. Rev. Lett.*, 57, 827, 1986.

# Spin blockade of Heavy-Holes in Double Quantum Dots

Jo-Tzu Hung,[1] * Bin Wang,[1] [2] Alexander R. Hamilton,[1] Dimitrie Culcer[1]

[1]*School of Physics, The University of New South Wales, Sydney NSW 2052, Australia*
[2]*University of Science and Technology of China, Hefei, Anhui, 230026, China*

**Abstract.** Spin-orbit interaction plays a crucial role in manipulating hole-spin qubits, and its coupling strength may be extracted from Pauli spin blockade. We investigate Pauli spin blockade for two heavy holes in a double quantum dot in an in-plane magnetic field. We include relevant spin-orbit interactions as well as complex Zeeman interaction, and calculate blockade leakage as a function of the in-plane field strength and direction. The leakage is anisotropic in the in-plane field direction. We further compare the spin-orbit coupling strength by extracting the relation between the leakage current and the field strength.

**Keywords:** spin qubit, quantum dot, hole, spin blockade

## 1 Lower-dimensional hole system

Holes, often symbolized as an alternate representation of electrons in the valence band, have the effective spin $J=\frac{3}{2}$ [see Fig. 1(a).] Owing to the atomic $p$-orbital, holes suffer from less spin-spin coupling to the nuclei and is expected to have a strong spin-orbit (SO) interaction[1]. Hole qubits then promise a less noisier magnetic environment and a purely electric control due to the strong SO mixture in the hole qubit [see Fig. 1(b).]

The $J=\frac{3}{2}$ Hilbert space comprises a heavy hole (HH) with a secondary quantum number $m_J=\pm\frac{3}{2}$ and a light hole (LH) with $m_J = \pm\frac{1}{2}$. For two-dimensional holes, when the HH-LH splitting is relatively large, the HH and LH states can be considered weakly coupled, and one may perform a unitary rotation to block-diagonalize the $J=\frac{3}{2}$ matrix[2]. In gated QDs, the ground state usually have a strong HH character and can be treated as a pseudospin.

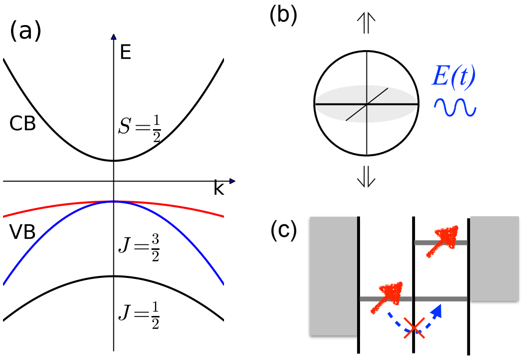

Figure 1: (a) The effective spin of bulk conduction band (CB) and valence band (VB) with $J = \frac{1}{2} \oplus 1$. The red and blue curves correspond to the HH and LH. (b) Both the logicals $|\Uparrow\rangle$ and $|\Downarrow\rangle$ in a HH are an strong SO mixture and can be driven by electric control $E(t)$. (c) PSB in a two-HH double QD. Practically, the spin of the left HH is unknown. PSB is often employed in quantum computing because it permits spin-selective charge readouts.

## 2 Spin-orbit lifted Pauli spin blockade

We theoretically investigate hole SO interaction by studying Pauli spin blockade [PSB, see Fig. 1(c)] of two HHs confined by coupled QDs in a magnetic field $\mathbf{B}=B(\cos\theta,\sin\theta,0)$. $\theta$ is measured from the $x$ axis.

We adapt the Pauli matrices $\vec{\sigma}$ to describe a HH pseudospin. The in-plane Zeeman interaction is given by $\hat{H}_Z=\hat{H}_{Zq}+\hat{H}_{[001]}+\hat{H}_{Zc}$, where $\hat{H}_{Zq}=-\frac{3}{2}q\mu_B B(e^{i\theta}\sigma_+ + e^{-i\theta}\sigma_-)$, and $\hat{H}_{[001]}=\frac{-f}{\hbar^2}\mu_B B(e^{-i\theta}\sigma_+ p_-^2+e^{i\theta}\sigma_- p_+^2)$ and $\hat{H}_{Zc}=F(\mu_B B)^3(e^{-3i\theta}\sigma_+ + e^{3i\theta}\sigma_-)$, with $\sigma_\pm = \frac{1}{2}(\sigma_x \pm i\sigma_y)$ and $p_\pm$ being the raising (lower) operator of the spatial momentum. $\mu_B$ denotes the Bohr magneton, $q$ is a dimensionless, material-dependent quantity, and both of $f$ and $F$ are subject to the dot confinement. The SO interaction $\hat{H}_{SO} = \hat{H}_R+\hat{H}_D$ includes Rashba and Dresselhaus couplings, with $\hat{H}_R=i\alpha(\sigma_+ p_-^3-\sigma_- p_+^3)$ and $\hat{H}_D=-\beta_3(\sigma_+ p_- p_+ p_- +\sigma_- p_+ p_- p_+)-\beta_1(\sigma_+ p_- +\sigma_- p_+)$.

Figure 1(c) shows a HH PSB from $(1,1)$ to $(0,2)$, where $(N_L,N_R)$ labels the number of HHs on the left and right. The two dots are coupled by a spin-perserving coupling $t_0$, and the lowest energy state is $|S_{02}\rangle$, a $(0,2)$ singlet. Due to the Pauli exclusion principle, the left spin, if it is parallel to the right spin, will be blocked. In the presence of the SO interaction, such PSB may be lifted[3].

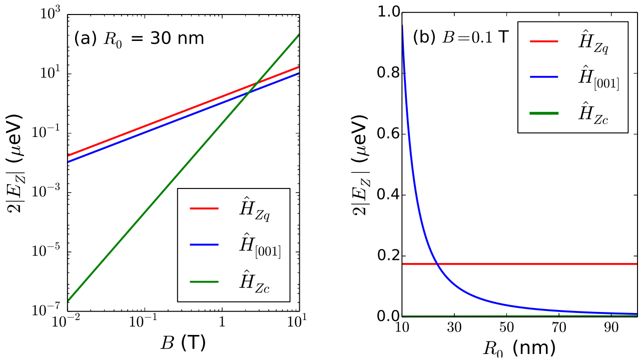

Figure 2: Individual DQD spin splittings (a) $2|E_Z(B)|$ with the dot radius $R_0 = 30$ nm and (b) $2|E_Z(R_0)|$ at $B = 0.1$ T, due to $\hat{H}_{Zq}$, $\hat{H}_{[001]}$ and $\hat{H}_{Zc}$, respectively.

We denote by $|S_{11}\rangle$ the $(1,1)$ singlet and by $|T_0\rangle$ the

*jo-tzu.hung@unsw.edu.au

Table 1: The $\theta$-dependent $\Delta_+(\theta)$ and $\Delta_0(\theta)$, with $t_{R(D)} \equiv \langle S_{02}| \hat{H}_{R(D)} |\Downarrow\Downarrow\rangle$ being the Rashba (Dresselhaus) coupling parameter.

| | $\Delta_+$ | $\frac{1}{\sqrt{2}}\Delta_0$ |
|---|---|---|
| $\hat{H}_{Zq}$ | $(t_R \cos\theta - t_D \sin\theta)$ | $i(t_R \sin\theta - t_D \cos\theta)$ |
| $\hat{H}_{[001]}$ | $(t_R \cos\theta + t_D \sin\theta)$ | $-i(t_R \sin\theta + t_D \cos\theta + t_B)$ |
| $\hat{H}_{Zc}$ | $(t_R \cos 3\theta + t_D \sin 3\theta)$ | $-i(t_R \sin 3\theta + t_D \cos 3\theta)$ |

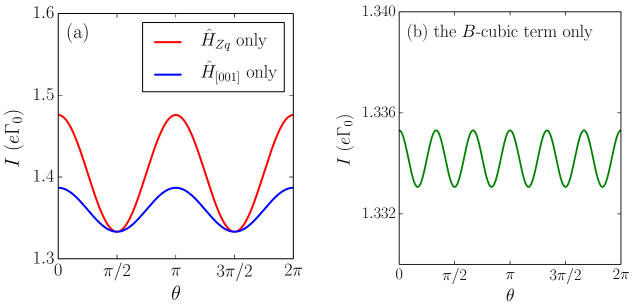

Figure 3: Individual PSB leakage currents $I(\theta)$ at $B = 1$ T when (a) only the $B$-linear terms in $\hat{H}_Z$ are included, and when (b) only $\hat{H}_{Zc}$ is included. The oscillation period in (b) is three times more than that in (a). $e$ is the elementary charge, and we set the $(1, 1)$ relaxation rate $\Gamma_0 = 3$ MHz and $t_R = 0.3t_0 \gg t_D$. $t_0 = 200$ $\mu$eV.

$(1, 1)$ unpolarized triplet, and by $|T_\pm\rangle$ the $(1, 1)$ polarized triplet. In the basis $\{S_{02}, M, M_\perp, T_+, T_-\}$, the effective tunneling Hamiltonian reads

$$\hat{H} = \begin{bmatrix} 0 & 0 & N_M(\theta) & \Delta_+(\theta) & -\Delta_+(\theta) \\ 0 & 0 & 0 & 0 & 0 \\ N_M(\theta) & 0 & 0 & 0 & 0 \\ \Delta_+^*(\theta) & 0 & 0 & E_Z & 0 \\ -\Delta_+^*(\theta) & 0 & 0 & 0 & -E_Z \end{bmatrix}, \tag{1}$$

Here we have used the superpositions of $|S_{11}\rangle$ and $|T_0\rangle$: $|M\rangle \equiv \frac{1}{N_M}[\Delta_0(\theta)\,|S_{11}\rangle - t_0\,|T_0\rangle]$ and $|M_\perp\rangle = \frac{1}{N_M}(t_0\,|S_{11}\rangle + \Delta_0^*(\theta)\,|T_0\rangle)$ with $N_M = \sqrt{t_0^2 + |\Delta_0(\theta)|^2}$. The in-plane Zeeman terms split the triplet by $E_Z$, whereas $\Delta_+(\theta)$ and $\Delta_0(\theta)$ correspond to the SO tunneling element between $|T_\pm\rangle$ and $|S_{02}\rangle$, and between $|T_0\rangle$ and $|S_{02}\rangle$. We list $\Delta_+(\theta)$ and $\Delta_0(\theta)$ in Table 1 by considering individual Zeeman terms.

## 3 Main Results

We diagonalize Eq. (1) and calculate the PSB leakage by solving the steady-state kinetic equations: $-\sum_\sigma W_{k\sigma} P_k - \sum_{k' \neq k} \Gamma_k P_k + \sum_{k' \neq k} \Gamma_{k'} P_{k'} + \sum_\sigma U_{\sigma k} P_\sigma = 0$ and $-\sum_k U_{\sigma k} P_\sigma + \sum_k W_{k\sigma} P_k = 0$. Here $P_k$ and $P_\sigma$ correspond to the probabilities in the eigenstate $|k\rangle$ and in $(0, 1)$ with the spin $\sigma$. $W_{k\sigma}$ ($U_{\sigma k}$) denotes the transition rate from $|k\rangle$ $[(0, 1)_\sigma]$ to $(0, 1)_\sigma$ ($|k\rangle$), and $\Gamma_k$ is the $(1, 1)$ relaxation rate out of $|k\rangle$.

Figure 2 shows individual spin splittings in a double QD due to the three terms in $\hat{H}_Z$. As expected, the two $B$-linear terms are significant at low and intermediate fields, whereas $\hat{H}_{Zc}$ is dominating at large fields. Figure 3 compares individual $I(\theta)$ at $B = 1$ T with a fixed SO coupling. The qualitative difference in $I(\theta)$ between the $B$-linear and $B$-cubic cases provides an indication of the power of the dominating in-plane Zeeman term in hole QDs. In Fig. 4, we find at low fields, where the $B$-linear terms dominates, the larger $|dI/dB|$, the stronger the SO coupling. To compare with electron PSB[4], we assume $t_R \ll t_0$ and $|E_Z| < t_0$, we obtain $I(B) \sim e\Gamma_{\text{DL}} P_M E_Z^2 \gamma^2 / (E_Z^2 + \frac{t_0^4}{|\Delta_+|^2}\gamma^2)$, with $\Gamma_{DL}$ the transition rate between the dot and lead, and $\gamma^2 = \Gamma_0/\Gamma_{DL}$.

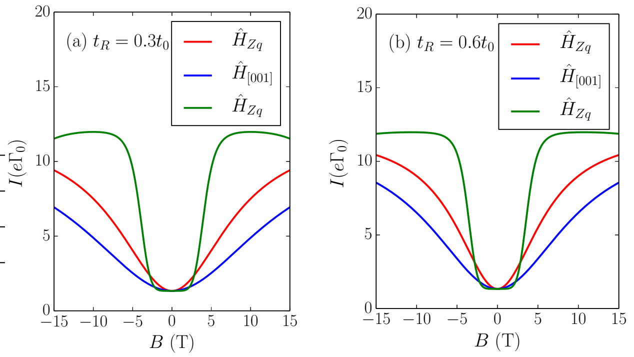

Figure 4: Individual PSB leakage currents $I(B)$ at $\theta = 0$ for (a) $t_R = 0.3t_0 \gg t_D$ and $(b) t_R = 0.6t_0 \gg t_D$.

## 4 Conclusion

We have found that (i) the $I(\theta)$ behavior suggests that the SO mixture in the hole qubit can be tuned by adjusting the field direction $\theta$, and (ii) the slope of $I(B)$ can be used in comparing the SO coupling strength.

**Acknowledgement** This work is supported by the ARC through the DP scheme.

## References

[1] C. Kloeffel and D. Loss. Prospects for spin-based quantum computing in quantum dots *Annu. Rev. Condens.Matter Phys.* 4:51–81, 2013.

[2] R. Winkler et al. Spin orientation of holes in quantum wells. *Semicond. Sci. Technol.*. 23:114017, 2008.

[3] R. Li et al. Pauli spin blockade of heavy holes in a silicon double quantum dot. *Nano Lett.*. 15:7314–7318, 2015; D. Q. Wang et al. Anisotropic Pauli spin blockade in GaAs double hole quantum dots. manuscript in preparation.

[4] J. Danon and Y. V. Nazarov. Pauli spin blockade in the presence of strong spin-orbit coupling. *Phys. Rev. B.* 80:041301, 2009.

[5] J. -T. Hung et al. Spin blockade of heavy holes in gate-defined quantum dots. manuscript in preparation.

# Unified View of Quantum Correlations and Quantum Coherence

Kok Chuan Tan[1] * Hyukjoon Kwon[1] † Chae-Yeun Park[1] ‡ Hyunseok Jeong[1] §

[1] *Center for Macroscopic Quantum Control, Department of Physics and Astronomy, Seoul National University, Seoul, 151-742, Korea*

**Abstract.** We present arguments that quantum coherence in a bipartite system can be contained either locally or in the correlations between the subsystems. The portion of quantum coherence contained within correlations can be viewed as a kind of quantum correlation which we call correlated coherence. We demonstrate that the framework provided by correlated coherence allows us to retrieve the same sets of quantum correlations as defined by the asymmetric and symmetric versions of quantum discord as well as quantum entanglement, thus providing a unified interpretation of these correlations. We also prove that correlated coherence can be formulated as an entanglement monotone, thus demonstrating that entanglement may be viewed as a specialized form of coherence.

**Keywords:** Quantum Coherence, Quantum Correlations, Quantum Discord, Entanglement

## 1 Introduction

Following the quantitative theories of entanglement, Baumgratz et al. [2] recently proposed a resource theory of quantum coherence. They first postulate a set of axioms that a measure of quantum coherence should satisfy, and then went on to demonstrate that several intuitive measures of quantum coherence satisfy these properties. Recent developments have since uncovered interesting connections between quantum coherence and correlation, such as their interconversion with each other [3, 4] as well as trade-off relations [5]. At the same time, it is well known in quantum information theory that within quantum theory, the set of all possible correlations can be categorized either as "classical" or "quantum". Here, we provide some arguments [1] to suggest that the "quantumness" of quantum correlations can be interpreted in terms of the language of the resource theory of quantum coherence, thus providing a bridge between the two concepts.

## 2 Preliminaries

We will frequently refer to a bipartite quantum state which we denote $\rho_{AB}$, where $A$ and $B$ refer to local subsystems held by different laboratories. Following convention, we say the subsystems $A$ and $B$ are held by Alice and Bob respectively. The local state of Alice is obtained by performing a partial trace on $\rho_{AB}$, and is denoted by $\rho_A = \text{Tr}_B(\rho_{AB})$, and $\{|i\rangle_A\}$ is a complete local basis of Alice's system. Bob's local state and local basis are also similarly defined. In general, the systems Alice and Bob holds may be composite, such that $A = A_1A_2 \cdots A_N$ and $B = B_1B_2 \cdots B_M$ so the total state may identically be denoted by $\rho_{A_1A_2\cdots A_N B_1B_2\cdots B_M}$.

We will adopt the axiomatic approach for coherence measures as shown in Ref. [2]. For a fixed basis set $\{|i\rangle\}$, the set of incoherent states $\mathcal{I}$ is the set of quantum states with diagonal density matrices with respect to this basis. Then a reasonable measure of quantum coherence $\mathcal{C}$ should satisfy following properties: (C1) $C(\rho) \geq 0$ for any quantum state $\rho$ and equality holds if and only if $\rho \in \mathcal{I}$. (C2a) The measure is non-increasing under incoherent completely positive and trace preserving maps (ICPTP) $\Phi$ , i.e., $C(\rho) \geq C(\Phi(\rho))$. (C2b) Monotonicity for average coherence under selective outcomes of ICPTP: $C(\rho) \geq \sum_n p_n C(\rho_n)$, where $\rho_n = \hat{K}_n \rho \hat{K}_n^\dagger / p_n$ and $p_n = \text{Tr}\hat{K}_n \rho \hat{K}_n^\dagger]$ for all $\hat{K}_n$ with $\sum_n \hat{K}_n \hat{K}_n^\dagger = \mathbb{1}$ and $\hat{K}_n \mathcal{I} \hat{K}_n^\dagger \subseteq \mathcal{I}$. (C3) Convexity, i.e. $\lambda C(\rho) + (1-\lambda) C(\sigma) \geq C(\lambda\rho + (1-\lambda)\sigma)$, for any density matrix $\rho$ and $\sigma$ with $0 \leq \lambda \leq 1$. Here, we will employ the $l_1$-norm of coherence, which is defined by $\mathcal{C}(\rho) := \sum_{i \neq j} |\langle i| \rho |j\rangle|$, for any given basis set $\{|i\rangle\}$ (otherwise called the reference basis). It can be shown that this definition satisfies all the properties mentioned [2].

## 3 Results

Consider a bipartite state $\rho_{AB}$, with total coherence $\mathcal{C}(\rho_{AB})$ with respect to local reference bases $\{|i\rangle_A\}$ and $\{|j\rangle_B\}$. Then $\mathcal{C}(\rho_A)$ and $\mathcal{C}(\rho_B)$ can be interpreted as the coherence that is local to $A$ and $B$ respectively. In general, the sum of the total local coherences is not necessarily the same as the total coherence in the system. It is therefore reasonable to suppose that a portion of the quantum coherences are not stored locally, but within the correlations of the system itself. This motivates the following definition:

**Definition 1** *With respect to local reference bases $\{|i\rangle_A\}$ and $\{|j\rangle_B\}$, the correlated coherence for a bipartite quantum system is the local coherences subtracted from the total coherence:*

$$\mathcal{C}_{cc}(\rho_{AB}) := \mathcal{C}(\rho_{AB}) - \mathcal{C}(\rho_A) - \mathcal{C}(\rho_B)$$

*where $\rho_A$ and $\rho_B$ are the reduced density matrices of $A$ and $B$ respectively.*

In general, the above quantity is basis dependent. However, it can be made a state dependent property by

*bbtankc@gmail.com

†tera900@snu.ac.kr

‡kaeri@gmail.com

§h.jeong37@gmail.com

choosing the local basis to be the the local eigenbasis. For every bipartite state $\rho_{AB}$, the reduced density matrices $\rho_A$ and $\rho_B$ have eigenbases $\{|\alpha_i\rangle\}$ and $\{|\beta_i\rangle\}$, respectively. In the even of degeneracy, where multiple local eigenbases exists, we will choose the basis that minimizes the total coherence. By choosing these local bases, $\rho_A$ and $\rho_B$ are both diagonal so the local coherences are zero. The implication of this is that for such a choice, *the coherence in the system is stored entirely within the correlations* and the correlated coherence becomes a state dependent property. We will assume that this choice of local bases will always be made.

Correlated coherence has many interesting properties. For instance, the following theorems suggests that it can properly define the set of states with symmetric/asymmetric quantum discord or quantum entanglement:

**Theorem 2 (Symmetric Quantum Discord)** *For a given state $\rho_{AB}$, $\mathcal{C}_{cc}(\rho_{AB}) = 0$ iff $\rho_{AB} = \sum_{i,j} p_{i,j} |i\rangle_A \langle i| \otimes |j\rangle_B \langle j|$.*

**Theorem 3 (Asymmetric Quantum Discord)** *For a given state $\rho_{AB}$, let $\{|i\rangle_A\}$ and $\{|j\rangle_B\}$ be the the eigenbases of $\rho_A$ and $\rho_B$ respectively. Define the measurement on A onto the local basis as $\Pi_A(\rho_{AB}) := \sum_i (|i\rangle_A \langle i| \otimes I_B)\rho_{AB}(|i\rangle_A \langle i| \otimes I_B)$. Then, with respect to these local bases, $\mathcal{C}_{cc}(\rho_{AB}) - \mathcal{C}_{cc}(\Pi_A(\rho_{AB})) = 0$ iff $\rho_{AB} = \sum_i p_i |i\rangle_A \langle i| \otimes \rho_B^i$, where $\rho_B^i$ is some normalized density matrix and $\{|i\rangle_A\}$ is some set of orthonormal vectors.*

**Theorem 4 (Entanglement)** *Let $\rho_{AA'BB'}$ be some extension of a bipartite state $\rho_{AB}$ and choose the local bases to be the eigenbases of $\rho_{AA'}$ and $\rho_{BB'}$ respectively. Then with respect to these local bases, $\min \mathcal{C}_{cc}(\rho_{AA'BB'}) = 0$ iff $\rho_{AB} = \sum_i p_i |\alpha_i\rangle_A \langle \alpha_i| \otimes |\beta_i\rangle_B \langle \beta_i|$ for some set of normalized vectors $|\alpha_i\rangle$ and $|\beta_i\rangle$ that are not necessarily orthogonal and may repeat. The minimization is over all possible extensions of $\rho_{AB}$ of the form $\rho_{AA'BB'}$.*

The above results already suggest a non-trivial relationship between coherence and quantum correlations. This relationship can be pushed further. We also demonstrate that it is possible to construct a new entanglement monotone from the coherence measure, suggesting that entanglement itself is a specialized form of coherence. This new entanglement monotone is first constructed by considering what we call unitarily symmetric extensions:

**Definition 5 (Unitarily Symmetric Extensions)** *Let $\rho_{AA'BB'}$ be an extension of a bipartite state $\rho_{AB}$. The extension $\rho_{AA'BB'}$ is said to be unitarily symmetric if it remains invariant up to local unitary operations on $AA'$ and $BB'$ under a system swap between Alice and Bob.*

*More formally, let $\{|i\rangle_{AA'}\}$ and $\{|j\rangle_{BB'}\}$ be complete local bases on $AA'$ and $BB'$ respectively. Define the swap operator $U_{\mathrm{swap}} |i,j\rangle_{AA'BB'} := |j,i\rangle_{AA'BB'}$ . Then $\rho_{AA'BB'}$ is unitarily symmetric if there exists local unitary operations $U_{AA'}$ and $U_{BB'}$ such that $U_{AA'} \otimes U_{BB'} \left(U_{\mathrm{swap}} \rho_{AA'BB'} U_{\mathrm{swap}}^\dagger\right) U_{AA'}^\dagger \otimes U_{BB'}^\dagger = \rho_{AA'BB'}$.*

It is possible then to define our entanglement measure:

**Definition 6** *Let $\rho_{AA'BB'}$ be some unitarily symmetric extension of a bipartite state $\rho_{AB}$ and choose the local bases to be the eigenbases of $\rho_{AA'}$ and $\rho_{BB'}$ respectively. Then the entanglement of coherence is defined to be:*

$$E_{cc}(\rho_{AB}) := \min \mathcal{C}_{cc}(\rho_{AA'BB'})$$

*The minimization is over all possible unitarily symmetric extensions of $\rho_{AB}$ of the form $\rho_{AA'BB'}$.*

From the above definition, it can then be shown that the above quantity satisfies the basic requirement of all entanglement measures:

**Theorem 7 (Entanglement monotone)** *The entanglement of coherence $E_{cc}$ is an entanglement monotone in the sense that it satisfies:*

*i.* *$E_{cc}(\rho_{AB}) = 0$ iff $E_{cc}(\rho_{AB})$ is separable.*

*ii.* *$E_{cc}(\rho_{AB})$ is invariant under local unitaries on A and B.*

*iii.* *$E_{cc}(\rho_{AB}) \geq E_{cc}(\Lambda_{\mathrm{LOCC}}(\rho_{AB}))$ for any LOCC procedure $\Lambda_{\mathrm{LOCC}}$.*

## 4 Conclusion

The framework of the correlated coherence allows us to identify the same non-classical correlations as those of (both symmetric and asymmetric) quantum discord and quantum entanglement. We also provide the first direct proof that entanglement can be viewed as a type of coherence by constructing an entanglement monotone through correlated coherence. The successful interpretation of quantum discord and entanglement in terms of the language of coherence suggests that tasks enabled by them actually derive their quantum advantage from a common source. This connection may eventually allow for the development of a new set of common tools in the treatment of various forms of quantum correlations and quantum coherence.

## References

[1] K. C. Tan, H. Kwon, C.Y. Park and H. Jeong, arXiv. 1603.01958 (2016).

[2] T. Baumgratz, M. Cramer, and M. B. Plenio, Phys. Rev. Lett. **113**, 140401 (2014).

[3] J. Ma, B. Yadin, D. Girolami, V. Vedral, and M. Gu, arXiv. 1510.06179 (2015).

[4] A. Streltsov, U. Singh, H. S. Dhar, M. N. Bera, and G. Adesso, Phys. Rev. Lett. **115**, 020403 (2015).

[5] Z. Xi, Y Li and H. Fan, Sci. Rep. **5**, 10922 (2015).